Landslides Caused by the 8/15/2007 Pisco, Peru (M_w = 7.9) Earthquake: A Case Study

Jennifer K. Diercksen

A thesis

submitted in partial fulfillment of the

requirements for the degree of

Master of Science in Engineering

University of Washington

2012

Committee:

Dr. Joseph Wartman

Dr. Pedro Arduino

Dr. Steven Kramer

Program authorized to offer degree:

Civil and Environmental Engineering

Table of Contents

List of Figures

List of Tables

Table Number Page

Acronyms

ASTER	Advanced Spaceborne Thermal Emission and Reflection Radiometer
CERESIS	Centro Regional de Sismología para América del Sur
CISMID	Centre for Seismic Research and Disaster Mitigation
EERI	Earthquake Engineering Research Institute
ESRI	Environmental Systems Research Institute
ERSDAC	Earth Remote Sensing Data Analysis Center
GSN	Global Seismic Network
IGP	Instituto Geofísico del Perú
INGEMMET	Instituto Geológico Minero y Metalúrgico
GEER	Geotechnical Earthquake Engineering Reconnaissance
MMI	Modified Mercalli Intensity
MSK	Medvedev Sponheuer Karnik (earthquake intensity scale)
NEIC	National Earthquake Information Center
NEHRP	National Earthquake Hazard Reduction Program
NSF	National Science Foundation
PGA	Peak Ground Acceleration
PUCP	Pontificia Universidad Católica del Perú
SA	Response Spectrum Acceleration
SEDAPAL	Servicio de Agua Potable y Alcantarillado de Lima
USGS	United States Geological Survey

Dedication

To my husband, Victor William Diercksen, who supported me in every way possible to make this happen, and to my thesis advisor, Dr. Joe Wartman, who provided direction and many, many great references.

Thank you both.

Landslides Caused by the M_w = 7.9, Pisco, Peru, Earthquake: A Case Study

Introduction

On August 15, 2007, at 6:41 pm local time, a M_w = 7.9 earthquake[1] occurred off the coast of central Peru. The earthquake occurred approximately 60 km west of Pisco and was recorded by 13 accelerograph stations within 200 km of the epicenter. The earthquake's rupture plane was determined to be about 170 km long and 130 km wide; the rupture propagated unilaterally with a predominantly reverse-fault mechanism. Maximum slip was on the order of 180 cm; earthquake duration was 210 seconds. The focus of the event was located at 13.49°S, 76.85°W, 18 km deep, a depth consistent with an interface event on the contact surface between the Nazca and South American plates (Tavera et al., 2008).

Alarcón et al. (2008) reported that the earthquake caused "519 deaths, 1366 injuries, and the collapse of more than 58,000 houses." In addition, the Pisco earthquake triggered over 290 ground failures, 254 of which were landslides.

The first part of this thesis describes the different landsliding modes observed in the affected area, and the parameters that affect landsliding susceptibility: ground motion, geology, geomorphology, slope, slope, slope aspect, ecological region, precipitation, proximity to rivers, and presence of roads or roadcuts. Three main landsliding regions are identified: the Paracas Peninsula, the Coastal Plains, and the Andes Mountains. For each region, the typical landsliding mode is described, as well as the specific parameters which contribute to landsliding susceptibility.

The second part of this paper attempts to determine whether several proposed landslide frequency-volume or earthquake magnitude-volume relationships are valid for the Pisco landsliding event, and whether any of them can be used to upscale the inventory; i.e. account for missing small-volume landslides.

Post-Earthquake Reconnaissance

290 ground failures were inventoried as a result of the earthquake (INGEMMET, 2007; Zavala et al., 2009, and Wartman, unpublished) including a 3 km-long, 1-km wide lateral spread along the Panamericana Sur highway—possibly the largest lateral spread ever recorded (Rodriguez-Marek, 2008). Ground failure inventories used in this report can be found in Appendix A.

[1] Moment magnitude was reported as 7.9 (Tavera and Bernal, 2008) and 8.0 (USGS, 2012.) The 7.9 value was chosen because of Tavera's previous experience and publications regarding the study area.

As-of-yet unpublished landslide data in this report comes from two earthquake reconnaissance trips and was provided by Joseph Wartman: the August 20, 2007, 6-day preliminary field reconnaissance trip sponsored by Geotechnical Earthquake Engineering Reconnaissance (GEER) and funded by the National Science Foundation (NSF); and a second NSF-sponsored 10-day trip starting March, 16, 2010.

Data Set

Ground failure data for this report was collected from three sources: INGEMMET (2007), Zavala et al. (2009), and Wartman (unpublished data). In this report, ground failure refers to landslides and lateral spreads, which have an associated volume, as well as settlement, cracks, and evidence of liquefaction, which have no associated volume. See Appendix A for original source data, as well as the final combined inventory.

INGEMMET (2007) detailed 157 ground failures immediately after the earthquake, in a report published the following month. Included were 128 landslides/lateral spreads. (Only 127 of these were used in analyses involving volume, as one lateral spread was without a volume estimate.)

Zavala (2009) expanded on the INGEMMET data, adding an additional 11 liquefaction sites and one settlement site.

Wartman (unpublished) inventoried 245 ground failures during two reconnaissance trips to Peru, in August of 2007, and again in March of 2010. 127 of these ground failures were not previously described by INGEMMET or Zavala. Volumes of some of the previously described INGEMMET ground failures were systematically measured and calculated, resulting in amended volumes in 25 cases.

The final combined inventory was created by mapping each of the ground failures from all 3 datasets in ESRI's ArcMap program, in order to determine which points were unique, and which were redundant. In some cases points were also viewed in Google Earth. The final inventory consisted of 290 ground failures, 254 of which were considered landslides (were associated with rock or soil volumes.)

Geologic and Geomorphic Setting

The area in which the earthquake-induced landslides occurred stretches from Lima on the central west coast of Peru, south 230 km to Nazca, and east 160 km to the ridge of the Andes. It consists of a relatively flat coastal plain to the west, and the mountainous Andes to the east. West of the Andes on the coastal plain, the geomorphology is characterized by cut-and-fill terraces, and Quaternary fluvial and alluvial fan deposits up to several tens of meters thick. Hillslopes here are less than 30°. The Andes themselves consist of Cretaceous and Tertiary volcanics and some pre-uplift (Jurassic or older) sedimentary rocks, all underlain by Mesozoic to Cenozoic intrusives (Steffen et al., 2009).

Between the coastal plain and the Andes is an area of slope discontinuity called the knickzone; in this area, the hillslope angles are very steep—up to 60°, and the alluvial channels are deeply incised into the bedrock. The geology in this area is not significantly different from that of the main Andes; the geomorphology here has been interpreted to indicate headward erosion in response to uplift during the late Miocene (Steffen et al., 2009).

Understanding the tectonic setting of the study area is useful to provide context for the geology and geomorphology of this area, in particular, to explain the absence of volcanism in most of the Peruvian Andes in an otherwise active volcanic chain. About 250 million years ago during the late Jurassic, a rift began to form in the continent of Gondwana. The western and eastern halves of this continent were split apart into what are now South America and Africa. As new crust was created in the mid-Atlantic spreading center, the South American plate was pushed westward into the Nazca plate. The denser oceanic crust of the Nazca plate subducted beneath the less-dense continental crust of the western margin of the South American plate, at a rate that is currently estimated to be about 7-8 cm/year, compressing the western margin of the South American plate and creating the Andean orogeny (DeMets et al., 2007).

For most of the length of the Nazca plate, subduction occurs in a "typical" fashion whereby the subducting plate dips at relatively steep angle (greater than 30°) and is consumed by the Peru-Chile trench. In these areas, volcanism is present. However, between the latitudes of 5°S and 14°S, there is a 1500 km long stretch (which includes our study area and most of the Peruvian Andes) where subduction is relatively flat (dipping at an angle less than 30°) and volcanism is absent. See Figure 1. Here the Nazca ridge, a thicker section of oceanic crust, subducts beneath the South American plate. (Barazangi and Isaaks (1976), Jordan et al. (1983), Nur and Benavraham (1982), McGeary et al. (1985), and Pilger (1981). Interestingly, seismic energy released into the upper, overriding South American plate in this area of flat subduction is 3-5 times greater than in areas of "typical" subduction. This increase is attributed to viscous coupling between the two plates across a larger area of contact. Dewey and Lamb, (1992) suggest that 90% of the intraplate motion here is taken up by slip between the two plates, and 10% by thickening and shortening of the overlying crust.

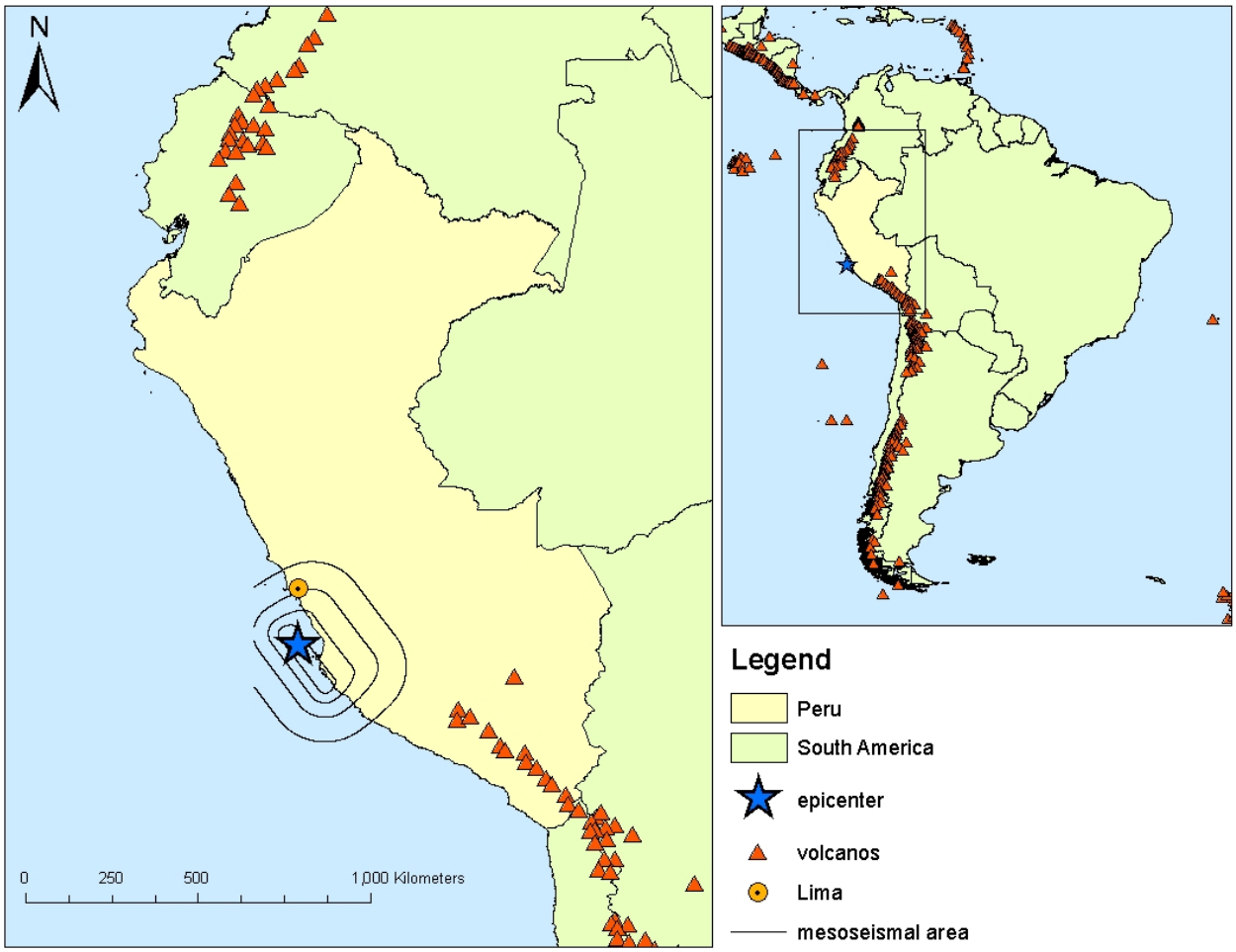

Figure 1. Gap in volcanism, seismic energy release 3-5 times greater in this area.

Climate and Moisture

The climate in the study area is very dry throughout most of the year, and most of the rivers are ephemeral (Casey, 2010; Steffen et al., 2009). Annual precipitation ranges from 700-800 mm/year in the Altiplano (high mountain plateau) region, to 30 mm/year in the knickzone, to almost zero on the coast. (Steffen et al., 2009). Precipitation is controlled by the positions of the sub-tropical jet stream and the Inter-Tropical Convergence Zone. During the Peruvian summer from December to February, when the sub-tropical jet stream is to the south, humidity from the tropical Amazon basin and the Atlantic is carried by easterlies to the high mountain areas. During the rest of the year when the subtropical jet stream is further north, there is a persistent, dry, westerly wind with almost no precipitation.

The study area encompasses 6 drainage basins which drain westward toward the Pacific Ocean (only one of which has a perennial river, the Rio Pisco) and one endorheitic drainage basin (a closed basin with no outflow) that drains to the east (Hearn et al., 2000).

Landslides

Types of Landslides

Landslides were classified using a modified version of the Keefer (1999) earthquake-induced landslide rubric. Not all subtypes were used, because information regarding the type of movement (e.g. rotational versus translational sliding) and amount of internal disruption was often not available— particularly for the INGEMMET and Zavala landslides. The 3 main categories of landslides were disrupted slides and falls, coherent landslides, and lateral spreads and flows.

Disrupted Slides and Falls

Disrupted slides and falls have high to very high internal disruption, consisting of numerous small blocks and individual soil grains and rock fragments. In cases of very high internal disruption there may be complete disaggregation into individual soil grains or rock fragments. **Rock falls** (Figure 2) are characterized by extremely rapid, bounding, rolling or free-fall motion. They occur at shallow (<3 m) depths, and are very abundant in earthquakes; they can occur in completely dry to saturated materials. **Debris/earth falls** (Figure 3) are identical in amount of internal disruption, speed, type of movement, depth, and water content, but are only moderately common. **Debris avalanches** (Figure 4) are distinguished from debris/earth falls by type of movement: rapid to extremely rapid translational sliding with subsidiary flow; Keefer (1994) considers them to be an abundant type of earthquake-induced landslide, however there are only 3 landslides of this type in our dataset.

Figure 2. Rockfall, mountains. Photo by Joseph Wartman, 8/23/2007.

Figure 3. Debris/earth fall, mountains. Photo by Joseph Wartman, 3/20/2010.

Figure 4. Debris/earth avalanche, Coastal Plains. Image from Google Earth.

Coherent Landslides

Both **rocks slumps** and **debris/earth slumps** (Figures 5 and 6) consist of one to several coherent blocks. Their motion is described as slow to rapid, deep (> 3 m) rotational sliding in materials that are moist to saturated. Keefer (1994) considers rock slumps to be moderately common, and soil slumps to be abundant.

Figure 5. Rock slump, Paracas. Photo by Joseph Wartman, 3/18/2010.

Figure 6. Debris/earth slump, mountains. Photo by Joseph Wartman, 3/20/2010.

Lateral Spreads and Flows

The motion of **lateral spreads and flows** (Figures 7 and 8) is very rapid translation upon a zone of liquefied or sensitive material which results in permanent deformation. Lateral spreads and flows occur in fully to partially saturated material, and can be either shallow or deep. Lateral spreads and flows are moderately common, according to Keefer (1999.)

Figure 7. Debris/earth lateral spreading, Coastal Plains. Photo by Joseph Wartman, 3/16/2010.

Figure 8. Debris/earth lateral spreading, mountains. Photo by Joseph Wartman, 3/20/2010.

Other Ground Failure Types

Also observed were cracks, settlement, and evidence of liquefaction (sand boils.) See Figures 9 and 10. None of these is associated with a rock or soil volume; these types of ground failures are not considered to be landslides.

Figure 9. Cracking, Paracas. Photo by Joseph Wartman, 3/18/2010.

Figure 10. Sand boil. Photo by Joseph Wartman, 8/26/2007.

Landsliding Parameters

Parameters investigated related to earthquake-induced landsliding were peak ground acceleration (PGA) and earthquake intensity, surface geology, ecological region, slope, slope aspect, moisture, and the presence of roads/roadcuts.

Peak Ground Acceleration

The McVerry ground motion attenuation relationship was selected to describe peak ground acceleration (PGA) based on the work of Tavera et al. (2008.)

Tavera et al. (2008) investigated predictive capability of 5 attenuation relationships developed for interface subduction earthquakes:

- Atkinson and Boore (2003) developed using worldwide data
- Kanno et al. (2006) developed using data from Japan
- Zhao et al. (2006b) developed using data from Japan
- McVerry et al. (2006) developed using data from New Zealand
- Ruiz and Saragoni (2005) developed using data from Chile

See Appendix B for information regarding the characteristics of each of the equations, as well as graphs comparing the predicted values to the observed values.

Using the Scherbaum et al. (2004) classification method, Tavera et al. (2008) assigned ratings to each of the attenuation relationships for peak ground acceleration (PGA) and 5% spectral analysis ($SA_{5\%}$) at 7 different periods. See Table 1. (Note: the Ruiz and Saragoni (2005) attenuation relationship is not included in the evaluation—possibly because it predicts PGA only.)

Table 1. A) Comparison of observed ground motions with predictions from selected equations, adapted from Tavera et al. (2008.) B) Classification rubric.

A

	Atkinson and Boore (2003)	McVerry et al. (2006)	Kanno et al. (2006)	Zhao et al. (2006b)
PGA	unacceptable	high	low	low
$SA_{5\%}$ at 0.05 s	unacceptable	-	intermediate	intermediate
$SA_{5\%}$ at 0.10 s	unacceptable	low	intermediate	intermediate
$SA_{5\%}$ at 0.20 s	unacceptable	intermediate	intermediate	low
$SA_{5\%}$ at 0.40 s	unacceptable	unacceptable	low	unacceptable
$SA_{5\%}$ at 1.00 s	unacceptable	unacceptable	unacceptable	unacceptable
$SA_{5\%}$ at 2.00 s	unacceptable	low	unacceptable	unacceptable
$SA_{5\%}$ at 3.00 s	unacceptable	low	unacceptable	unacceptable

B

	mean normalized residual	median normalized residual	st. deviation of normalized residual	median likelihood
high	< 0.25	< 0.25	< 1.125	> 0.4
intermediate	< .050	< .050	< 1.250	> 0.3
low	< 0.75	< 0.75	< 1.50	> 0.2
unacceptable	all other combinations of parameters			

The McVerry relationship was determined to be the overall best fit, and is used to predict PGA for ground failure sites described later in this paper.

Implementation of McVerry Attenuation Relationship

Peak ground acceleration (PGA) was calculated using the following equations and parameters from the McVerry (2006) subduction zone model:

$$PGA_{A/B} = SA_{A/B}(T=0) \qquad \text{McVerry et al. (2006) equation (5)}$$

Where

$$\begin{aligned} \ln SA_{A/B}(T) = {} & C_{11}(T) + (C_{12Y} + (C_{15}(T) \\ & - C_{17}(T))C_{19Y})(M-6) \\ & + C_{13Y}(T)(10-M)^3 \\ & + C_{17}(T)\ln(r+C_{18Y}\exp(C_{19Y}M)) \\ & + C_{28}(T)H_C + C_{24}(T=0)SI \\ & + C_{46}(T)r_{VOL}(1-DS) \end{aligned} \qquad \text{McVerry et al. (2006) equation (2)}$$

Details of the McVerry equations, as well as tables of the coefficients used can be found in Appendix C. A/B refers to the New Zealand site class categories, “strong rock” and “rock,” which are nominally equivalent to National Earthquake Hazards Reduction Program (NEHRP) site classes A and B, however they are defined slightly differently—see also Appendix C. Note that the unprimed versions of the equations and coefficients were used. (Unprimed coefficients are for the geometric mean of the acceleration response components; primed are for the stronger horizontal components.)

Parameters used in the equations were:

Moment magnitude	M = 7.9
Shortest distance in km from site to source	r = varies, depending on location
Centroid depth in km	H_C = 18
Interface earthquakes, <50 km depth	SI = 1
Length of path in volcanic zone	r_{VOL} = 0
Deep slab earthquakes, >50 km depth	DS = 0
Coefficients of the attenuation model	$C_i(T)$ = varies, from table

MATLAB code implementation of the the McVerry ground motion attenuation relationship, as well as the calculation of site-to-source distance, r, can be found in Appendix E. PGA values were calculated for 1061 points on a square grid spaced 0.05 degrees apart. Point values were then imported into ESRI’s ArcMap program to create PGA contours in units of g. See Figure 11.

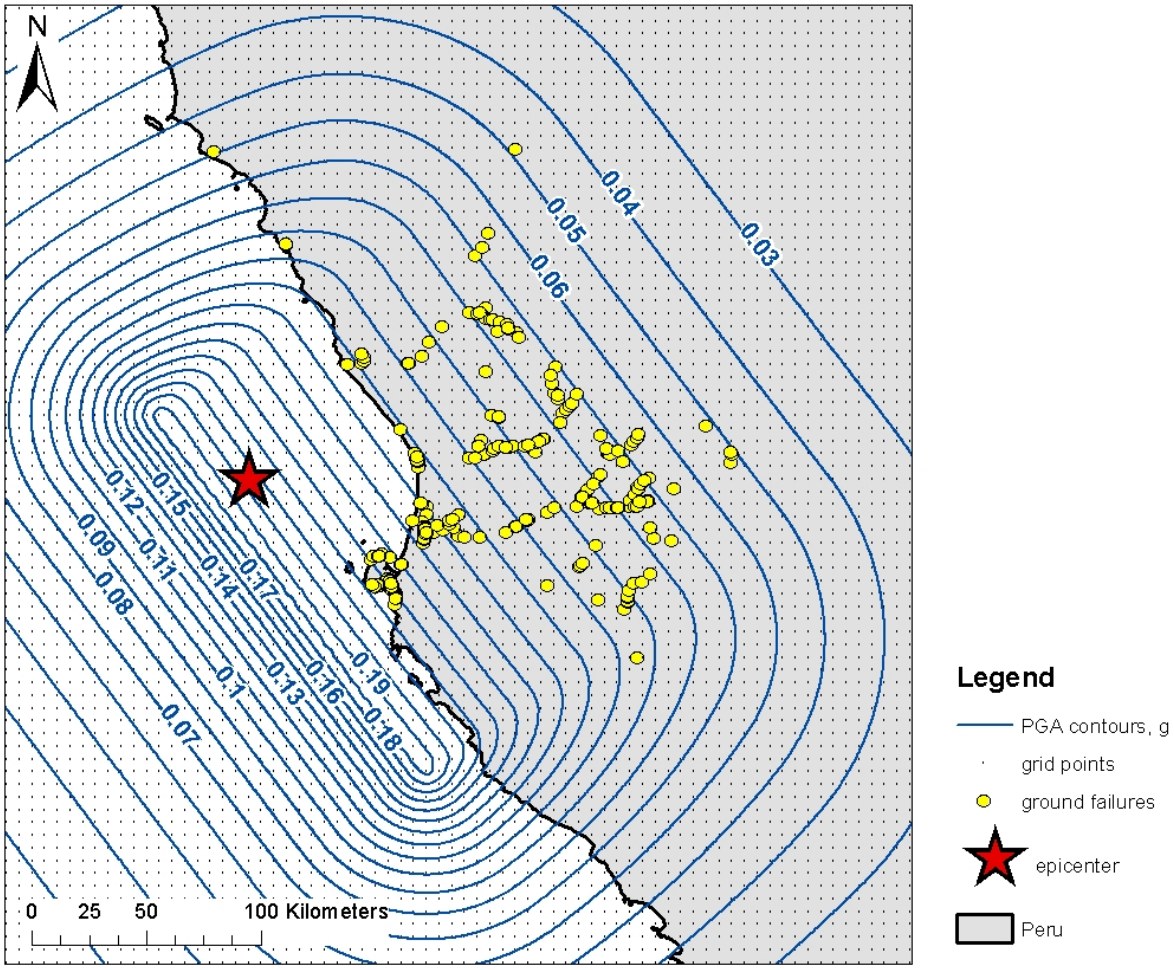

Figure 11. McVerry peak ground acceleration contours.

These PGA values correspond to a period of T=0. They do not take into account effects of local site conditions, specifically amplification due to soils. See Figure 12 for a comparison of the McVerry contours with accelerograph station PGA values.

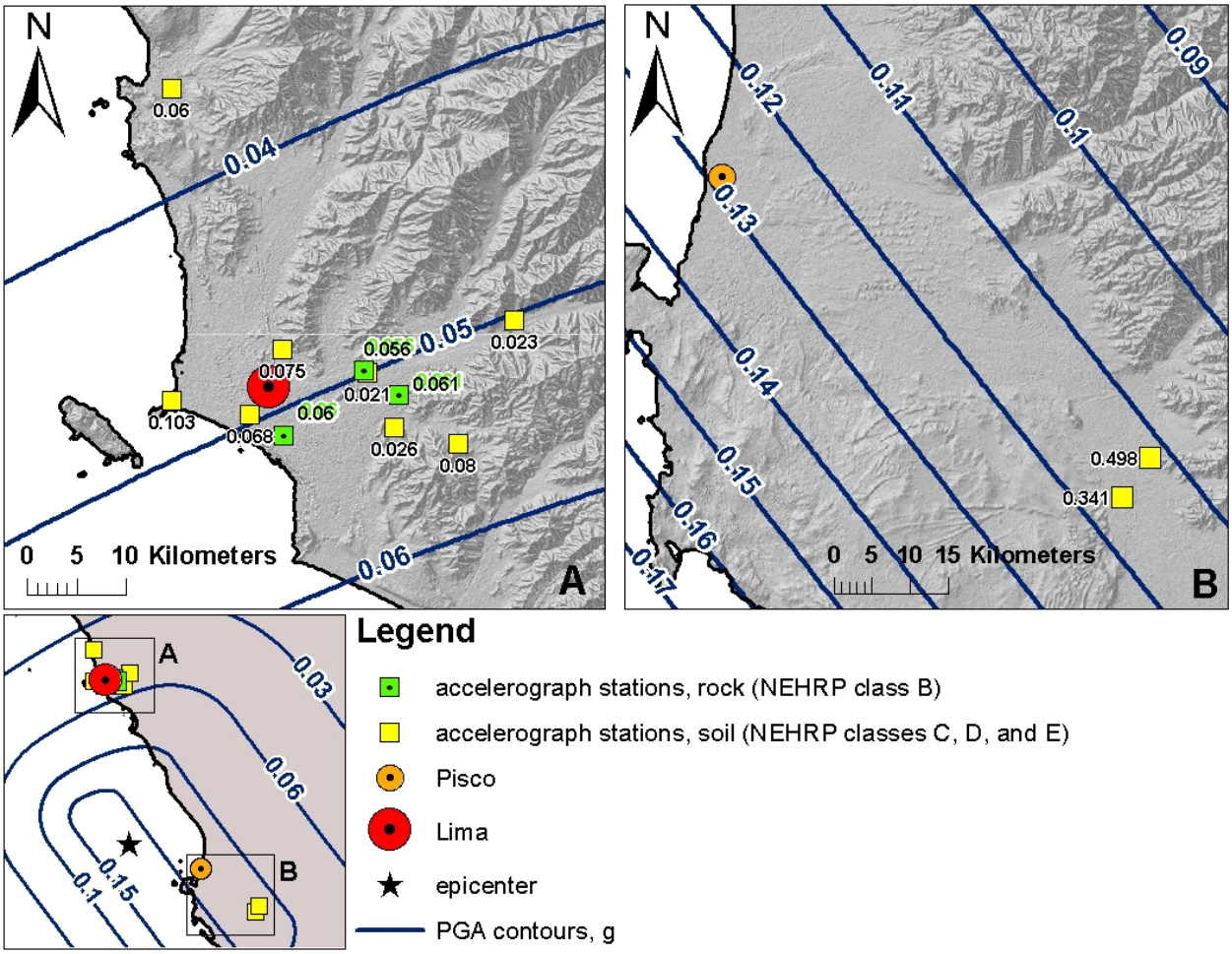

Figure 12. PGA contours calculated using McVerry compared to A) North accelerograph station PGA values, and B) South accelerograph station PGA values.

For rock sites (158 out of 254 ground failures) the McVerry contours are a reasonably good predictor of PGA. For soil sites, actual PGAs will be larger than predicted by the McVerry attenuation relationship. In general, landslide density (number of landslides per square kilometer) and volume of landsliding material decrease as PGA decreases (Figures 13 and 14) however two factors, slope and moisture, can have a controlling effect locally. This will be examined in further detail later in this paper.

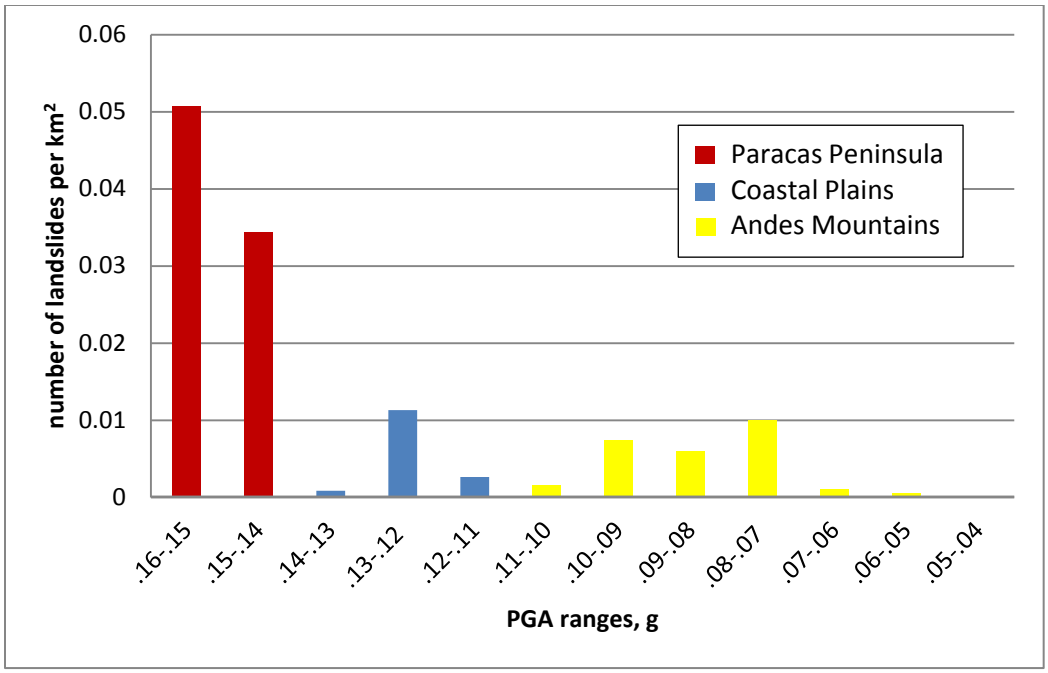

Figure 13. Number of landslides normalized by area.

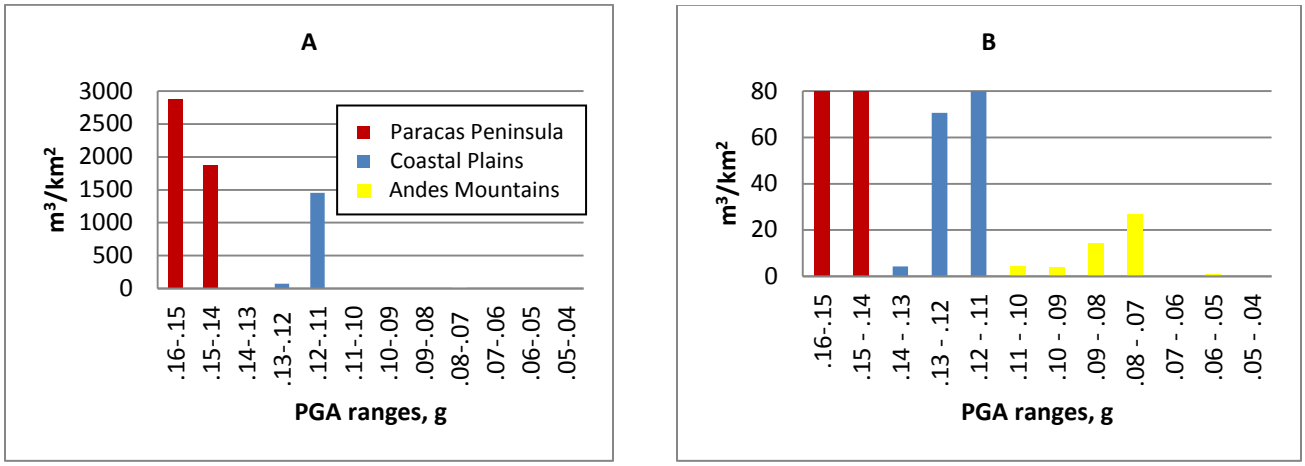

Figure 14. A) Landslide volumes normalized by area; B) vertical axis expanded to show Andes Mountains region.

Modified Mercalli Intensity (MMI) Scale

An alternative method of presenting ground shaking intensity is the MMI (Modified Mercalli Intensity) scale. MMI contours (Tavera et al., 2008) were produced by surveying earthquake damage, primarily to structures. [2] See Figure 15 for a comparison of MMI contours with accelerograph PGA values. Table 2 shows PGA equivalents to MMI values, using the Wald et al. (1999) relationship:

$$MMI = 3.66*\log(PGA) - 1.66$$

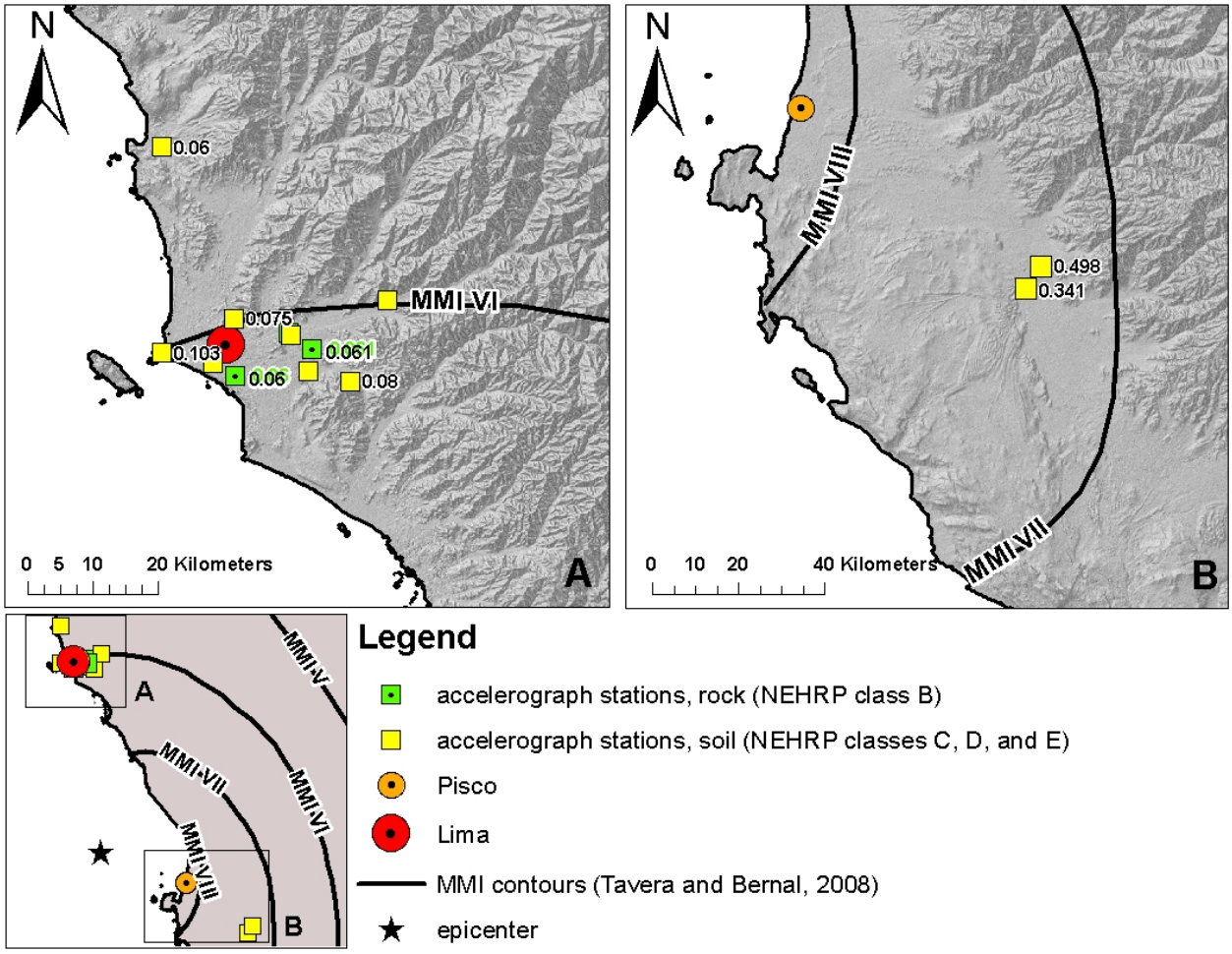

Figure 15. MMI intensities compared to accelerograph stations. PGA for stations in g.

[2] Many buildings in Pisco and the surrounding area were constructed with adobe or unreinforced concrete, and were severely damaged during the earthquake. Because the MMI scale is calibrated to structures typically found in in more developed countries, the large amount of damage assessed could lead to higher MMI values than would otherwise be assigned for the same amount of ground shaking elsewhere.

Table 2. Wald et al. (1999) empirical relationship between PGA and MMI.

MMI	III	IV	V	VI	VII	VIII
PGA (g)	0.02	0.04	0.07	0.13	0.24	0.44

MMI values are a better fit for soil sites than for rock sites.

Medvedev Sponheuer Karnik (MSK) Intensity Scale

Also evaluated was the MSK earthquake intensity, an earthquake intensity scale developed in Eastern Europe, which is similar to the MMI scale. Contours were created in ArcMap, using the latitude, longitude, and MSK intensity values from 54 towns, as reported in Astroza (2007.) See Figure 16.

Table 3 shows the conversion between PGA and MSK intensity values; conversion is from Mohindra et al. (2012.)

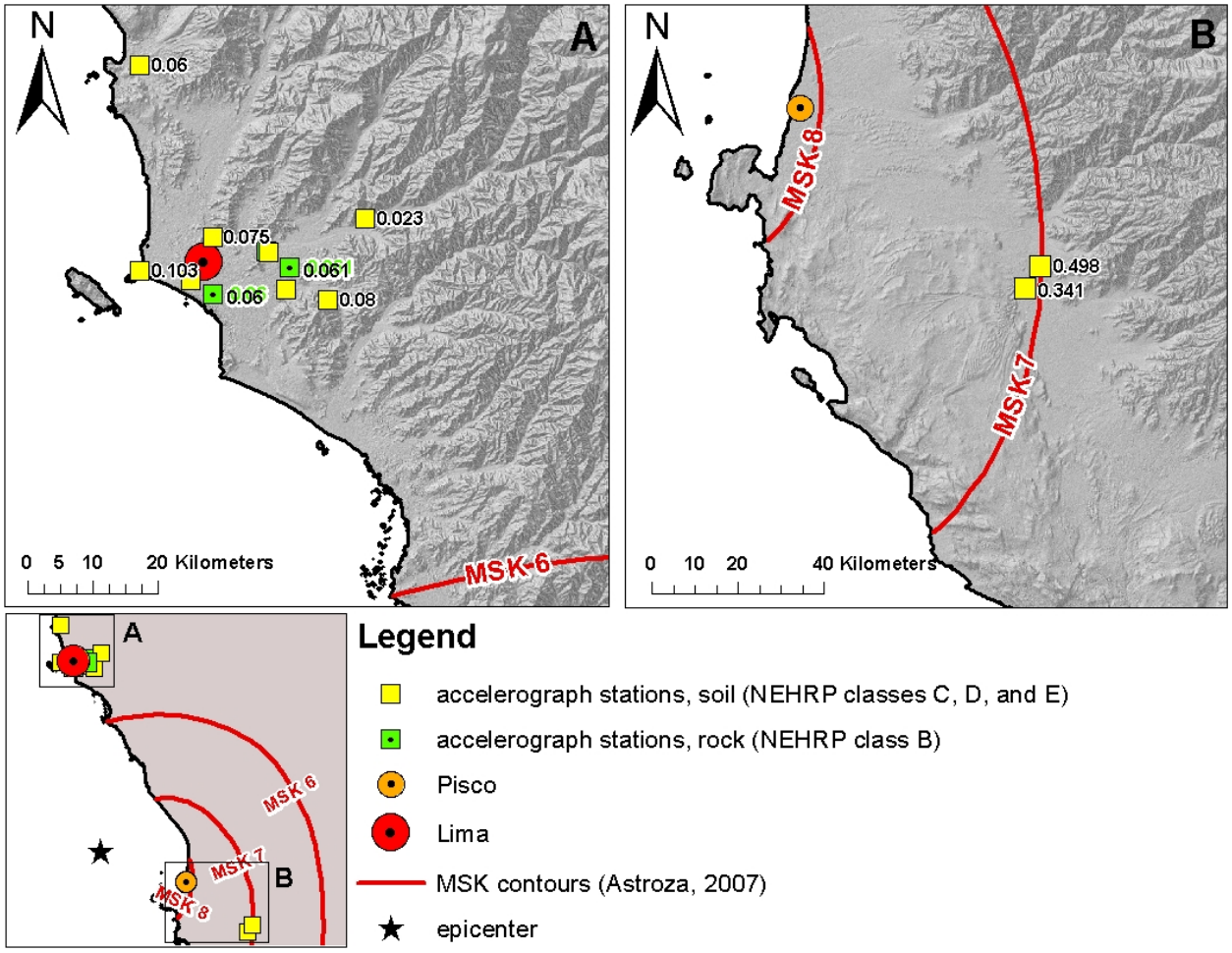

Figure 16. MSK intensities compared to accelerograph stations. PGA for stations in g.

Table 3. Mohindra et al. (2012) PGA-MSK intensity conversion table.

MSK	4	5	6	7	8	9	10	11	12
PGA (g)	0.03	0.05	0.09	0.18	0.32	0.53	0.82	1.20	1.60

The values in Table 3 were taken directly from Mohindra et al. (2012.) A regression performed in Excel returned the following mathematical relationship:

$$PGA = 1.9187 \ln(MSK) + 10.542$$

With $R^2 = 0.988$.

Like MMI values, MSK values are a better fit for soil sites than for rock sites.

Comparison of McVerry, MMI, and MSK PGA Predictions

For rock sites, the difference between the predicted PGA values and the measured PGA values is smallest for the McVerry attenuation relationship. For soil sites, MSK values are a slightly better fit. See Figure and 17 Table 4. PGA values were derived by interpolating MMI or MSK values from the contours, and converting them to PGA with the appropriate mathematical relationship.

Throughout the rest of this text, McVerry PGA values will be used for two main reasons: the McVerry PGA values for soil are quite close to the MSK values, and data for the MSK contours does not extend to contours lower than MSK=6 and therefore cannot be used in the Andes Mountains region.

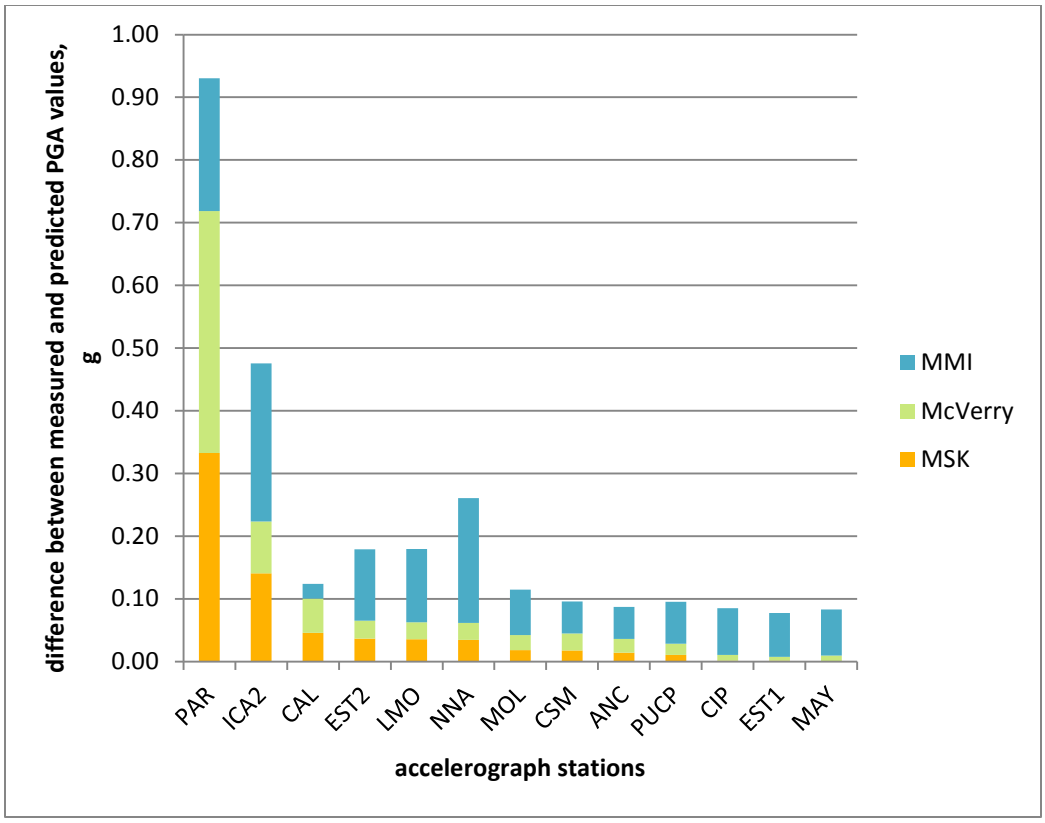

Figure 17. Comparison of PGA predictions with accelerograph station measurements.

Table 4. Comparison of McVerry, MMI, and MSK predictive values.

station	PGA from accelerograph	PGA from McVerry attenuation relationship	difference between accelerograph and McVerry	PGA from MMI contours	difference between accelerograph and MMI	PGA from MSK contours	difference between accelerograph and MSK	NEHRP site class	NEHRP site description
EST2	0.021	0.112	0.386	0.286	**0.212**	0.166	0.332	-	unknown
LMO	0.026	0.117	**0.083**	0.286	0.252	0.175	0.141	-	unknown
NNA	0.023	0.048	0.055	0.126	**0.023**	0.057	0.046	-	unknown
CIP	0.060	0.050	**0.029**	0.134	0.113	0.057	0.036	B	rock
EST1	0.056	0.053	**0.027**	0.143	0.117	0.062	0.036	B	rock
MAY	0.061	0.050	**0.027**	0.222	0.199	0.057	0.034	B	rock
ANC	0.080	0.056	0.024	0.152	0.072	0.062	**0.018**	C	very dense soil/soft rock
MOL	0.080	0.048	0.027	0.126	0.051	0.057	**0.018**	C	very dense soil/soft rock
PUCP	0.068	0.038	0.022	0.111	0.051	0.046	**0.014**	C	very dense soil/soft rock
CSM	0.075	0.050	0.018	0.134	0.066	0.057	**0.011**	C,D	stiff to very dense soil
ICA2	0.034	0.051	0.009	0.134	0.074	0.062	**0.002**	C,D	stiff to very dense soil
PAR	0.498	0.050	0.006	0.126	0.070	0.057	**0.001**	C,D	stiff to very dense soil
CAL	0.103	0.052	0.009	0.134	0.073	0.062	**0.001**	E	soft soil

Values in bold indicate best fit for intensity measure/attenuation relationship and accelerograph PGAs.

Geology

The geologic maps used in this report were created by the Instituto Geológico Minero y Metalúrgico (INGEMMET) of Peru, and downloaded as .kml files from OneGeology.org. The maps, including brief unit descriptions, can be found in Appendix D. Figure 18 shows locations of landslides on the geologic map.

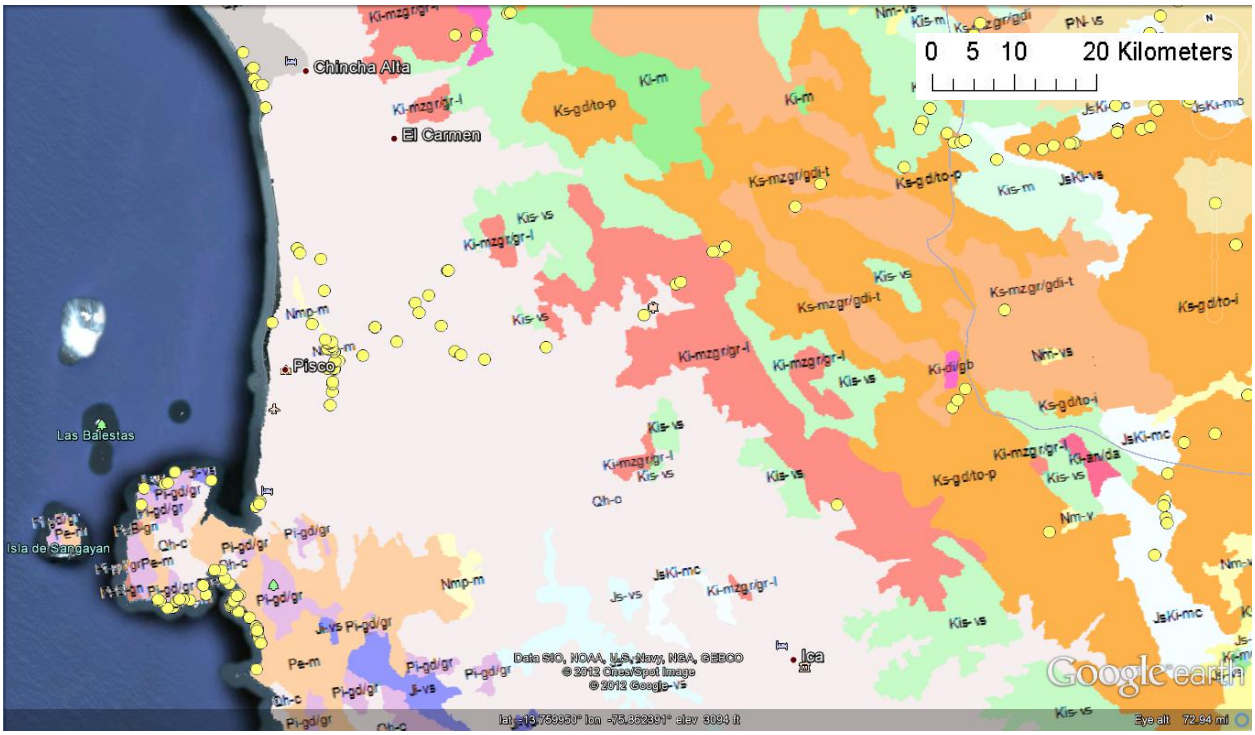

Figure 18. Geologic map of study area. Unit descriptions can be found in Appendix D. Yellow circles are ground failures.

Geology is clearly a factor in landsliding susceptibility for the Paracas Peninsula and Coastal Plains regions, and will be explained in further detail, later in the sections that describe these regions. In the Andes Mountains region, sedimentary rock units appear to be more susceptible to landsliding; however other factors such as slope and the presence of soils appear to contribute more to landsliding susceptibility than geologic unit.

Ecological Regions

Shapefiles for ecological region data come from a USGS database of Central and South America (Hearn et al., 2000.) Ground failures were mapped on top of ecological regions in an attempt to discern a relationship; see Figure 19. It appears that the extent of ground failures ends at the boundary between the Sechura desert (desert and xeric shrublands) and the Central Andean wet puna (montane grasslands.) It is possible that increases in moisture or vegetation reduce the landsliding susceptibility. This idea will be further explored later in this paper when landslides are mapped relative to rainfall contours.

It should be noted, however, that it is also possible that landsliding is not controlled by ecological region, but instead both landsliding and ecological region are functions of another factor such as slope. At the boundary between the Sechura desert and the Central Andean wet puna there is a distinct reduction in slope steepness. See Figure 20.

In addition, ecological region boundaries parallel PGA attenuation contours—it may be that landsliding ends simply because the ground shaking has diminished below a triggering threshold.

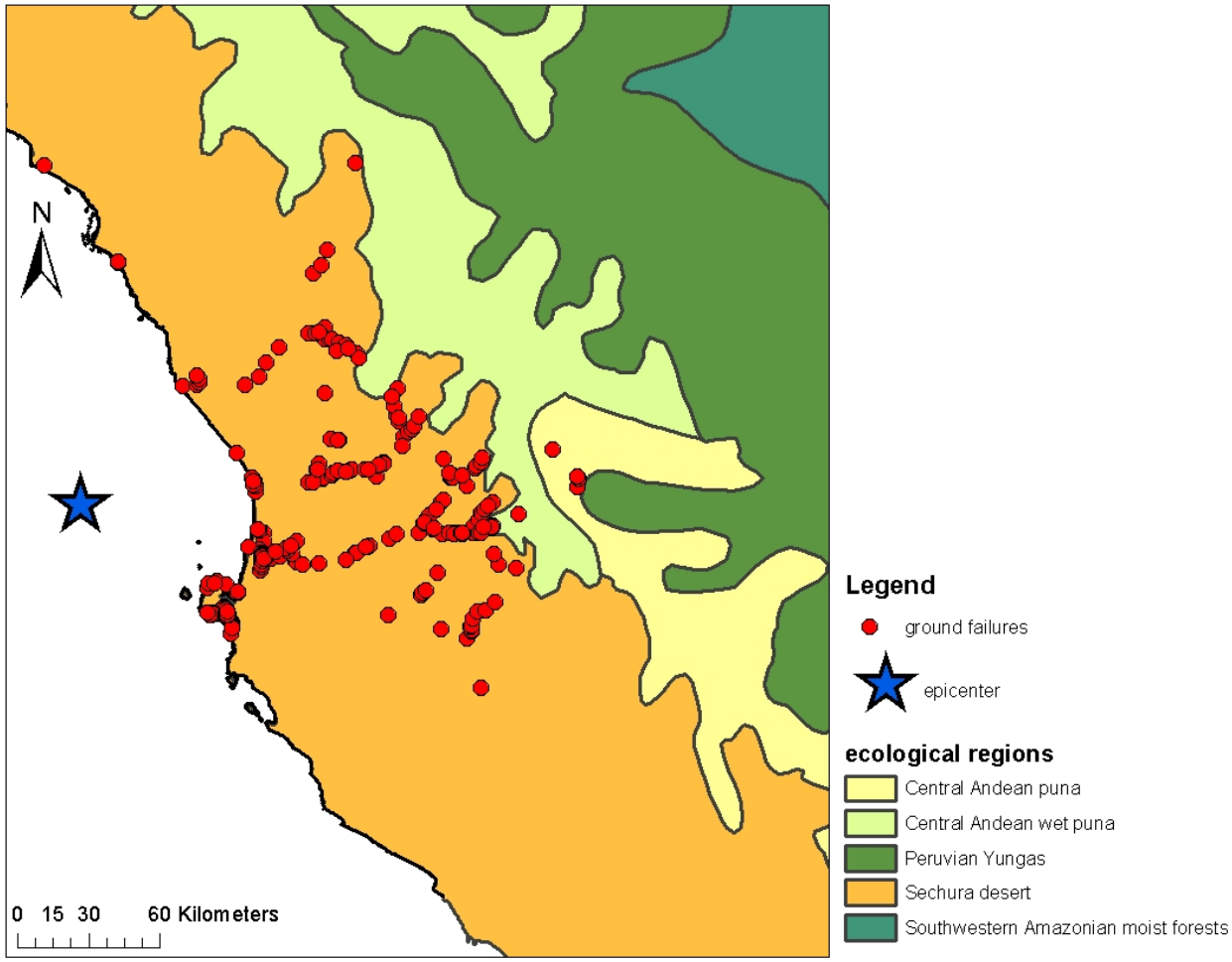

Figure 19. Ground failures relative to ecological region.

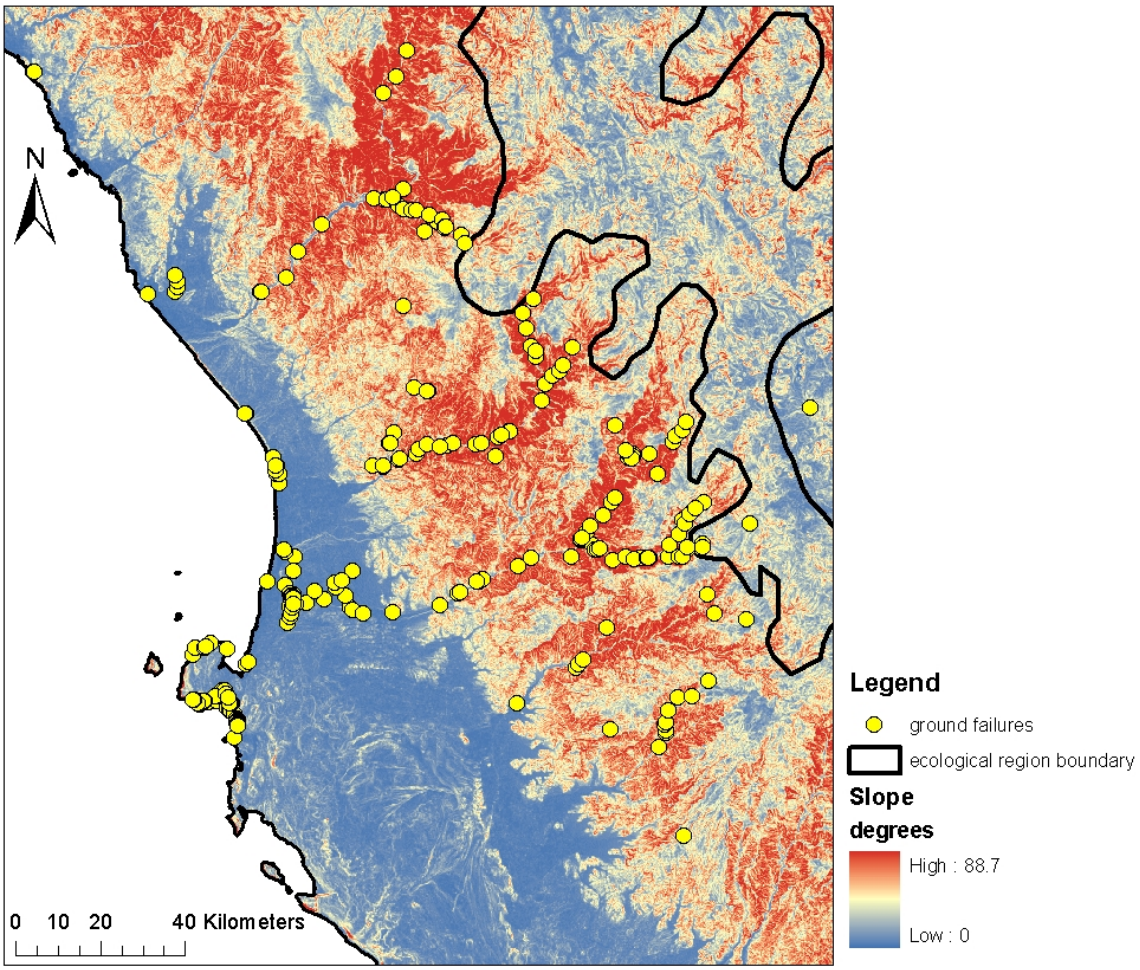

Figure 20. Ecological region boundary coincides with distinct decrease in slope.

Slope

Slope was calculated using a built-in analysis tool in ArcMap from 30-m resolution ASTER (Advanced Spaceborne Thermal Emission and Reflection Radiometer) data, which was downloaded from the ERSDAC (Earth Remote Sensing Data Analysis Center) website (NASA, 2011.)

The algorithm used to calculate slope comes from Burrough and McDonell (1998):

a	b	c
d	e	f
g	h	i

Figure 21. 3x3 grid of cells for calculation of slope at cell e. Cellsize is 30 m for Pisco region data.

slope (degrees) = $\tan^{-1}((\ [dz/dx]^2 + [dy/dx]^2\ )^{½}\ )\ * 180/\pi$

where dz/dx is the rate of change in the x direction:

$$dz/dx = ((c + 2f + i) – (a + 2d + g)) / (8 * \text{cellsize})$$

and dz/dy is the rate of change in the y direction:

$$dz/dy = ((g + 2h + i) – (a + 2b + c)) / (8 * \text{cellsize})$$

Slope is clearly a major contributing factor for landsliding. Most of the landslides with the largest volumes occur on the near-vertical slopes of the Paracas Peninsula sea cliffs, although the largest and most notable landslide, at 2.7×10^6 m^3 (a lateral spread at the base of the Canchamana formation) occurred in relatively flat area. In the mountains, landslides are clustered linearly along the steep-sided river valleys and are absent where the slopes are more moderate. See Figure 22.

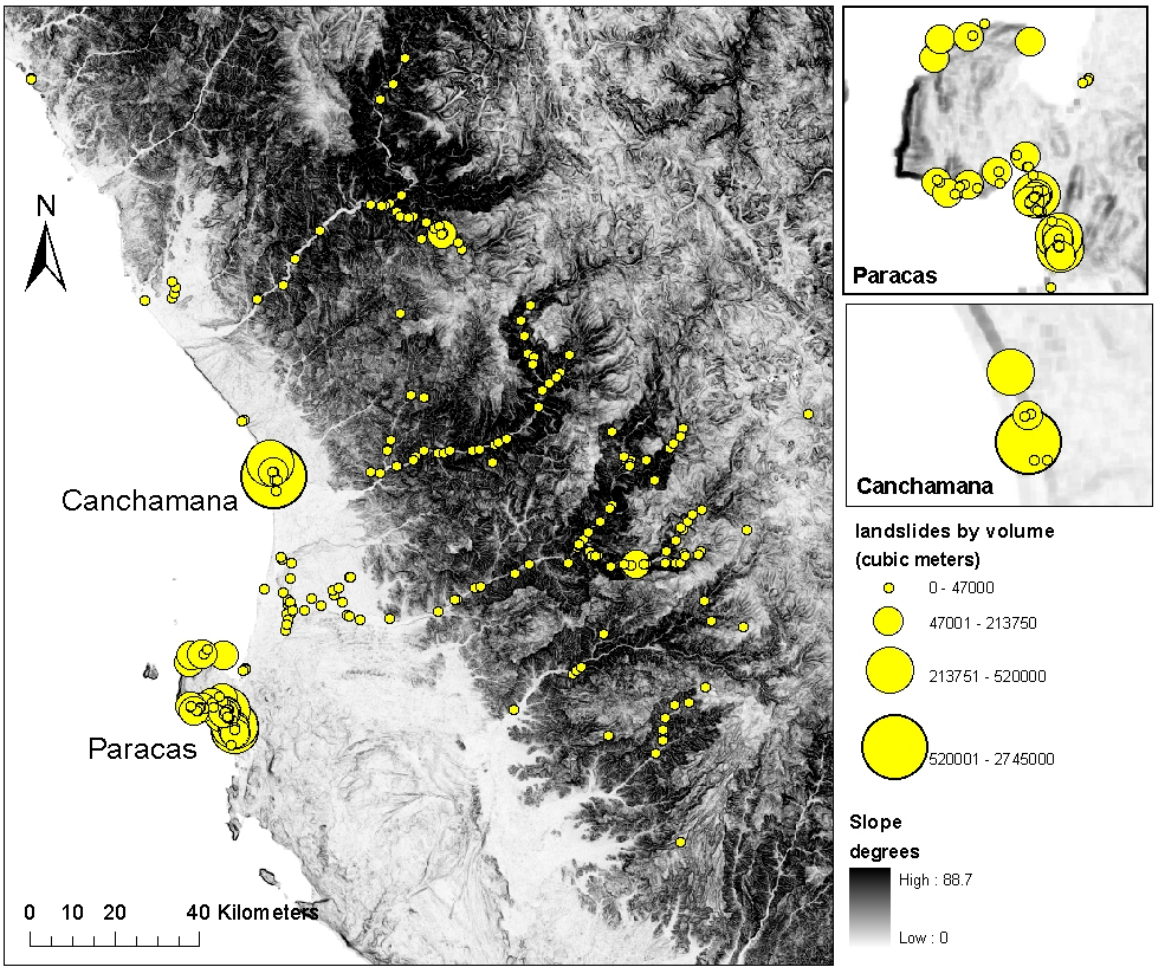

Figure 22. Landslide volumes relative to slope.

Figure 23 shows ground failure type relative to slope. Unsurprisingly, lateral spreads, liquefaction, and cracks/settlement are more likely to be found in flatter areas, while falls and slumps (disrupted and coherent landslides) are found on steeper slopes.

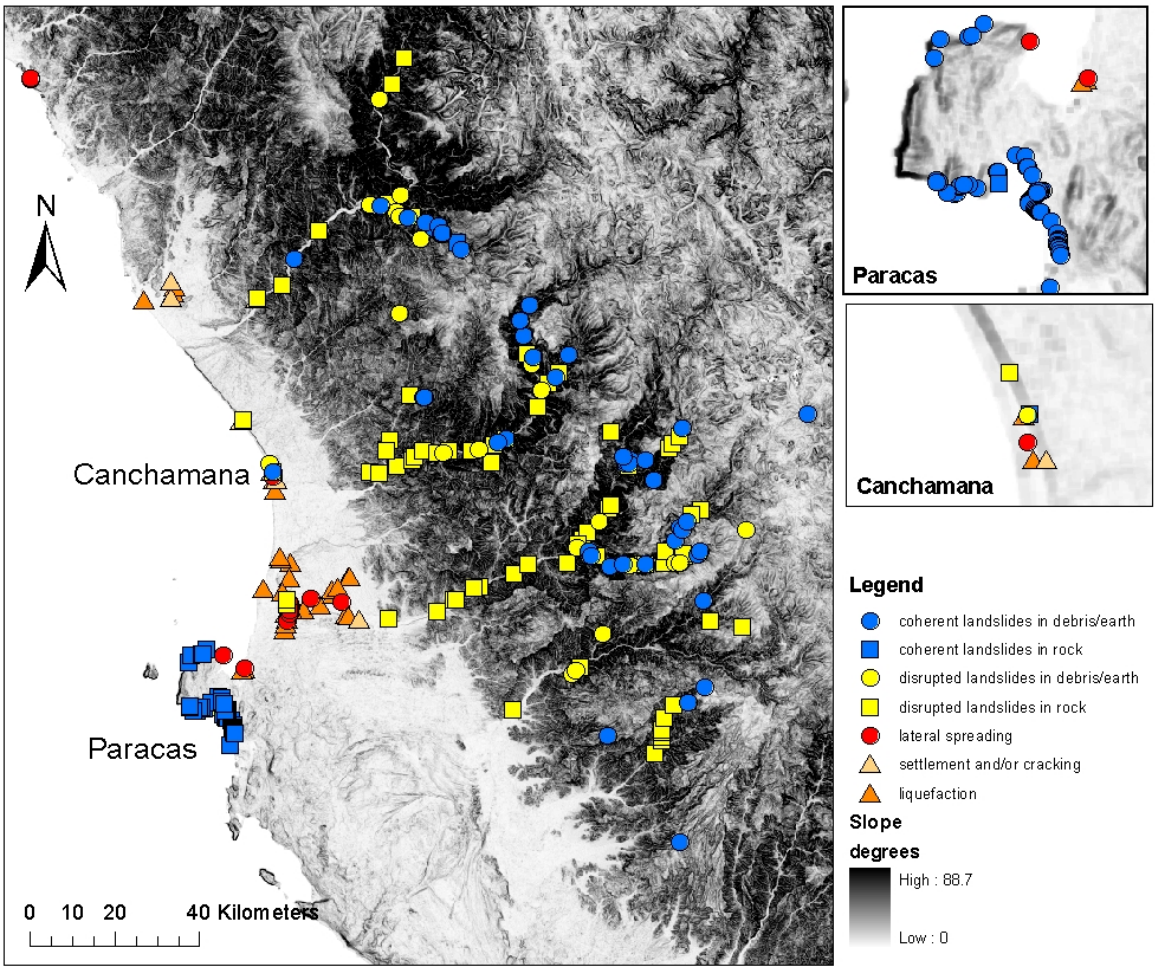

Figure 23. Landslide type relative to slope.

Slope Aspect

Landslides are more likely to form on slopes facing NNW or SE, which is approximately perpendicular to both the PGA contours and the trend of the secondary tributaries. See Figure 24. There is a smaller group of landslides oriented at 90° to the main group, facing ENE or WSW, which is perpendicular to the trend of the primary tributaries. It is interesting to speculate that secondary tributaries (which are often dry) accumulate more landslide-susceptible material.

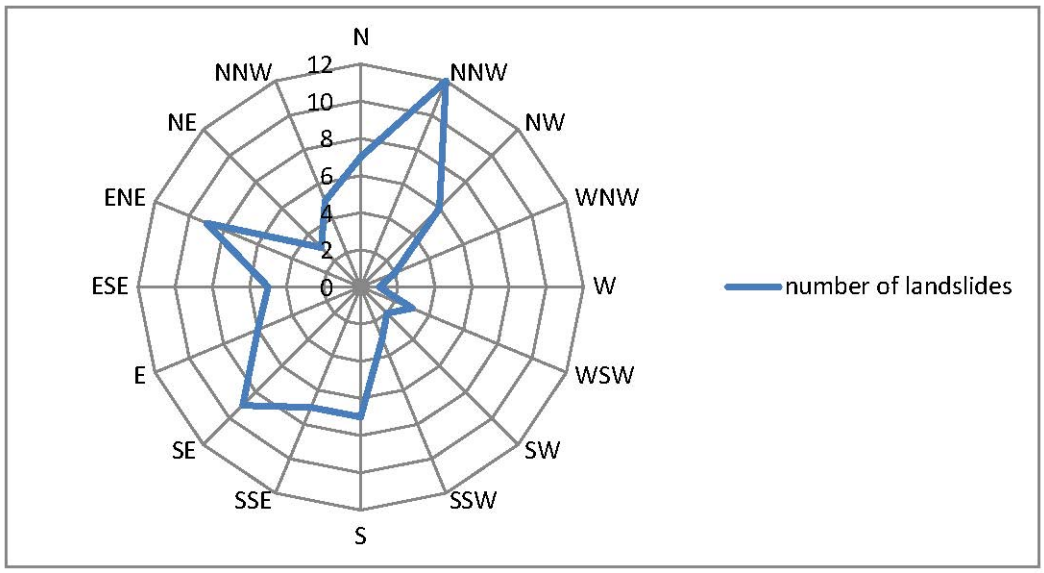

Figure 24. Number of landslides relative to slope aspect.

Moisture

Rainfall

Precipitation contours were created from data downloaded from Agrotechnologica Amazonica (Cochrane, 2010.) It appears that as rainfall levels increase, coherent landslides in soil also increase, and disrupted landslides in rock decrease. See Figure 25. This possible relationship is confounded by the fact that as rainfall increases, PGA decreases; so it is also possible that diminishing PGA is fully or partially responsible for the decrease in disrupted landslides/increase in coherent landslides.

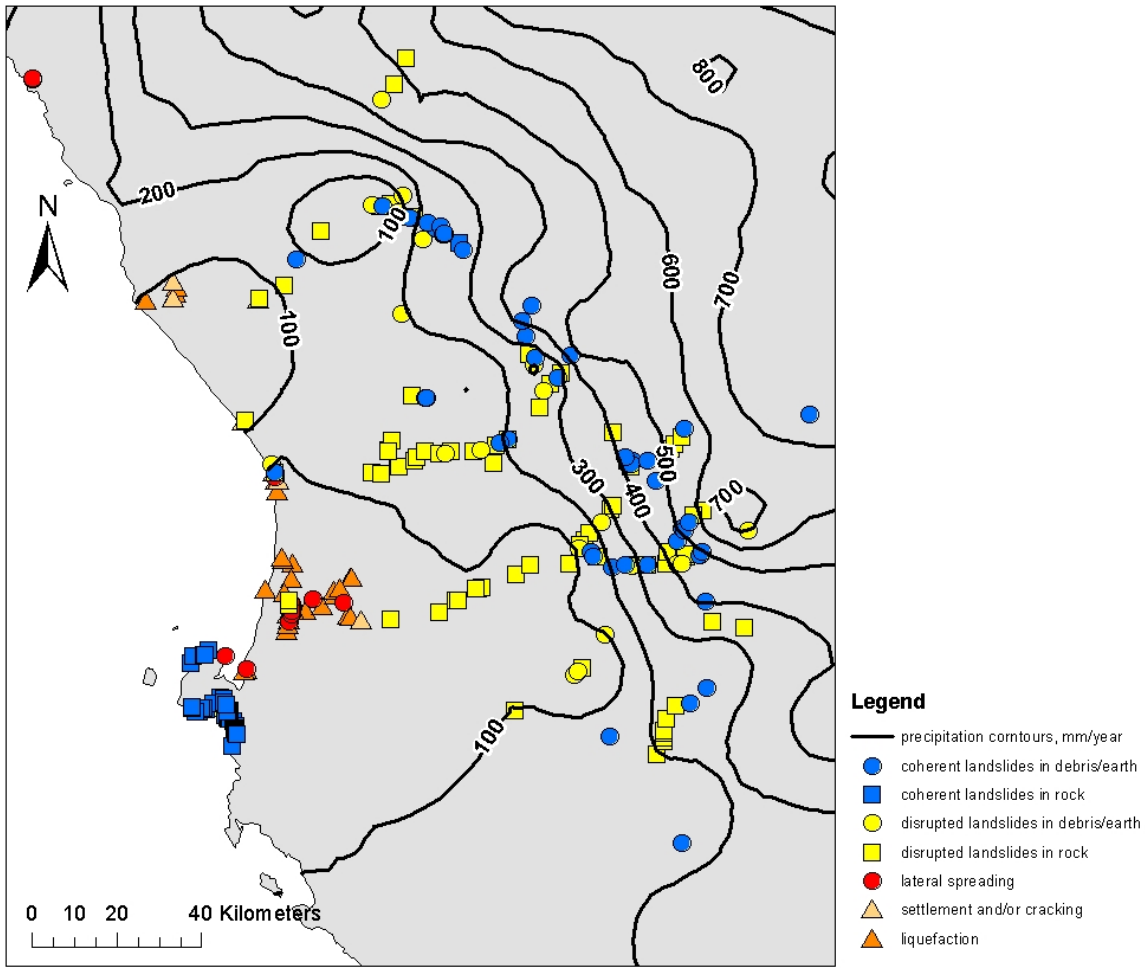

Figure 25. Ground failure type relative to amount of yearly precipitation.

Rivers and Drainage Basins

Data for rivers and drainage basins come from a USGS database of Central and South America (Hearn et al., 2000.) Figure 26 shows landslides clustering linearly along drainages, which is unsurprising since slopes are steepest in these areas. Landslide density appears to be greater along perennial rivers than ephemeral rivers. The Rio San Juan may be misidentified as an ephemeral river, since by inspection in Google Earth, it appears to be flowing in July (the dry season.) Additionally, significant agricultural activity can be seen in the Rio San Juan delta.

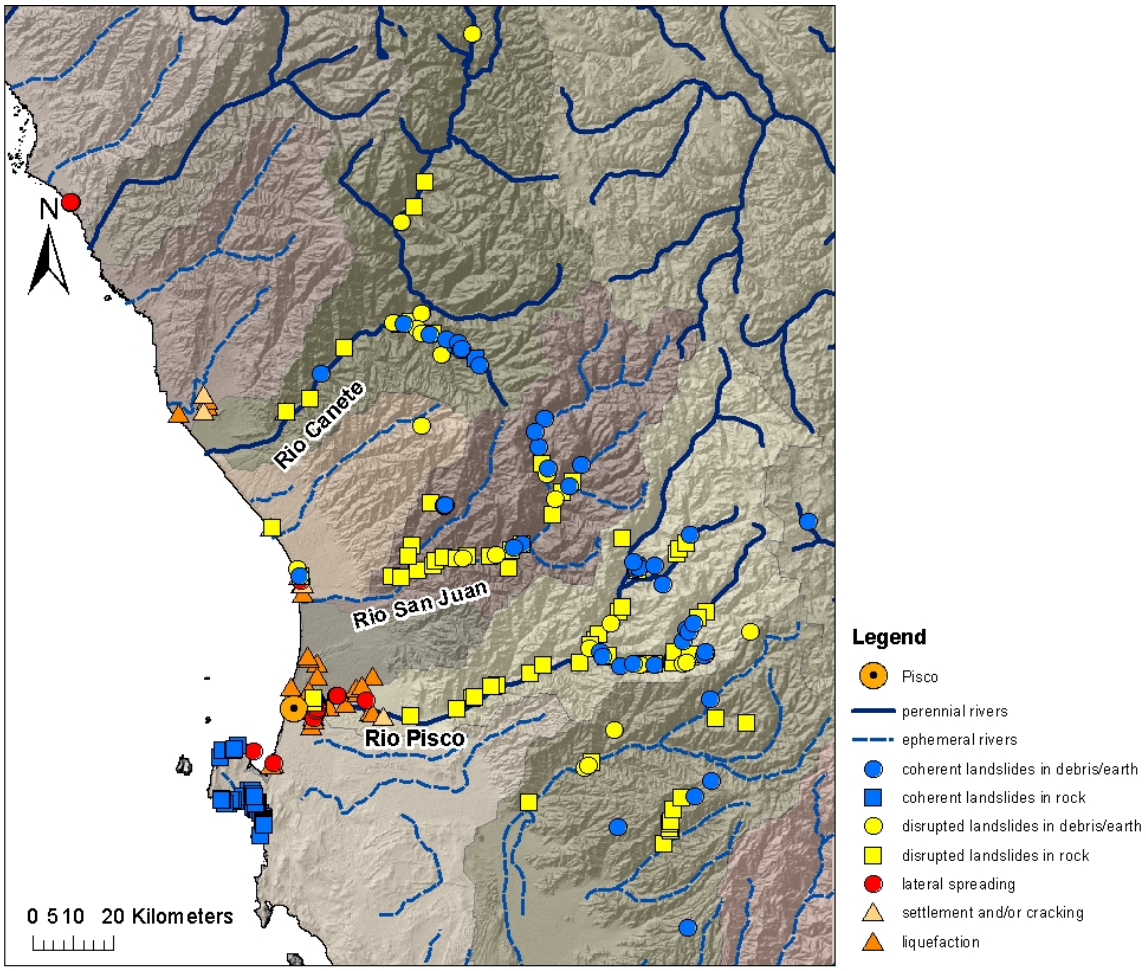

Figure 26. Ground failures relative to rivers; shaded areas are drainage basins.

Roads and Roadcuts.

In the Coastal Plains region, lateral spreads and settlement/cracking are more likely to be associated with roads. Disrupted landslides are more likely to be associated with roads/roadcuts in the Andes Mountains region. (No landslides in Paracas are associated with roads.) Figure 27 shows the locations of landslides in relation to roads; those landslides directly associated with roads or which blocked roads are marked. The same pattern of linear clustering of landslides can be observed with roads as with rivers, in part because many (but not all) roads are aligned with rivers.

Toward the far extent of the landslide distribution, the influence of roads and roadcuts diminishes. The slopes become shallower, and annual rainfall increases. Landslides (debris/earth slumps) are more likely to be found located along the river banks and in farmed areas than along roads.

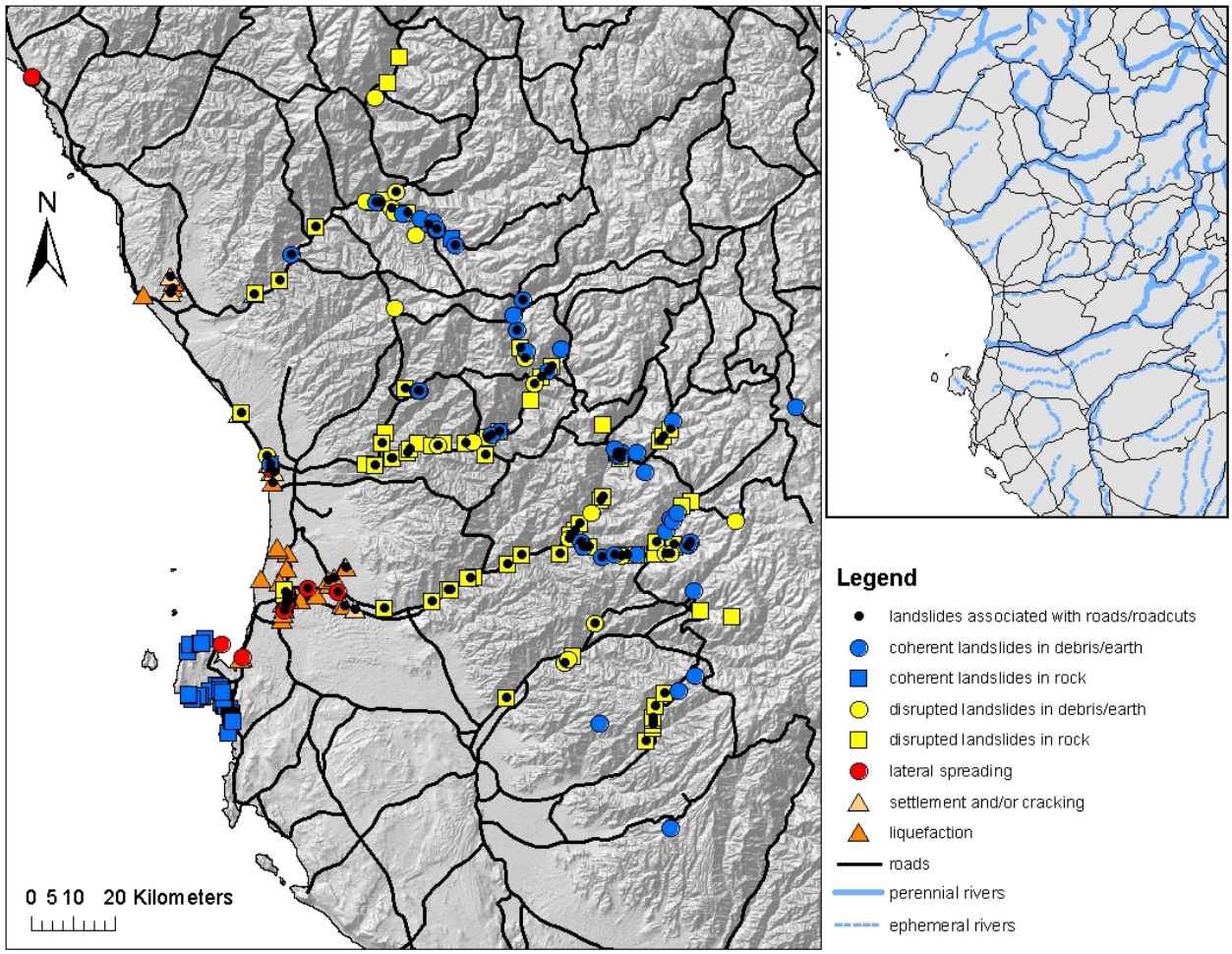

Figure 27. Ground failures relative to roads. Inset shows alignment of roads with rivers.

Three Main Landsliding Settings

Landsliding triggered by the Pisco earthquake occurred in the three distinct geomorphic-geologic settings: the Paracas Peninsula sea cliffs, the Coastal Plains, and the Andes Mountains. See Figure 28. Each geomorphic setting displays a typical or predominant style of ground failure: rock slumps in Paracas, liquefaction/lateral spreading in the Coastal Plains, and disrupted landslides in the Andes. Factors which are most influential for each setting will be described in the following sections.

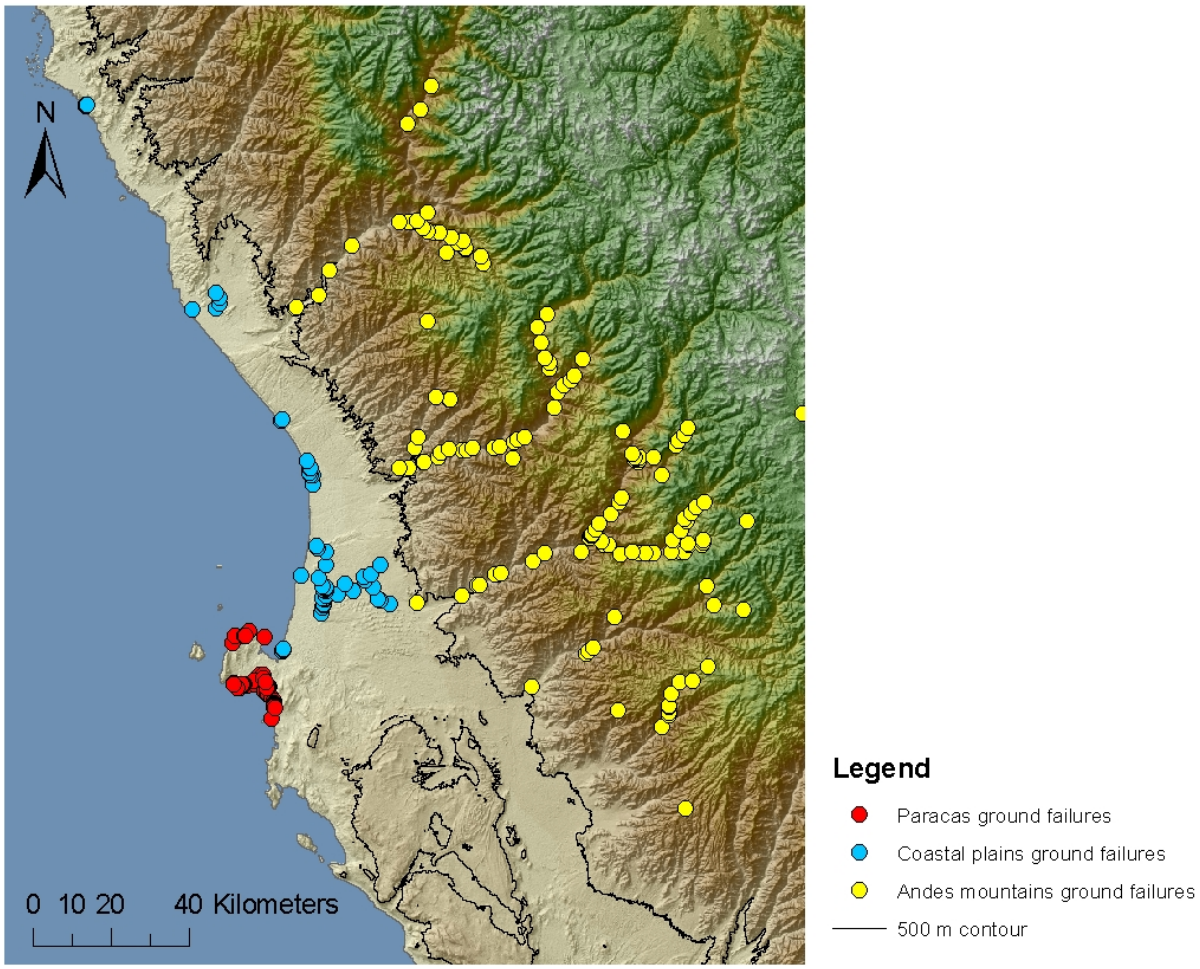

Figure 28. Geomorphic settings.

Paracas Peninsula

Paracas is a peninsula of approximately 120 km^2, located about 200 km south of Lima. The geomorphology of Paracas is typified by near-vertical sea cliffs with narrow beaches. Paracas is a National Reserve, protecting many kinds of animals including migratory birds and sea mammals. A total of 71 ground failures occurred in this area, with volumes ranging from 10 m^3 to 470,000 m^3. Of these ground failures, all but two were rock slumps; there was a single lateral spread that occurred in a parking area, possibly in man-made fill, and a small (volume = 10 m^3) rockfall. See Figures 29-31.

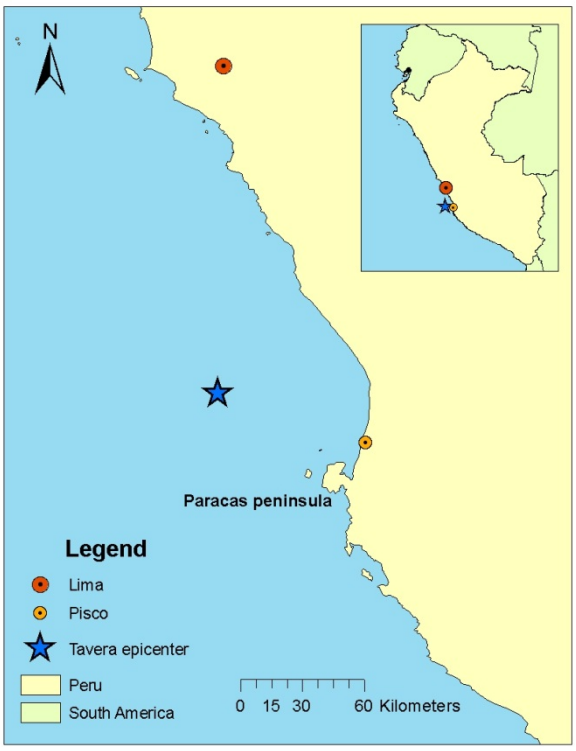

Figure 29. Location of the Paracas Peninsula.

Figure 30. Landslides on the Paracas Peninsula.

Figure 31. Typical Paracas Peninsula sea cliffs. Photo by Joseph Wartman, 3/18/2010.

After slope (landslides occur exclusively on the margins of the Paracas Peninsula) geologic unit is the factor that has that has the greatest contribution to landsliding susceptibility. PGA/earthquake intensity does not vary significantly in this small area, and there are no rivers or roadcuts.

There are 5 rock units and one soil unit found in Paracas. From oldest to youngest, the rock units are a Pre-Cambrian gneiss, a Paleozoic granodiorite/granite, a Carboniferous shale, a Jurassic volcano-sedimentary unit (possibly a welded ash tuff or ignimbrite) and a Paleogene-Eocene marine sandstone. These rock units outcrop only in the Paracas Peninsula and the coastal margin to the south of Paracas (up to about 55 km.) Because they are relatively resistant to day-to-day erosion, they tend to form cliffs, however, this property also makes them susceptible to earthquake-induced landsliding. See Figure 32 for a map of the Paracas geologic units. Unit descriptions can be found in Appendix D.

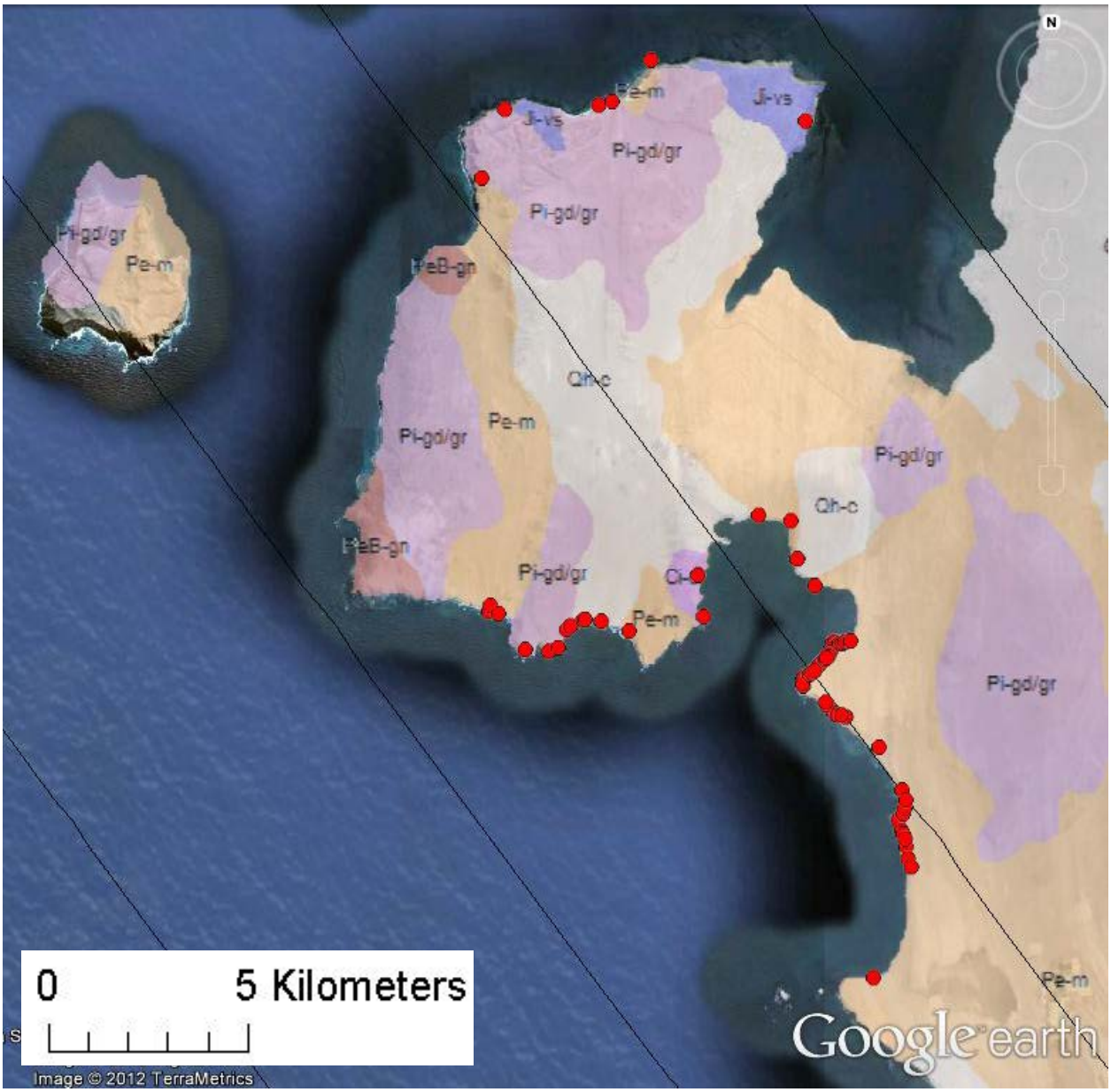

Figure 32. Paracas landslides.

The older, plutonic rocks (gneiss and granodiorite/granite) and also the intermediate-aged volcano-sedimentary unit are least susceptible to either erosion or landsliding. There are few or no landslides occurring in these units, and the units themselves form the headward prominence of the peninsula as well as the western half of Isla de Sangayan, the small island to the west of the Paracas Peninsula. The two youngest rock units, which are marine sedimentary units, are the most susceptible to both erosion and landsliding. The sandstone unit not only has the highest landslide density, but can be seen to form bays along the coastline. See Figure 33 for a comparison of landslide density by unit.

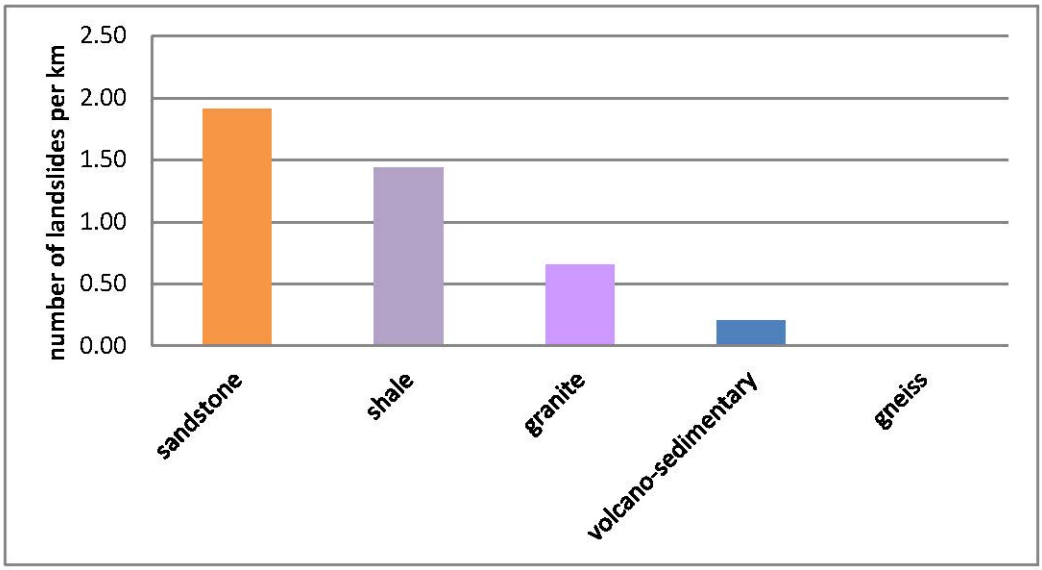

Figure 33. Paracas landslide density. Colors match units in geologic map of Figure 32.

Landslides that mapped onto the Quaternary colluvium were reassigned to either the sandstone unit (1 landslide) or the granite unit (2 landslides) because the geologic map shows only surficial geology, and the landslides undoubtedly occurred in a lithologic unit underlying the colluvium. The singular landslide (a lateral spread) that mapped onto in the Jurassic volcano-sedimentary unit may be over-representative; upon inspection in Google Earth, this landslide appears to be located in a parking lot, and is possibly occurring in man-made fill.

To determine landslide density, the number of landslides occurring in each unit was normalized by length of the cliff-forming portion of the unit, as measured in Google Earth. Table 5 shows landslide counts and susceptible coastline measurements. Data from this table was used to create the bar graph in Figure 33.

Table 5. Paracas landslide density.

unit	description	length of susceptible coastline (km)	number of landslides	landslide density (km^{-1})
Qh-c	Quaternary colluvium	7.87	3	0.38
Pe-m	Paleogene-eocene marine sandstone	28.2	54	1.91
Ji-vs	Jurassic volcano-sedimentary	4.8	1	0.21
Ci-c	Carboniferous shale	2.08	3	1.44
Pi-gd/gr	Paleozoic granodiorite/granite	13.67	9	0.66
PeB-gn	Pre-Cambrian gneiss	7.22	0	0.00

Coastal Plains

Between the Pacific Ocean and the Andes is a broad, relatively flat coastal plain, composed of Quaternary alluvial fans and eolian deposits. These deposits are dissected by river valleys and ravines, locally with wetlands and/or a shallow water table. See Figures 34 and 35. To the south of Paracas in the wide coastal plain, bedrock is exposed in an eroded remnant of the coastal cordillera (Zavala, 2009.) No ground failures were observed in this area.

The factors which contribute most to ground failures in the Coastal Plains area are 1) the presence of soil, as opposed to rock, and 2) shallow ground water. All of the Coastal Plains ground failures were found in river deltas, or other areas of local shallow ground water (indicated by vegetation.) See Figure 36.

A third factor, the presence of roads, may also increase the likelihood of some types of ground failures, particularly lateral spreading

Figure 34. Coastal Plains, dissected alluvial fan deposits.

Figure 35. Coastal Plains, eolian deposits with local shallow water table.

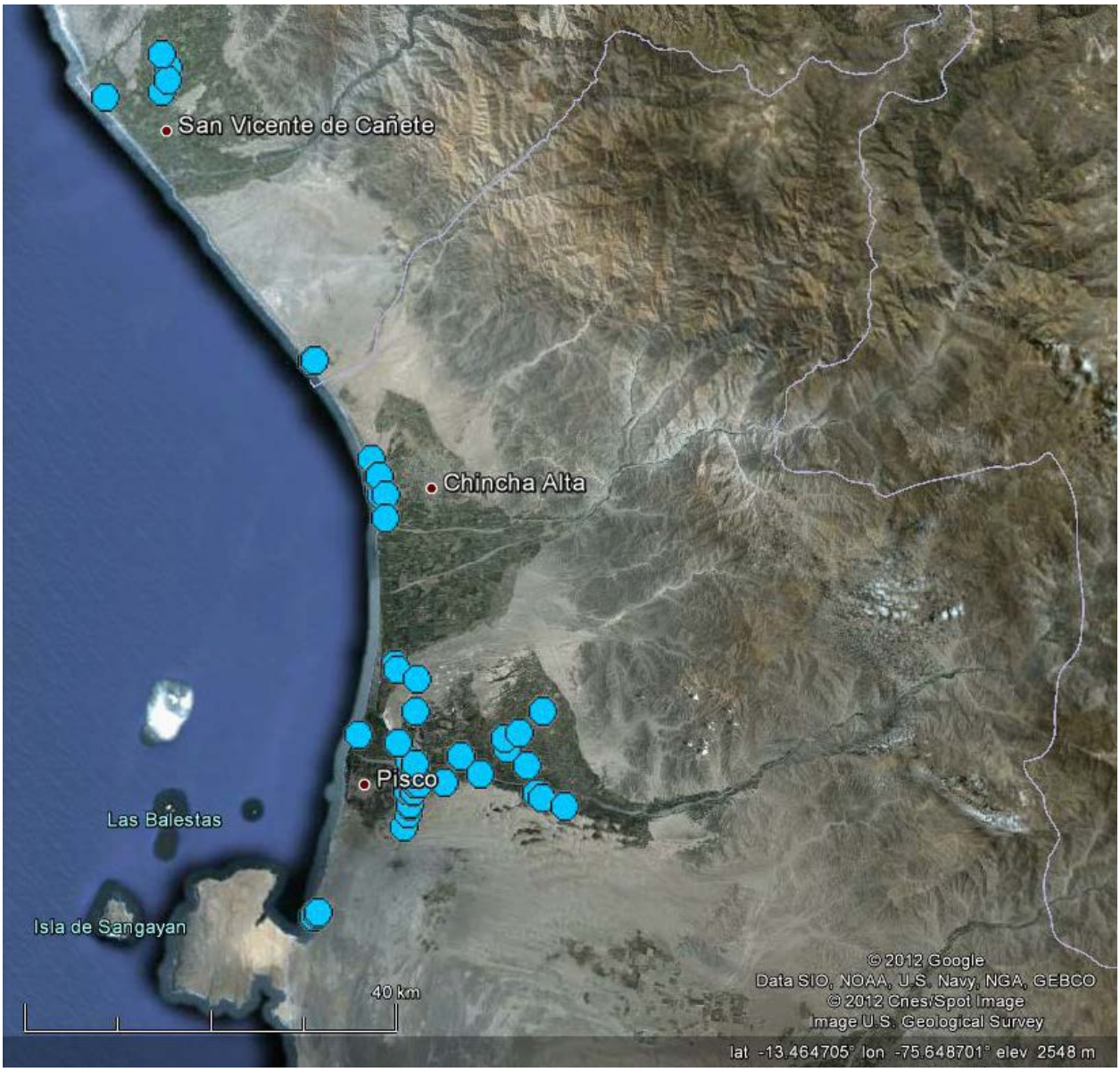

Figure 36. Coastal Plains ground failures relative to vegetation, an indication of shallow ground water.

Of the 65 ground failures observed in the Coastal Plains area, 29 occurred by liquefaction and 23 by lateral spreading, which are the two dominant modes of ground failure. There were 7 disrupted landslides, 1 coherent landslide, and 5 observations of settlement/cracking. See Figure 37.

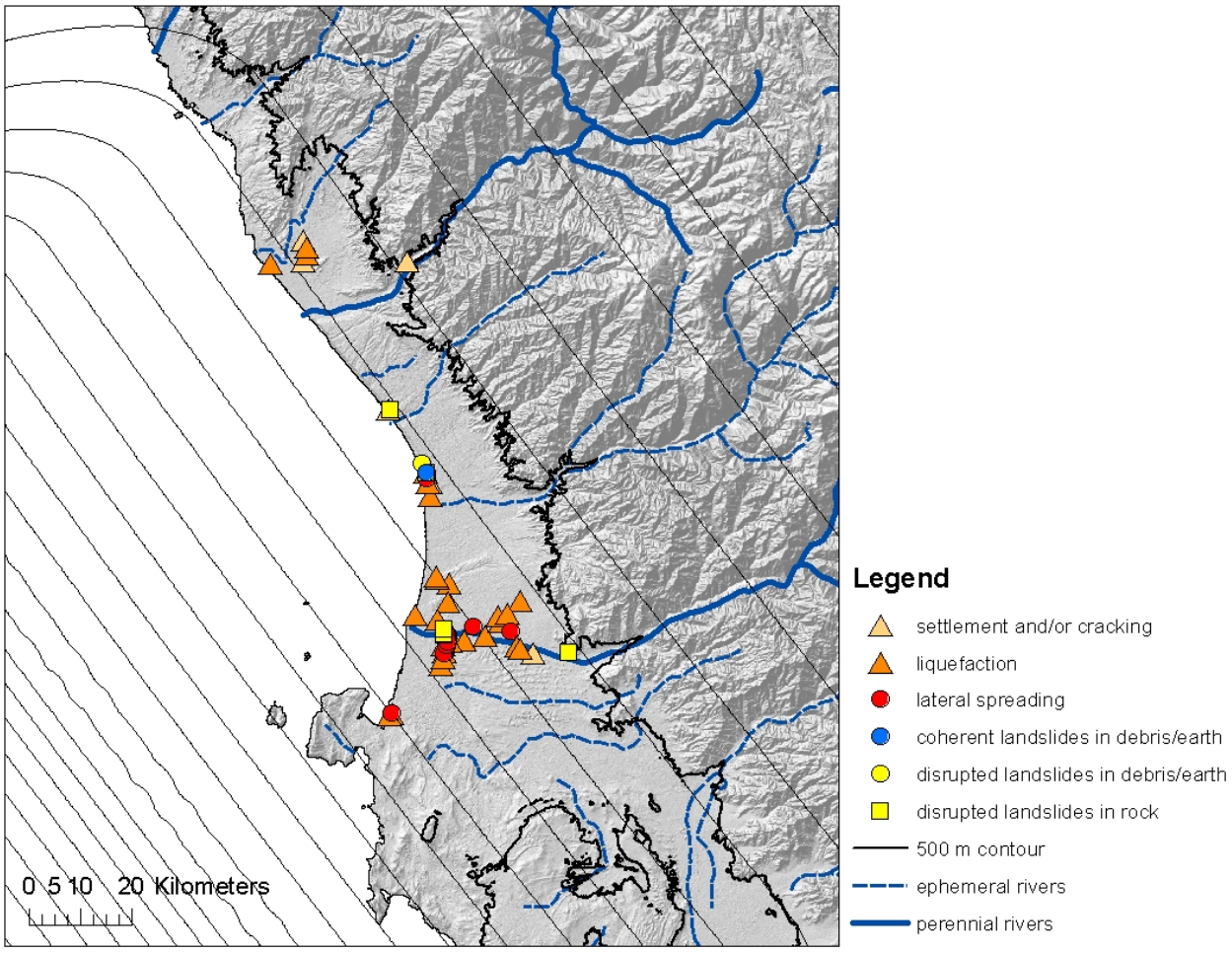

Figure 37. Coastal Plains, location of various types of ground failures.

Unlike Paracas, ground failures in the Coastal Plains area occurred primarily in soils (colluvium and alluvium) typically as either liquefaction or lateral spreading. A few falls and slumps occurred along the cut banks of the Rio Pisco, and an avalanche on the fault scarp of the Canchamana formation. Although many types of rocks outcrop in the Coastal Plains, ground failures occurred in only 3 units: Quaternary-Holocene colluvium (Qh-c), Quaternary -Pleistocene alluvium (Qpl-c), and a Neogene uplifted marine-terrace deposit (Nmp-m) which is well-known for containing abundant marine vertebrate fossils, including whales. See Figures 38 and 39 for locations of ground failures relative to geologic unit, and Table 6 for a count of ground failure type by geologic unit. Geologic maps and brief unit descriptions can be found in Appendix D.

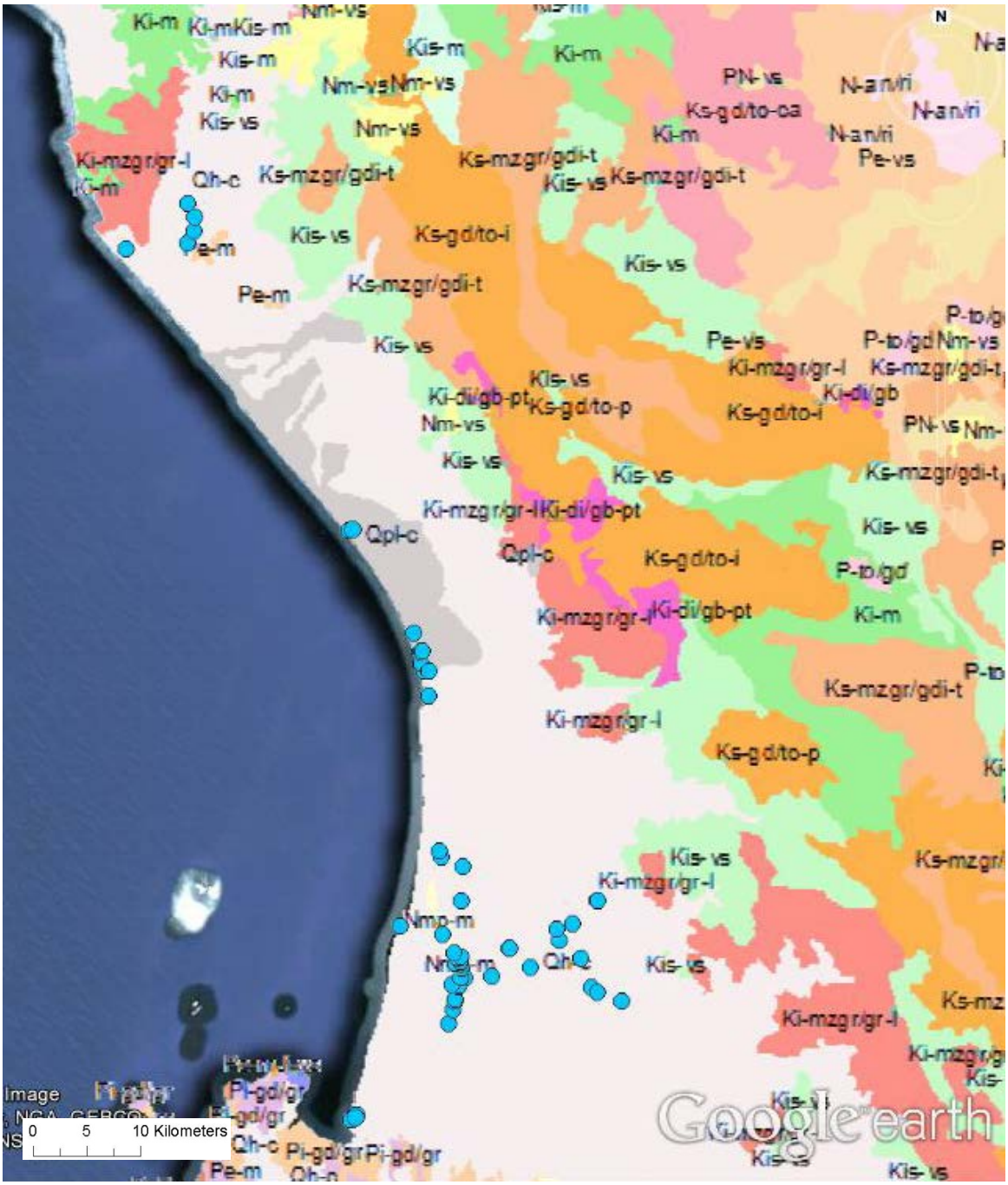

Figure 38. Coastal Plains landslides by geologic unit.

Figure 39. Landslides in the Neogene marine terrace deposits.

Table 6. Coastal Plains: ground failure type by geologic unit.

unit	description	liquefaction	lateral spreading	disrupted landslides	coherent landslides	cracks and settlement
Qh-c	Quaternary (Holocene) colluvium	27	15	0	0	3
Qpl-c	Quaternary (Pleistocene) alluvium	2	1	3	1	2
Nmp-m	Neogene marine terrace deposits	0	7	4	0	0
total		29	23	7	1	5

The majority of the ground failures (45 out of 65) fall within the off-white unit, Qh-c , probably not so much because that unit is more susceptible to ground failures, but because that is the unit which covers the greatest area within the Coastal Plains. Figure 40 shows the number of ground failure types by geologic unit; after normalizing for area (Figure 41) it can be seen that Qh-c has the smallest landsliding density of the 3 units.

The Pleistocene alluvium (Qpl-c) has a small number of all types of ground failures, including a single coherent landslide. It may be that this unit has become somewhat indurated over time, hence the

coherent landslide. Alternatively, the distinction between soil slump and lateral spread may be small in this case.

Upon inspection in Google earth, the area designated on the map as Neogene uplifted marine terrace (Nmp-m) is visually indistinguishable from the Quaternary colluvium. It appears to be primarily farmland, with 7 lateral spreads adjacent to a road, and 4 disrupted landslides along the bank of the Rio Pisco. After normalizing for area (Figure 41) the Neogene marine terrace deposits seem much more susceptible to lateral spreading and disrupted landslides, however it should be considered that the sample size here is quite small (11 landslides total.)

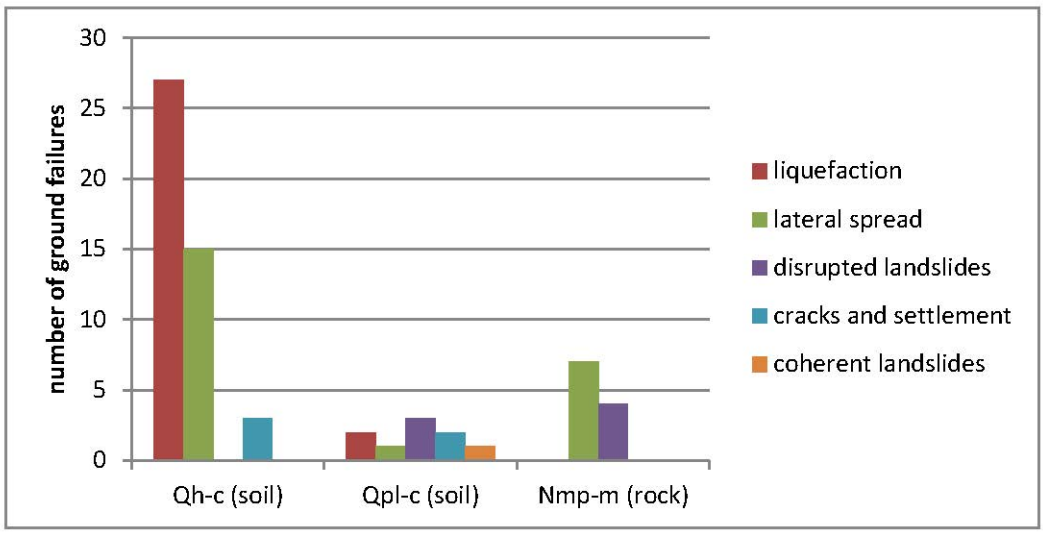

Figure 40. Number of ground failures by surficial geologic unit.

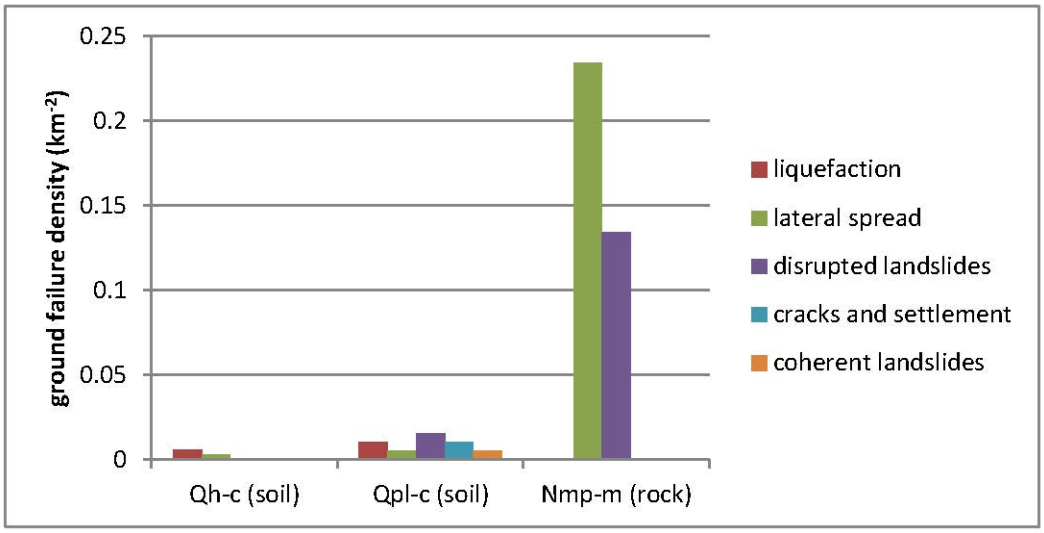

Figure 41. Density of ground failure types by geologic unit.

The last factor that seems to contribute to ground failure susceptibility is the presence of roads. In the Coastal Plains region, association of ground failures with roads was determined by inspection in Google Earth. Lateral spreads and settlement/cracking are more likely to be associated with roads (Figure 42.) Overall, there is a large proportion of ground failures associated with roads, considering that the total area that roads represent is quite small. It should also be considered that observations of ground failures on or near roads are over-represented due to sampling bias, as those ground failures are more likely to be discovered.

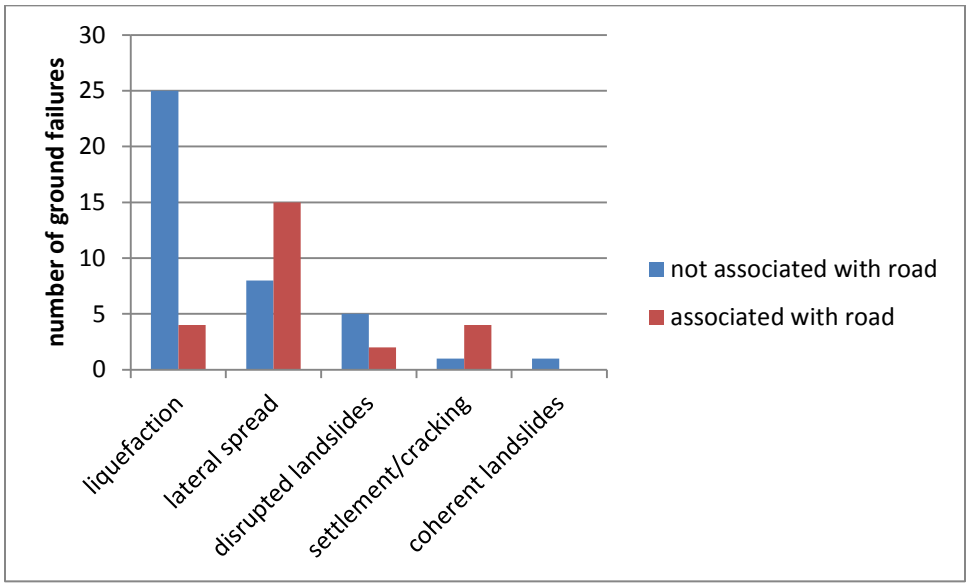

Figure 42. Ground failures in the Coastal Plains region associated with roads.

Other parameters considered, which do not seem to contribute significantly to the patterns of ground failures in the Coastal Plains area are:

- PGA. The range of PGA in the Coastal Plains area is small, and there are areas with larger PGA, but fewer ground failures. Landslide volume actually increases as PGA decreases. There is not enough area in the Coastal Plains region (and consequently not enough variability in PGA) to develop a relationship between PGA and landsliding volume or style.
- Ecological Region. The entire Coastal Plains area is categorized in the same ecological region: Sechura desert (deserts and xeric shrublands.)
- Precipitation. All ground failures in the Coastal Plains have less than 100 mm/year precipitation.
- Slope, slope aspect, and relief. With the exception of the Canchamana fault scarp and associated earth/debris avalanche, there is minimal relief in the Coastal Plains area. A few disrupted landslides were associated with cut-banks of the Rio Pisco.

Andes Mountains

154 ground failures (153 landslides and 1 incidence of settlement/cracking) were observed in the Andes Mountains region. Eighty-two landslides occurred in rock (81 falls, 1 slump) and 71 occurred in soil (46 slumps, 22 falls, and 2 avalanches.) Volumes ranged from 5 to 75,000 cubic meters. About 60% (93 out of 154) of landslides were associated with roads or roadcuts.

For simplicity, the geologic units of the Andes can be divided into 6 main groups, which are described in the next section. Deeply incised into these units are steep-sided v-shaped river valleys, with alluvial deposits on the valley floor and talus cones at the base of the slopes. See Figure 43.

Figure 43. V-shaped mountain valley, with talus cone on right. Photo by Joseph Wartman, 3/21/2010.

Landsliding in the Andes is controlled by different factors in different areas. Where the PGA is highest and the mountains first start to rise up out of the plains, there are actually very few landslides, possibly due to shallower slopes, but also because the convergence of tributaries results in fewer steep river valleys. See Figures 44 and 45. As the slopes increase (and tributaries diverge) rockfalls increase. Further away from the earthquake epicenter, as PGA decreases and precipitation increases, the valley floor widens and there is more soil and terraced farming; in this area there are many soil slumps and falls. The incidence of landsliding diminishes sharply after this, as ground shaking is no longer sufficient to trigger ground failures.

Disrupted landslides (rock and soil falls) are more likely to be associated with roads. Like Paracas, sedimentary rock units in the Andes Mountains region are more susceptible to landsliding, although this factor seems less influential than slope or the presence of moisture (which is coincident with the presence of soil.)

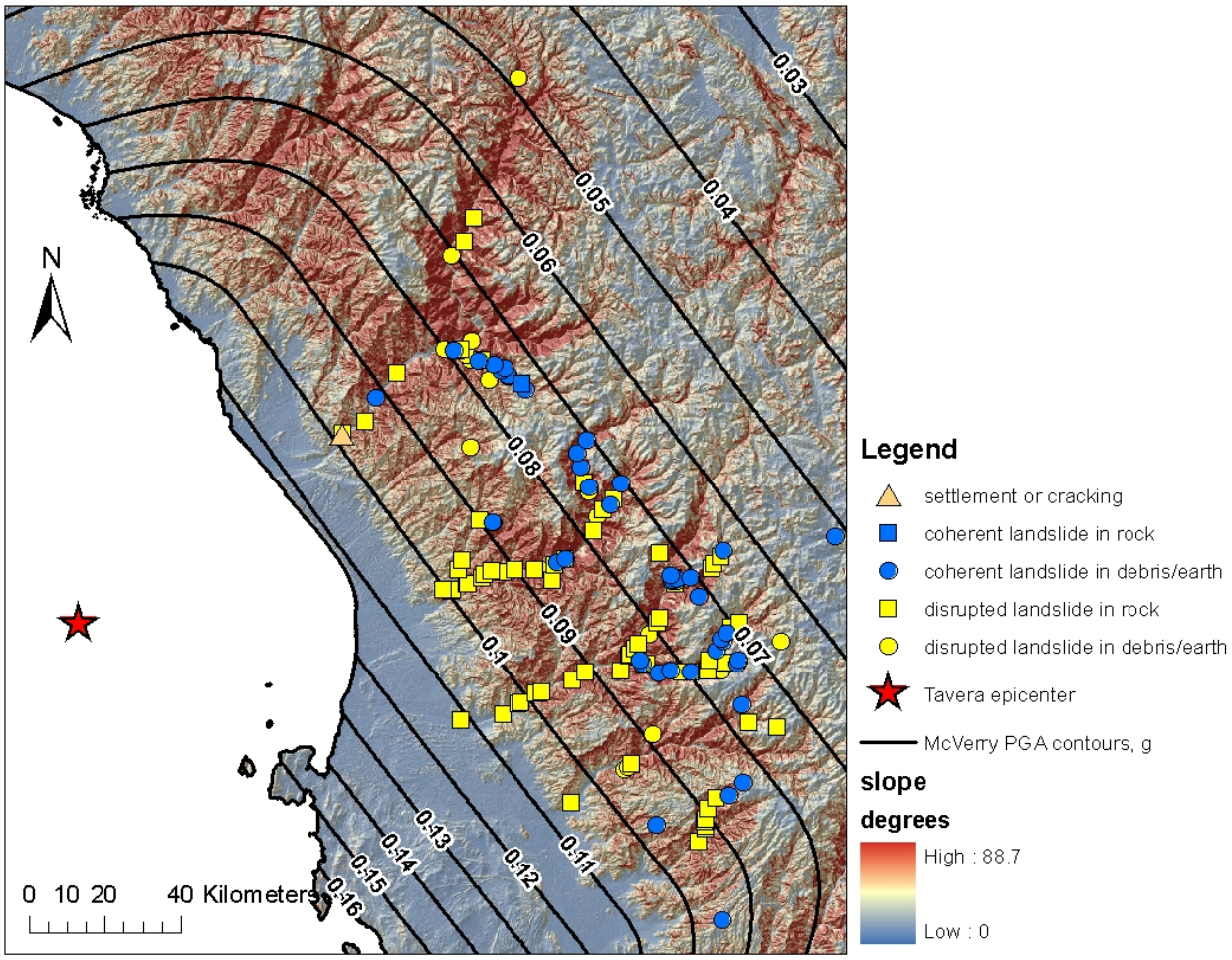

Figure 44. Andes Mountains ground failures relative to PGA and slope.

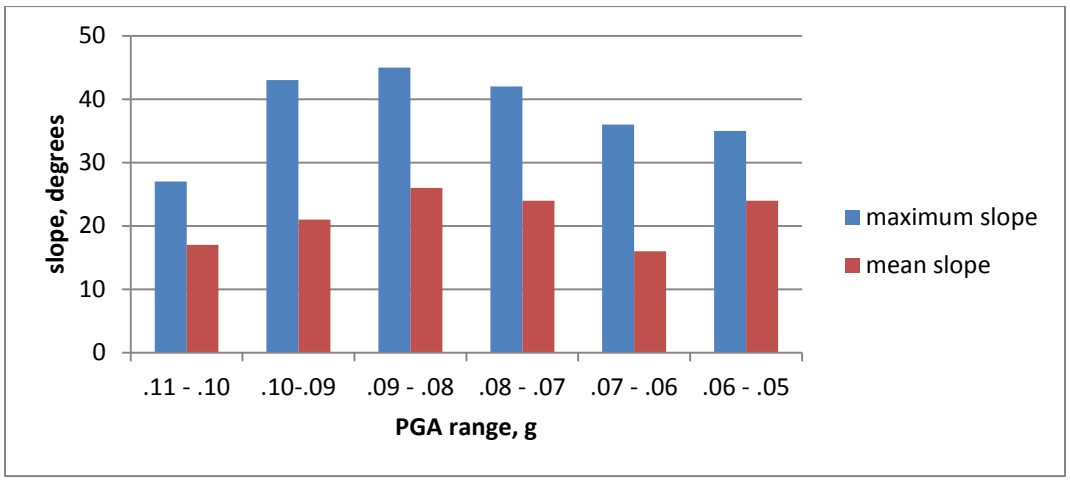

Figure 45. Changes in slope in Andes Mountains region by PGA range.

A simplified geologic map was used for analysis in the Andes Mountains region: Mapa Litológico (INGEMMET, 2002.) The geologic units of the Andes are divided into 6 main groups:

Superficial deposits
I alluvium, colluvium, eolian, lacustrine, fluvial, marine, and pyroclastic deposits
Intrusive rocks
II granite, granodiorite, diorite, gabbro
Volcanic rocks
III-1 basalt, tuff
III-2 tuff
Volcano-sedimentary rocks
IV ash tuff, mudstone, black limestone, shale, andesite, rhyolite
Sedimentary rocks
V-1 quartzite, sandstone, shale, coal
V-2 slate, shale, sandstone, schist
V-3 red sandstone, shale, gypsum
V-4 limestone, sandstone, shale
V-5 conglomerate, sandstone, shale, evaporite deposits
Metamorphic rocks
VI schist, gneiss

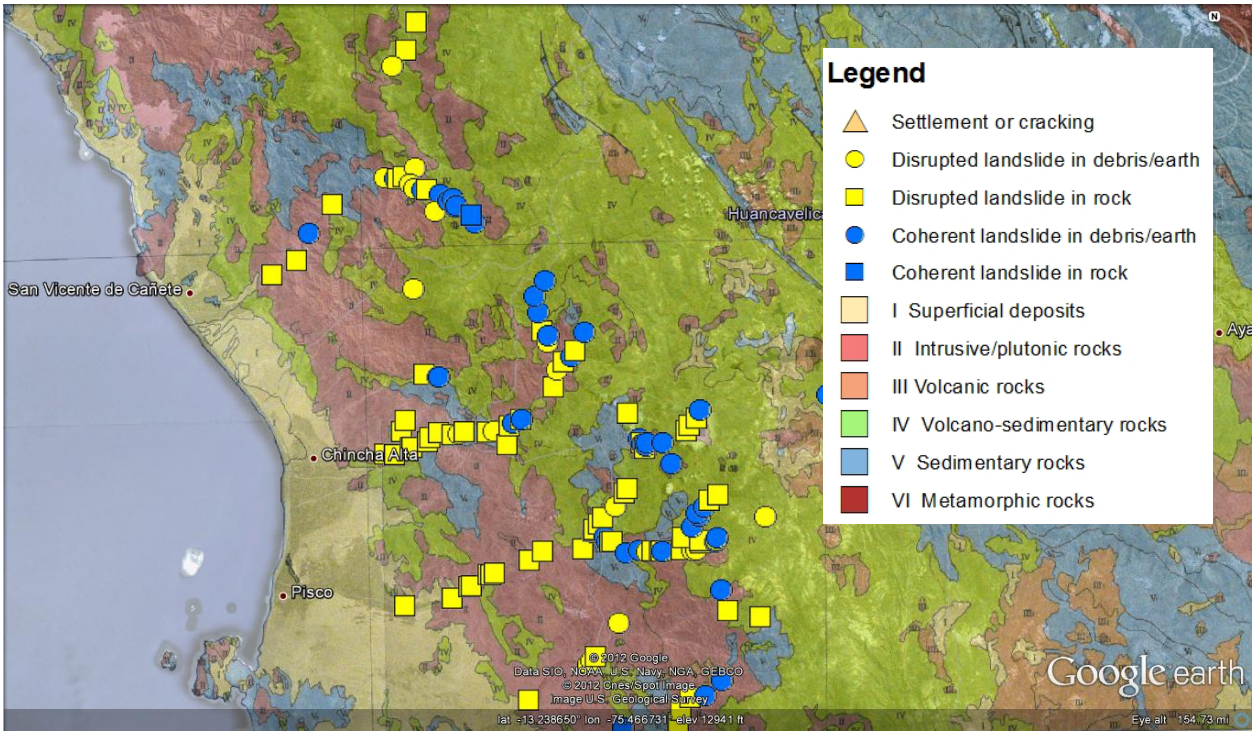

Figure 46. Landslides by type and geology.

Landslides are much more likely to occur in the sedimentary rock units (unit V, mapped in blue in Figure 46.) Table 7 and Figure 47 show ground failure density by unit; note that the ground failure density of

the sedimentary units is greater than twice that of the next-most susceptible unit. After the sedimentary units, units I, II, and IV (superficial deposits, intrusive/plutonic rocks, and volcano-sedimentary rocks, respectively) are similar in landsliding susceptibility. Unit III (volcanic rocks) is significantly less susceptible. This may be because the unit III rock is stronger, but also possible is that it outcrops the furthest away from the earthquake epicenter.

Table 7. Mountains landslides data.

		count					normalized by road length				
unit	road length (km)	disrupted landslides, rock	disrupted landslides, soil	coherent landslides, rock	coherent landslides, soil	cracks and settlement	disprupted landslides, rock	disrupted landslides, soil	coherent landslides, rock	coherent landslides, soil	cracks and settlement
I	9.8	2	0	0	0	0	0.203	0.000	0.000	0.000	0.000
II	321.9	41	11	0	14	2	0.127	0.034	0.000	0.043	0.006
III_2	21.7	0	0	0	1	0	0.000	0.000	0.000	0.046	0.000
IV	311.4	23	8	1	26	0	0.074	0.026	0.003	0.083	0.000
V_1	11.8	2	0	0	2	0	0.169	0.000	0.000	0.169	0.000
V_4	72.2	10	5	0	3	0	0.139	0.069	0.000	0.042	0.000
total	748.9	78	24	1	46	2	0.712	0.129	0.003	0.384	0.006

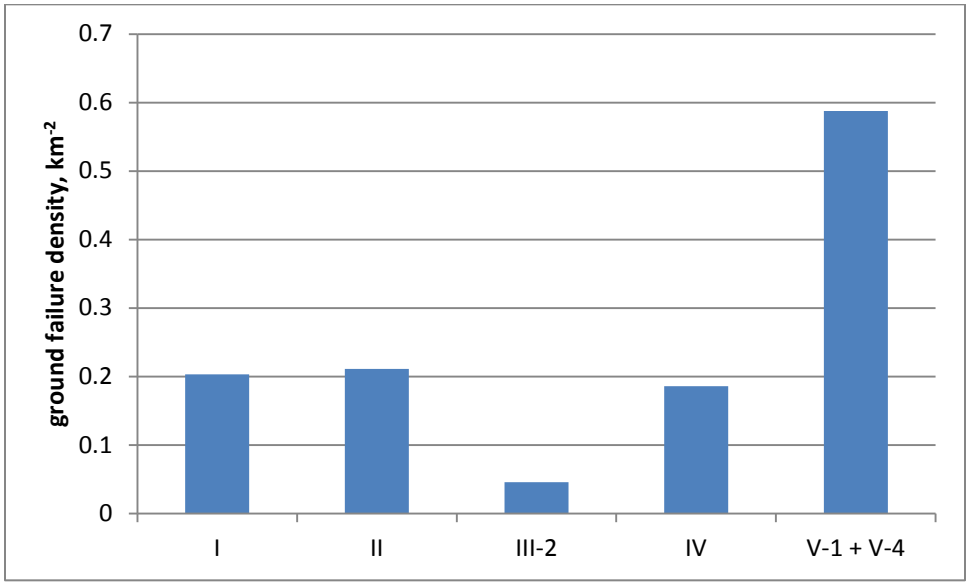

Figure 47. Number of ground failures per unit, normalized by area.

Average landslide volumes are much larger in unit I (superficial deposits.) The volcanic rock unit (unit III) has the smallest average landslide volume, although it should be noted that there is only one landslide in this unit. See Table 8 and Figure 48.

	I	II	III	IV	V
sum	16018	151459	60	70790	40098
max	8000	75000	60	56394	35000
min	18	5	60	2	5
avg	5339	2195	60	1242	2005
st dev	4608	10265	0	7495	7781

Table 8. Landslide volumes by geologic unit, m^3.

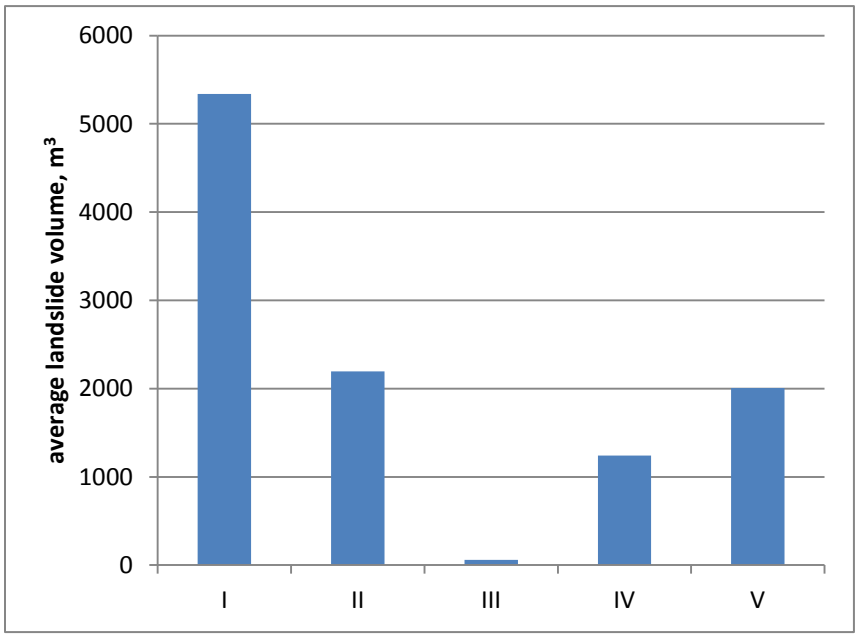

Figure 48. Average landslide volume by geologic unit.

Table 9 shows the number of each type of landslide in each geologic unit. Superficial deposits exhibited only one mode of landsliding: disrupted landslides (rockfalls.) Volcanic rocks also had only one mode of landsliding: coherent landslides in debris/earth (soil slumps.) The remaining 3 units exhibited primarily disrupted landslides (rock and soil falls) followed by coherent landslides in (soil and rock slumps.) See Figure 49. Because geologic unit types were determined from a map, instead of in the field, these results should be considered preliminary for the purpose of suggesting further investigation—unit boundaries on maps are interpolated, and consequently imprecise.

Table 9. Landslide types by geologic unit.

unit	disrupted landslides, rock	disrupted landslides, soil	coherent landslides, rock	coherent landslides, soil	cracks and settlement	total
I	2	0	0	0	0	2
II	41	12	0	14	1	68
III_2	0	0	0	1	0	1
IV	23	8	1	26	0	58
V_1	2	0	0	2	0	4
V_4	10	5	0	3	0	18
total	78	25	1	46	1	151

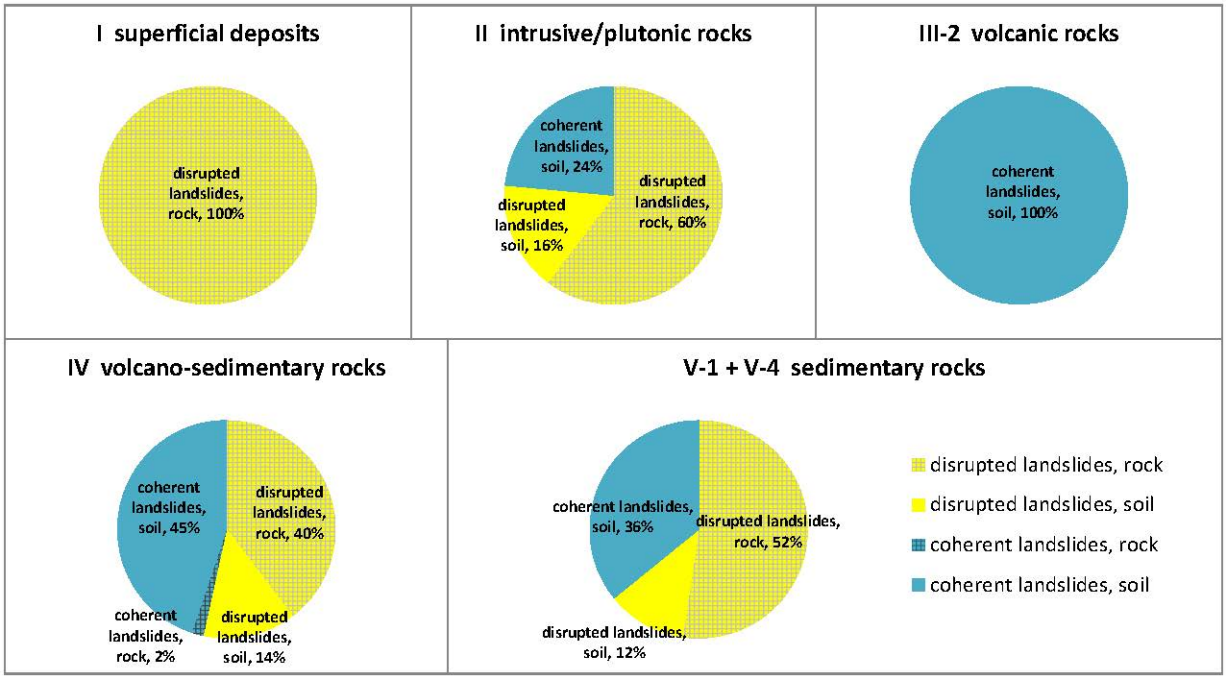

Figure 49. Landslide type by geologic unit.

In the Andes Mountains region, PGA does not affect landsliding in an intuitive way. One might expect that as PGA decreases, so would the number of landslides and the volume of the average landslide. In fact, both the number of landslides and the mean volume of the landslides increase as PGA decreases to between .08 and .07 g, and then both number and volume drop off dramatically. See Figure 50 A-D. Clearly there is some factor other than PGA which is has a controlling influence on landsliding susceptibility. Slope, geology, and precipitation were considered as controlling factors, but did not show any pattern of concentrating landslides in the PGA range of .08 - .07 g. After inspection in Google earth,

it appears that what is happening is a change in the geomorphology from narrow river valleys to wide, accompanied by the presence of terraced farming. See Figure 51.

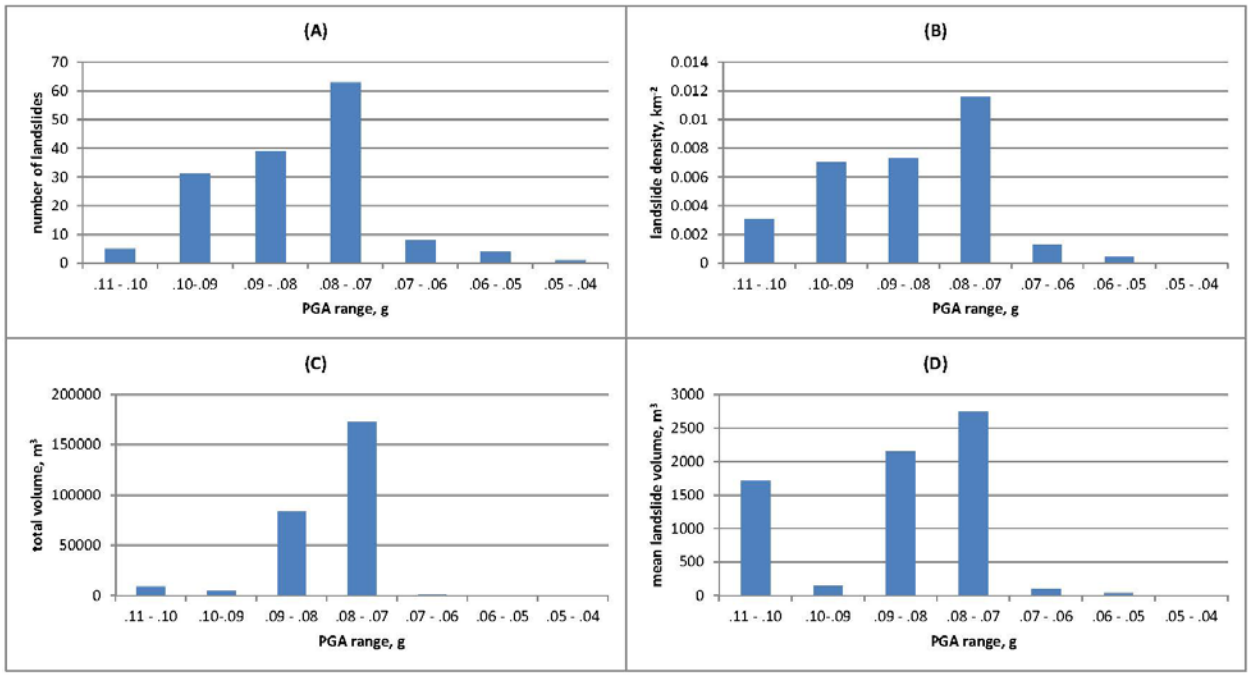

Figure 50. A) Number of landslides within each PGA range. B) Number of landslides normalized by area. C) Total landslide volume within each PGA range. D) Mean landslide volume.

Figure 51. Narrow river valley to left (PGA > .08 g.) Wide river valley with terraced farming to right (PGA < .08 g.)

Figure 52 shows how the mode of landsliding changes as PGA decreases. The number of disrupted rock landslides reaches a maximum at a PGA range of .10 - .09 g, and then drops off as PGA decreases. Landslides in soil reach a maximum at a lower PGA range of .08 - .07 g, which coincides with the location of the wider river valleys and terraced farming.

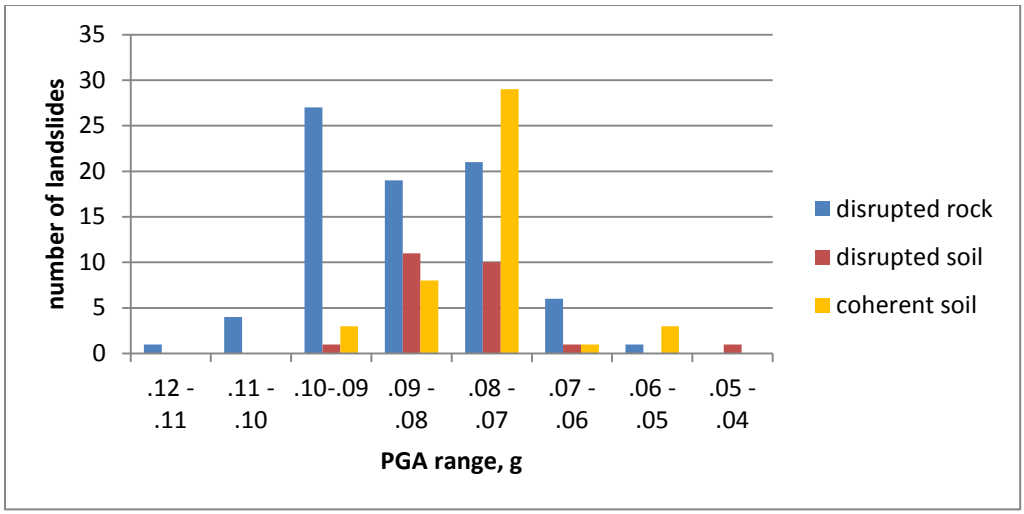

Figure 52. Number of landslide by type within each PGA range.

Figure 53 shows the transition from a predominant mode of failure in rock, to a predominant mode of failure in soil. This change of mode occurs as precipitation increases.

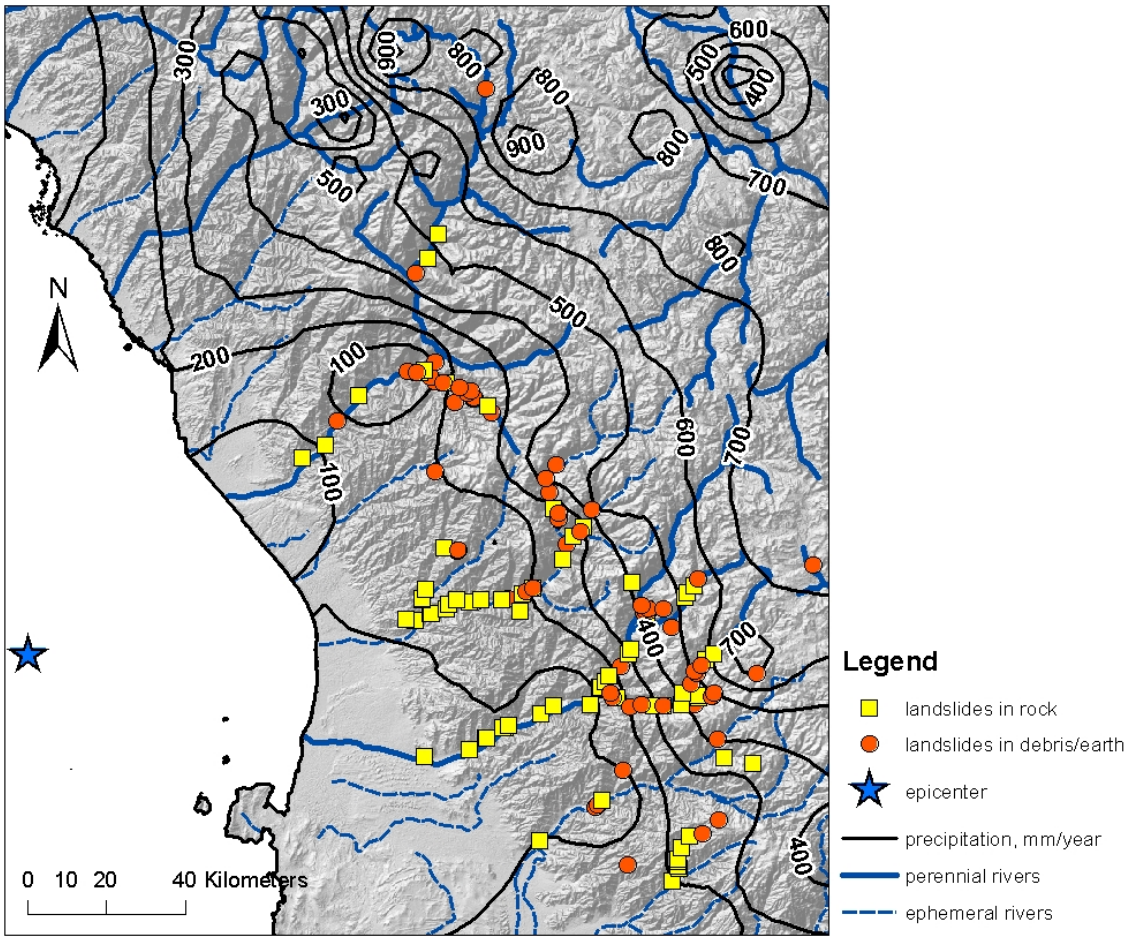

Figure 53. Rock and soil landslides relative to moisture.

As with the Coastal Plains region, ground failures in the Andes Mountains are often associated with roads and roadcuts. Disrupted landslides, both rock and soil, are more likely to be associated with roads. See Figure 54.

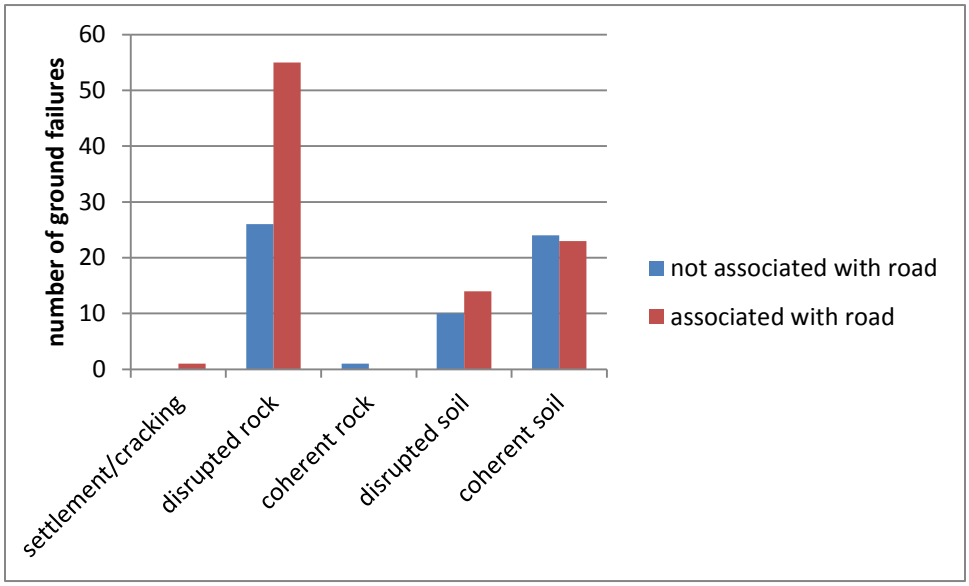

Figure 54. Ground failures in the Andes Mountains region associated with roads.

Landslide Frequency-Size Models

Landslide frequency-size models are used to estimate the total number and size of landslides, when the landslide inventory is incomplete. The premise is that the distributions for the medium and large landslide areas/volumes are self-similar regardless of triggering mechanism, terrain, or any other factor. (Malamud et al., 2003.) That is, for an event of any magnitude, the proportions of the different sizes of landslides will be the same. Given a partial inventory of the largest landslide volumes, the remainder of the landslide volumes can be determined for a complete inventory.

There are several different empirical landslide frequency-size models that have been proposed. Three are described here: inverse power law distribution, 3-parameter inverse gamma distribution, and lognormal distribution. The intent of the following sections is to determine which, if any, model is a good fit for the Pisco data, so that the landslide inventory may be upscaled to represent any landslides that may have been omitted during field reconnaissance.

The total volume of landsliding material for the Pisco earthquake event was estimated to be 7.72×10^6 m^3, a value that is two orders of magnitude smaller than the estimated landslide volume from a 1970, M_w=7.9 earthquake in Peru that had an estimated volume of 1.41×10^8 m^3 (Keefer, 1994.) The next section attempts to determine if the Pisco total landslide volume is smaller due to missing data in the inventory, or if it is smaller for some other reason.

Inverse Power Law (Pareto) Distribution

Distributions of the type

$$p(x) = Cx^{-\alpha}$$

follow a power law, where x is any variable and α is the exponent of the power law. The constant C is determined by the requirement that that the sum of p(x) = 1. The following section uses the Newman (2006) method to determine if the Pisco dataset for landslide volumes follows a power law distribution.

The method is first presented using an artificial dataset with a power-law distribution, where C and α are known; and then presented using the Pisco landslide volume data, from which C and α will be extracted. The artificial dataset was created by generating a uniform distribution of one million random numbers between 0 and 1, and then transforming the uniform distribution into a power law distribution where C = 1.5 and α= 2.5. See Appendix E for the MATLAB code implementation of the Newman method.

Figure 55A shows a histogram of the artificial dataset. The blue bars are the random data and the red line is the function $p(x) = 1.5x^{-2.5}$. It can be seen in Figure 55B that when the data is graphed in logarithmic scales, the power law distribution plots in a straight line, which is characteristic of power law distributions. It can also be seen that the tail of the distribution is quite noisy, because as the number of samples in the bins becomes very small, the fraction that those samples represent is quite large and magnifies any statistical fluctuations.

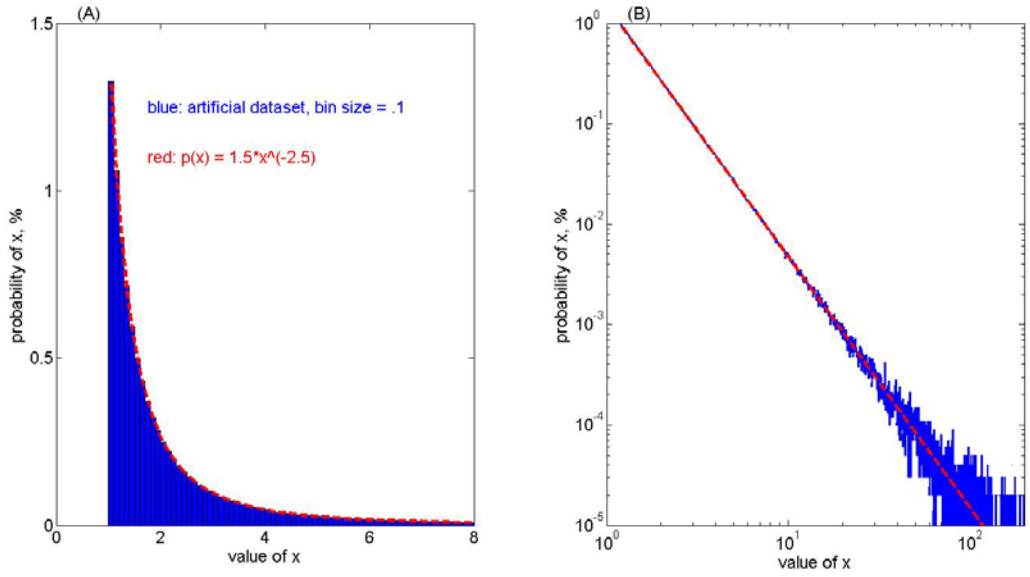

Figure 55. A) Histogram of artificial dataset. B) Log-log plot of same data.

According to Brunetti et al. (2009):

> *…landslide volumes almost inevitably obey a negative power-law scaling. Variability exists in the exponent of the power-law tails of the distributions. Part of the variability is natural, i.e., due to different landslide types and local morphological and lithological settings. However, part of the variability is fictitious, and caused by the different methods used to collect the data and to estimate the distributions.*

Since the tail of the Pisco dataset is very important in estimating a complete dataset, it is useful to have a method to reduce noise. Binning the data in log-2 bins accomplishes this goal nicely; see Figure 56 for histogram and equivalent logarithmically plotted graph.

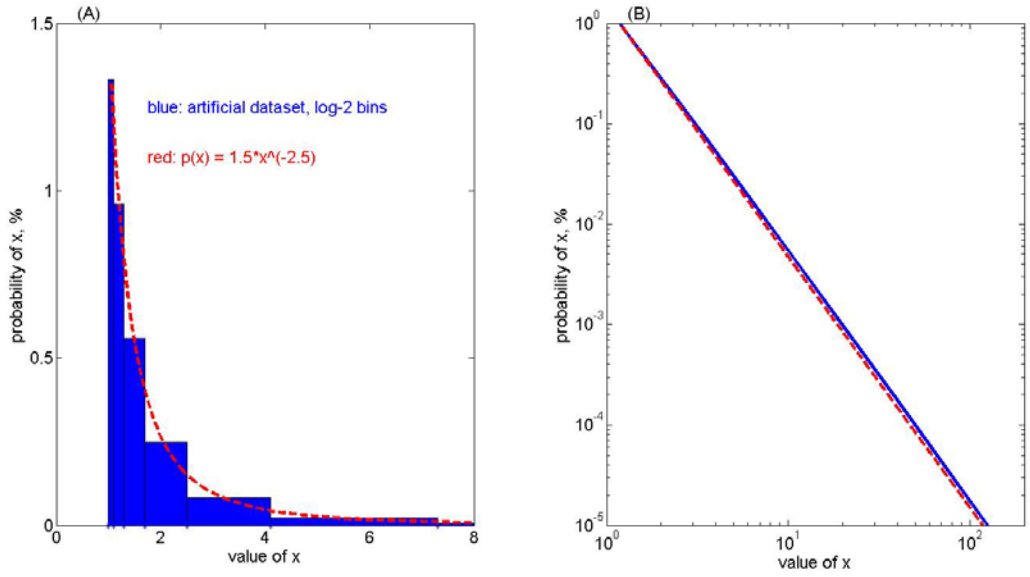

Figure 56. A) Histogram of log-binned artificial dataset. B) Log-log plot of same data.

A superior method for noise reduction, according to Newman (2006) is to plot the cumulative distribution function, or the probability that x has a value greater than or equal to X:

$$P(X \leq x) = \int_{-\infty}^{x} f_x(x)\, dx$$

Or, if the distribution follows a power law, $p(x) = Cx^{-\alpha}$

$$P(X \leq x) = C \int_{x}^{\infty} x^{-\alpha}\, dx = \frac{C}{\alpha - 1} x^{-(\alpha-1)}$$

It is not necessary to bin the data or determine what sizes the bins ought to be. According to Newman (2006):

> *…P(x)is well-defined for every value of x and so can be plotted as a perfectly normal function without binning…binning of the data lumps all samples of a given range together into the same bin and so throws out any information that was contained in the individual values of the samples within that range. Cumulative distributions don't throw away any information; it's all there in the plot.*

If the original function follows a power law, then the cumulative distribution function will also follow a power law, with a different exponent, α-1. See Figure 57 for artificial dataset plotted cumulatively.

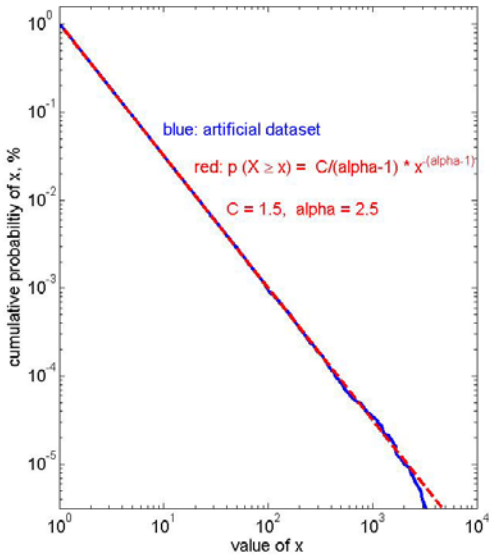

Figure 57. Cumulative probability of artificial dataset, log-log plot --no binning!

The artificial dataset was used as a test to ensure the MATLAB program was working correctly. Using a slightly modified program with actual Pisco landslide volume data, the inventory appears to have an inverse power law relationship when graphed in histogram form: see Figure 58A. Figure 58B shows the same data plotted in logarithmic scales. It is now less clear if the data is plotting in the characteristic straight line (particularly in the tail region) and if the data does indeed follow a power law relationship. MATLAB code can be found in Appendix E.

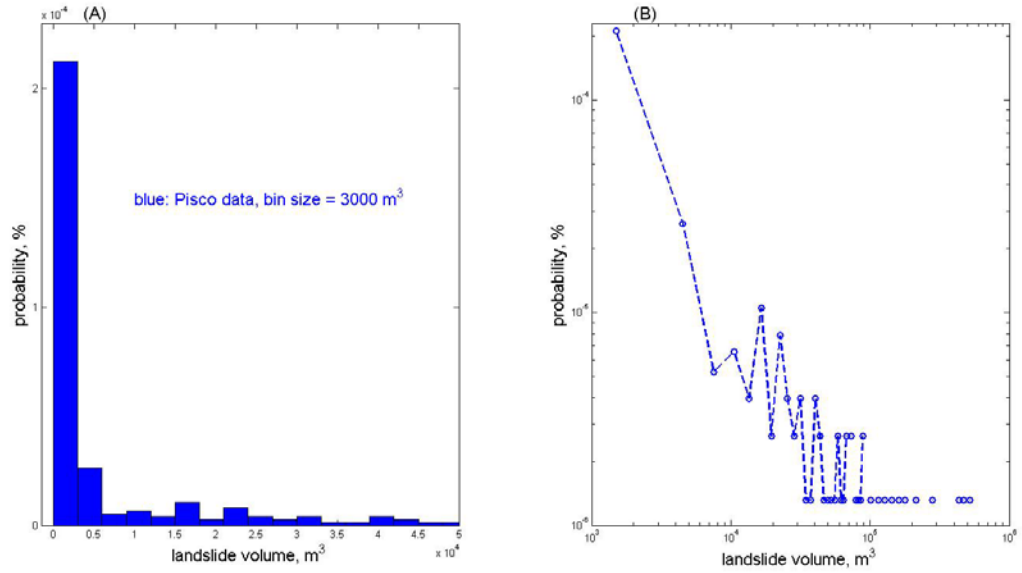

Figure 58. A) Histogram of uniformly-binned Pisco data. B) Log-log plot of same data.

Figure 59 shows the Pisco data plotted cumulatively. Here it is clear that the data (in blue) do not plot in a straight line, and that smaller volumes are under-represented for a true power-law distribution. For the small-volume landslides, the probability of a landslide being larger is quite high.

The relative dearth of small-volume landslides could mean that the Pisco landslide volumes cannot be appropriately modeled with a power-law; alternatively, it could mean that the inventory is incomplete for small-volume landslides. Assuming the latter is the case, a power-law function has been fit to the tail of the curve, with the hope of eventually extrapolating the "missing" data.

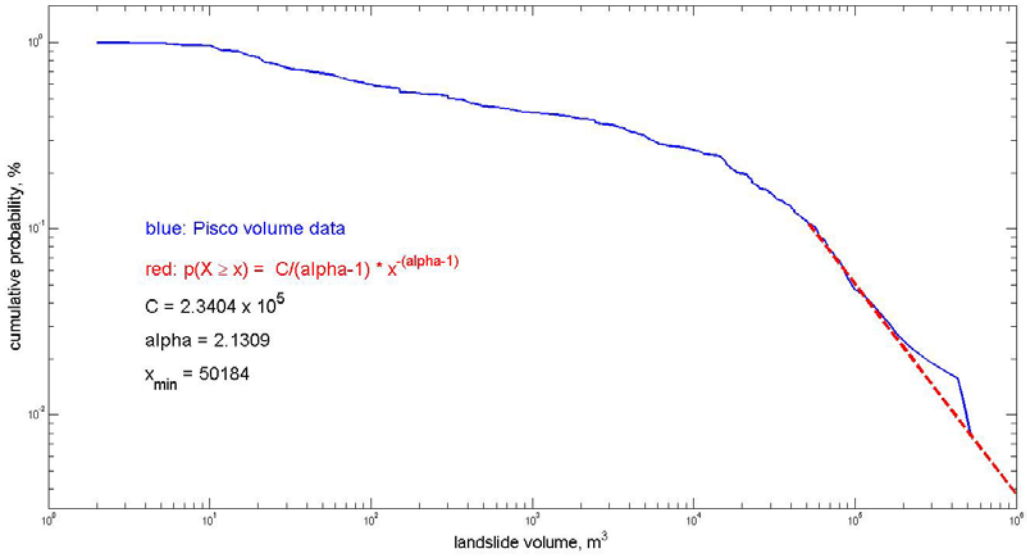

Figure 59. Cumulative probability of the Pisco landslide volume data.

The dashed red line shows the power-law function, $p(X \geq x) = \frac{C}{\alpha-1} x^{-(\alpha-1)}$. Alpha and x_{min} were determined by using Clauset's plfit.m function (see Appendix E) downloaded from http://tuvalu.santafe.edu/~aaronc/powerlaws/plfit.m.

> *PLFIT(x) estimates x_min and alpha according to the goodness-of-fit based method described in Clauset, Shalizi, Newman (2007). x is a vector of observations of some quantity to which we wish to fit the power-law distribution p(x) ~ x^-alpha for x >= xmin.*
> *PLFIT automatically detects whether x is composed of real or integer values, and applies the appropriate method. For discrete data, if min(x) > 1000, PLFIT uses the continuous approximation, which is a reliable in this regime.*

The fitting procedure works as follows:
1) For each possible choice of x_min, we estimate alpha via the method of maximum likelihood, and calculate the Kolmogorov-Smirnov goodness-of-fit statistic D.
2) We then select as our estimate of x_min, the value that gives the minimum value D over all values of x_min.

The value of x_{min} could also be roughly "eyeballed" from the graph by selecting a value that occurs after the slope break, or one could select x_{min} by choosing a landslide volume above which it is certain that all landslides are accounted for. The plfit.m method was chosen because it is not subjective, and therefore reproducible.

Plfit.m also provided alpha, although alpha could also be calculated given x_{min}. C was calculated from a relationship provided by Clauset and Newman (2009):

$$\alpha = 1 + n\left[\sum_{i=1}^{n} ln\frac{x_i}{x_{min}}\right]^{-1} = 2.1309 \qquad \text{Newman (2006)}$$

$$C = (\alpha - 1)x_{min}^{(\alpha-1)} = 2.3404 \times 10^5 \qquad \text{Clauset and Newman (2009)}$$

Where x_i, i=*1*…n, are the measured values of x.

Figure 60 shows the Pisco probability data plotted with the appropriate power-law function, $p(x) = Cx^{-\alpha}$ using C, alpha, and x_{min} as previously determined. Ideally, this power-law function could be used to "upscale" the Pisco data (extrapolate missing volumes.)

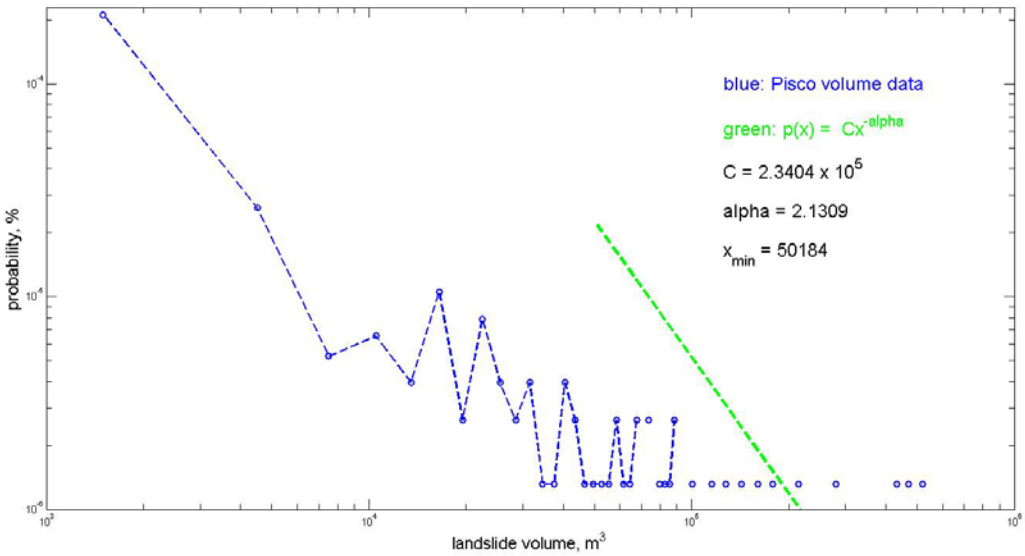

Figure 60. Log-log plot of the Pisco landslide probability data.

The area beneath the green line is very close to 100%:

$$\int_{x_{min}}^{x_{max}} Cx^{-\alpha}\,dx = \int_{50184}^{2745000} 234040x^{-2.1309}\,dx = .989165$$

Where x_{max} is the volume of the largest landslide in the inventory. This 98.9% represents a volume of 6,598,574 m^3, which is the sum of all landslide volumes equal to or greater than 50184 m^3. If we were to extend the green line to the smallest landslide in the inventory, the new area under the curve would be:

$$\int_{x_{min}}^{x_{max}} Cx^{-\alpha}\,dx = \int_{2}^{2745000} 234040x^{-2.1309}\,dx = 94{,}499.8$$

We can now say that:

$$\frac{6{,}598{,}574\ m^3}{.989165} = \frac{upscaled\ volume}{94{,}499.8} \rightarrow upscaled\ volume = 6.30 \times 10^{11}\ m^3$$

Compare this upscaled value to 7.72 x 10^6 m^3, the total volume of all landslides in the Pisco inventory, or 1.41 x 10^8 m^3, the volume of landslide material reported by Keefer (1994) from a 1970, M_w = 7.9 earthquake in Peru. It is 5 orders of magnitude greater than the first value, and 3 orders greater than the second! It seems highly unlikely that so many landslides were omitted from the inventory.

Even if we were to ignore this problem, we still cannot convert probability to frequency without knowing the total number of landslides in the inventory. Malamud (2003) solves this problem (with a different function) by the assumption of self-similarity and the use of congruent landslide-magnitude curves; this method will be described in the next section. For the time being, we will conclude that the inverse power law function does not fit the data.

3-Parameter Inverse Gamma Distribution

One of the shortcomings of modeling landslide volume distributions using the inverse power law distribution is the failure of the model to fit the entire range of data. Misfit for the smallest landslides has been attributed to undersampling of these sizes, possibly due to erosion of the evidence or limitations in the mapping resolution. Guzetti et al. (2001) argue that the "rollover" (fewer small landslides than medium ones) is real, and is associated with surface morphology. Malamud et al. (2003) say that

> *If the rollover were an artifact, there would be very large numbers of small landslides in nature. Field experience from many regions suggests that the required numbers of small landslides do not exist. We conclude that the rollover of the distribution for small landslides is real and not an artifact of inventory resolution.*

The 3-parameter inverse gamma distribution (also known as the Pearson 5 distribution) is proposed by Turcotte and Malamud (2004a) as a best-fit model for landslide frequency-size distributions, after a comparative test of over 300 statistical distributions. For medium or large landslide sizes, this distribution decays as a power law with an exponent of -2.40, "despite large differences in landslide

types, sizes distributions, patterns, and triggering mechanisms" (Turcotte and Malamud, 2004a.) For small landslide sizes, there is an exponential "rollover." One caveat: the proposed distribution does not work well for rockfall dominated inventories—the Pisco inventory consists of about 35% rockfalls.

The probability distribution for the 3-parameter inverse gamma function is:

$$p(A_L;\ \rho, a, s) = \frac{1}{a\Gamma(\rho)} \left[\frac{a}{A_L - s}\right]^{\rho+1} exp\left[-\frac{a}{A_L - s}\right]$$

where

A_L = landslide area
ρ = controls decay for medium and large landslides
a = controls location of maximum probability
s = controls decay for small landslides
$\Gamma(n) = (n-1)!$ or alternatively, $\Gamma(z) = \int_0^\infty t^{z-1} e^{-t} dt$

The inverse gamma distribution f(y) is obtained by substituting x = 1/y into the gamma distribution, f(x).

Figure 61 from Malamud et al. (2003) shows the probability density versus landslide area for 3 landslide inventories, which were considered to be substantially complete. The data agree very well with the 3-parameter inverse gamma distribution with parameter values ρ = 1.40, a = 1.28 x 10^{-3}, s = -1.32 x 10^{-4}, and Γ(ρ) = 0.88726, despite differences in total number of landslides in each inventory. (Northridge has 11,111; Umbria has 4233; and Guatemala has 9594.)

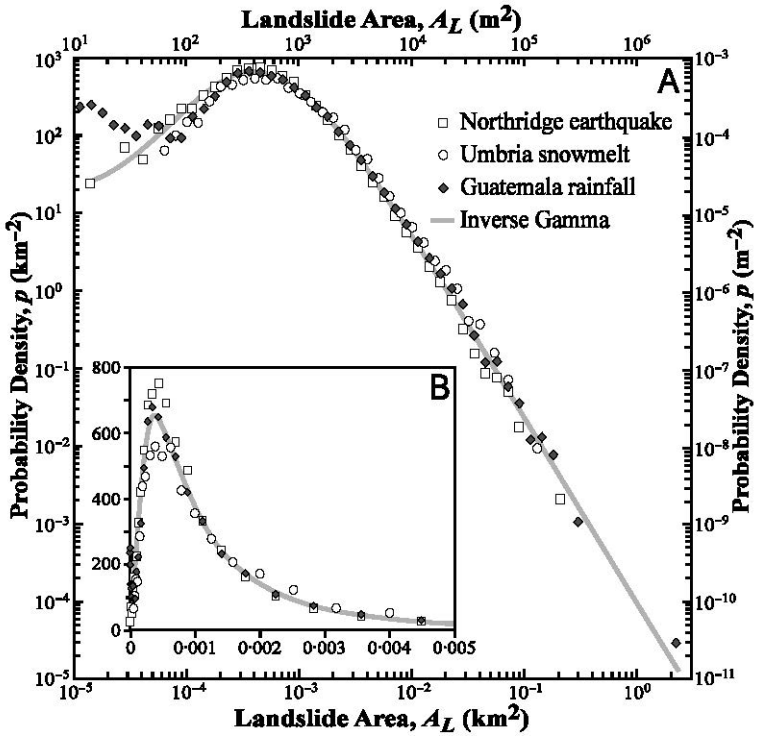

Figure 61. From Malamud et al. (2003.) Comparison of landslide inventories with 3-parameter inverse gamma distribution.

Notice how in Figure 61, the landslide size with the greatest probability is the same regardless of the number of landslides in the inventory. This is feature is characteristic of the model:

> *One implication of our landslide distribution is that since the probability distribution always has the same mean, then all landslide events should have the same mean landslide area, $\bar{A}_L$ = 3.07 x 10^{-3} km^2 = 3070 m^2 (Malamud et al., 2003.)*

Mean landslide area was determined to be:

$$\bar{A}_L = \frac{a}{\rho - 1} + s$$ Malamud et al. (2003)

Given the total number of landslides in a complete inventory (N_{LT},) the total area of all the landslides (A_{LT}) can be determined:

$$A_{LT} = N_{LT}\bar{A}_L = \left(\frac{a}{\rho - 1} + s\right) N_{LT}$$ Malamud et al. (2003)

Particularly useful is the ability to extrapolate a complete inventory (N_{LT}) from a partial inventory of the cumulative area of all landslides ($A_{LC}(\geq A_L)$) with areas greater than some value (A_L.) A_L should be large enough to be confident that no landslides with areas greater than A_L have been omitted from the inventory:

$$A_{LC}(\geq A_L) = \frac{N_{LT}}{a\Gamma(\rho)} \int_{A_L}^{\infty} \left[\frac{a}{A_L - 1}\right]^{\rho+1} exp\left[-\frac{a}{A_L - s}\right] A_L dA_L$$ Malamud et al. (2003)

In the next section, the Pisco landslide data will be plotted against Malamud et al.'s (2003) 3-parameter inverse gamma probability distribution for comparison of fit. If the fit is good, the next step is to determine if the Pisco inventory is complete, and if not, what the complete inventory ought to be according to the model. See Figure 63.

The Pisco landslide volumes were converted to areas using the relationship:

$V = \alpha A^{\gamma}$ Larsen et al. (2010)

Where

log α =-0.836 ∓ 0.015 (intercept)
γ = 1.35 ∓ 0.01 (scaling exponent for rock)

The probability density function used for the Pisco landslide data is:

$$p(A_L) = \frac{1}{N_{LT}} \frac{\delta N_L}{\delta A_L}$$ Malamud et al. (2003)

Where

$$N_{LT} = total\ number\ of\ landslides\ in\ inventory$$
$$\delta N_L = number\ of\ landslides\ in\ bin$$
$$\delta A_L = size\ of\ bin$$

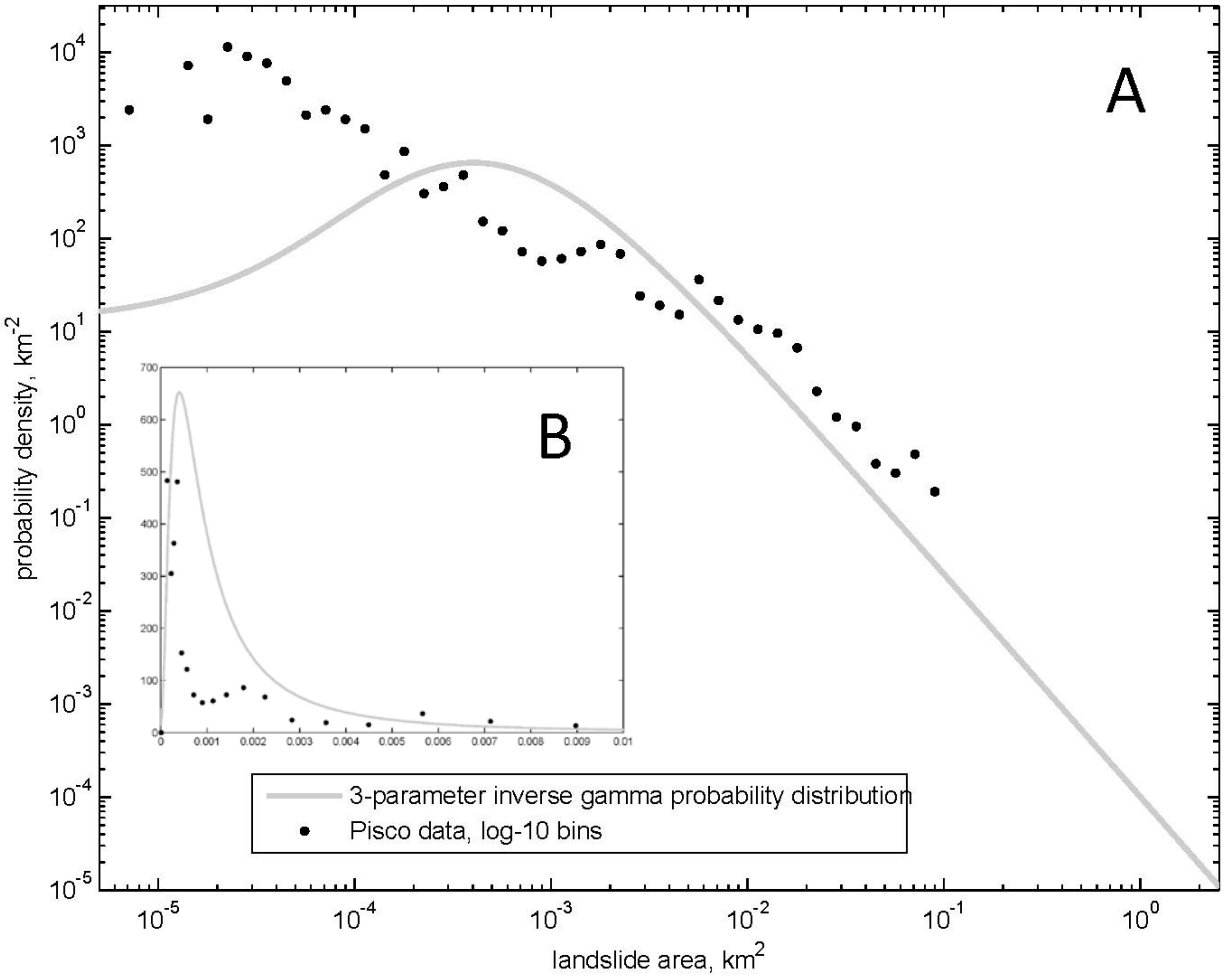

Figure 62. Pisco data plotted relative to probability distribution proposed by Malamud et al. (2003.)

Figure 62 shows a reasonably good fit for the Pisco landslide data with the tail of the 3-parameter inverse gamma distribution. However the rollover, if indeed it is a rollover and not just scatter in the data, does not fit well.

Malamud et al. (2003) predict a mean landslide area for all landslide events of $\bar{A} = 3.07 \times 10^{-3}$. The mean landslide area for the Pisco data is $\bar{A} = 1.42 \times 10^{-3}$, which is low, but within the same order of magnitude. Actual mean landslide areas for Umbria, Northridge, and Guatemala were closer to the prediction at $\bar{A} = 3.01 \times 10^{-3}$, $\bar{A} = 2.14 \times 10^{-3}$, and $\bar{A} = 3.07 \times 10^{-3}$, respectively.

For an alternative comparison, Malamud et al. 2004b show a rollover that is *less than* the predicted distribution for *incomplete* inventories; see Figure 63. Note that the data in this figure are not normalized for number of landslides in the inventory, and the graph is therefore a frequency density versus area graph, instead of a probability density versus area graph. Landslide magnitude curves are obtained using the relationship:

$$m_L = log\ A_{LT} + 2.51$$ Malamud et al. (2003)

Where

m_L = landslide magnitude is t
A_{LT} = total area of all landslides in inventory

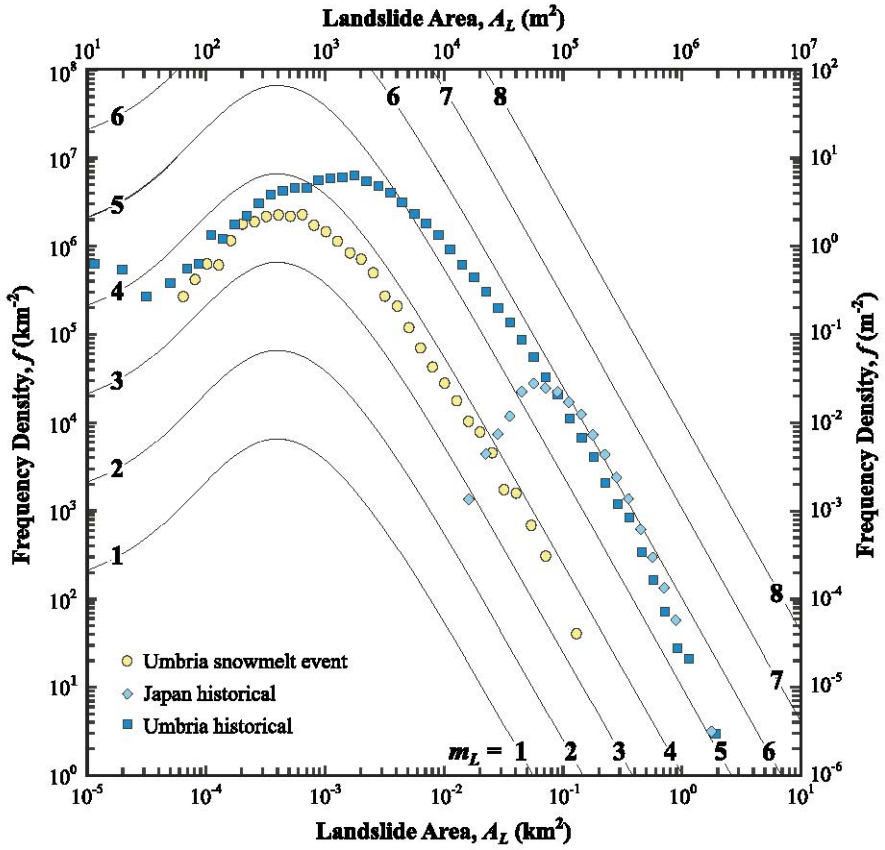

Figure 63. Frequency density of incomplete landslide inventories, from Malamud et al. (2004b.)

The equivalent frequency-density versus area graph for the Pisco data is shown in Figure 64. If the dataset is incomplete, it should be incomplete for the smaller landslide areas in the rollover part of the curve; the data in the rollover part of the curve should plot below the landslide magnitude curve, which is defined by the (presumably complete) data for the large landslides. This is not what is occurring: instead, the large landslides are defining a landslide magnitude of $m_L \cong 3$. Small-area landslides are plotting significantly above the $m_L \cong 3$ curve, and medium-area landslides are plotting below the $m_L \cong 3$ curve.

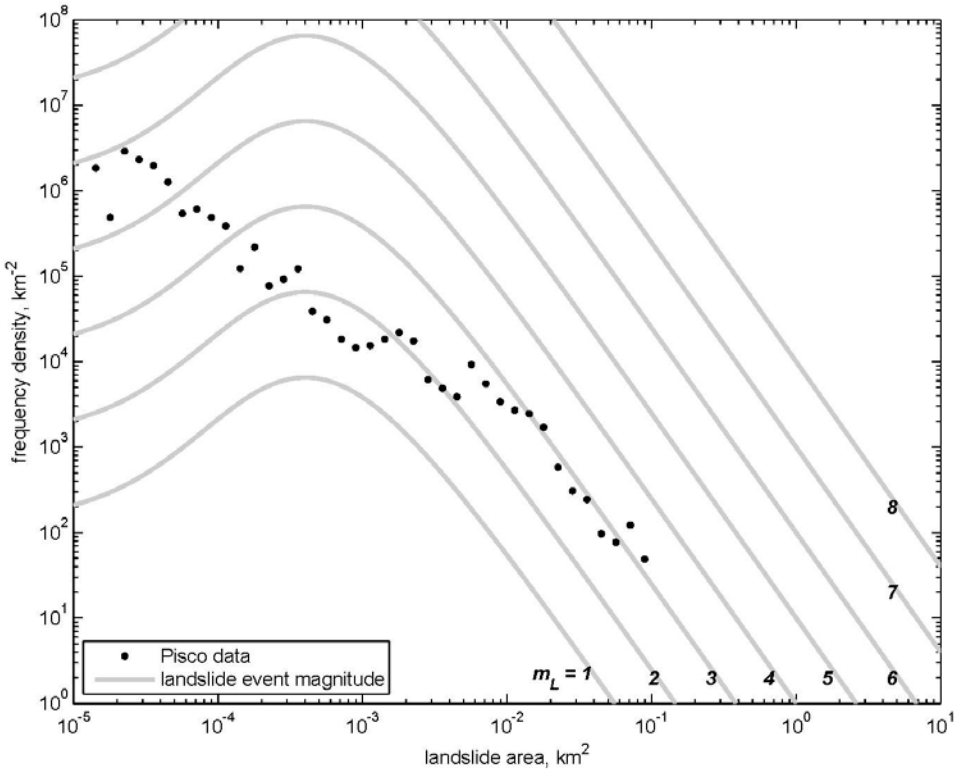

Figure 64. Frequency density of Pisco data with landslide magnitude curves.

The 3-parameter inverse gamma distribution, with parameters ρ, a, and s, as given by Malamud (2003) does not fit the Pisco data well, and unfortunately cannot be used to upscale the data.

Recall the caveat at the beginning of this section: the 3-parameter inverse gamma distribution does not work well for rockfall dominated inventories, and the Pisco inventory consists of about 35% rockfalls. Malamud (2003) does have a *power-law* correlation for rockfall dominated inventories:

$$\log f = -1.07 \log(V_R) + .37$$ Malamud et al. (2003)

Where

$$f = frequency\ density$$
$$V_R = landslide\ volume$$

Figure 65 shows the Malamud et al. (2003) power-law curve; Figure 66 shows the same curve with the Pisco data plotted. The fit seems quite good; unfortunately there is no upscaling method suggested for determining a complete inventory from a partial one.

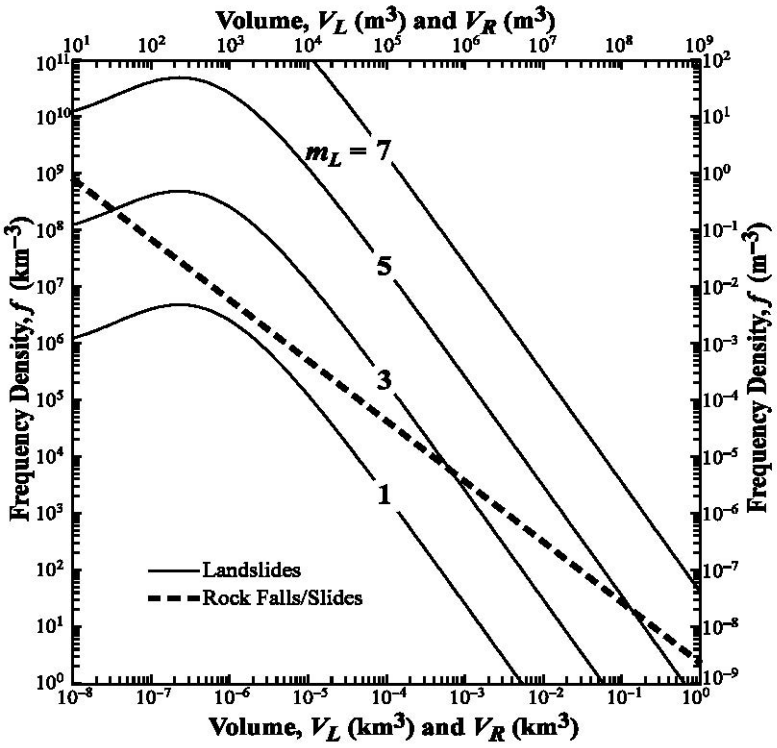

Figure 65. Power-law curve for rockfall dominated inventories from Malamud et al. (2003.)

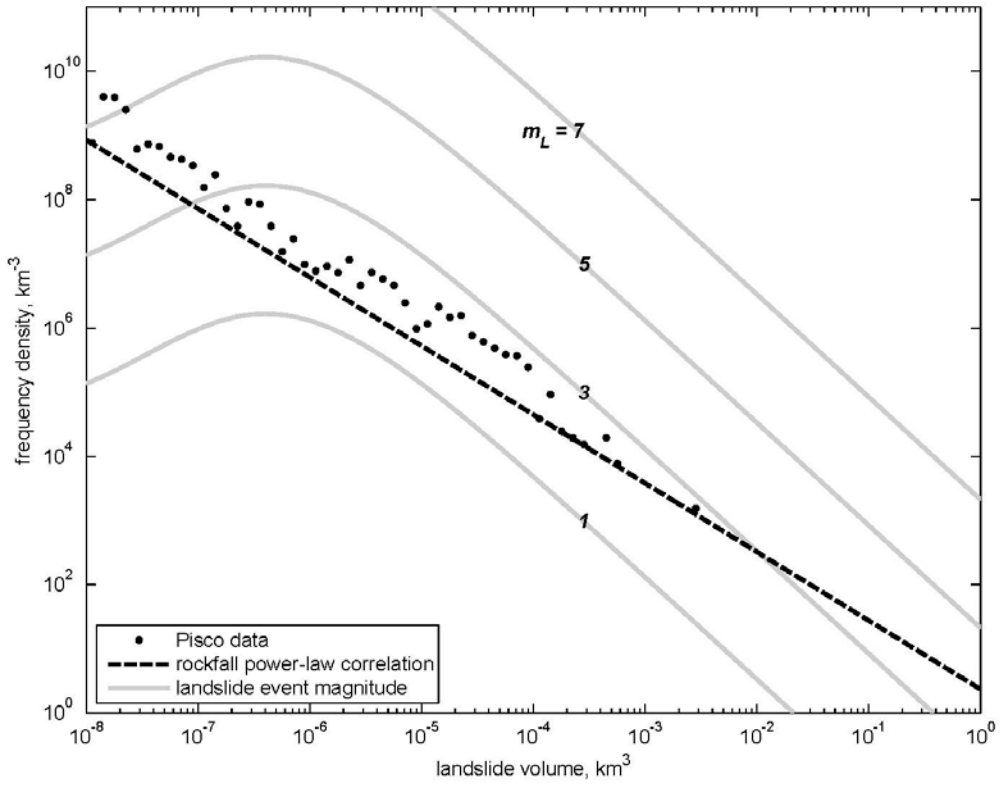

Figure 66. Malamud et al. (2003) power-law curve for rockfalls with Pisco data.

To upscale, the data is plotted as frequency versus volume, for the purpose of integrating the resulting power-law regression. See Figure 67. The Malamud (2003) rockfall correlation is included for reference.

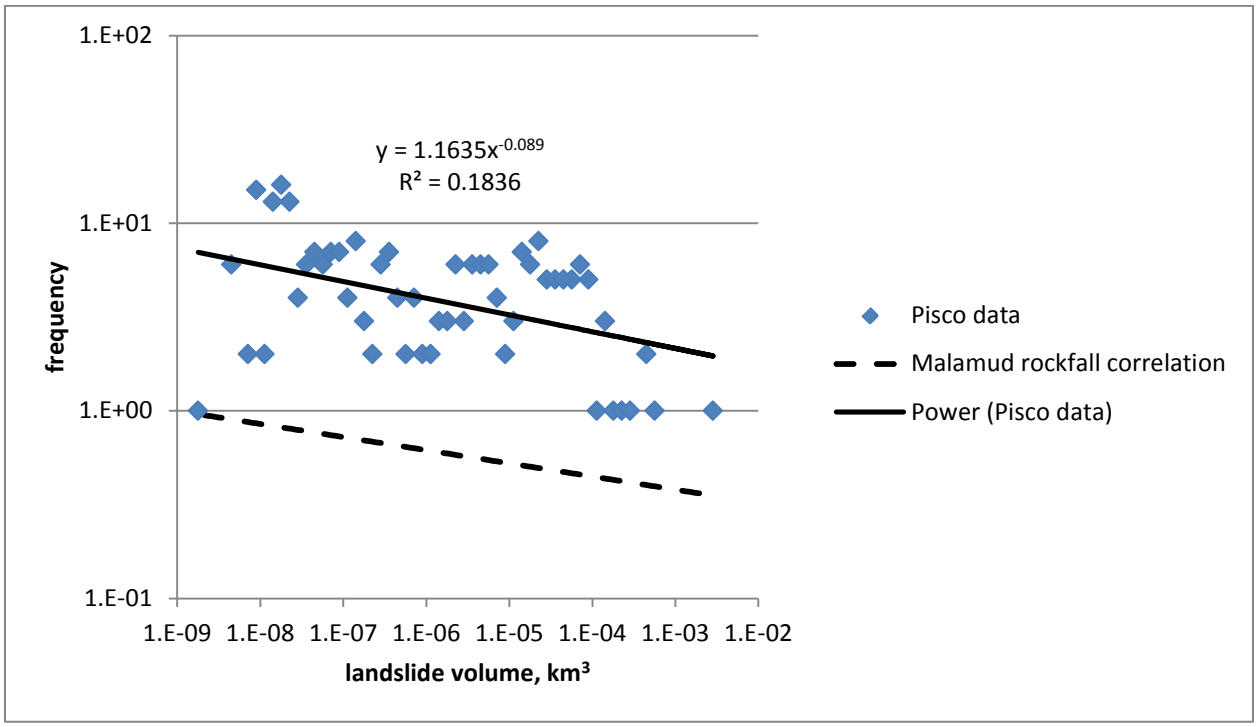

Figure 67. Best-fit power law to Pisco landslide volumes.

The definite integral

$$\int_{vol_{min}}^{vol_{max}} 1.1635x^{-0.089}\,dx \;=\; \int_{1\ m^3}^{2{,}745{,}000\ m^3} 1.1635x^{-0.089}\,dx \;=\; 9.37 \times 10^5\ m^3$$

returns a value that is smaller than the sum of the already-accounted-for landslide volumes, 7.72 x 10^6 m^3, making it useless for upscaling. This outcome is not wholly unsurprising, given the goodness-of-fit value (R^2) of 0.1836.

Lognormal Distribution

Ten Brink et al. (2009) suggests that some landslides are better approximated by a lognormal distribution, where the log of the landslide volumes is normally distributed:

> *A few landslide datasets, however, have distributions that are not easily approximated by an inverse power law distribution. Issler et al. (2005) obtained a logarithmic distribution for the volume of depositional lobes from the Storegga slide. Lognormal distributions were found for the areas of landslides in Kashmir (Dunning et al., 2007), and for volumes of deposits of pre-historic turbidity currents in Italy (Talling et al., 2007). Most recently, Chaytor et al. (2009) obtained an excellent lognormal fit to the size distribution of areas and volumes of 106 submarine slope failures along the Atlantic continental slope…*

Landslides in the Pisco inventory do not appear to be lognormally distributed; when the number of landslides is graphed relative to log of volume, the distribution is clearly not a typical bell-shape. See Figure 68.

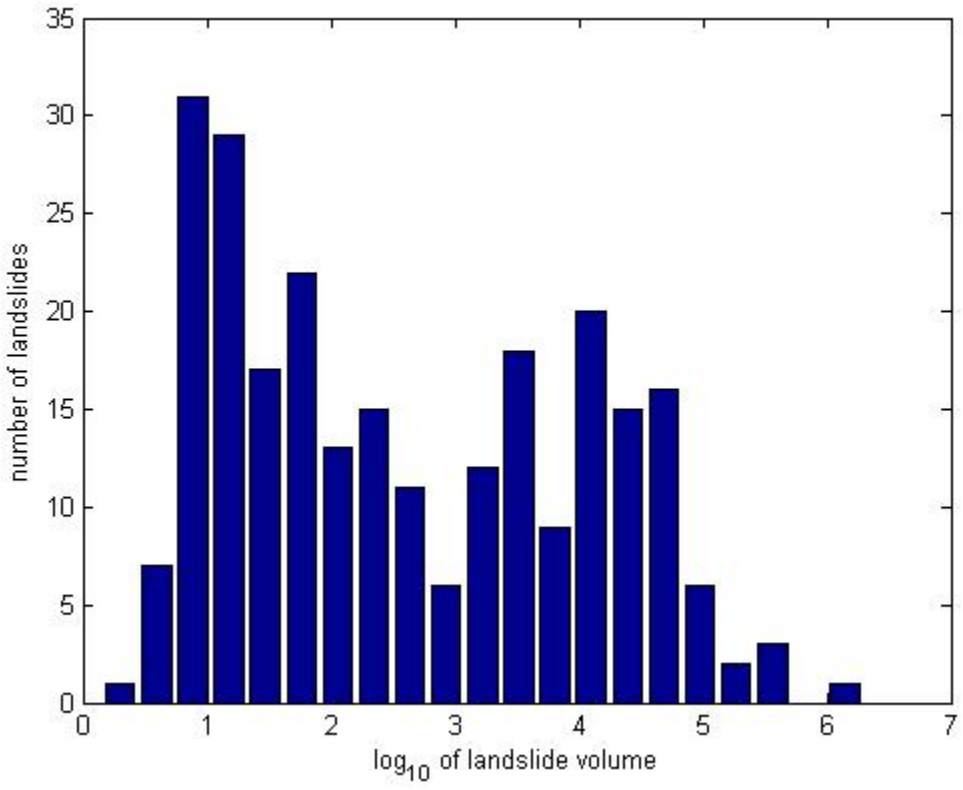

Figure 68. Histogram of log of landslide volumes.

It is interesting to compare Figure 69 with Figure 65; both figures show a deficit of mid-sized landslides and a surfeit of small landslides, compared to a typical distribution.

Conclusion for Landslide Frequency-Size Models

While it may be true that some smaller landslides were omitted from the inventory, the data in the inventory is more accurate as-is than it might be by attempting to use a power-law or other relationship to upscale it. There appears to be a deficit of mid-sized landslides in the Pisco landslide inventory relative to predictions made by frequency-size models; this deficit is probably due to a much wider Coastal Plains region (flat region) in the study area than anywhere else in Peru, along with the presence of a remnant of the landslide-resistant Coastal Cordillera. See Figure 69.

The Coastal Plains are arbitrarily delimited to elevations lower than 500 meters (the gray area to the west of the 500 m contour.) The base of Coastal Cordillera can be seen within the Coastal Plains region to the south of Pisco as an area enclosed by the 500 m contour, with a slightly higher elevation.

Ultimately, attempting to upscale the Pisco data using a frequency-size model results in upscaled values that are far too large to be reasonable.

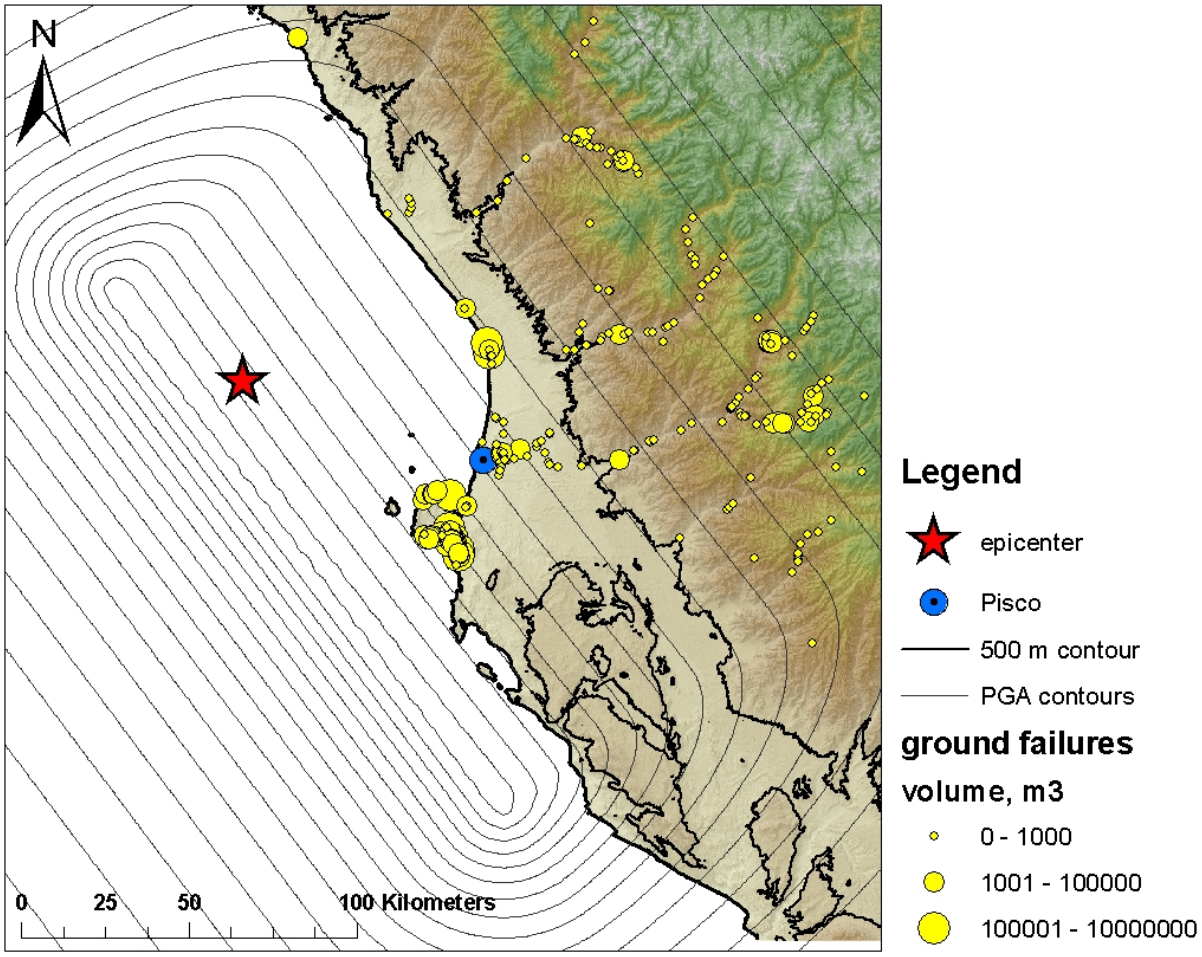

Figure 69. Wide Coastal Plains in study area, along with landslide-resistant Coastal Cordillera remnant.

Moment Magnitude-Size Model

Keefer (1994) found the following relationship between earthquake moment magnitude and landslide volume for 15 shallow (focal depth < 60km) earthquakes:

$$log_{10}V = 1.45M - 2.50 \qquad \text{Keefer (1994)}$$
$$5.3 \leq M \leq 8.6$$

Where

M = moment magnitude
V = total volume of landslide material

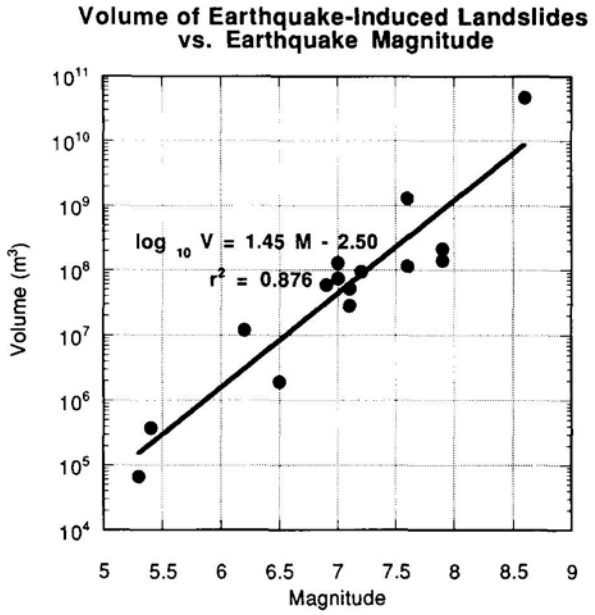

Figure 70. Keefer (1994) volume-magnitude relationship.

Applying this relationship to the Pisco data, we predict:

$$V = 10^{1.45(7.9)-2.50} = 9.02 \times 10^8\ m^3 = .902\ km^3$$

This volume prediction can be further reduced to account for the fact that the earthquake epicenter is 60 km offshore, and 57% of the area with shaking strong enough to trigger landslides is under water:

$$.43V = 3.89 \times 10^8\ m^3 = .389\ km^3$$

This predicted volume is still 2 orders of magnitude larger than sum of the individual volumes (7.72×10^6 m^3) in the Pisco inventory.

Keefer's model produces a very high predicted total volume, in part because it is not corrected for decreasing landslide density with distance from the earthquake epicenter. The mathematical model resembles Figure 71A, where 43% each of the high, medium and low landslide density areas is calculated. Physically, when considering the relationship of the epicenter to the coastline, a smaller proportion of high-density landslide area should be included in the calculation, resulting in a smaller predicted volume. See Figure 71B.

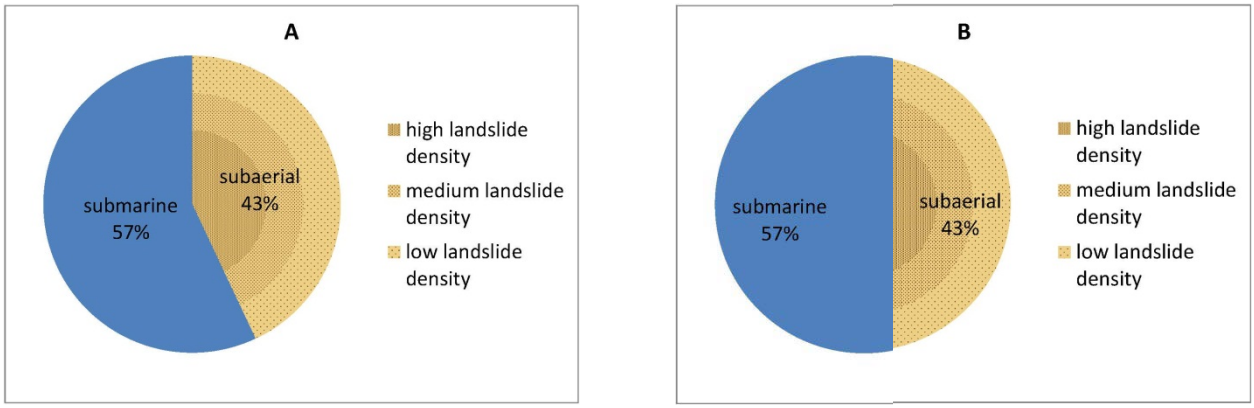

Figure 71. A) Mathematical model of susceptible area. B) Physical model of susceptible area.

In order to correct for decreasing landslide density in a portion of the total area, a relationship for landslide density with distance from the earthquake epicenter is necessary. Keefer (1994) does not include this relationship (which is probably not generalizable by earthquake magnitude, but requires additional information such as earthquake focal depth.)

Compared to volume predictions using the power-law, inverse 3-parameter gamma distribution, or lognormal distributions, Keefer's prediction is closest to the observed data. Since many subduction earthquakes have offshore epicenters, and since Keefer's (1994) model is otherwise quite good, landslide-density with distance relationships might be a worthwhile direction for further research.

Figure 72 shows the Pisco data in comparison with historical earthquake data from Peru. The Pisco landslide volume has been multiplied by the frequency of M_w=7.9 earthquakes (0.04/year) to get volume per year, and divided by 43% to account for the land area. Data for historic earthquake frequencies is from Espinosa et al. (1985) and Kanamori (1977) as reported by Keefer (1994.)

From the graph, it is apparent that the Pisco landslide volume is not only lower than the Keefer model prediction, but also quite low compared to the range of the data scatter. Conclusion: the Pisco volume is probably not typical for an M_w=7.9 earthquake in Peru, and the Keefer relationship is probably more valid than it would appear from comparison with a single earthquake event.

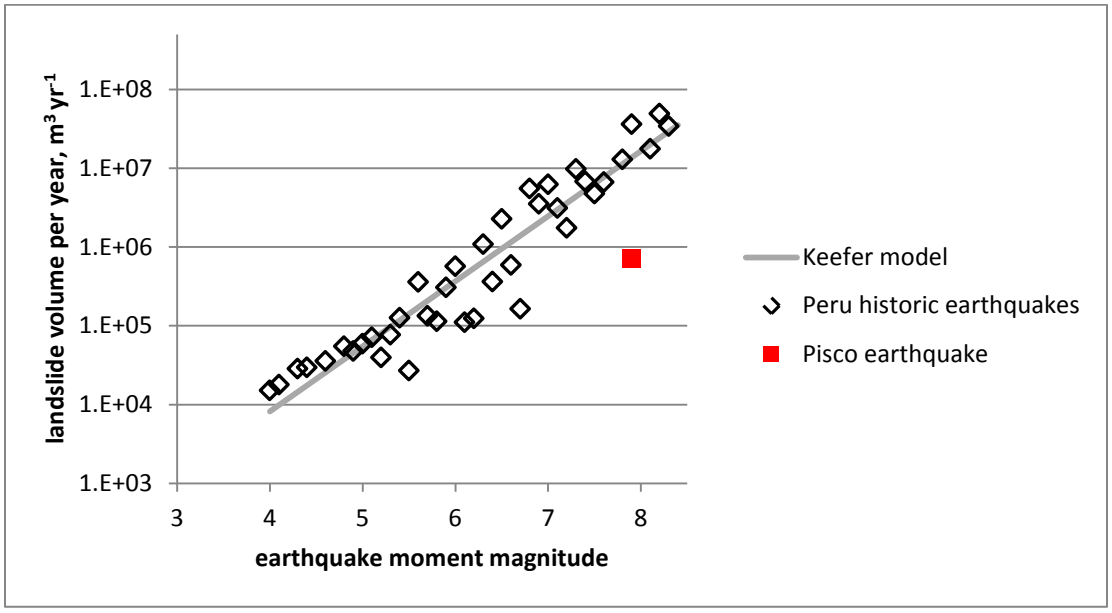

Figure 72. Pisco landslide volume, relative to historic landslide volumes for Peru and adjacent regions (parts of Ecuador, Columbia, Brazil, Bolivia, and Chile.)

As suggested in the section on frequency-size models, the Pisco landslide volumes may be unusually low because of the unusual width of the Coastal Plains in the study area, along with the presence of a remnant of the Coastal Cordillera. The area in which ground shaking might otherwise trigger medium-sized landslides is too flat, too dry, or too rocky to be susceptible.

Regional Rate of Erosion

Using earthquake magnitude-frequency data for Peru, and the Keefer (1994) magnitude-volume relationship, Keefer (1994) found the mean rate of production of earthquake-induced landslide material to be 1.70 x 10^8 m^3/year for Peru and adjacent regions. For an area of 2,308,000 km^2, this rate of landslide material production translates to a mean erosion rate of 54.63 m^3/km^2/yr, or 54.63 mm/1000 years.

Keefer (1994) also suggests that mean rate of erosion can be calculated using data from events of M ≥ 6 only:

> *…most of the total volume of earthquake-induced landslides over time is generated by a few large events; in this region, only 0.1 percent of the landslide volume over time was associated with events of M ≥ 5.0, and only 1 percent was associated with events of M ≥ 6.0, whereas 92 percent was attributable to events of M ≥ 7.0… This relation has two implications: first, the determination of V' [mean rate of production of earthquake-induced landslide material] is relatively sensitive to the F [frequency] and M [magnitude] of the largest events in the region, and, second, for practical purposes, events of M < 6 (or, in some regions, even M < 7) may be disregarded with only a negligible effect on the calculated V'.*

A single landslide event such as the Pisco earthquake-induced landslides is not sufficient to calculate regional erosion. As more data is collected, particularly high-quality before-and-after satellite imagery, the estimation of the rate of regional erosion can be further refined.

Summary and Conclusion

Landslides induced by the Pisco earthquake can be categorized by the three distinct geologic-geomorphic settings within which they occur: the Paracas Peninsula, the Coastal Plains, and the Andes Mountains. Each setting displays a predominant style of landsliding, and landslides within each setting are controlled by different sets of landslide parameters.

On the Paracas Peninsula, landslides are controlled primarily by two factors: slope and geology. Landslides occur almost exclusively along the near-vertical cliffs as rock slumps. Sedimentary units (Paleogene-Eocene marine sandstone and Carboniferous shale) are most susceptible to landsliding; by contrast, there were very few landslides in the older volcanic and plutonic units (Jurassic volcano-sedimentary and Paleozoic granite/granodiorite) and none in the Pre-Cambrian gneiss. PGA, moisture, ecological region, and roads/roadcuts are not factors that affect landsliding patterns in this region, as there is little or no variability among these parameters.

Within the Coastal Plains, ground failures are typically found in soils with shallow groundwater (Quaternary and Pleistocene alluvium and colluvium, and a Neogene uplifted marine terrace deposit) as either lateral spreads or liquefaction; no ground failures were observed in rock units. Lateral spreads are more likely to be found adjacent to roads than elsewhere. Like the Paracas Peninsula, PGA and ecological region do not affect landsliding susceptibility significantly in the Coastal Plains region.

In the Andes Mountains, there are several factors which affect landsliding susceptibility. In areas closest to the epicenter (with the highest ground shaking) rockfalls predominate. Slopes are very steep, and landslides are often associated with roads/roadcuts. There is very little moisture in this part of the Andes Mountains region. Further away from the epicenter, there is a transition from rockfalls to soil falls and soil slumps, as precipitation increases and the valley floors widen. Landslides here are still associated with roads, but in this region they begin to be increasingly associated with terraced farming and river cutbanks. Sedimentary units appear to be more susceptible to landsliding, although this factor is not as predictive of landsliding as are slope and the presence of moisture/soils. The cut-off for landsliding susceptibility coincides with an ecological region boundary, but it is likely that the concurrent decrease in slope, along with diminishing PGA, result in conditions whereby the threshold for landslide-triggering is no longer reached.

Due to the inaccessibility of much of the study area, as well as the low resolution of Google Earth imagery, it seemed likely that some landslides (particularly the smaller ones) may have been missed during reconnaissance. In addition, the total volume of landslide material for the Pisco earthquake-induced landslides is much smaller than volumes estimated for similar-magnitude earthquakes in Peru.

Three frequency-size distributions (inverse power law, 3-parameter inverse gamma, and lognormal) and one magnitude-size distribution were evaluated to determine if they could be used to upscale landslide data. Upscaling landslide volumes depends on two things: first, the premise that landslide distributions

are self-similar, regardless of triggering event, geology, geomorphology, or any other factor, and second, that the landslide inventory is complete for at least the largest landslides.

None of the distribution models fit the Pisco landslide data well; all resulted in upscaled values that were either far too large, or too small to be reasonable. Two possible explanations for this are presented: first, the landslide inventory has a significant proportion (about 35%) of rockfalls, the physics of which are so fundamentally different that the frequency-size models do not apply (as suggested by Malamud, 2003) or alternatively, while self-similarity allows for comparison of inventories with widely different characteristics, those characteristic must be consistent within the inventory itself. The Pisco inventory is too internally inconsistent to fit any of the models. Of particular note, there are far fewer medium-sized landslides than the models predict given the volume of the largest landslides. Ultimately, the landslide inventory for the Pisco earthquake-induced landslides was determined to be more accurate without modification than with any attempt at upscaling.

References

References Cited

Alarcón, J. E., Taucer, F., & So, E. (2008, October). *The 15 August 2007 Pisco, Peru, earthquake-post-earthquake field study*. Paper presented at The 14th World Conference on Earthquake Engineering, Beijing, China.

Astroza, M. Instituto Geofísico del Perú, (2007).*Intensidades y daños del terremoto de Pisco del 15 de Agosto del 2007*. Retrieved from website: http://www.igp.gob.pe/sismologia/libro/trabajo_11.pdf

Atkinson, G. M., & Boore, D. M. (2003). Empirical ground-motion relations for subduction-zone earthquakes and their application to Cascadia and other regions. *Bulletin of the Seismological Society of America*, *93*(4), 1703-1729. doi: 10.1785/0120020156

Barazangi, M., & Isaaks, B. L. (1976). Spatial distribution of earthquakes and subduction of the Nazca plate beneath South America. *Geology*, *4*(11), 686-692. doi: 10.1130/0091-7613(1976)4<686:SDOEAS>2.0CO;2

Brunetti, M. T., Guzzetti, F., & Rossi, M. (2009). Probability distributions of landslide volumes. *Nonlinear Processes in Geophysics*, *16*, 179-188. Retrieved from http://www.nonlin-processes-geophys.net/16/179/2009/npg-16-179-2009/

Burrough, P. A., & McDonell, R. A. (1998). *Principles of geographical information systems*. New York: Oxford University Press.

Casey, J.B. (2010). *Pisco Peru: Climate, global warming, and daylight charts data*. Retrieved from http://www.climate-charts.com/Locations/p/PR84691.php

Clauset, A. (2012). *Plfit*. Retrieved from http://tuvalu.santafe.edu/~aaronc/powerlaws/plfit.m

Clauset, A., Shalizi, C. R., & Newman, M. E. J. (2009). Power-law distributions in empirical data. *SIAM Review*, *51*(4), 1-43. doi: 10.1137/070710111

Cochrane, T. (2010, July 23). *Compiled data for Bolivia/Peru/Paraguay*. Retrieved from http://www.agteca.com/climate.htm

DeMets, C., Gordon, R. G., Argus, D. F., & Stein, S. (2007). Current plate motions. *Geophysical Journal International, 101(2)*, 425-478. doi: 10.1111/j.1365-246X.1990.tb06579.x

Dewey, J. F., & Lamb, S. H. (1992). Active tectonics of the Andes. *Tectonophysics, 205(1-3)*, 79-95. doi: 10.1016/0040-1951(92)90419-7

Espinoza, A. F., Casaverde, L. A., Michael, J. A., Alva-Hurtado, J., & Vargas-Neumann, J. U.S. Geological Survey, (1985). *Earthquake catalog of Peru: U.S. Geological Survey open-file report, 85-286, p. 615.*

Guzetti, F., Malamud, B. D., Turcotte, D. L., & Reichenbach, P. (2002). Power-law correlations of landslide areas in central Italy. *Earth and Planetary Science Letters*, *195*, 169-183.

Hearn, P. P., & Geological Survey (U.S.). (2000). Global GIS database: Digital atlas of Central and South America. Flagstaff. AZ: USGS.

Instituto Geológica Minero Y Metalúrgico, (1995). *Geologia del Perú; Boletin no 55; Serie a: Carta geólica nacional*. Lima, Perú: Fimart S.A.

Instituto Geológica Minero Y Metalúrgico, (2007). *Movimientos en masas y deformaciones superficiales asociados al sismo de Pisco, 2007*. Lima, Perú: INGEMMET.

Jordan, T. E., Isaaks, B. L., Allmendinger, R. W., Brewer, J. A., Ramos, V. A., & Ando, C. J. (1983). Andean tectonics related to geometry of subducted Nazca plate. *Geological Society of America Bulletin*, *94*(3), 341-361. doi: 10.1130/0016-7606(1983)94<341:ATRTGO>2.0.CO;2

Kanno, T., Narita, A., Morikawa, N., Fujiwara, H., & Yoshimitsu, F. (2006). A new attenuation relation for strong ground motion in Japan based on recorded data. *Bulletin of the Seismological Society of America*, *96*(3), 879-897. doi: 10.1785/0120050138

Keefer, D. K. (1984). Landslides caused by earthquakes. *Geological Society of America Bulletin*, *95*, 406-421.

Keefer, D. K. (1994). The importance of earthquake-induced landslides to long-term slope erosion and slope-failure hazards in seismically active regions. *Geomorphology*, *10*, 265-284.

Keefer, D.K. (1999). Earthquake-induced landslides and their effects on alluvial fans. *Journal of Sedimentary Research*, 69-1, 84-104.

Larsen, I. J., Montgomery, D. R., & Korup, O. (2010). Landslide erosion controlled by hillslope material. *Nature Geoscience*, *3*, doi: 10.1038/NGEO776

Malamud, B. D., Turcotte, D. L., Guzzetti, F., & Reichenbach, P. (2004). Landslides, earthquakes, and erosion. *Earth and Planetary Science Letters*,*229*, 45-59.

Malamud, B. D., Turcotte, D. L., Guzzetti, F., & Reichenbach, P. (2003). Landslide inventories and their statistical properties. *Earth surface Processes and Landforms*, *29*, 687-711. doi: 10.1002/esp.1064

McGeary, S., Nur, A., & Ben-Avraham, Z. (1985). Spatial gaps in arc volcanism: The effect of collision or subduction of oceanic plateaus. Tectonophysics, 119(1-4), 195-221. doi: 10.1016/0040-1951(85)90039-3

McVerry, G. H., Zhao, J. X., Abrahamson, N. A., & Somerville, P. G. (2006). New Zealand acceleration response spectrum attenuation relations for crustal and subduction zone earthquakes. *Bulletin of the New Zealand Society for Earthquake Engineering*, *39*(1), 1-58.

Mohindra, R., Nair, A. K. S., Gupta, S., Sur, U., & Solokov, V. (2012). Probabilistic seismic hazard analysis for Yemen. *International Journal of Geophysics*, *2012*, doi: 10.1155/2012/304235

National Aeronautics and Space Administration (NASA) and Ministry of Economy, Trade and Industry of Japan (METI). (2011). *ASTER Global digital elevation model* [Data files]. Retrieved from http://www.gdem.aster.ersdac.or.jp/search.jsp

Newman, M. E. J. (2006). *Power laws, Pareto distributions and Zipf's law*. *Contemporary Physics*, *46*(5), 323-351. doi: 10.1080/00107510500052444

Nur, A., & Ben-Avraham, Z. (1982). *Oceanic plateaus, the fragmentation of continents, and mountain building*. Journal of Geophysical Research, 87(B5), 3644-3661. doi: 10.1029/JB087iB05p03644

One geology. (n.d.). Retrieved from http://portal.onegeology.org/

Pilger, R. H. (1981*). Plate reconstructions, aseismic ridges, and low-angle subduction beneath the Andes*. Geological Society of America Bulletin, 92(7), 448-459. doi: 10.1130/0016-7606(1981)92<448:PRARAL> 2.0.CO;2

Rodrigez-Marek, A. (2008, May 20). *Geotechnical aspects of the August 15, 2007, M_w 8.0 Pisco, Peru earthquake: Preliminary observations*. Retrieved from http://www.geerassociation.org/GEER_Activities/GEESD_IV/GEESDIV_RodriguezMarek.pdf

Ruiz, S., & Saragoni, G. (2005). Attenuation equations for subduction zone earthquakes in Chile considering two seismogenic mechanisms and site effects. *IX Jornadas Chilenas de Sismologia e Ingeneria Antisismica*, Concepcion, Chile. Paper No. A01-15 (in Spanish)

Scherbaum, F., Cotton, F., & Smit, P. (2004). On the use of response spectral-reference data for the selection and ranking of ground-motion models for seismic hazard analysis in regions of moderate seismicity: The case of rock motion. *Bulletin of the Seismological Society of America*, *94*(6), 2164-2185. doi: 10.1007/s000240050240

Steffen, D., Schlunegger, F., & Preussner, F. (2009). Drainage basin response to climate change in the Pisco valley, Peru. *Geological Society of America*, *37*(6), 491-494. doi: 10.1130/G25475A.1

Tavera, H., Bernal, I., Strasser, F. O., Arango-Gaviria, M. C., Alarcón, J. E., & Bommer, J. J. (2008). Ground motions observed during the 15 August 2007 Pisco, Peru, earthquake. *Bulletin of Earthquake Engineering*, *7*(1), 71-111. doi: 10.1007/s10518-008-9083-4

Tavera, H., & Bernal, I. (2008). The Pisco (Peru) earthquake of 15 August 2007. *Seismological Research Letters*, *79*(4), 510-515. doi: 10.1785/gssrl.79.4.510

ten Brink, U. S., Barkan, R., Andrews, B. D., & Chaytor, J. D. (2009). Size distributions and failure initiation of submarine and subaerial landslides. *Earth and Planetary Science Letters*, *287*, 31-42. doi: 10.1016/j.epsl.2009.07.031

Turcotte, D. L., & Malamud, B. D. (2004). Landslides, forest fires, and earthquakes: Examples of self-organized criticality. *Physica A*, *340*, 580-589. doi: 10.1016/j.physa.2004.05.009

U.S. Geological Survey, National Earthquake Information Center. (2012). *Magnitude 8.0 - near the coast of central Peru*. Retrieved from World Data Center for Seismology website: http://earthquake.usgs.gov/earthquakes/eqinthenews/2007/us2007gbcv/

Wald, D. J., Quitoriano, V., Heaton, T. H., & Kanamori, H. (1999). Relationships between peak ground acceleration, peak ground velocity, and modified Mercalli intensity in California. *Earthquake Spectra*,*15*(3), doi: http://dx.doi.org/10.1193/1.1586058

Wartman, J. (2010). [Pisco, Peru, earthquake-induced landslides]. Unpublished raw data.

Wipf, M. A. (2006). *Evolution of the western cordillera and coastal margin of Peru: Evidence from low-temperature thermochronology and geomorphology (Doctoral dissertation)*. Swiss Federal Institute of Technology, Zürich.

Zavala, B., Hermanns, R., Valderrama, P., Costa, C., & Rosado, M. (2009). Procesos geológicos e intensidad macrosísmica inqua del sismo Pisco del 15/08/2007, Perú. *Revista de la Asociatión Geológica Argentina*, *65*(4), 760-779.

Zhao, J. X., Zhang, J., Asano, A., Ohno, Y., Oouchi, T., & Takahashi, T., et al. (2006b). Attenuation relations of strong ground motion in Japan using site classification based on predominant period. *Bulletin of the Seismological Society of America*, *96*(3), 914-925. doi: 10.1785/0120050122

Additional References

Allmendiger, R. W., & González, G. (2010). Neogene to quaternary tectonics of the coastal cordillera, northern Chile. *Tectonophysics*, *495*(1-2), 93-110. Retrieved from http://dx.doi.org/10.1016/j.tecto.2009.04.019

Atkinson, P. M., & Massari, R. (1998). Generalised linear modeling of susceptibility to landsliding in the central Apennines, Italy. *Computers and Geosciences*, *24*(4), 373-385.

Barrientos, S. E. (2007). Earthquakes in Chile. In T. Moreno & W. Gibbons (Eds.), *The Geology of Chile* (pp. 263-395). Barcelona: The Geological Society of London.

Cembrano, J., Lavenu, A., Yañez, G., Riquelme, R., García, M., González, G., & Hérail, G. (2007). Neotectonics. In T. Moreno & W. Gibbons (Eds.), *The Geology of Chile* (pp. 231-262). Barcelona: The Geological Society of London.

Chigara, M., Wu, X., Inokuchi, T., & Wang, G. (2010). Landslides induced by the 2008 Wenchuan earthquake, Sichuan, China. *Geomorphology*, *118*(3-4), 225-238. doi: 10.1016/j.geomorph.2010.01.003

Cobbold, P. R., Rossello, E. A., Roperch, P., Arriagada, C., Gómez , L., & Lima, C. (2007). Distribution, timing, and causes of Andean deformation across South America. *Geological Society of London, Special Publications*, *272*, 321-343. doi: 10.1144/GSL.SP.2007.272.01.17

Deneven, W. M., Stewart, N. R., & Velasquez, M. T. (2012). Andes mountains. In *Encyclopædia Britannica* Retrieved from http://www.britannica.com/EBchecked/topic/23692/Andes-Mountains

Dorbath, L., Cisternas, A., & Dorbath, C. (1990). Assessment of the size of large and great historical earthquakes in Peru. *Bulletin of the Seismological Society of America*, *80*(3), 551-576.

Elnashai, A. S., Alva-Hurtado, J., Pineda, O., Kwon, O. S., Moran-Yunez, L., Huaco, G., & Pluta, G. University of Illinois at Urbana-Champagne, Civil and Environmental Engineering Department. (2008). *The Pisco-Chincha earthquake of August 15, 2007*. Urbana: Mid-America Earthquake Center.

Gallant, J. Commonwealth Scientific and Industrial Research Organisation Land and Water, (2001).*Topographic scaling for the NLWRA sediment project*. Canberra: CSIRO.

Gansser, A. (1973). Facts and theories on the Andes: Twenty-sixth William Smith lecture. *Journal of the Geological Society*, *129*(2), 93-131. doi: 10.1144/gsjgs.129.2.0093

Gentry, A. H., Herrera-MacBryde, O., Huber, O., Nelson, B., & Villamil, C. B. (1995). *South America regional overview*. Retrieved from http://botany.si.edu/projects/cpd/sa/sa.htm

Gorum, T., Fan, X., van Westen, C. J., Huang, R. Q., Xu, Q., Tang, C., & Wang, G. (2010). Distribution pattern of earthquake-induced landslides triggered by the 12 May 2008 Wenchuan earthquake. *Geomorphology*, doi: 10.1016/j.geomorph.2010.12.030.

Johansson, J., Mayorca, P., Torres, T., & Leon, E. (2007, November 15). *A reconnaissance report on the Pisco, Peru earthquake of August 15, 2007*. Retrieved from http://shake.iis.u-tokyo.ac.jp/Peru2007/JSCE_JAEE_Report/Index.htm

Keefer, D. K., & Moseley, M. E. (2004). Southern Peru desert shattered by the great 2001 earthquake: Implications for paleoseismic and paleo-El Niño--southern oscillation records. *Proceedings of the National Academy of Sciences*, *101*(30), 10878-10883.

Keefer, D. K., & Wilson, R. C. (1989). Predicting earthquake-induced landslides with emphasis on arid and semi-arid environments. In P. M. Sadler & D. M. Morton (Eds.), *Landslides in a Semi-arid Environment with Emphasis on the Inland Valleys of Southern California* (pp. 118-149). Riverside: Inland Geological Society of Southern California Publications.

Malamud, B. D., Turcotte, D. L., Guzzetti, F., & Reichenbach, P. (2004). Landslides, earthquakes, and erosion. *Earth and Planetary Science Letters*,*229*, 45-59.

Meunier, P., Hovius, N., & Haines, A. J. (2007). Regional patterns of earthquake-triggered landslides and their relation to ground motion. *Geophysical Research Letters*, *34*(LGL03133720408), doi: 10.1029/2007GL031337

McVerry, G. H., Zhao, J. X., Abrahamson, N. A., & Somerville, P. G. (2000). *Subduction zone attenuation relations for New Zealand earthquakes*. Paper presented at 12th world conference on earthquake engineering.

Moon, A. T., Wilson, R. A., & Flentjie, P. N. (2005, June). *Developing and using landslide size frequency models*. Paper presented at International conference on landslide risk management, 18th annual Vancouver geotechnical society symposium.

O'Connor, J. S., Mesa, L., & Nykamp, M. A. National Technical Information Service, (2008). *Damage to the highway system from the Pisco, Peru earthquake of August 15, 2007*. Buffalo: MCEER, State University of New York.

One geology. (n.d.). Retrieved from http://portal.onegeology.org/

Pedoja, K., Ortlieb, L., Dumont, J. F., Lamothe, M., Ghaleb, B., Auclair, M., & Labrousse, B. (2006). *Quaternary coastal uplift along the Talera arc (Ecuador, northern Peru) from new marine terrace data*. *Marine Geology*, *228*, 73-91. doi: 10.1016/j.margeo.2006.01.004

Rodriguez-Marek, A., Hurtado, J. A., Cox, B., Meneses, J., Moreno, V., Olcese, M., Sancio, R., & Wartman, J. (2007, September 8). *Preliminary reconnaissance report on the geotechnical engineering aspects of the August 15, 2007 Pisco, Peru earthquake*. Retrieved from http://www.geerassociation.org/GEER_Post EQ Reports/Peru_2007/Cover_Peru2007.html

Stark, C. P., & Hovius, N. (2001). The characterization of landslide size distributions. *Geophysical Research Letters*, *28*(6), 1091-1094.

Sufri, O., Koper, K., & Lay, T. (2012). Along-dip seismic radiation segmentation during the 2007 M_w 8.0 Pisco, Peru earthquake, *Geophysical Research Letters*, 39, L08311, doi:10.1029/2012GL051316

Tavera, H., Bernal, I., Strasser, F. O., Arango-Gaviria, M. C., Alarcón, J. E., & Bommer, J. J. (2008). Ground motions observed during the 15 August 2007 Pisco, Peru, earthquake. *Bulletin of Earthquake Engineering*, *7*(1), 71-111. doi: 10.1007/s10518-008-9083-4

Turner, T. R., Duke, S. D., Fransen, B. R., Reiter, M. L., Kroll, A. J., Ward, J. W., … Bilby, R. E. (2010). Landslide densities associated with rainfall, stand age, and topography on forested landscapes, southwestern Washington, USA. *Forest Ecology and Management*, *259*, 2233-2247. doi: 10.1016/j.foreco.2010.01.051

van den Eeckhaut, M., Vanwalleghem, T., Poesen, J., Govers, G., Verstraeten, G., & Vandekerckhove, L. (2006). Prediction of landslide susceptibility using rare events logistic regression: A case study in the Flemish Ardennes (Belgium). *Geomorphology*, *76*, 392-410. doi: 10.1016/j.geomorph.2005.12.003

Wartman, J., & Malasavage, N. E. (2010). Spatial analysis for identifying concentrations of urban damage. In A. C. de Pina Filho & A. C. de Pina (Eds.), *Methods and Techniques in Urban Engineering* (pp. 85-108). India: InTech.

Wipf, M. A. (2006). *Evolution of the western cordillera and coastal margin of Peru: Evidence from low-temperature thermochronology and geomorphology (Doctoral dissertation)*. Swiss Federal Institute of Technology, Zürich.

Wortel, M. J. R. (1984). Spatial and temporal variations in the Andean subduction zone. *Journal of the Geological Society*, *141*, 783-791. doi: 10.1144/gsjgs.141.5.0783

Appendix A: Landslide Inventories

Introduction

The INGEMMET landslide data in Appendix A are directly excerpted from INGEMMET (2007). Text in red (numbering) has been added by the author for clarification.

The Zavala (2009) landslide points are identical to the INGEMMET points for landslides in Cuadro 2. Cuadro 1 points are unique to Zavala, and are primarily classified as liquefaction (with some cracking and/or settlement.)

Dr. Joseph Wartman inventoried at total of 245 landslides during his 2007 and 2010 field reconnaissance trips to Peru. In some cases, careful measurement using tape measures and GPS points of landslides previously inventoried by INGEMMET resulted in amended landslide volumes. These amended landslides are presented in a separate table.

The landslides for each inventory were mapped and compared against each other to remove any redundancy, and create the final combined landslide inventory. In cases where the landslide descriptions (for landsliding type and volume) were inconsistent, the data from Dr. Joseph Wartman was used.

CUADRO Nº 1
MOVIMIENTOS EN MASA DETONADOS POR EL SISMO EN LOS ACANTILADOS DE LA RNP

SECTOR/ PARAJE	COORDEN. (WGS84)	MORFOLOGÍA	DESCRIPCIÓN DE MOVIMIENTOS EN MASA Y VOLUMEN	SUBSTRATO ROCOSO /SUELO	INTENS. INQUA	DAÑOS OCASIONADOS	DISTANCIA AL EPICENTRO
Playa Talpo 1	8474902 N 356397 E	Acantilado y planicie costera	Grandes colapsos de material rocoso sedimentario; agrietamientos y asentamientos de terrenos. Volumen: 30 m³.	Areniscas y limolitas de la Formación Paracas.	VII	No se registran daños.	48.77
Lechuza Baja (Playa Los Choros) 2	8461600 N 352520 E	Planicie costanera que termina hacia el mar como acantilados de 20 a 50 m de altura.	Derrumbes o colapsos de material sedimentario. Volumen: 70 m³.	Sedimentitas compuestas de areniscas y limolitas de la Formación Paracas	VI-VII	No se reportaron daños	50.52
Punta Arquillo: Mirador de Lobos Nº 3 3	8460490 N 353963 E	Acantilado rocoso	Fuertes agrietamientos en el acantilado; derrumbes y deslizamientos en cuñas. Fractura principal N170°. 83°O; otras fRacturas N20°, N 165° y N40° en el sector. Volumen: 15 m³	Sedimentitas compuestas de areniscas y limonitas de la Formación Paracas	VII	Rajaduras en el acceso hacia el mirador. Afectación de hábitat de fauna marina (lobos) en actual período de fecundación.	52.31
Punta Arquillo (Mirador de Lobos Nº 2) 4	8460580 N 354189 E	Acantilado marino	Fallamiento superficial con fracturas abiertas en el substrato rocoso; formación de bloques inestables en cuñas con caída de rocas y colapsos, zona muy	Sedimentitas compuestas de areniscas y limonitas de la Formación Paracas	VII	Rajaduras en el mirador y el acceso hacia éste. Afectación de hábitat de fauna marina en actual período de fecundación.	52.32

			inestable. Sistemas de fracturas abiertas: 1) N90°; 2) N8°; 3) N110°. Aberturas de 3 a 7 cm y profundidad de 0,68 m. Cuña favorable con abertura de 20 a 40 cm y profundidad de 3,5 a 4 m. Volumen: 15 m³.				
Punta Arquillo 5 Mirador de Lobos Nº 1	8461020 N 354370 E	Acantilado subvertical	Caída de rocas en el sector. Disturbación de habitat de lobos. Volumen: 15 m³.	Areniscas y limonitas de la Formación Paracas	VII	Se recomienda mover mirador unos 15-20 m hacia el sur para poder apreciar nuevo habitat de lobos.	52.22
Playa Arquillo 6	8461114 N 354465 E	Terraza amplia que termina como acantilado de 15 a 25 m de altura.	Abundantes derrumbes con caída de grandes bloques de rocas. Deslizamiento al borde acantilado, con asentamiento de 25 a 30 cm de terreno, profundidad mayor a 10 m, aparentemente reactivado con réplicas. Hacia el lado sur del acantilado agrietamientos a 5-8 m del acantilado con aberturas de 5-15 cm. Profundidad de 1,80 m. Volumen: 250 m³.	Secuencias horizontales de la Formación Paracas	VII	No se reportan daños. Zona de pescadores.	52.57
Punta Prieto 7	8460994 N 355915 E	Acantilados rocosos y conos de talus de detritos.	Zona con grandes agrietamientos y grandes derrumbes y caída de rocas en una longitud de 500 m en	Sedimentitas compuestas de areniscas y limonitas de la	VII	No se reportan daños. Zona de pescadores.	53,72

			forma discontinua. Bloques de material caído de 0,10 m hasta 0,50 m, excepcionalmente 1,0 m de diámetro. Volumen: 150 m³.	Formación Paracas			
Playa La Mina 8	8461352 N 357748 E	Acantilado marino subvertical y playa angosta de arena	Agrietamientos a 15 y 20 m del acantilado con aberturas de 0,15-0,20 m y profundidades de 1,0 m; reactivaciones de fracturas del substrato rocoso (Ambo). Pequeños sectores con caída de rocas (tamaños de 0,50 a 1,50 m de diámetro); cuñas. Sistemas de fracturas: 1) N38°.74°E; 2) N165°.90°; 3) N86°.87°S; 4) N35°. Volumen: 10 m³.	Lutitas negras con niveles de carbón; sedimentitas de la Formación Paracas	VI-VII	No se reportaron daños	55,08
Entre Frontón y La Mina acceso a La Mina 9	8462360 N 357586 E	Ladera de colina alta con pendiente mayor a 60° que termina abruptamente hacia el acantilado	Gran deslizamiento rotacional con escarpa semicircular de 100 m, asentamientos en la plataforma de carretera; agrietamientos y derrumbes en el acantilado. Profundidad de escarpa principal de 2,30 a 5,50 y salto de 0,70 a 0,93 m y abertura de 0,60 a 1,03 m; dos grietas secundarias;	Lutitas y limoarcillitas muy fisibles y fracturadas de la Formación Paracas.	VII	Afectó tramo de trocha de acceso a La Mina	32,04

			desnivel entre escarpa y pie de 15 a 20 m. Volumen: 12 000 m³.				
Playa Roja 10	8463830 N 359080 E	Planicie baja que termina en acantilados de 8 a 10 m de altura	Agrietamientos en zona de planicie; caída de rocas y derrumbes en la zona de acantilado en un tramo de 600 m de acantilado. Cuñas inversas y agrietamientos paralelos al acantilado. Sistemas de fracturas: N87°.51°N; N76° y N160°. Volumen: 120 m³.	Secuencias de la Formación Paracas	VII	No se registraron daños.	55,22
Cerca de Punta Santa María 11	8463696 N 359861 S		Agrietamientos y deformaciones en el terreno de dirección N140. Volumen: 30 m³.	Secuencias de la Formación Paracas con niveles de lumaquelas con fósiles	VII	No se registraron daños	55,94
Acantilados en Playa Yumaque 12	8460947 N 361498 E	Acantilado marino menor a 12 m de altura	Agrietamientos en secuencias de lutitas muy fisibles. Fracturas N36°; N80° a N75°; caída de rocas, derrumbes y deslizamientos hacia la playa. Volumen: 80 m³.	Secuencias de la Formación Paracas	VII	No se registraron daños; gran disturbación de acantilados.	58,56
Punta del Cielo 13	8460083 N 360487 E	Acantilado marino subvertical	Zona con fuertes agrietamientos, mostrando zonas inestables con presencia de deslizamientos y caída de rocas.	Lutitas y limoarcillitas muy fisibles y fracturadas.	VII-VIII	Desprendimiento de grandes masas rocosas en un área de 500 m	57,84

Punta del Cielo 14	8459863 N 360157 E	Acantilado marino subvertical	Fuertes agrietamientos en el substrato. Fracturamientos antiguos reactivados (N160°); Sistemas actuales N128° y N98°. Caída de rocas en un tramo de 450 m. Volumen: 250 m³.	Lutitas y limoarcillitas muy fisibles y fracturadas. Diques sedimentarios.	VII-VIII		58,27
Punta del Cielo 15	8460718 N 361162 E	Acantilado marino subvertical	Bloques fracturados que forman cuñas; aberturas de 0,30 a 0,45 m y 2 a 3 m de profundidad. Desprendimiento de grandes masas rocosas en un área de 500 m; deslizamientos y derrumbes. Volumen: 350 m³.	Lutitas y limoarcillitas muy fisibles y fracturadas.	VII-VIII		58,46
La Catedral y La Bóveda 16	8459850 N 360050 E	Acantilados de 50-60 m de altura	Agrietamientos y fracturas abiertas de hasta 0,80 m y 3 m de profundidad, en el talud o acantilado; Tres fracturas abiertas principales: N110-115°; N15°.42°=; N75°.90° y una principal N-S.59°O que afectó principalmente La catedral; grandes derrumbes y deslizamientos en cuñas en un tramo de 1500. Volumen: 750 m³.	Substrato de la Formación Paracas con lutitas muy fisibles y muy fracturadas	VII-VIII	Destrucción de lugar turístico de la RNP; agrietamientos en el mirador y obstrucción en el sector de La Bóveda	57,49

Playa Salinas y Frayles 17	8456115 N 362631 E	Acantilados de 20 a 50 m de altura	Zona muy fuertemente disturbada con grandes derrumbes y caída de rocas hacia la playa en un tramo de 3 km, discontinuo; abundantes agrietamientos que forman cuñas y bloques desde el borde o acantilado hasta 80 m hacia tierra adentro. Volumen: 600 m³.	Substrato de la Formación Paracas con lutitas muy fisibles y muy fracturadas	VII	Desprendimiento de grandes masas rocosas en un área de 1000 m	62,31
Sector Puente 18	8452572 N 361970 E	Zona de acantilados y planicie costanera; playa de cantos.	Agrietamientos en la zona de planicie hasta una longitud de 80 m desde el acantilado, derrumbes y caída de grandes bloques en los acantilados en un tramo de 300 m. Volumen: 45 m³.	Lutitas muy fisibles de la Formación Paracas; delgada cobertura eólica	VII	No se reportaron daños.	63,78

CUADRO N° 2
MOVIMIENTOS EN MASA DETONADOS POR EL SISMO EN LOS ACANTILADOS COSTEROS ENTRE CAÑETE Y CHINCHA

SECTOR/ PARAJE	COORDEN. (WGS84)	MORFOLOGÍA	DESCRIPCIÓN DE MOVIMIENTOS EN MASA Y VOLUMEN	SUBSTRATO ROCOSO /SUELO	INTENS. INQUA	DAÑOS OCASIONADOS	DISTANCIA AL EPICENTRO
Entre Cerro Colorado y Jahuay 19	8528900 N 364346 E	Acantilado de mar; taludes de corte de carretera (superior e inferior)	Suelo muy fracturado y agrietado; deslizamiento o asentamiento vertical en la plataforma de carretera y en los taludes superiores. Se distinguen también deslizamientos antiguos en el pie del acantilado. Caída de detritos a lo largo de los acantilados entre Cañete y Chincha, derrumbes y caída de rocas en playa Wakama. Volumen: 5250 m^3.	Conglomerados y areniscas estratificados semicompactos; depósitos eólicos y marinos.	V-VI	Daños en tramos de carretera	
Jahuay (Chincha) 20	8516784 N 371352 E	Ladera de colinas, playa y planicie costera	Fracturas y asentamientos en pavimento; deslizamientos superficiales y caída de rocas en los taludes superiores de la carretera en un tramo de 10 km. Volumen: 125 m^3.	Conglomerados, areniscas y lutitas estratificadas semicompactas; depósitos eólicos y marinos.	VI-VII	Fuertes daños en varios tramos de l a plataforma de carretera	

CUADRO Nº 3 MOVIMIENTOS EN MASA DETONADOS EN LA CARRETERA LIBERTADORES-WARI

TRAMO: SAN CLEMENTE INDEPENDENCIA-HUMAY-LETRANO-HUANCANO- PAMPANO-HUAYTARÁ-PUENTE RUMICHACA

SECTOR/ PARAJE	COORDEN. (WGS84)	MORFOLOGÍA	DESCRIPCIÓN DE MOVIMIENTOS EN MASA Y VOLUMEN	SUBSTRATO ROCOSO /SUELO	INTENS. INQUA	DAÑOS OCASIONADOS	DISTANCIA AL EPICENTRO
Quebrada Cocanansaño. (Km. 59+800) 21	8493126 N 427040 E	Laderas de Montaña de fuerte pendiente y valle fluvial	Derrumbe de material coluvial inconsolidado, por efecto de cara libre por el corte de la carretera. Volumen: 375 m³	Material coluvial con clastos mayores a los 2 metros con un matriz limo-arcillosa	VII	Afecto 25 m de la carretera, sin mayores daños. Pobladores restituyeron el tránsito vehicular.	117,59
Pasando Patipampa. (Km. 83+250) 22	8499242 N 441342 E	Laderas de montaña de fuerte a moderada pendiente y valle fluvial	Avalancha de material coluvial inconsolidado por efecto de cara libre en el corte de la carretera. Volumen 35 m³	Material coluvial con clastos mayores a los 2 m. en un matriz limo-arcillosa	VII	Ocasionó el cierre parcial de 7 metros de la vía, pero sin afectarla seriamente.	132,29
Cerro Jajahuacce. (Km. 83+360) 23	8498326 N 444081 E	Laderas de montaña de fuerte a moderada pendiente y valle fluvial	Derrumbe de rocas provenientes de materiales aluviales antiguos inestabilizados por el sismo. Volumen: 24 m³	Material aluvial con clastos no mayores al metro, con matriz limosa.	V	Cubrió 6 metros de la cuneta y bloqueó parcialmente la carretera.	134,96
Pasando quebrada Uchupata (Km. 84+900) 24	8497216 N 444617 E	Laderas de Montaña de fuerte a moderada pendiente y valle fluvial	Derrumbe de rocas provenientes de materiales aluviales antiguos inestabilizados por el sismo. Volumen: 15 m³	Material aluvial con clastos no mayores al metro, con matriz limosa.	V	Cubrió la cuneta de la carretera y no produjo daños mayores.	135,39
Quebrada Cacahuacce.	8497170 N 445379 E	Laderas de montaña de	Pequeñas caídas de rocas, con planos de rotura irregulares.	Andesitas grises verdosas, con	IV	Cubrió la cuneta de la carretera y no	136,09

Km. 85+700 25		fuerte a moderada pendiente y valle fluvial	Volumen: 15 m³	material aluvial no consolidado		produjo daños mayores.	
Frente a la mina Santa Elena (Km. 90+250) 26	8494794 N 448899 E	Laderas de montaña de fuerte a moderada pendiente	Pequeño derrumbe de rocas con bloques no mayores a 1 m, con superficie de rotura irregular. Volumen: 67,5 m³	Andesitas grises verdosas, con material aluvial no consolidado	V	Afecto cartel de señalización vial y cubrió parcialmente 15 metros de la carretera.	139,49
Tullpa (Km. 93+500) 27	8495390 N 451861 E	Laderas de montaña de fuerte a moderada pendiente.	Pequeño derrumbe de rocas con bloques de diámetro inferior a 1 m; superficie de rotura irregular. Volumen: 15 m³	Andesitas grises verdosas, con material aluvial no consolidado.	V	Cubrió la cuneta de la carretera y no produjo daños mayores.	142,54
Capana (Km. 95+200) 28	8495130 N 454921 E	Laderas de Montaña de fuerte pendiente y valle fluvial	Reactivación parcial de un deslizamiento antiguo con derrumbe de material aluvial inconsolidado. La altura del material caído es de 10 m, con una escarpa a 25 m de altura. Volumen: 8750 m³	Material aluvial inconsolidado con clastos mayores al metro, con matriz arcillosa.	VIII	Obstrucción total de 70 metros de vía, al momento de la inspección el transito estaba interrumpido parcialmente.	145,29
Jerque 29	8495634 N 461624 E	Laderas de montaña de fuerte a moderada pendiente y valle fluvial	Pequeñas caídas de rocas con bloques no mayores al metro y con rotura irregular. Volumen: 23 m³	Areniscas lutitas, cuarcitas y material coluvial inconsolidado.	V	No se produjo ningún daño.	152,29
Km. 118 -123 30	Point not mapped due to lack of coordinates	Ladera de montaña con muy fuerte pendiente.	Pequeños conos de talus de detritos, con caídas de rocas y derrumbes en los taludes de corte, con bloques de 0,60-0,80 m de diámetro en 500 m de	Roca intrusiva muy fracturada y meteorizada, material coluvial de talud arenoso(coluvial	IV-V	Deposito que obstruye la carretera.	

			distancia. Volumen de 100 m³.	residual)			
Quebrada Sayauma 31	8497500 N 469200 E	Ladera de montaña de pendiente moderada, disectada y en taludes corte banqueteados	Deslizamiento en el sector de la quebrada Sayauma con caída de detritos cara libre a quebrada y en los taludes de corte Volumen: 10 m³.	Lutitas, muy fracturadas y alteradas.	IV-V	Afecta carretera asfaltada.	159,96
Km. 130 + 100 32	8498465 N 469583 E	Talud de montaña, corte cerrado de carretera.	Caída de rocas, fracturas abiertas en el substrato rocoso con bloques de 1,8 m de diámetro sobre una distancia de 100 m. Volumen: 10 m³.		IV-V	Obstrucción de carretera y vía.	160,39
Km. 182 33	8514863 N 504735 E		Derrumbes en macizo rocoso muy fracturado y alterado, con bloques de 1,50 m de diámetro sobre una distancia de 120 m. Volumen: 15 m³.	Rocas volcánicas macizo fracturado, estratificada, alterada.	IV-V	Carretera no asfaltada; zona inestable en los cortes de talud.	197,38
Km. 185 +900 – 186 +000 34	8518163 N 505289 E	Ladera de montaña con taludes de corte de hasta 20 m de altura.	Deslizamiento traslacional en roca muy fracturada y alterada. Altura: 20m y longitud: 60 m; bloques de 1,5 m de diámetro como máximo, en 100 m.l. Volumen: 70 m³.	Lutitas, arcillolita, arenisca.	IV-V	Afectó tránsito en carretera en tramo de 60 m.	197,77
Km 188+450— 188+250 35	8519201 N 504819 E	Taludes subvertical en laderas de montaña de fuerte pendiente.	Caída de rocas en los taludes de corte; vuelcos, pequeños conos de material fino. Bloques de hasta 1,20 m de diámetro, en una longitud de 500 m. Volumen: 60 m³.	Alternancia de areniscas y limo-arcillitas abigarradas.	IV-V	Obstrucción de cunetas y vía por sectores	198,24

CUADRO Nº 4 MOVIMIENTOS EN MASA DETONADOS EN LA CARRETERA

PUENTE RACRA-PAMPA BLANCA-TICRAPO-PUENTE INFIERNILLO-CASTROVIRREYNA

SECTOR/ PARAJE	COORDEN. (WGS84)	MORFOLOGÍA	DESCRIPCIÓN DE MOVIMIENTOS EN MASA Y VOLUMEN	SUBSTRATO ROCOSO /SUELO	INTENS. INQUA	DAÑOS OCASIONADOS	DISTANCIA AL EPICENTRO
Cerro Racra 36	8501668 N 4429601 E	Montaña con acumulación de detritos en la ladera.	Caída de rocas y detritos con bloques < 0.20 m de diámetro, sobre una distancia de 1800 m, estim ándose un volumen total de 450 m³ de material.	Intrusivo, con sedimentos coluvial de talud.	IV-V	Afecta carretera de acceso a mina abandonada.	133,83
Cerro Matacaballo 37	8502694 N 443695 E	Ladera de montaña con pendiente de 35-50° y acumulación de detritos de vertiente en la margen izquierda del río Pisco.	Cortes de carretera entre 2 y 5 m de altura con caída de rocas y detritos, vuelcos, con bloques de 0.30 m de diámetro, sobre una longitud de 1500 m. Volumen: 150 m³.	Rocas intrusivas y material coluvial de talud.	IV-V	Obstrucción de carretera a Ticrapo en tramo de 1,5 km.	134,71
Pampa Blanca 38	8508325 N 448600 E	Talud de montaña con talus de detritos.	Caída de rocas con bloques de 1.0 m de diámetro sobre una distancia de 300 m y un volumen de 45 m³.	Intrusivo, sedimentos coluviales.	IV	Obstrucción moderada de 300 m de carretera a Ticrapo, por sectores.	140,53
Quebrada Venturosa 39	8509346 N 449284 E	Ladera de montaña de fuerte pendiente, margen izquierda del río Pisco.	Caída de rocas con bloques de 0.80-1.0 m de diámetro, en 500 m de longitud. Zona ya activa parcialmente. Volumen: 90 m³	Intrusivos fracturados y alterados y acumulación de depósitos coluviales gruesos en los taludes de corte.	IV	Obstrucción de carretera por sectores en tramo de 500 m.	141,38

Km. 105 +800 40	8518962 N 452390 E	Talud de montaña	Zona reactivada con derrumbe de detritos; bloques menores a 0.30 m de diámetro, distancia de 100 m Volumen: 8-10 m³.	Volcánico-sedimentarias, sedimentos coluviales de talud	IV-V	Sin daños registrados; material puede ser removido en próximas lluvias originando huaycos.	146,25
Cabracancha 41	8519455 N 452550 E	Talud de montaña, vertiente de detritos.	Deslizamiento rotacional, y en parte caída de rocas, hasta la otra margen del río; bloques de rocas de hasta 0.60 m de diámetro, longitud 35 m. Volumen: 60 m³.	Depósitos proluviales	IV-V	Obstrucción de carretera a Ticrapo.	146,47
Buenavista / Ticrapo 42	8519804 N 452454 E	Talud de montaña, vertiente de detritos y plataforma de carretera.	Asentamiento de orden de 10-20 m y 90 m de longitud; deslizamiento en progreso.	Deposito proluvial		Carretera y terrenos de cultivo en talud inferior.	146,36
Cabracancha 43	8519750 N 453500 E	Ladera de montaña con pendiente escalonada por deslizamiento	Deslizamiento reactivado con pequeñas remociones de suelo en cara libres a carretera, con bloques de 0,40 m de diámetro; distancia de 150 m. Volumen: 20 m³.	Rocas sedimentarias, detritos de vertiente coluvial proluvial , gravo-arcilloso	IV-V	Carretera Ticrapo-Castrovirreyna. Zona activa con abundantes filtraciones.	147,4
Km. 112 + 500 44	8519067 N 453421 E	Talud de montaña.	Ladera con acumulación de detritos, fracturas en el terreno, con asentamientos en el terreno entre 5-8 cm. Fractura N150° de 35 m de longitud, sinuosa, desplazamiento de 2-3 cm y máxima abertura de 5 cm.	Material coluvial de talud y relleno de carretera.	IV-V	Deslizamiento compromete en un futuro con lluvias, carretera Ticrapo-Castrovirreyna.	147,63

Km. 113 + 000 - 113 + 100 45	8518534 N 453200 E	Talud de montaña, talud de corte en la ladera de carretera.	Deslizamiento planar en roca, ausencia de humedad, con bloques de 1,0 m de diámetro, en una distancia de 100 m.l. Volumen estimado: 20 m³.	Rocas sedimentarias muy fracturadas; predominan fracturas planares favorables al talud de corte.	IV-V	Obstrucción de 100 m de carretera Ticrapo-Castrovirreyna.	146,78
Pata Pata 46	8522557 N 462587 E	Talud de montaña con cortes de carretera de 5-10 m de altura.	Derrumbes en los taludes de corte de carretera; bloques caídos de hasta 0,40 m de diámetro sobre una distancia de 900 m. Volumen: 180 m³.	Rocas volcánicas y material coluvial de talud.	IV-V	Obstrucción por sectores de tramo Puente Infiernillo-Castrovirreyna	157,75
Chuncacc 47	8523785 N 463249 E	Valle intermontano; laderas de montaña con acumulación de detritos, tierras de cultivo en la parte inferior.	Derrumbes de detritos en los taludes de corte de carretera (altura 5 m), en tramo de 50-60 m de longitud. Volumen 10 m³.	Suelo grano limoso, arcilloso y húmedo.	IV-V	Obstrucción de tramo de 60 m de carretera.	157,71
Km. 140 +150 (Entre Sinto y Pucaya) 48	8525411 N 464889 E	Taludes de corte subverticales en ladera de moderada pendiente	Caída de rocas; bloques de 1,60 m de diámetro sobre un a distancia de 15 m. Volumen: 8 m³.	Rocas volcánicas	IV-V	Obstrucción de vía 15 m.	160,69

CUADRO Nº 5 MOVIMIENTOS EN MASA EN EL TRAMO DE CARRETERA
SAN VICENTE DE CAÑETE – LUNAHUANÁ – ZÚÑIGA-CATAHUASI-YAUYOS Y RUTAS VECINALES

SECTOR/ PARAJE	COORDEN. (WGS84)[1]	MORFOLOGÍA	PROCESOS GEOLÓGICOS OBSERVADOS	SUBSTRATO ROCOSO /SUELO	INTENS. INQUA	DAÑOS OCASIONADOS Y VOLUMEN	DISTANCIA DEL EPICENTRO
Caltopa Alto 49	8557378 N 367381 E	Laderas de montaña de fuerte pendiente	Grietas a favor de cara libre del corte artificial del talud de carretera; presencia posible de un deslizamiento antiguo.	Material aluvial no consolidado con bloques de tamaño promedio de un metro.	VI-V	Agrietamientos en la carretera	90,17
Socsi 50	8557590 N 367612 E	Laderas de montaña de fuerte pendiente	Caída de rocas, por efecto de cara libre y la poca compactación del suelo. Volumen: 15 m³	Material aluvial no consolidado con bloques promedio de un metro	IV	Bloqueo parcialmente un canal de regadío en varios tramos.	91,17
San Agustín 51	8560824 N 373356 E	Ladera de colina de fuerte pendiente	Caída de bloques y bloqueo de carril hacia la costa de carretera. Volumen: 10 m³	Material aluvial no consolidado con bloques de 1 m.	V	Bloqueo parcial de la carretera hacia la costa, en 100 m.	97,22
Entrada a Patapampa. Km 38+750 52	8566972 N 376090 E	Ladera de montaña, taludes de corte de carretera y valle fluvial.	Deslizamiento - Derrumbe por cara libre hacia el valle, por efectos del sacudimiento y la poca compacidad del suelo. Volumen: 50 m³	Terraza fluvial y material aluvial poco compactado.	VII	Destrucción parcial de 50 metros de la pista, en la salida de Lunahuaná.	103,33
Frente al cerro Riverón 53	8573514 N 381650 E	Acantilado de rio y corte de carretera	Derrumbe de un tramo del acantilado, por efecto del sacudimiento y la cara libre. Volúmen: 35 m³	Material aluvial no consolidado con bloques promedio de un metro.	VII	Daños en 8metros de la carretera.	111,79
Frente a San Miguel 54	8579430 N 395861 E	Ladera de montaña, corte de carretera y acantilado de río.	Fracturas en el suelo que muestran evidencias de afloramientos de agua y licuación. Asentamiento de plataforma de carretera y	Roca intrusiva muy fracturada	VII	Bloqueo total de la carretera por más de 30 horas, se derruyó un pequeño tubo que	125,7

			deslizamientos en los taludes superiores. Volumen: 250 m³			transportaba agua para los terrenos de cultivo.	
Puente a San Miguel 55	8579384 N 395934 E	Ladera de montaña, corte de carretera y acantilado de río.	Durante el derrumbe explicado en el ítem anterior, un bloque golpeo uno de los pilares del puente San Miguel destruyéndolo, y dejando al puente completamente inutilizado.	Roca intrusiva muy fracturada, material fluvial proveniente del río Cañete	VIII	Destrucción de puente peatonal dejó aislada comunidad de San Miguel, quienes tienen que cruzar por un puente artesanal.	125,63
Catahuasi 56	8581822 N 400457 E	Ladera de montaña, corte de carretera y acantilado de río.	Derrumbe de material aluvio-coluvial inconsolidado producto de replica sísmica del 15/08/2007, desestabilizado por terremoto principal. Volumen: 300 m³	Material coluvial y aluvial al pie de la ladera muy inestabilizado.	VIII	Destrucción total de 45 metros de carretera, que interrumpió el transito por 54 horas.	131,04
TRAMO SAN JERÓNIMO DE YANAC-HUANGASCAR-VIÑAC-MADEÁN-AZÁNGARO-CHOCOS							
Quebrada Huangascar 57	8578092 N 399369 E	Ladera de montaña con acumulación de detritos de talud y terrazas aluviales al pie.	Varios sectores con caída de detritos en las laderas (ambas márgenes de valle), como en los cortes de carretera. Algunas caídas por rodamiento de coluvios sueltos: Tamaños máximo: 0,40 m en 1000 m.l. Volumen: 25 m³.	Rocas intrusivas y coluvios de talud con grandes bloques.	IV-V	Obstrucción parcial de vía hacia Chocos, Azángaro, Viñac y Madeán.	127,242
Entre Huangascar y Chocos 58	8574200 N 408315 E	Ladera de montaña con pendiente de 45°-50° y talud de corte de carretera	Derrumbes de rocas sobre la carretera en tramo de 250 m, por sectores; bloques mayores de 0,60 m. Volumen: 15 m³.	Rocas intrusivas y coluvios de talud.		Obstrucción de vía Huangascar-Chocos.	132,05

CUADRO Nº 6 MOVIMIENTOS EN MASA EN EL TRAMO DE CARRETERA CHINCHA-CULEBRILLA-SAN JUAN-PUENTE HUACHINGA- HUANCHO CHICO-PALCA-SAN JUAN DE CASTROVIRREYNA-TANTARÁ-SAN PEDRO DE HUACARPANA Y RUTAS VECINALES.

SECTOR/ PARAJE	COORDEN. (WGS84)[1]	MORFOLOGÍA	PROCESOS GEOLÓGICOS OBSERVADOS	SUBSTRATO ROCOSO /SUELO	INTENS. INQUA	DAÑOS OCASIONADOS Y VOLUMEN	DISTANCIA DEL EPICENTRO
Hacienda San Juan 59	8516473 N 395824 E	Laderas de Montaña de fuerte pendiente y valle fluvial	Pequeñas caídas de rocas con planos de rotura principalmente en cuña, que al pie del talud formo pequeños conos de detritus. Volumen: 105 m³	Roca intrusiva muy fracturada y material coluvial en la parte alta	V	Obstrucción de 14 m de la carretera, pasando la hacienda San Juan, pequeños derrumbes.	90,82
Frente a Caruya 60	8518285 N 399535 E	Laderas de Montaña de fuerte pendiente y corte artificial de carretera.	Pequeñas caídas de rocas con sistema de rotura muy irregular con bloque no mayores a un metro. Volumen: 60 m³	Roca intrusiva muy fracturada	IV	Obstrucción por pequeños tramos de carretera, sin mayores daños.	94,67
Huanchor (Km. 29) 61	8518345 N 399869 E	Laderas de Montaña de fuerte pendiente y corte artificial de carretera.	Grandes caídas de roca, con bloques mayores a los 2 metros, con superficies de rotura irregulares. Volumen: 800 m³	Roca intrusiva muy fracturada, con material coluvial acumulado en canchales	VI	Obstrucción de 160 metros de la trocha carrozable, pero no se produjo fuertes daños a la carretera.	95,33
Huanchor. Km. (30 + 800) 62	8519149 N 421831 E	Laderas de Montaña de fuerte pendiente y corte artificial de carretera.	Grandes caídas de roca, con bloques mayores a los 2 m., con superficies de rotura irregulares. Volumen: 450 m³	Roca intrusiva muy fracturada, con material coluvial acumulado en canchales	VI	Obstrucción de 90 m de carretera, pero no se produjo fuertes daños.	116,11
Huauyapa. (Km. 33 + 200)	8519673 N 403479 E	Laderas de Montaña de	Pequeñas caídas de rocas, con bloques no mayores al metro,	Roca intrusiva muy fracturada	IV	Formación de pequeños	99,07

63		fuerte pendiente y corte artificial de carretera.	con superficies de rotura mayormente en cuña. Volumen: 30 m³			canchales en los bordes cubrieron la cuneta.	
Hda. Atahuaranga. (Km. 35). 64	8520636 N 404007	Laderas de Montaña de fuerte pendiente, abanicos coluviales y corte artificial de carretera.	Caídas de rocas de proporciones medias, con bloques mayores a los 2 m, con superficies de rotura irregulares. Volumen: 40 m³	Roca intrusiva muy fracturada, y conos aluviales en el fondo del valle fluvial	VI	Afecto un terreno de cultivo y bloqueo parcialmente 7 m de carretera.	99,87
Cabecera de Huachinga. (Km. 42) 65	8521443 N 410508 E	Laderas de Montaña de fuerte pendiente y corte artificial de carretera.	Caída de material aluvial por efecto de cara libre y una escarpa de deslizamiento antigua que mostró reactivación parcial por el terremoto. Volumen: 400 m³	Material aluvial inconsolidado con clastos mayores al metro y matriz areno-arcillosa	IV	Obstrucción de 20 m de la carretera, que al momento de la inspección se venían limpiando con maquinaria pesada.	105,92
Km 48-50 San Juan- Tantará (Cerro Carhuay Pata) 66	8523393 N 422290 E	Talus de detritos acumulados en ladera de montaña de pendiente mayor a 40°	Caída de rocas y rodamiento de detritos de forma superficial por sacumiento sísmico. Bloques caídos en un tramo de 2000 m, con tamaños menores a 0,40 m. Volumen 150 m³.	Coluvial de talud sobre substrato intrusivo	IV-V	Obstrucción por sectores de carretera San Juan –Tantará, San Juan- Palca- Villa de Arma.	118,36
Santa María de Yanapampa 67	8524849 N 424893 E	Talus de detritos en ladera de fuerte pendiente	Caída y rodamiento de detritos en tramo de 100 m de carretera; bloques de 0,50 m Volumen: 5 m³.	Coluvial de talud compuesto por grava angulosa con clastos de hasta 0,50 m de diámetro de depósitos de talus antiguos.	IV	Interrupción parcial de vía hacia la Costa desde Tantará y Villa de Arma.	121,64

Huancho Grande 68	8524820 N 425000 E	Ladera rocosa con acumulación de detritos de talud; pendiente 40°-50°.	Derrumbes en los taludes superiores e inferiores, tanto en el substrato fracturado como talus de detritos antiguos; remoción superficial de detritos en una distancia de 250 m. Volumen: 20 m³.	Intrusivos muy fracturados con acumulación de coluvios	IV-V	Interrupción de carretera de acceso a Tantará y Villa de Arma	122,18
Chata 69	8542321 N 430999 E	Depósitos de vertiente de ladera y mezcla de aluviales, con cortes de talud	Caída de detritos reciente de fragmentos de rocas de hasta 0,80 m en una distancia de 150 m. Volumen: 15 m³.	Suelo aluvial con bloques de hasta 1,20 m	IV	Obstrucción parcial de vía a Tantará y San Pedro de Huacarpana.	133
Palca 70	8536113 N 433109 E	Ladera de montaña con acumulación de detritos de vertiente, con fuerte declive	Abundantes talus de detritos con caída de detritos o derrumbes sobre una distancia de 350 m.l. Volumen: 180 m³.	Suelo gravo limoso a gravo arcilloso	V	Obstruccón de carretera hacia San Juan de Castrovirreyna y Tantará, antes de desvío a Palca	135,56
Frente a Lunche 71	8544868 N 429821 E	Ladera de montaña con taludes de corte mayores a 65°	Caída de rocas en varios sectores con bloques hasta de 1,20 m sobre una distancia de 400 m.l. Volumen: 80 m³ aprox.	Rocas intrusivas	IV-V	Interrupción de vía hacia Tantará y San Pedro de Huacarpana. Zona parcialmente activa.	132,95
Pache 72	8549000 N 428867 E	Corte de carretera en talud rocoso con fuerte pendiente; ladera media del río San	Derrumbes de detritos superficiales en los taludes de corte y laderas naturales; varios sectores en tramo de 1 km con clastos removidos de 0,25 m de diámetro. Volumen: 15 m³.	Intrusivos muy fracturados y meteorizados con acumulación de coluvios	IV	Interrupción de vía hacia Tantará y San Pedro de Huacarpana.	133,83

		Juan					
Entre Tambo y Huacasca 73	8556102 N 430406 E	Taludes de corte de 2 a 5 m de altura en ladera de montaña con pendiente moderada	Derrumbes y caída de detritos en taludes de corte de hasta 0,80 m en una longitud de 300 m. Volumen: 20 m³.	Suelo coluvial gravoarcilloso a gravo limoso	IV-V	Obstrucción de vía de acceso a San Pedro de Huacarpana en dos desarrollos de carretera afirmada.	138,65
TRAMO: SAN JUAN -YANAC-LISCAY							
Huayto 74	8535024 N 402824 E	Ladera de montaña con acumulación de detritos	Caída de rocas en corte de carretera y rodamiento de bloques de depósitos coluviales superiores. Bloques de hasta 1 m en una distancia de 350 m. Volumen: 90 m³.	Roca intrusiva	IV	Obstrucción de carretera entre San Juan y Yanac	104,38
Cerro Rupasca 75	8534400 N 406150 E	Ladera de montaña con moderada a fuerte pendiente, escasa vegetación, disectada por surcos.	Deslizamiento rotacional en talud superior de carretera, así como derrumbes de detritos en los taludes de corte de carretera. Detritos de 0,10 m en una longitud de 300 m. Escarpa semicircular con salto entre 1,80 a 2,0 m. Volumen: 60 m³ aprox.	Roca intrusiva muy meteorizada; suelo residual.	IV-V	Obstrucción de vía de acceso a Yanac y Liscay.	107,11
TRAMO: PALCA-VILLA DE ARMA							
Palca 76	8537952 N 434705 E	Terraza alta en la margen derecha del río Huanchos con cortes subverticales de 8-12 m de	Caída de detritos; derrumbes en la terraza de enfrente. Bloques subsredondeados caídos de hasta 1,20 m en una distancia de 300 m y bloques angulosos en varios sectores. Volumen: 150 m³.	Depósitos aluviales con grandes ; bloques, por sectores susbstrato rocoso intrusito	IV-V	Obstrucción de carretera Palca-Villa de Arma	132,09

		altura.					
Frente a Pumani 77	8539150 N 436390 E	Terraza y vertiente de detritos contigua en la margen derecha del río Huanchos	Derrumbes de detritos y agrietamientos de plataforma de carretera hacia cara libre al río. Pequeños derrumbes en la terraza de enfrente. Bloques de hasta 0,60 m en una distancia de 150 m.l. Volumen: 10 m³ aprox.	Depósito aluvial con gravas y arenas	V	Afectó carretera hacia Villa de Arma; actualmente zona inestable por agrietamientos en la plataforma de carretera y terrenos de cultivos.	136,35
Entre Huachacmarán y Acomachay 78	8540479 N 437299 E	Ladera con pendiente mayor a 45º y taludes de corte de 4-10 m de altura	Taludes de corte con acumulación de material al pie producto de múltiples caída de rocas y derrumbes en tramo de 4 km de carretera; bloques de hasta 1,50 m. Volumen: 300 m³.	Roca intrusiva muy alterada y fracturada	V	Obstrucción de carretera en varios sectores.	138,27

CUADRO N° 7 MOVIMIENTOS EN MASA EN LOS TRAMOS DE CARRETERA DESDE ICA HACIA LA SIERRA

SECTOR/ PARAJE	COORDEN. (WGS84)	MORFOLOGÍA	DESCRIPCIÓN DE MOVIMIENTOS EN MASA Y VOLUMEN	SUBSTRATO ROCOSO /SUELO	INTENS. INQUA	DAÑOS OCASIONADOS	DISTANCIA AL EPICENTRO
TRAMO DE CARRETERA: ICA-COCHARCAS-PAMPAHUASI-ANDAYMARCA-SANTIAGO DE CHOCORVOS							
Cerro Puca Puca 79	8450791 N 459384 E	Talud de montaña con taludes de corte de carretera con pendiente 40-55°.	Caidas de rocas y de detritos de hasta 1 m de diámetro en una longitud de 200 m. Conos o talus de detritos 8-10 x 3-10 m, rocas fracturadas inestables zona ya activa. Volumen: 20 m³.	Rocas volcánicas con estratificación, muy fracturadas, material coluvial de talud.	IV- V	Afectó 200 m de carretera a Santiago de Chocorvos; necesita desquinchar taludes.	154,33
Tingo 80	8454012 N 461092 E	Ladera de montañas de moderada a fuerte pendiente.	Caídas de detritos y rocas, pequeños vuelcos. Talus de detritos con pendiente natural de 25-35°, con taludes de corte >60° desde 2-8 m de altura, Bloques de 0,35 m de diámetro en una distancia de 400 m. Volumen: 10 m³.	Volcánico-sedimentario areniscas. buzamientos de capas contra talud	IV-V	Área afectada 400 m.	155,34
Entre Tingo y Sauces. 81	8454632 N 461007 E	Talud de montaña con laderas de moderada a fuerte pendiente > 50°.	Caída y deslizamiento de rocas; bloques de 0,80 m de diámetro, sobre una distancia de 180 m. Volumen: 25 m³.	Roca volcánica o subvolcanica muy fracturada.	IV-V	Obstrucción de vía en tramo de 200 m.	155,11
Sauces 82	8455929 N 460916 E	Ladera de montaña con pendiente >40°. Taludes de corte de 6 m de altura.	Caída de grandes bloques de rocas, de 1,5 a 3,5 m de diámetro. Volumen:18-20 m³.	Rocas intrusivas y material coluvial de talud.	IV-V	Afectó 150 m de carretera por sectores.	154,78

Quebrada Andaymarca 83	8456462 N 461074 E	Talud de montaña con taludes de corte de 5-8 m de altura.	Caída de roca y detritos en los taludes de carretera; derrumbes pequeños sobre terrazas aluviales, bloques de > 0.60 m. sobre una distancia de 180 m y un volumen estimado de 15 m³.	Rocas intrusivas y material coluvial de talud. Depósitos aluviales en el pie de valle (Terrazas).	IV-V	Afectó 180 m de tramo de carretera.	154,89
San Antonio de Andaymarca . 84	8459300 N 461650 E	Talud de montaña, ladera con pendiente >45°y talud de corte >60-70°, altura de talud < a 5m.	Derrumbes pequeños y caídas de rocas en los taludes de corte, dimensiones de los bloques <0.20 m, con 400 m de distancia. Se estima volumen inferior a 80 m³.	Rocas sedimentarias.	IV-V	Afectó 400 m de carretera.	154,78
Puccquillua 85	8462311 N 463707 E	Ladera de montaña de moderada pendiente con taludes de corte	Caída de rocas y derrumbes en los taludes de corte en desarrollo de carretera, acumulación de detritos en la plataforma de charretera con dimensiones de 0.30 m, sobre una distancia de 450 m. Volumen: 90 m³.	Intrusivo muy fracturado y alterado.	IV-V	Afectó 2 a 3 desarrollos de carretera en tramo de 450 m entre Andaymarca y Santiago de Chocorvos.	156,24
TRAMO DE CARRETERA: ICA-SAN JOSÉ DE LOS MOLINOS-HUAMANÍ LA LAJA-TAMBILLOS-CHAULISMA-AYAVI-TRANCA-TAMBO-SANTODOMINGO DE CAPILLAS-SANTIAGO DE CHOCORVOS							
Labanda /Bocatama La Achirana 86	8460937 N 426800 E	Ladera de colina con taludes de corte	Caída de rocas y derrumbes en taludes y terraplén con bloques de 0.80 m de diámetro, distancia de 350 m . Volumen: 12 m³.	Intrusivo muy meteorizado, arenoso material coluvial de talud.	IV	Carretera no asfaltada	120,35
Sector Socavón 87	8469450 N 440400 E	Ladera de montaña de fuerte pendiente en la margen derecha del río Ica.	Caída de detritos en los taludes de corte y talud inferior de carretera ; bloques con dimensiones de 0.50 m	Intrusivos muy fracturados, gravas, y material coluvial de talud.	IV-V	Por sectores en tramo de 1500 m de carretera.	131,38

			de diámetro, distancia recorrida 1500 m Volumen: 150 m³.				
Quebrada Dos Aguas 88	8478904 N 447355 E	Ladera de montaña con fuerte pendiente y cortes de talud	Caída de detritos por sectores en los taludes de corte; bloques menores a 0,20-0,30 m de diámetro en un tramo de 6 km. Volumen estimado: 250 m³		IV-V	Interrupción parcial de vía por sectores en un tramo de 6 km.	138,17
Entre Tambo y Capilla. 89	8482070 N 472159 E	Ladera de montaña.	Caída de rocas, movimiento rápido presenta fracturas en el terreno con desplazamiento de bloques de 1 m de diámetro en una distancia de 300 m Volumen: 10 m³.	Intrusivas muy fracturada y alterada.			162,57
Cerro Huañacancha 90	8480742 N 479485 E	Talud de colina, colina con pendiente escarpada en la parte superior y ladera suave.	Movimiento del talud, rodamiento de roca /detritos de 1,10 m de tamaño a una distancia de 105 m Volumen: 5 m³.	Rocas volcánicas pseudo estratificadas.			170,39

CUADRO Nº 8 MOVIMIENTOS EN MASA DETONADOS POR EL SISMO EN LA CUENCA DEL RÍO CAÑETE

SECTOR/PARAJE	COORDEN. (WGS84)	MORFOLOGÍA	DESCRIPCIÓN DE MOVIMIENTOS EN MASA Y VOLUMEN	SUBSTRATO ROCOSO /SUELO	INTENS. INQUA	DAÑOS OCASIONADOS	DISTANCIA AL EPICENTRO
Cerro Campana 91	8577060 N 400400 E	Ladera superior de montaña con fuerte pendiente	Múltiples caída de detritos de forma superficial en varios las laderas y cárcavas de montaña (medias a superiores); detritos pequeños con diámetros inferiores a 0,20 m en una distancia acumulada de 1500 m.l. Volumen: 18-20 m³.	Rocas volcánico sedimentarias	IV-V	No se reportan daños	127,36
San Jerónimo de Yanac (ladera NO del cerro Pishcullay) 92	8554250 N 400450 E	Ladera de montaña de fuerte pendiente con acumulación de talus de detritos.	Caída de detritos en la parte superior de ladera de formas angulosas y tamaños de hasta 1,o m en una distancia lineal de 100 m. Volumen: 5 m³.	Rocas intrusivas	IV-V	No se reportan daños.	112,57
Frente a Zañín 93	8604500 N 395500 E	Ladera de fuerte pendiente (>50º), con acumulación de detritos	Caída de detritos superficiales en un sector de 150 m de ladera con altura mayor a 120 m; bloques menores a 0,30 m. Volumen 35-40 m³	Rocas intrusivas muy fracturadas y coluviales acumulados en su vertiente.	IV-V	Material caído hasta pie del valle fluvial con obstrucción reducida del cauce del río .	145,17
Huanchac 94	8608225 N 398650 E	Ladera con pendiente mayor a 50º y terraza media a alta.	Caídas de rocas múltiples y discontinuos en ladera media e inferior en tramo de 600 m.l., con clastos máximos menores a 0,30 m. Volumen 15 m³.	Rocas intrusivas muy fracturadas y coluviales	IV-V	No se reportan daños; afectación leve de caminos de herradura.	149,88

Entre Yaca y Caullama 95	8614350 N 401100 E	Talus de detritos en ladera de montaña de fuerte declive, en la margen izquierda del río Cañete.	Múltiples eventos de caídas de rocas en laderas medias del valle del río Cañete, sobre una longitud de 1500. Volumen: 20 m³.	Suelo coluvio-residual	IV-V	No se registran daños.	156,64
Quichca 96	8576725 N 402300 E	Abanico secundario proluvial en la margen izquierda del río Huangascar	Derrumbes o caída de detritos en el pie de terrazas/abanico; caída de rocas en este sector sobre la carretera. Varios sectores con caída de bloques de hasta 0,20 m en una longitud de 150 m. Volumen: 10 m³.	Suelo proluvial gravolimoso, sucio, beige.	IV-V	No se registran daños.	128,39
Entre Suquia y Quichca 97	8576850 N 403345 E	Valle fluvial con laderas de montaña de fuerte pendiente y cortes de carretera.	Caída de rocas en los taludes de corte y caída de detritos en las laderas naturales en ambas márgenes; derrumbes. Bloques de hasta 1 m de diámetro en 1500 m.l. Volumen: 30-35 m³.	Intrusivos muy fracturados y acumulaciones coluviales en las laderas.	IV-V	Obstrucción en varios sectores de la carretera hacia Viñac y Chocos.	129,28
Frente a Pallca 98	8575650 N 406350 E	Valle fluvial tributario con márgenes de depósito en abanico y terraza adyacentes; ladera de moderada a	Caídas y derrumbes de detritos en varios sectores en forma discontinua, con clastos máximos de hasta 0,50 m. en un sector de 350 m.l. Volumen: 15 m³.	Roca intrusiva muy alterada que muestra zona de brecha de falla antigua (margen izquierda del río Chocos). Depósitos aluviales.	IV-V	Obstrucción de cauce fluvial del río Chocos.	130,51

		fuerte pendiente.					
Cerro Pucahuasi (Huangascar) 99	8574700 N 409250 E	Depósito de remoción antiguo con ladera cóncavo-convexa, disectado por cárcavas. Margen izquierda del río Viñac,.	Deslizamiento rotacional múltiple de gran magnitud, reactivado en un pequeño sector del cuerpo como derrumbe de detritos (2 a 3 eventos). Área de 550 m de longitud Volumen: 8-10 m³.	Depósito de movimiento en masa con suelo gravo-limoso y terrenos de cultivo.	IV	Áreas de cultivo.	132,15
Tranca (Huangascar) 100	8572850 N 409900 E	Ladera con movimiento en masa antiguo, disectado por cárcavas.	Derrumbes cara libre a cárvcavas en cuerpo de deslizamiento antiguo. 250 m de longitud con remoción superficial. Volumen: 10 m³.	Rocas volcánicas.	IV	No se registram daños.	131,37
Río Viñac 101	8570945 N 413680 E	Ladera de montaña en valle superior del río Viñac.	Derrumbe o colapso de rocas reactivado por sismo en tramo de 60 m.l. Máximo tamaño de bloques de 2 m Volumen: 8-10 m³.	Volcánicos gris violáceos muy fracturados	IV-V	Afectó canal de riego artesanal.	133,1
Quebrada Catacancha 102	8569150 N 414450 E	Ladera de montaña con fuerte pendiente y cortes de talud de carretera.	Derrumbe superficial de rocas, cara libre a quebrada. Área afectada de 200 m de longitud con bloques máximos de rocas de 0,50 m. Volumen: 20 m³.	Roca volcánica, brechosa, alterada.	IV-V	Afecta tramo de carretera a Madeán.	132,6
Frente a Chocos 103	8571800 N 405300 E	Ladera de montaña muy disectada por	Caída de detritos cara libre a cárcavas, en forma superficial en una longitud de 350-400	Roca intrusita muy alterada.	IV	No se registran daños.	127,32

		cárcavas	m.l. Volumen: 10 m3				
Entre Cascajal y Huayabo (Cerro Poquio) 104	8579600 N 393500 E	Laderas disectadas de montaña con fuerte pendiente en la margen izquierda del río Cañete	Múltiples caídas de detritos superficiales, cara libre a cárcavas, desde laderas superiores hasta el pie del valle. Volumen estimado de 25 m³.	Roca intrusita muy alterada en contacto con rocas sedimentarias	IV-V	No se registran daños	124,25
Frente a Huancaya 105	8651070 N 412650 E	Ladera disectada por quebrada o cárcava	Caída de detritos en margen derecha de quebrada, con poco volumen de remoción (5 m³), en una longitud de 50 m.	Depósitos fluvioglaciares gravo arenosos	IV	No se registraron daños.	192,92

CUADRO Nº 9 MOVIMIENTOS EN MASA DETONADOS POR EL SISMO EN LA CUENCA DEL RÍO SAN JUAN-CHINCHA

SECTOR/PARAJE	COORDEN. (WGS84)	MORFOLOGÍA	DESCRIPCIÓN DE MOVIMIENTOS EN MASA Y VOLUMEN	SUBSTRATO ROCOSO /SUELO	INTENS. INQUA	DAÑOS OCASIONADOS	DISTANCIA AL EPICENTRO
Tripunca, Distrito de Huacro, Huancavelica. (Frente a Km 46, carretera a Tantará). 106	8521975 N 411902 E	Laderas de Montaña de fuerte pendiente en la margen izquierda del río San Juan.	Sistemas de cárcavas reactivadas por el terremoto con pequeñas caídas de rocas, que en la época de lluvias podría causar flujos de detritos con el material suelto. Volumen: 20 m³.	Rocas intrusivas y sedimentarias que forman esa parte de la Cordillera de los Andes	VI	No ocurrió daños ni a vías de comunicación ni a terrenos de cultivo.	107,81
Cantupuquio 107	8552640 N 428060 E	Ladera de montaña de fuerte pendiente en la margen derecha del río Tantará.	Deslizamiento rotacional en la ladera inferior del valle con reactivación cara libre en forma de caída o derrumbe de detritos. Dimensión de bloques menores a 0,50 m en una distancia de 100 m. Volumen: 10 m³.	Rocas volcánicas andesíticas	IV	Compromete tramo de carretera de acceso a Cantupuquio.	135,05
Cerca de Ayacuchito 108	8524019 N 423024 E	Terrazas y abanicos en ambas márgenes del río San Juan	Derrumbes y caída de detritos; tramo de 100 m con bloques de hasta 0,30 m de diámetro. Volumen: 8-10 m³.	Depósitos aluviales gravo-arenosos	IV	Compromete un tramo de carretera Chincha-Tantará	119,09
Songo Chico 109	8532250 N 432400 E	Ladera de montaña con pendiente mayor a 50º con escasa	Caída de rocas en laderas inferiores, dispersos y de poco volumen de remoción. Volumen: 20 m³.	Rocas intrusivas muy fracturadas y meteorizadas.	IV-V	No se reportaron daños.	130,56

		vegetación.					
Cascanni 110	8543810 N 431120 E	Ladera convexa con forma redondeada, pendiente moderada a fuerte	Derrumbes y deslizamientos superficiales de detritos en una distancia de 600 m.l., de ladera. Volumen: 50 m³.	Rocas intrusivas	IV-V	Remoción de escombros hacia ladera oeste y hacia cárcava.	133,73
Quebrada Jasa Huishcana 111	8544600 N 439305 E	Ladera de montaña cara libre a quebrada con pendiente mayor a 50º.	Derrumbe de detritos que genera flujo de material canalizado aguas abajo. Zona reactivada superficialmente con remoción de bloques de 0,50 m en una distancia de 60 m.l. Volumen 5 m³.	Roca intrusita muy alterada y fracturada	IV-V	No se reportaron daños.	141,79
Molienda 112	8455000 N 448400 E	Montaña con ladera cóncavo-convexa en la margen izquierda del río Arma.	Deslizamiento traslacional reactivado parcialmente con caída de detritos o derrumbes de la escarpa principal y secundaria, hacia el valle. Volumen: 10 m³.	Coluvial de talud y/o residuo-coluvial en substrato sedimentario (areniscas)	IV-V	No se reportan daños.	142,8
Río Castrovirreyna 113	8430000 N 465260 E	Valle fluvial con laderas (terrazas o morrenas) y substrato rocoso	Derrumbes de detritos (roca meteorizada), y caída de detritos en las terrazas, con bloques < a 0.50 m de diámetro, en una distancia del cauce de 700 m. Volumen 150 m³.	Depósitos fluvioglaciares grava arenosas y talus de detritos, roca muy fracturada y meteorizada.	IV-V		166,09

CUADRO Nº 10 MOVIMIENTOS EN MASA DETONADOS POR EL SISMO EN LA CUENCA DEL RÍO PISCO

SECTOR/PARAJE	COORDEN. (WGS84)	MORFOLOGÍA	DESCRIPCIÓN DE MOVIMIENTOS EN MASA Y VOLUMEN	SUBSTRATO ROCOSO /SUELO	INTENS. INQUA	DAÑOS OCASIONADOS	DISTANCIA AL EPICENTRO
Jatumpampa 114	8508225 N 469800 E	Talud de corte de carretera con pendiente entre 40º a 55º	Caída de detritos superficiales, con flujo de material pendiente abajo; máximo dimensión de bloques de 1,50 m en una longitud de 25 m. Volumen: 5 m³.	Rocas volcánicas piroclásticas	IV	Obstrucción de camino de herradura	161,99
Río Pisco 115	8505200 N 446500 E	Talud de colina con fuerte pendiente.	Avalancha de detritos, tamaño de bloques 1.0 m de diámetro Volumen: 300 m³.	Intrusivo muy fracturado y meteorizado suelo coluvial.	IV	Obstrucción leve del cauce.	138,29
Pampanito. (Frente a Km. 101) 116	8495214 N 457167 E	Laderas de Montaña de fuerte pendiente y valle fluvial	Derrumbes y deslizamientos reactivados por el sismo en la margen derecha del río Huaytara. Volumen: 5279 m³.	Areniscas lutitas, cuarcitas y material coluvial inconsolidado.	VIII	No producen ningún daño, debido a que donde se encuentran no hay ninguna carretera, ni poblado.	147,75
Río Vizcacha 117	8497250 N 466025 E	Talud de montaña, movimiento en la ladera antiguo reactivado en la margen derecha del Río Vizcacha.	Deslizamiento traslacional en el cuerpo de deslizamiento antiguo, derrumbe de detritos a cara libre y al pie del deposito, distancia 100 m.l. Volumen:10-12 m³.	Rocas volcánicas	V		156,78
Valle del Rio Arma/Río Vizcacha 118	8498415 N 461894 E	Valle fluvial con laderas de fuerte pendiente,	Caídas de rocas en los cortes de talud de carretera en construcción,	Rocas intrusivas muy fracturadas.	IV	Afecta carretera.	152,74

		terrazas y detritos de vertiente.	pequeños derrumbes en las laderas del valle y terrazas, bloques de tamaño de 0.60 m de diámetro, en una longitud de 300 m. Volumen: 20 m³.				
Quito Arma /Collcapampa 119	8500850 N 463900 E	Valle fluvial, márgenes del río arma con deslizamientos.	Deslizamientos, pequeños reactivaciones en la escarpa y cuerpo de deslizamiento activos como derrumbes y asentamientos de tierra, con bloques < 0.20 m, a una distancia de 1000 Volumen: 25 m³.	Lutita arcillosa, deposito de remoción en masa grano-limosos.	IV-V		155,02
Quito Arma 120	8504025 N 464900 E	Talud de montaña; vertiente de detritos con ocupación de áreas de cultivo y carretera.	Derrumbe y deslizamiento de detritos, en la margen derecha del río, en una distancia de 1000 m. Volumen: 60 m³.	Rocas sedimentarias	IV-V	Afecta tierras de cultivo.	156,17
Huayacundo Arma 121	8503300 N 465500 E	Ladera de montaña y vertiente de detritos.Pendiente suave a moderada, terreno escalonado del antiguo depósito	Deslizamiento reciente cara libre a cárcava y reactivaciones en derrumbes / deslizamiento en el corte de carretera de forma superficial, bloques de 1,5 m de diámetro, longitud 500 m.l. Volumen: 75 m³.	Rocas volcánicas	IV-V	Afecta pastizales y tierras de cultivo.	156,74

		de movimiento de masa.					
Río Quito Arma 122	8505400 N 466550 E	Talud de montaña con pendiente pronunciada, gran deposito de remoción en masa; superficie cóncava – convexa, margen izquierda del río.	Colapso o derrumbe en el cuerpo de deslizamiento antiguo, avance cara libre a quebrada, acumulación de detritos superficiales, con bloques de 1.80 m de diámetro a una distancia de 360 m. Volumen: 110 m³.	Rocas volcánicas, tobas rocosas muy fracturadas, y material coluvial perteneciente a movimiento en masa antiguo	IV-V	Afecta pequeña acequia o canal.	159,33
San Antonio de Cusicancha 123	8506979 N 467817 E	Talud de montaña y valle intermontano.	Deslizamiento reactivado en los cortes de carretera, como derrumbe y caídas de rocas (margen derecha), margen izquierda en el pie del valle, con bloques de 1,0 m de diámetro, a distancias de 250 m Volumen: 15 m³.	Rocas piroclásticas fracturada.	IV-V	Afecta canal.	159,37
Taurcarpata / Ticrapo 124	8520650 N 451800 E	Valle fluvial intermontano, con laderas de moderada pendiente, terraza con inclinación al valle.	Derrumbe y/o avalancha de detritos en tres sectores al pie del valle en una longitud de 300 m. Volumen: 60 m³.	Material coluvial de talud.	IV-V	No registra daños. Parcialmente desvío de curso fluvial.	145,78
Tarayocc 125	8526400 N 449300 E	Laderas de montaña disectada con cárcavas.	Derrumbes cara libre en cabecera de cárcavas de escarpas irregulares. Bloques de rocas 0,30 m	Material residual/coluvial detritico.	IV-V	No se registraron daños.	145,05

			de diámetro Volumen: 40 m³.				
Chalma 126	8515100 N 459150 E	Talud de montaña, disectada por cárcavas, en la margen izquierda del río Castrovirreyna.	Deslizamiento de material detrítico (roca alterada), en cabecera de cárcava que presenta reactivación por sismo (caída de detritos) en varios sectores de la ladera., con bloques de 0.30 m sobre una distancia de 500 m.l. Volumen: 35 m³.	Rocas volcánicas y sedimentarías, arcillas , limo y gravas.	IV-V	No se registraron daños.	152,14
Quebrada Infiernillo 127	8519800 N 457150 E	Ladera de montaña, muy disectada en cárcavas, terreno escalonado con escarpas de deslizamiento	Deslizamiento y derrumbes en cuerpo de deslizamiento activo, reactivado con el sismo; derrumbes en cabecera de quebrada de naturaleza superficial. Volumen: 100 m³.	Rocas volcánicas y sedimentarías, muy meteorizadas.	IV-V	Sin daños registrados.	151,2
Río Castrovirreyna 128	8527200 N 465550 E	Valle fluvial con terrazas y/o depósitos fluvioglaciares	Caída de detritos y derrumbes a nivel del cauce y laderas (morrenas o terrazas); pequeños derrumbes en los taludes superiores de carretera, con bloques de 1,0 m de diámetro; distancia 1500 m. Zona activa por erosión fluvial en las márgenes del río. Volumen: 25 m³	Rocas volcánicas, y grava arenosas arcillosa parcialmente húmeda.	IV-V	Material caído al cauce fluvial sin generar daños.	160,91

CUADRO N° 11 MOVIMIENTOS EN MASA DETONADOS POR EL SISMO EN LA CUENCA ICA

SECTOR/PARAJE	COORDEN. (WGS84)	MORFOLOGÍA	DESCRIPCIÓN DE MOVIMIENTOS EN MASA Y VOLUMEN	SUBSTRATO ROCOSO /SUELO	INTENS. INQUA	DAÑOS OCASIONADOS	DISTANCIA AL EPICENTRO
Quebrada Chincao 129	8462750 N 467050 E	Talud de montaña, valle ínter montano.	Derrumbe /deslizamiento en zona de cárcavas, con escarpa semicircular. Varios sectores. Volumen: 20 m³.	Rocas intrusivas alteradas	IV-V	Sin daños registrados	159,57
Morro / Río Ica 130	8470150 N 441100 E	Terraza aluvial y abanico de la quebrada Buenavista.	Caída de detritos, con bloques < a 0.20 m de diámetro en una distancia de 150 m. Volumen: 30 m³.	Limo, arena, gravas, estructura semicoherente masiva.	IV		132,92
Santa Rosa de Tambo 131	8486680 N 470525 E	Terraza aluvial margen de río.	Deslizamiento de tierras en margen izquierda de quebrada, de 40 m de longitud. Volumen: 15 m³.	Limo, arena, gravas, sedimento aluvial masivo grano-arcillosos.	IV-V		160,93
Santa Rosa de Tambo 132	8466300 N 470800 E	Margen de Río, Vertiente de detritos ocupada por tierras de cultivo	Deslizamiento rotacional de tierras en la margen derecha de quebrada, deslizamiento de detritos sobre una distancia de 90 m, reactivado con el sismo. Volumen: 60 m³.	Lutitas arcillosita masiva, arcillas y limos.	IV-V		162,77
Vivanco 133	8471200 N 442150 E	Talud de colina en la margen izquierda del río Ica.	Caída de rocas por movimiento de talud, acumulación de bloques en el talud, y talus de detritos menores, con 1,50 m de	Intrusiva, material coluvial, rocas muy fracturadas	IV	No se registran daños	133,65

			diámetro, en una distancia de 350 m Volumen: 25 m³.				
CUENCA RÍO PAMPAS							
Río Pampas /Colcapampa 134	8530710 N 494300 E	Colinas onduladas con ladera concava-convexa por movimiento en masa convexo, en la margen izquierda del río Pampas.	Deslizamiento activo de gran magnitud, con pequeños reactivaciones en el cuerpo en una longitud de 500-600 m; remoción superficial de cuerpo por movimiento, que involucra un volumen superficial menor a 10 m³. Deslizamiento activo con grandes filtraciones de agua.	Roca volcánico-sedimentaria muy alterada. Volumen: < 10 m³.	IV-V	No se registran daños.	

CUADRO Nº OTRAS ÁREAS CON DEFORMACIONES SUPERFICIALES GENERADAS POR EL SISMO DE PISCO

SECTOR/ PARAJE	COORDEN. (WGS84)[1]	MORFOLOGÍA	PROCESOS GEOLÓGICOS OBSERVADOS	SUBSTRATO ROCOSO /SUELO	INTENS. INQUA	DAÑOS OCASIONADOS
Monte Fuerte (Chongos) 135	8485256 N 382362 E	Llanura y cauce fluvial	Fracturas y agrietamientos en el terreno (N95º); presencia de volcanes de arena. Proceso de licuación en la margen izquierda del río Pisco.	Depósitos aluviales (arenas y limos), parcialmente saturados.	VI-VII	No se registro daños.
Cuchilla Vieja (Valle de Pisco) 136	8483297 N 388444 E	Llanura aluvial	Asentamiento de terreno por licuación. Salto de 0,30 a 0,45 m, abertura de 10 a 25 cm y profundidad de 0,50 a 0,60 m; zona húmeda.	Depósitos aluviales (arenas y limos), parcialmente saturadas.	VI-VII	Afecta terrenos de cultivo
Frente a Huarangal (valle de Pisco) 137	8482820 N 389047 E	Llanura aluvial	Asentamiento de vivienda y agrietamientos en el suelo por proceso de licuación. En el mismo sector asentamientos en el camino.	Depósitos aluviales (arenolimosos), parcialmente saturados.	VI-VII	Afectó una vivienda
Cerca de caserío de Paracas (valle de Pisco) 138	8481961 N 391488 E	Llanura aluvial	Pequeño sector con asentamiento de terreno (60 m), con salto de 0,15 a 0,20 m. Agrietamientos e inclinación de árboles y poste de luz.	Depósitos aluviales.	VI-VII	Afecta tramo de trocha y un poste de luz.
San Juan de Cóndor (Valle de Pisco) 139	8486210 N 387382 E	Terraza aluvial y terrenos de cultivo	Fuertes agrietamientos y asentamientos de terreno en un área semicircular, muy húmeda que produjo en conjunto deslizamiento-flujo de tierra. Podrían corresponder a desplazamientos laterales.	Depósitos aluviales (areno-limosos), saturados.	VII	Afectación de terrenos de cultivo.
Cabeza de Toro (Valle de Pisco) 140	8491972 N 388952 E	Planicie aluvial con humedales y totorales	Agrietamientos en el terreno de rumbo N-S y N160º de tipo "roll ver"; proceso de licuación de suelos en un área de aproximadamente 20 has, con abundantes volcanes de arena con emisión de gases.	Depósitos aluviales (areno-limosos), saturados. Substrato de la Formación Pisco.	VII-VIII	Afecta terrenos de cultivos (algodón); colapso de drenes

Cabeza de Toro (Valle de Pisco) 141	8491986 N 389043 E	Planicie aluvial y terrenos de cultivo	Agrietamientos en las chacras; presencia de grietas con expulsión de arenas y afloramiento de agua por licuación. Dueño de parcela menciona que procesos se afloramiento de agua una semana antes del sismo (¿?).	Depósitos aluviales (areno-limosos). Substrato de la Formación Pisco.	VII-VIII	Afecta terrenos de maizales, algodón y vid.
José Olaya (Valle de Pisco) 142	8487978 N 385229 E	Planicie aluvial y terrenos de cultivo	Agrietamientos y asentamientos de tierras; emanaciones de agua y lodo por licuación. Pérdida de agua por grietas al intentar regar sus cultivos.,	Depósitos aluviales areno-arcillosos a areno-limosos. Substrato de la Formación Pisco.	VII-VIII	Agrietamientos en la trocha y gran afectación de tierras de cultivo (maíz, pallar).
Toscania (Valle de Pisco) 143	8489080 N 384970 E	Planicie aluvial y terrenos de cultivo	Agrietamientos de tierras, afloramiento de agua. Asentamiento de terreno de hasta 0,40 m.; licuación de suelos.	Depósitos aluviales areno-limosos. Substrato de la Formación Pisco.	VII-VIII	Asentamientos en las trochas o caminos entre parcelas de cultivos. Colapso y cierre de algunas acequias.
Manrique hacia Montalbán y Benavides (Valle de Pisco) 144	8489655 N 386535 E	Planicie aluvial, terrenos de cultivo y zona de humedales.	Fuertes agrietamientos , volcanes de lodo y asentamientos de tierras producidos por licuación.	Depósitos aluviales areno-limosos. Substrato de la Formación Pisco.	VII-VIII	Colapso de drenes y agrietamientos de trochas. Gran afectación de terrenos de cultivo con alfalfa (20 has)
Sector Salinas (La Hoyada) 145	8488485 N 373542 E	Zona de humedales y colinas	Agrietamientos ay asentamientos de tierras tipo "roll over" en borde de humedales. Predomina la dirección Norte-Sur. Podrían considerarse desplazamientos laterales (Lateral Spreads).	Suelo salitroso; Substrato de la Formación Pisco.	VI-VII	No se registran daños.
Camacho / San Martín 146	8496254 N 373374 E	Planicie aluvial, terrenos de cultivo	Agrietamientos y asentamientos de hasta 1,0 m de salto; grietas en el terreno con aberturas de hasta 0,30-	Depósitos aluviales areno-limosos.	VI-VII	Afecta terrenos de cultivos.

			0,40 m y profundidad de 1,20 m. Presencias de volcanes de arena indicativos de procesos de licuación de arenas.			
Callejón (Camacho) 147	8496821 N 373156 E	Planicie aluvial y terrenos de cultivo	Emanación de agua y lodo; agrietamientos y asentamientos en el terreno.	Depósitos aluviales areno-limosos.	VI-VII	Afectó terrenos de cultivo y trocha carrozable
Polvareda, Mariategui y Santa Cruz 148	8489307 N 369268 E	Planicie aluvial, terrenos de cultivo	Agrietamientos de tierras y expulsión de agua	Depósitos aluviales y marinos, areno-limosos.	VI-VII	Afectó terrenos de cultivo con maizales.
Tambo de Mora (Calle Nueva) 149	8512341 N 372019 E	Planicie costera y playa	Intensa licuación de arenas. Fuertes agrietamientos y asentamientos de estructuras. Afloramiento de agua y lodo.	Depósitos marinos.	VII-VIII	Colapso y hundimiento de viviendas de uno a más pisos. Agrietamientos de pistas y veredas y caída de postes de alumbrado publico.
Penal de Tambo de Mora (Chincha). 150	8514799 N 371520 E	Planicie costera y playa	Licuación de suelos; agrietamientos de tierras, emanación de agua y lodo en volcanes y grietas alineadas. Algunas fracturas en echelón.	Depósitos marinos	VII-VIII	Caída de gran número de postes de alumbrado, colapso de estructuras en penal
Entre Penal y carretera a Sunampe (Chincha) 151	8514799 N 372049 E	Planicie costanera; acantilados	Área con asentamientos y agrietamientos tipo "roll over" en el pie de borde de acantilados con dirección predominante N-S. Alineamientos se presentan desde la subida de Jahuay hacia Chincha.	Depósitos aluviales con mezcla de arenas, limos; gravas en los acantilados.	VI-VII	No se reportan daños.
Casaya hasta cerca de carretera (San	8484157 N 375821 E	Colinas bajas y humedales	Asentamientos y agrietamientos, producida por licuación de suelos, relacionada a zona con pequeño	Formación Pisco y depósitos aluviales.	VI-VII	Colapso de viviendas y tuberías de desague.

Clemente, Pisco) 152			humedal. Licuación de suelos.			
Fundo Don Oscar (Cañete) 153	8556816 N 341569 E	Planicie aluvial y terrenos de cultivo	Deslizamientos en la margen derecha de canal o acequia	Depósitos aluviales arcillo-arenosos		Afecta acequia en un tramo de 60 m de longitud.
Puente La quebrada / canal San Miguel (Cañete) 154	8557397 N 347716 E	Planicie aluvial y terrenos de cultivo	Asentamientos hacia el dren o acequia	Suelo con relleno antrópico y depósitos aluviales	VI-VII	60-65 m.l. de acequia obstruidos
La Quebrada (San Luis, Cañete) 155	8558609 N 348367 E	Planicie aluvial y terrenos de cultivo	Asentamientos y agrietamientos en plataforma de carretera y bordes de canales hacia los cultivos. Licuación de suelos por probable indicio de nivel freático superficial	Suelo aluvial gravo arenoso.	VI-VII	Afectó 450 m.l. de acceso carretera a La Quebrada afectados. Grietas en las chacras.
Compradores y sector de La Huaca (San 156 Luis, Cañete)	8559993 N 348426 E	Planicie aluvial y terrenos de cultivo	Licuación de suelos; procesos de afloramiento de aguas, agrietamientos y asentamientos de terreno tipo roll over	Suelo aluvial gravo arenoso.	VII-VIII	Gran afectación de tierras de cultivo y una vivienda; trocha carrozable
Canta Gallo (San Luis, Cañete) 157	8561356 N 347716 E	Planicie aluvial y terrenos de cultivo	Agrietamientos y asentamientos en borde de canal (ambas márgenes), en tramo de 300 m de longitud. Fracturamientos de dirección N 45º	Suelo aluvial gravo arenoso.	VII-VIII	Afecta tramo de trocha carrozable, obstrucción de canal

Landslides from Zavala et al. (2009) Report

CUADRO 1: Deformaciones superficiales asociadas al sismo de Pisco del 15/08/2007

	Paraje	Morfología	Características	Daños	Dist. al epicentro (Km)	Intens. Inqua
1	Entre Cerro Colorado y Jahuay	Ladera con depósitos eólicos y residuales.	Agrietamientos y hundimientos de terreno	Asentamientos en talud inferior de carretera.	68,16	VI
2	Jahuay	Acantilado y playa	Licuación; agrietamientos que muestran evidencias de afloramiento de agua.	Hundimiento de carretera.	68,00	VII
3	Pampa Camacho	Planicie costanera y zona de bofedal	Licuación; grietas de 0,50 m de ancho y 0,60 m de profundidad	Caída de poste de luz; agrietamientos en la carretera	66,39	VI-VII
4	(Km 218 al 222)	Planicie costera bofedal	Licuación	Agrietamientos en la carretera.	65,98	VI-VII
5	Entre puente Huamaní y Casaya	Valle de Pisco y terrazas aluviales.	Licuación; depósitos aluviales y secuencias de la Formación Pisco.	Agrietamientos en el puente.	66,11	VI-VII
6	Km 229	Planicie costanera.	Licuación; Agrietamientos con azimut 10°.	Agrietamientos y asentamientos en la carretera.	58,05	VI-VII
7	Playa Chaco, Paracas	Litoral y playa.	Licuación; agrietamientos de terreno; depósitos marinos y napa freática superficial.	Viviendas agrietadas, hundimientos en las veredas ,colapso de muros.	57,66	VI-VII
8	Pisco Playa	Costa y playa	Licuación; volcanes de lodo	Agrietamientos de paredes de viviendas.	65,11	VI-VII
9	Entre Pisco y Panamericana Sur	Planicie costanera	Licuación	Agrietamientos en viviendas y carretera. Rotura detuberías de agua potable.	65,55	VI-VII
10	Km 232	Planicie costanera y zona de bofedal	Licuación	Agrietamientos y asentamientos en la carretera.	65,67	VI-VII
11	Km 235 + 300	Planicie costanera y zona de bofedal	Licuación		65,39	VI-VII
12	Entre Villa Túpac Amaru y Chongos	Planicie aluvial	Licuación; fracturas en el terreno y expansión lateral. Azimut 90°	Terrenos de cultivo.	69,09	VI-VII
13	Monte Fuerte (Chongos)	Valle del río Pisco.	Volcanes de arena; agrietamientos con azimut 95°.	Agrietamientos en la carretera.	72,78	VI-VII
14	Cuchilla Vieja	Terraza aluvial	Agrietamientos con azimut 75°, desplazamiento 0,50 m.	Asentamiento de viviendas	78,93	VI-VII
15	Frente a Huarangal	Terraza aluvial	Licuación	Agrietamientos en la carretera.	79,67	VI-VII
16	Caserío de Paracas	Terraza aluvial	Licuación	Agrietamientos en la carretera.	82,15	VI-VII
17	San Juan de Cóndor	Terraza aluvial y bofedal	Expansión lateral. Fracturas con azimut 120° y desplazamientos de 1 m.	Terrenos de cultivo y canal.	77,69	VII
18	Cabeza de Toro	Planicie aluvial y bofedales.	Licuación; volcanes de lodo; grietas con azimut 160°.	Terrenos de cultivo y acequias.	79,45	VII-VIII
19	Cabeza de Toro	Planicie aluvial y bofedales.	Licuación; agrietamientos en el terreno con aberturas de 0,05 a 0,10 m y 0,40 m de profundidad.	Terrenos de cultivo .	79,46	VII-VIII
20	José Olaya	Lomadas y piedemontes Bofedales	Licuación; expansión lateral Fracturas con azimut 15° y desplazamientos de 0,50 m.	Terreno eriazo, salitral.	75,67	VII-VIII
21	Toscanía	Planicie aluvial	Licuación;agrietamientos, asentamientos en varios sectores; fracturas en echelón.	Terrenos de cultivos, caminos o trochas carrozables y linderos de parcelas. Obstrucción de acequias.	75,33	VII-VIII
22	Manrique hacia Montalbán y Benavides	Planicie aluvial y. zona de bofedales	Licuación;agrietamientos, asentamientos; volcanes de lodo alineados en grietas principales.		76,90	VII-VIII
23	Sector Salinas (La Hoyada)	Planicie aluvial	Licuación;agrietamientos, y asentamientos.		64,06	VI-VII
24	Camacho / San Martín	Planicie aluvial	Licuación; agrietamientos con azimut 90° y asentamientos de terreno.	Agrietamientos de terrenos de cultivo y en los límites de parcelas.	64,23	VI-VII
25	Polvareda, Mariátegui y Santa Cruz	Planicie aluvial			59,79	VI-VII
26	Callejón (Camacho)	Planicie aluvial	Licuación; volcanes de arena.	Agrietamientos de terrenos de cultivo.	65,85	VI-VII
27	Tambo de Mora (Calle Nueva)	Zona litoral	Licuación; agrietamientos, hundimientos y expulsión de agua. Volcanes de lodo.	Colapso de viviendas	67,07	VII-VIII

Continúa Cuadro 1

	Paraje	Morfología	Características	Daños	Dist. al epicentro (Km)	Intens. Inqua
28	Penal de Tambo de Mora.	Planicie aluvial y zona cercana al litoral.	Licuación; expansión lateral, agrietamientos y volcanes de lodo.	Colapso de muros y estructuras.	67,52	VII-VIII
29	Entre Penal Tambo de Mora y Sunampe	Acantilado y planicie aluvial	Licuación; expansión lateral del terreno, agrietamientos y asentamientos.	Hundimiento de terrenos.	67,93	VII-VIII
30	Casaya hasta cerca de carretera	Planicie aluvial	Licuación; relleno antrópico y zona de bofedal. Agrietamientos de terreno	Daños en estructuras de viviendas, grietas en la carretera.	66,42	VI-VII
31	Fundo Don Oscar	Planicie aluvial	Licuación; agrietamientos.	Agrietamiento de terraplenes de carretera.	76,16	VI
32	Puente La Quebrada y canal San Miguel	Planicie aluvial	Licuación	Agrietamientos y asentamientos en la carretera que accede a La Quebrada.	78,99	VI-VII
33	La Quebrada	Planicie aluvial	Licuación		80,46	VI-VII
34	Compradores y sector de La Huaca	Planicie aluvial y lomadas con nivel freático superficial	Licuación; Surgimientos de arena, lodo y agua en gran cantidad, alineados a lo largo de las fracturas.	Viviendas colapsadas; terrenos de cultivo agrietados.	82,07	VII-VIII
35	Canta Gallo	Planicie aluvial	Licuación	Chacras agrietadas y colapso de acequias.	82,70	VII-VIII

CUADRO 2: Movimientos en masa detonados por el sismo de Pisco del 15/08/2007

	Paraje	Tipo de MM	Vol. (m^3)	Intens. INQUA	Dist. al epicentro(Km)
	Reserva Nacional de Paracas				
1	Playa Talpo	Derrumbe	30	VII	48,77
2	Lechuza Baja (Playa Los Choros)	Derrumbe	70	VII	50,52
3	Punta Arquillo: Mirador de Lobos N° 3	Derrumbe y deslizamiento	15	VII	52,31
4	Punta Arquillo: Mirador de Lobos N° 2)	Caída de rocas y derrumbe	15	VII	52,32
5	Punta Arquillo: Mirador de Lobos N° 1	Caída de rocas	15	VII	52,22
6	Playa Arquillo	Caída de rocas y derrumbe	250	VII	52,57
7	Punta Prieto	Caída de rocas y derrumbe	150	VII	53,72
8	Playa La Mina	Caída de rocas	10	VII	55,08
9	Entre Frontón y La Mina	Deslizamiento	12000	VII	32,04
10	Playa Roja	Caída de rocas y derrumbe	120	VII	55,22
11	Cerca de Punta Santa María	Caída de rocas	30	VII	55,94
12	Playa Yumaque	Caída de rocas y derrumbe	80	VII	58,56
13	Punta del Cielo	Derrumbe, deslizamiento y caída de rocas	200	VIII	57,84
14	Punta del Cielo	Derrumbe, deslizamiento y caída de rocas	250	VIII	58,27
15	Punta del Cielo	Derrumbe, deslizamiento y caída de rocas	350	VIII	58,46
16	La Catedral y La Bóveda	Derrumbe, deslizamiento y caída de rocas	750	VIII	57.49
17	Playa Salinas y Frayles	Derrumbe, deslizamiento y caída de rocas	600	VII	62,31
18	Sector Puente	Caída de rocas	600	VII	63,78
	Acantilados costeros entre Cañete y Chincha				
19	Entre Cerro Colorado y Jahuay	Caída de rocas y de detritos	5250	VI	53,73
20	Jahuay (Chincha)	Caída de rocas y de detritos	125	VII	52,25
	Tramo de carretera: San Clemente-Humay-Huancano-Pampano-Huaytará-Puente Rumichaca				
21	Quebrada Cocanansaño. (Km. 59+800)	Derrumbe	45	VII	117,59
22	Pasando Patipampa. (Km. 83+250)	Caída de rocas	35	VII	132,29
23	Cerro Jajahuacce. (Km. 83+360)	Derrumbe	24	V	134,96
24	Pasando quebrada Uchupata (Km. 84+900)		Derrumbe		15 V 135,39
25	Quebrada Cacahuacce. Km. 85+700	Caída de rocas	15	IV	136,09
26	Frente a la mina Santa Elena (Km. 90+250)		Derrumbe		67.5 V 139,49
27	Tullpa (Km. 93+500)	Derrumbe	15	V	142,54
28	Capana (Km. 95+200)	Derrumbe y deslizamiento	8750	VIII	145,29
29	Jerque	Caída de rocas	23	V	152,29
30	Km. 118 -123	Caída de rocas	100	V	
31	Quebrada Sayauma	Deslizamiento	10	V	159,96
32	Km. 130 + 100	Caída de rocas	10	V	160,39
33	Km. 182	Derrumbe	15	V	197,38
34	Km. 185 +900 - 186 +000	Deslizamiento	70	V	197,77
35	Km 188+450-188+250	Caída de rocas	60	V	198,24
	Tramo de Carretera: Puente Racra-Ticrapo-Puente Infiernillo-Castrovirreyna				
36	Cerro Racra	Caída de rocas	450	V	133,83
37	Cerro Matacaballo	Caída de rocas	150	V	134,71
38	Pampa Blanca	Caída de rocas	45	IV	140,53
39	Quebrada Venturosa	Caída de rocas	90	IV	141,.38
40	Km. 105 +800	Derrumbe	10	V	146,25
41	Cabracancha	Caída de rocas y deslizamiento	60	V	146,47
42	Buenavista / Ticrapo	Agrietamiento y asentamiento		IV	146,36
43	Cabracancha	Deslizamiento	20	V	147,4
44	Km. 112 + 500	Agrietamiento y asentamiento		V	147,63
45	Km. 113 + 000 - 113 + 100	Deslizamiento	20	V	146,78
46	Pata Pata	Derrumbe	180	V	157,75
47	Chuncacc	Derrumbe	10	V	157,71
48	Km. 140 +150 (Entre Sinto y Pucaya)	Caída de rocas	8	V	160,69
	Tramo de carretera: Cañete-Lunahuaná-Yauyos-Chocos-Huangascar y rutas vecinales				
49	Caltopa Alto	Agrietamiento y asentamiento		V	90,17
50	Socsi	Caída de rocas	15	IV	91,17
51	San Agustín	Caída de rocas	10	V	97,22
52	Entrada a Patapampa. Km 38+750	Derrumbe y deslizamiento	50	VII	103,33
53	Frente al cerro Riverón	Derrumbe	35	VII	111,79
54	Frente a San Miguel	Agrietamiento y asentamiento	250	VII	125,7
55	Puente San Miguel	Derrumbe	5	V	125,63
56	Catahuasi	Derrumbe	300	VI	131,04
57	Quebrada Huangascar	Caída de detritos	25	V	127,24
58	Entre Huangascar y Chocos	Derrumbe	15	V	132.05
	Tramo de Carretera: Chincha-San Juan de Castrovirreyna-Tantará-San Pedro de Huacarpana y rutas vecinales				
59	Hacienda San Juan	Caída de rocas	105	V	90,82
60	Frente a Caruya	Caída de rocas	60	IV	94,67
61	Huanchor (Km. 29)	Caída de rocas	800	VI	95,33
62	Huanchor. Km. (30 + 800)	Caída de rocas	450	VI	116,11
63	Huauyapa. (Km. 33 + 200)	Caída de rocas	30	IV	99,07
64	Hda. Atahuaranga. (Km. 35).	Caída de rocas	40	VI	99,87
65	Cabecera de Huachinga. (Km. 42)	Caída de detritos	400	IV	105,92
66	Km 48-50 San Juan-Tantará	Caída de rocas	150	V	118,36
67	Santa María de Yanapampa	Caída de rocas	5	IV	121,64
68	Huancho Grande	Derrumbe	20	V	122,18
69	Chata	Caída de detritos	15	IV	133
70	Palca	Caída de detritos	180	V	135,56

Continúa Cuadro 2

Paraje	Tipo de MM	Vol. (m^3)	Intens. INQUA	Dist. al epicentro(Km)
Reserva Nacional de Paracas				
71 Frente a Lunche	Caída de rocas	80	V	132,95
72 Pache	Derrumbe	15	IV	133,83
73 Entre Tambo y Huacasca	Derrumbe y caída de detritos	20	V	138,65
Tramo: San Juan -Yanac-Liscay				
74 Huayto	Caída de rocas	90	IV	104,38
75 Cerro Rupasca	Deslizamiento	60	V	107,11
Tramo: Palca-Villa de Arma				
76 Palca	Caída de detritos	150	V	132,09
77 Frente a Pumani	Derrumbe	10	V	136,35
78 Entre Huachacmarán y Acomachay	Caída de rocas y derrumbe	300	V	138,27
Tramo de carretera: Ica-Cochiarcas-Pampahuasi-Andaymarca-Santiago de Chocorvos				
79 Cerro Puca Puca	Caída de rocas y de detritos	20	V	154,33
80 Tingo	Caída de rocas y de detritos	10	V	155,34
81 Entre Tingo y Sauces.	Caída de rocas y deslizamiento	25	V	155,11
82 Sauces	Caída de rocas	20	V	154,78
83 Quebrada Andaymarca	Caída de rocas	15	V	154,89
84 San Antonio de Andaymarca.	Caída de rocas y derrumbe	80	V	154,78
85 Puccquillua	Caída de rocas y derrumbe	90	V	156,24
Tramo de carretera: Ica-San José de los Molinos-Huamani -Tambo-Santo Domingo de Capillas-Santiago de Chocorvos				
86 Labanda /Bocatama La Achirana	Caída de rocas y derrumbe	12	IV	120,35
87 Sector Socavón	Caída de detritos	150	V	131,38
88 Quebrada Dos Aguas	Caída de detritos	250	V	138,17
89 Entre Tambo y Capilla.	Caída de rocas	10	V	162,57
90 Cerro Huañacancha	Caída de rocas	5	V	170,39
Cuenca río Cañete				
91 Cerro Campana	Caída de detritos	20	V	127,36
92 San Jerónimo de Yanac	Caída de detritos	5	V	112,57
93 Frente a Zañin	Caída de detritos	40	V	145,17
94 Huanchac	Caída de rocas	15	V	149,88
95 Entre Yaca y Caullama	Caída de rocas	20	V	156,64
96 Quichca	Derrumbe	10	V	128,39
97 Entre Suquia y Quichca	Caída de rocas	35	V	129,28
98 Frente a Pallca	Caída de rocas y derrumbe	15	V	130,51
99 Cerro Pucahuasi (Huangascar)	Deslizamiento	10	IV	132,15
100Tranca (Huangascar)	Derrumbe	10	IV	131,37
101Río Viñac	Derrumbe	10	V	133,1
102Quebrada Catacancha	Derrumbe	20	V	132,6
103Frente a Chocos	Caída de detritos	10	IV	127,32
104Entre Cascajal y Huayabo (C° Poquio)	Caída de detritos	25	V	124,25
105Frente a Huancaya	Caída de detritos	5	IV	192,92
Cuenca río San Juan-Chincha				
106Tripunca	Caída de detritos	20	VI	107,81
107Canlupuquio	Deslizamiento	10	IV	135,05
108Cerca de Ayacuchito	Caída de rocas y derrumbe	10	IV	119,09
109Songo Chico	Caída de rocas	20	V	130,56
110Cascanni	Derrumbe y deslizamiento	50	V	133,73
111Quebrada Jasa Huishcana	Derrumbe	5	V	141,79
112Molienda	Deslizamiento	10	V	142,8
113Río Castrovirreyna	Derrumbe	150	V	166,09
Cuenca río Pisco				
114Jatumpampa	Caída de detritos	5	IV	161,99
115Río Pisco	Caída de detritos	300	IV	138,29
116Pampanito. (Frente a Km. 101)	Derrumbe y deslizamiento	5279	VIII	147,75
117Río Vizcacha	Deslizamiento	12	V	156,78
118Valle del Río Arma/Río Vizcacha	Caída de rocas	20	IV	152,74
119Quito Arma / Collcapampa	Deslizamiento	25	V	155,02
120Quito Arma	Derrumbe y deslizamiento	60	V	156,17
121Huayacundo Arma	Deslizamiento	75	V	156,74
122Río Quito Arma	Derrumbe	110	V	159,33
123San Antonio de Cusicancha	Deslizamiento	15	V	159,37
124Taurcarpata / Ticrapo	Derrumbe y caída de detritos	60	V	145,78
125Tarayocc	Derrumbe	40	V	145,05
126Chalma	Deslizamiento	35	V	152,14
127Quebrada Infiernillo	Derrumbe y deslizamiento	100	V	151,2
128Río Castrovirreyna	Derrumbe y caída de detritos	25	V	160,91
Cuenca río Ica				
129Quebrada Chincao	Derrumbe y deslizamiento	20	V	159,57
130Morro / Río Ica	Caída de detritos	30	IV	132,92
131Santa Rosa de Tambo	Deslizamiento	15	V	160,93
132Santa Rosa de Tambo	Deslizamiento	60	V	162,77
133Vivanco	Caída de rocas	25	IV	133,65
134Río Pampas / Colpabamba	Deslizamiento	10	IV	173,96

Fuente: Elaboración propia con datos de campo (Zavala, B., Valderrama, P., Hermanns, R. y Costa, C.).

Landslides from Dr. Joseph Wartman's Reconnaissance

Landslides Mapped by Dr. Wartman				
ID	Latitude	Longitude	Volume	Landslide Type
2	-12.578949	-76.704961	4875	Debris/earth lateral spread
3	-12.578241	-76.704392	2400	Debris/earth lateral spread
4	-12.576867	-76.702954	5600	Debris/earth lateral spread
5	-12.576696	-76.703523	3200	Debris/earth lateral spread
11	-13.805212	-76.293526	128100	Debris/earth lateral spread
15	-13.832828	-76.248636	5040	Debris/earth lateral spread
61-1	-13.696428	-76.157231	1851	Rock fall
61-2	-13.696022	-76.157633	4519	Rock fall
61-3	-13.695861	-76.157881	1800	Rock fall
62	-13.686583	-76.158595	294	Rock fall
64	-13.682302	-76.107686	3384	Debris/earth lateral spread
65	-13.726999	-75.940756	18	Rock fall
71	-13.686133	-75.803277	94	Rock fall
72	-13.684679	-75.798267	450	Rock fall
80	-13.661177	-75.756306	360	Rock fall
81	-13.65754	-75.748715	10	Rock fall
100	-13.611487	-75.646325	15	Rock fall
113	-13.608134	-75.562152	25	Rock fall
116	-13.571211	-75.540383	22	Rock fall
117	-13.570363	-75.539986	20	Rock fall
118	-13.56922	-75.539294	18	Rock fall
119	-13.567997	-75.538747	18	Rock fall
125	-13.59233	-75.500295	25	Rock fall
129	-13.612592	-75.427848	5000	Debris/earth fall
130	-13.610306	-75.415864	75000	Rock fall
133	-13.611009	-75.400297	4500	Rock fall
137	-13.608987	-75.332544	3500	Debris/earth fall
139	-13.608037	-75.32447	400	Debris/earth fall
143	-13.587384	-75.282644	700	Debris/earth fall
145	-13.538273	-75.181391	2	Debris/earth fall
153	-13.588366	-75.316097	35000	Rock fall
157	-13.610559	-75.396901	42000	Rock fall
225	-13.425046	-76.189182	2745000	Debris/earth lateral spread
626	-13.922649	-76.288436	39840	Rock slump
642	-13.923072	-76.288293	281996	Rock slump
659	-13.9051	-76.318092	89240	Rock slump
670	-13.915318	-76.340096	18368	Rock slump
681	-13.914977	-76.341173	34342	Rock slump
694	-13.914947	-76.343779	5899	Rock slump
697	-13.915089	-76.344268	4186	Rock slump
880	-13.922178	-76.28792	99792	Rock slump
900	-13.923446	-76.288664	179377	Rock slump
905	-13.923816	-76.289217	58317	Rock slump
910	-13.924083	-76.28957	6698	Rock slump
913	-13.92456	-76.290059	11475	Rock slump
919	-13.924969	-76.290413	5706	Rock slump
927	-13.925383	-76.290852	22933	Rock slump
937	-13.926334	-76.291541	86238	Rock slump
950	-13.926738	-76.292199	22825	Rock slump

Landslides Mapped by Dr. Wartman				
ID	Latitude	Longitude	Volume	Landslide Type
960	-13.92715	-76.292745	28925	Rock slump
973	-13.927732	-76.293803	51548	Rock slump
986	-13.928259	-76.294168	114688	Rock slump
990	-13.9292	-76.294197	13733	Rock slump
1A	-12.211545	-76.985117	2400	Debris/earth lateral spread
1B	-12.211544	-76.985117	6000	Debris/earth lateral spread
3A	-13.414375	-75.982924	25	Rock fall
4A	-13.415545	-75.96185	7	Rock fall
6A	-13.367466	-75.947468	75	Rock fall
7A	-13.3451	-75.938845	25	Rock fall
16A	-13.256934	-75.868747	12	Debris/earth fall
19A	-13.255948	-75.868081	32	Debris/earth fall
37A	-13.38905	-75.891603	20	Rock fall
38A	-13.370109	-75.867979	50	Rock fall
40A	-13.374501	-75.839363	1200	Rock fall
44A	-13.368889	-75.764611	150	Rock fall
46A	-13.367103	-75.751717	50	Debris/earth fall
50A	-13.224595	-75.602029	22.5	Rock fall
53A	-13.121317	-75.658873	50	Rock fall
204A	-13.415465	-75.961769	202	Rock fall
225A	-13.368161	-75.946971	151	Rock fall
230A	-12.848967	-75.958953	120	Rock fall
231A	-12.827063	-75.91722	200	Debris/earth fall
232A	-12.844352	-75.940985	2400	Rock fall
243A	-12.909169	-75.829798	56394	Debris/earth slump
257A	-12.9062	-75.828814	6760	Debris/earth slump
296A	-13.710666	-75.839304	8000	Rock fall
334A	-13.66034	-75.761908	140	Rock fall
358A	-13.929626	-76.294045	24896	Rock slump
475A	-13.920119	-76.287332	15574	Rock slump
483A	-13.919888	-76.286744	32167	Rock slump
502A	-13.920254	-76.285817	21336	Rock slump
505A	-13.920211	-76.28508	44850	Rock slump
516A	-13.919693	-76.283278	29250	Rock slump
522A	-13.901628	-76.295502	21670	Rock slump
540A	-13.892775	-76.298516	213750	Rock slump
594A	-13.933211	-76.289048	15810	Rock slump
605A	-13.933841	-76.288678	40325	Rock slump
611A	-13.935507	-76.287246	3980	Rock slump
613A	-13.93605	-76.286425	9585	Rock slump
619A	-13.936023	-76.28549	15300	Rock slump
626A	-13.936395	-76.284539	14910	Rock slump
630A	-13.94308	-76.276987	25512	Rock slump
646A	-13.954719	-76.270936	433080	Rock slump
660A	-13.952515	-76.271815	159960	Rock slump
704A	-13.95666	-76.271248	18272	Rock slump
716A	-13.957812	-76.27161	72668	Rock slump
733A	-13.959153	-76.272578	80298	Rock slump
762A	-13.961394	-76.271858	11150	Rock slump

Landslides Mapped by Dr. Wartman				
ID	Latitude	Longitude	Volume	Landslide Type
771A	-13.962173	-76.271503	3887	Rock slump
783A	-13.963296	-76.271038	21728	Rock slump
803A	-13.964984	-76.270771	469620	Rock slump
815A	-13.967628	-76.270356	141723	Rock slump
832A	-13.969472	-76.269635	67459	Rock slump
A	-13.39745	-76.196286	520000	Debris/earth avalanche
B	-13.414117	-76.189478	67000	Debris/earth slump
A36	-13.717097	-76.154353	900	Debris/earth lateral spread
A37	-13.708965	-76.152353	375	Debris/earth lateral spread
A38	-13.69983	-76.151518	375	Debris/earth lateral spread
A39	-13.697677	-76.152678	16100	Debris/earth lateral spread
A41	-13.691563	-76.156006	47000	Debris/earth lateral spread
A42	-13.69056	-76.156192	375	Debris/earth lateral spread
A43	-13.691107	-76.155376	1500	Debris/earth lateral spread
A45	-13.694335	-76.15303	3750	Debris/earth lateral spread
A46	-13.69659	-76.153147	23000	Debris/earth lateral spread
A126	-13.730499	-76.157933	300	Debris/earth lateral spread
A127	-13.715946	-76.154101	300	Debris/earth lateral spread
A128	-13.709308	-76.152375	300	Debris/earth lateral spread
A131	-13.682337	-76.10706	10000	Debris/earth lateral spread
J1	-13.793392	-76.328061	1400	Rock slump
J10	-13.892322	-76.303981	301	Rock slump
P63	-13.916303	-76.347092	42108	Rock slump
P66	-13.920986	-76.34954	11250	Rock slump
P67	-13.921645	-76.35168	2465	Rock slump
P69	-13.921578	-76.357173	60240	Rock slump
P88	-13.90166	-76.295341	14762	Rock slump
P95	-13.919748	-76.283475	17544	Rock slump
P104	-13.919899	-76.284557	24196	Rock slump
P109	-13.920206	-76.285838	36680	Rock slump
P121	-13.919857	-76.287087	31464	Rock slump
P128	-13.92145	-76.287714	16688	Rock slump
S1	-13.913617	-76.363243	30450	Rock slump
S2	-13.913193	-76.365401	65472	Rock slump
S3	-13.818031	-76.367106	83040	Rock slump
S4	-13.802798	-76.361798	59150	Rock slump
S5	-13.80177	-76.340405	50184	Rock slump
S6	-13.800925	-76.337319	3738	Rock slump
S7	-13.907572	-76.291322	15844	Rock slump

INGEMMET Landslides Modified during Dr. Joseph Wartman's Reconnaissance

INGEMMET Points Modified by Dr. Wartman				
ID	Latitude	Longitude	Volume	Landslide Type
J5	-13.91719	-76.347949	3140	Rock slump
J7	-13.917503	-76.333653	16820	Rock slump
J10	-13.892322	-76.303981	301	Rock slump
J18	-13.993936	-76.278037	45	Rock slump
J19	-13.30404	-76.252396	5250	Rock fall
J21	-13.629693	-75.674533	375	Rock fall
J29	-13.607677	-75.354768	600	Rock fall
J32	-13.582173	-75.281161	500	Rock fall
J40	-13.396607	-75.439744	2815	Debris/earth slump
J41	-13.392152	-75.438258	2045	Debris/earth slump
J42	-13.388995	-75.439139	1700	Rockfall
J43	-13.389499	-75.429479	1316	Debris/earth slump
J44	-13.395674	-75.43022	1044	Debris/earth slump
J45	-13.40049	-75.43227	807	Rock fall
J46	-13.364246	-75.345516	645	Rock fall
J47	-13.353151	-75.339387	72	Rock fall
J51	-13.015821	-76.167858	30	Rock fall
J53	-12.901422	-76.090885	749	Rock fall
J78	-13.201768	-75.578664	561	Rock fall
J84	-13.936209	-75.355023	85	Rock fall
J114	-13.493923	-75.279053	40	Rock fall
J117	-13.59312	-75.314064	30	Rock fall
J121	-13.538408	-75.318844	2452	Debris/earth slump
J123	-13.505168	-75.29739	80	Rock fall
J125	-13.3293	-75.468154	150	Rock fall

Final Combined Landslide Inventory

Landslide Inventory Combined from 3 Sources: INGEMMET, Zavala, and Wartman							
INGEMMET ID	Zavala ID	Wartman ID	Name	Latitude	Longitude	LS type	volume (m^3)
1	C2-1	J1	Playa Talpo	-13.7918041	-76.3284774	Rock slump	1400
2	C2-2		Lechuza Baja (Playa Los Choros)	-13.9118515	-76.3650384	Rock slump	70
3	C2-3	P67	Punta Arquillo: Mirador de Lobos Nº 3	-13.9219597	-76.3517433	Rock slump	2465
4	C2-4	P66	Punta Arquillo (Mirador de Lobos Nº 2)	-13.9211578	-76.3496471	Rock slump	11250
5	C2-5	J5	Punta Arquillo Mirador de Lobos Nº 1	-13.9171896	-76.347949	Rock slump	3140
6	C2-6	P63	Playa Arquillo	-13.9163448	-76.347065	Rock slump	42108
7	C2-7	J7	Punta Prieto	-13.9175033	-76.3336527	Rock slump	16820
8	C2-8		Playa LaMina	-13.9143593	-76.3166713	Rock fall	10
9	C2-9	659	Entre Frontón y La Mina acceso a La Mina	-13.9052392	-76.3181188	Rock slump	89240
10	C2-10	J10	Playa Roja	-13.8920251	-76.3042192	Rock slump	301
11	C2-11	540A	Cerca de Punta Santa María	-13.893275	-76.296999	Rock slump	213750
18	C2-18	J18	Sector Puente	-13.9939363	-76.278037	Rock slump	45
19	C2-19	J19	Entre Cerro Colorado y Jahuay	-13.3040403	-76.2523958	Rock fall	5250
20	C2-20		Jahuay (Chincha)	-13.4138855	-76.1882605	Rock fall and debris/earth fall and reactivated former landslide	125
21	C2-21	J21	Quebrada Cocanansaño (Km 59+800)	-13.6296928	-75.6745332	Rock fall	375
22	C2-22		Pasando Patipampa (Km 83+250)	-13.5747163	-75.5421865	Debris/earth avalanche	35
23	C2-23		Cerro Jajahuacce (Km 83+360)	-13.5830524	-75.5168881	Debris/earth slump	24
24	C2-24		Pasando quebrada Uchupata (Km 84+900)	-13.5930992	-75.5119553	Debris/earth slump	15
25	C2-25		Quebrada Cacahuacce Km 85+700 Cacahuacce Km 85+700	-13.5935295	-75.5049125	Rock fall	15
26	C2-26		Frente a la mina Santa Elena (Km 90+250)	-13.615077	-75.4724173	Debris/earth slump	67.5
27	C2-27		Tullpa (Km 93+500)	-13.6097385	-75.4450248	Debris/earth slump	15
28	C2-28	130	Capana (Km 95+200)	-13.610306	-75.415864	Rock fall	75000
29	C2-29	J29	Jerque	-13.6076772	-75.3547681	Rock fall	600
30	C2-30		Km 118 -123			Rock fall and rock slump	100
31	C2-31		Quebrada Sayauma	-13.5908944	-75.284712	Debris/earth slump and reactivated former landslide	10
32	C2-32	J32	Km 130 + 100	-13.5821727	-75.2811614	Debris/earth slump	500
33	C2-33		Km 182	-13.4340509	-74.9562586	Debris/earth slump	15
34	C2-34		Km 185 +900 – 186 +000	-13.4042099	-74.9511468	Debris/earth slump and reactivated former landslide	70
35	C2-35		Km 188+450—188+250	-13.3948247	-74.9554898	Rock fall	60
36	C2-36		Cerro Racra	-13.556575	-75.529025	Rock fall and debris/earth fall	450
37	C2-37		Cerro Matacaballo	-13.5435498	-75.52037	Rock fall and debris/earth fall	150
38	C2-38		Pampa Blanca	-13.4927243	-75.4749384	Rock fall	45
39	C2-39		Quebrada Venturosa	-13.4835043	-75.4686004	Rock fall	90
40	C2-40	J40	Km 105 +800	-13.396607	-75.439744	Debris/earth slump	2815
41	C2-41	J41	Cabracancha	-13.3921518	-75.4382581	Debris/earth slump	2045
42	C2-42	J42	Buenavista / Ticrapo	-13.3889945	-75.4391391	Rock fall	1700
43	C2-43	J43	Cabracancha	-13.3894994	-75.4294792	Debris/earth slump	1316
44	C2-44	J44	Km 112 + 500	-13.3956739	-75.4302198	Debris/earth slump	1044
45	C2-45	J45	Km 113 + 000 - 113 + 100	-13.4004899	-75.4322696	Rock fall	807
46	C2-46	J46	Pata Pata	-13.3642464	-75.3455157	Rock fall	645
47	C2-47	J47	Chuncacc	-13.3531507	-75.3393866	Rock fall	72
48	C2-48		Km 140 +150 (Entre Sinto y Pucaya)	-13.3384677	-75.3242221	Rock fall	8
49	C2-49		Caltopa Alto	-13.0467209	-76.2231011	Settlement and cracking	
50	C2-50		Socsi	-13.0448143	-76.2209616	Rock fall	15
51	C2-51	J51	San Agustín	-13.0158208	-76.1678578	Rock fall	30
52	C2-52		Entrada a Patapampa Km 38+750	-12.9603495	-76.1423955	Debris/earth slump and reactivated former landslide	50
53	C2-53	J53	Frente al cerro Riverón	-12.9014223	-76.0908845	Rock fall	749

Landslide Inventory Combined from 3 Sources: INGEMMET, Zavala, and Wartman							
INGEMMET ID	Zavala ID	Wartman ID	Name	Latitude	Longitude	LS type	volume (m^3)
54	C2-54		Frente a San Miguel	-12.8484461	-75.9597057	Settlement and cracking	250
55	C2-55		Puente a San Miguel	-12.8488644	-75.9590346	Debris/earth slump	5
56	C2-56	231A	Catahuasi	-12.8269698	-75.9172762	Debris/earth fall	200
57	C2-57		Quebrada Huangascar	-12.8606599	-75.9274247	Debris/earth fall	25
58	C2-58		Entre Huangascar y Chocos	-12.8961291	-75.8451021	Debris/earth slump	15
59	C2-59		Hacienda San Juan	-13.4176607	-75.9622606	Rock fall	105
60	C2-60		Frente a Caruya	-13.4014064	-75.9279229	Rock fall	60
61	C2-61		Huanchor (Km 29)	-13.4008752	-75.9248362	Rock fall	800
62	C2-62		Huanchor Km (30 + 800)	-13.3942671	-75.7219807	Rock fall	450
63	C2-63	37A	Huauyapa (Km 33 + 200)	-13.3889882	-75.891452	Rock fall	20
64	C2-64		Hda Atahuaranga (Km 35)	-13.3802986	-75.8865441	Rock fall	40
65	C2-65		Cabecera de Huachinga (Km 42)	-13.3732054	-75.8264837	Debris/earth fall	400
66	C2-66		Km 48-50 San Juan- Tantará (Cerro Carhuay Pata)	-13.3559061	-75.717628	Rock fall	150
67	C2-67		Santa Mariade Yanapampa	-13.3428082	-75.6935538	Rock fall	5
68	C2-68		Huancho Grande	-13.3430731	-75.6925665	Debris/earth slump	20
69	C2-69		Chata	-13.1849748	-75.6367609	Debris/earth fall	15
70	C2-70		Palca	-13.2411555	-75.6174311	Debris/earth fall	180
71	C2-71		Frente a Lunche	-13.1619176	-75.6475708	Rock fall	80
72	C2-72		Pache	-13.1245336	-75.656274	Debris/earth slump	15
73	C2-73		Entre Tambo y Huacasca	-13.0603526	-75.6419095	Debris/earth slump and debris/earth fall	20
74	C2-74		Huayto	-13.2501727	-75.8969896	Rock fall	90
75	C2-75		Cerro Rupasca	-13.2559206	-75.8663112	Debris/earth slump and reactivated former landslide	60
76	C2-76	50A	Palca	-13.2245623	-75.6026591	Rock fall	22.5
77	C2-77		Frente aPumani	-13.2137661	-75.5870816	Debris/earth slump	10
78	C2-78	J78	Entre Huachacmarán y Acomachay	-13.2017682	-75.5786641	Rock fall	561
79	C2-79		Cerro Puca Puca	-14.0131146	-75.3761251	Rock fall and debris/earth fall	20
80	C2-80		Tingo	-13.9840149	-75.360263	Rock fall and debris/earth fall	10
81	C2-81		Entre Tingo y Sauces	-13.9784078	-75.3610413	Rock fall and reactivated former landslide	25
82	C2-82		Sauces	-13.9666793	-75.3618656	Rock fall	20
83	C2-83		Quebrada Andaymarca	-13.9618622	-75.3603952	Rock fall and debris/earth fall	15
84	C2-84	J84	San Antonio de Andaymarca	-13.9362092	-75.3550232	Rock fall	85
85	C2-85		Puccquillua	-13.9090111	-75.3359415	Rock fall and debris/earth slump	90
86	C2-86		Labanda/BocatamaLa Achirana	-13.9207246	-75.67759	Rock fall and debris/earth slump	12
87	C2-87		Sector Socavón	-13.8440702	-75.5515215	Debris/earth fall	150
88	C2-88		Quebrada Dos Aguas	-13.7587253	-75.4869863	Debris/earth fall	250
89	C2-89		Entre Tambo y Capilla	-13.7304446	-75.257511	Rock fall	10
90	C2-90		Cerro Huañacancha	-13.742514	-75.1897602	Rock fall	5
91	C2-91		Cerro Campana	-12.8700243	-75.9179577	Debris/earth fall	20
92	C2-92		San Jerónimo de Yanac (ladera NO del cerro Pishcullay)	-13.0762641	-75.9182533	Debris/earth fall	5
93	C2-93		Frente a Zañín	-12.6217606	-75.9621769	Debris/earth fall	40
94	C2-94		Huanchac	-12.5881829	-75.9330544	Rock fall	15
95	C2-95		Entre Yaca y Caullama	-12.5328791	-75.9103062	Rock fall	20
96	C2-96		Quichca	-12.873114	-75.9004588	Debris/earth slump and debris/earth fall	10
97	C2-97		Entre Suquia y Quichca	-12.8720167	-75.8908244	Rock fall	35
98	C2-98		Frente a Pallca	-12.8829595	-75.8631681	Debris/earth slump and debris/earth fall	15
99	C2-99		Cerro Pucahuasi(Huangascar)	-12.8916359	-75.8364694	Debris/earth slump and reactivated former landslide	10

Landslide Inventory Combined from 3 Sources: INGEMMET, Zavala, and Wartman							
INGEMMET ID	Zavala ID	Wartman ID	Name	Latitude	Longitude	LS type	volume (m^3)
100	C2-100		Tranca (Huangascar)	-12.9083824	-75.8305338	Debris/earth slump and reactivated former landslide	10
101	C2-101		Río Viñac	-12.9257156	-75.795747	Rock slump and debris/earth slump	10
102	C2-102		Quebrada Catacancha	-12.9419673	-75.7887002	Debris/earth slump	20
103	C2-103		Frente a Chocos	-12.9177381	-75.8729658	Debris/earth fall	10
104	C2-104		Entre Cascajal y Huayabo (Cerro Poquio)	-12.8468286	-75.9814556	Debris/earth fall	25
105	C2-105		Frente a Huancaya	-12.2011867	-75.8029898	Debris/earth fall	5
106	C2-106		Tripunca, Distrito de Huacro, Huancavelica (Frente a Km 46, carretera a Tantará)	-13.3684371	-75.8135945	Rock fall	20
107	C2-107		Cantupuquio	-13.0916015	-75.6636308	Debris/earth slump and reactivated former landslide	10
108	C2-108		Cerca deAyacuchito	-13.350265	-75.7108335	Debris/earth slump and debris/earth fall	10
109	C2-109		Songo Chico	-13.2760688	-75.6240643	Rock fall	20
110	C2-110		Cascanni	-13.171514	-75.6356095	Debris/earth slump and reactivated former landslide	50
111	C2-111		Quebrada Jasa Huishcana	-13.1645467	-75.5600666	Debris/earth slump	5
112	C2-112		Molienda	-13.9748789	-75.4777618	Debris/earth slump and reactivated former landslide	10
113	C2-113		Río Castrovirreyna	-14.2011805	-75.3219747	Debris/earth slump and debris/earth fall	150
114	C2-114	J114	Jatumpampa	-13.4939229	-75.2790527	Rock fall	40
115	C2-115		Río Pisco	-13.5209432	-75.4944002	Debris/earth avalanche	300
116	C2-116		Pampanito (Frente a Km 101)	-13.6114127	-75.3959766	Debris/earth slump and reactivated former landslide	5279
117	C2-117	J117	Río Vizcacha	-13.5931197	-75.3140641	Rock fall	30
118	C2-118		Valle del RioArma/Rio Vizcacha	-13.5825346	-75.3522349	Rock fall	20
119	C2-119		Quito Arma/Collcapampa	-13.5605424	-75.3336618	Debris/earth slump and reactivated former landslide	25
120	C2-120		Quito Arma	-13.5318457	-75.3243803	Debris/earth slump and reactivated former landslide	60
121	C2-121	J121	Huayacundo Arma	-13.5384084	-75.3188441	Debris/earth slump	2452
122	C2-122		Río Quito Arma	-13.5194319	-75.3091158	Debris/earth slump and reactivated former landslide	110
123	C2-123	J123	San Antonio de Cusicancha	-13.5051684	-75.2973897	Rock fall	80
124	C2-124		Taurcarpata /Ticrapo	-13.3813343	-75.4451653	Debris/earth slump and debris/earth avalanche	60
125	C2-125	J125	Tarayocc	-13.3293001	-75.468154	Rock fall	150
126	C2-126		Chalma	-13.431629	-75.3773616	Debris/earth slump and reactivated former landslide and rock fall	35
127	C2-127		Quebrada Infiernillo	-13.3891023	-75.3957672	Debris/earth slump and reactivated former landslide	100
128	C2-128		Río Castrovirreyna	-13.3222987	-75.3180972	Debris/earth slump and debris/earth fall	25
129	C2-129		Quebrada Chincao	-13.9050823	-75.3049926	Debris/earth slump and debris/earth fall	20
130	C2-130		Morro / Río Ica	-13.8377555	-75.5450294	Debris/earth fall	30

Landslide Inventory Combined from 3 Sources: INGEMMET, Zavala, and Wartman							
INGEMMET ID	Zavala ID	Wartman ID	Name	Latitude	Longitude	LS type	volume (m^3)
131	C2-131		Santa Rosa deTambo	-13.6887443	-75.2725762	Debris/earth slump and reactivated former landslide	15
132	C2-132		Santa Rosa deTambo	-13.8730242	-75.2702448	Debris/earth slump and reactivated former landslide	60
133	C2-133		Vivanco	-13.8282831	-75.5352919	Rock fall	25
134	C2-134		Río Pampas/Colcapampa	-13.2907533	-75.0526249	Debris/earth slump and reactivated former landslide	10
	C1-1		Entre CerroColorado yJahuay	-13.3049083	-76.2552333	Cracks	
	C1-2		Jahuay	-13.4149333	-76.1905194	Liquefaction	
	C1-3		Pampa Camacho	-13.6084722	-76.1506667	Liquefaction	
	C1-4		Km 218 al 222	-13.6394806	-76.1520694	Liquefaction	
	C1-5		Entre puente Huamani y Casaya	-13.6900056	-76.15235	Liquefaction	
	C1-6		Km 229	-13.8351694	-76.2495028	Liquefaction	
	C1-7		Playa Chaco, Paracas	-13.8372389	-76.2533833	Liquefaction	
	C1-8		Pisco Playa	-13.7151194	-76.1605611	Liquefaction	
	C1-9		Entre Pisco Playa y Panamerica Sur	-13.7284278	-76.1577167	Liquefaction	
	C1-10		Km 232	-13.7504583	-76.1637028	Liquefaction	
	C1-11		Km 232 + 300	-13.7378667	-76.1595556	Liquefaction	
	C1-12		Entre Villa Tupac Amaru y Chongos	-13.7076583	-76.1235528	Liquefaction	
135	C1-13		Monte Fuerte(Chongos)	-13.6993787	-76.087876	Liquefaction	
136	C1-14		Cuchilla Vieja (Valle de Pisco)	-13.7173304	-76.0317157	Liquefaction	
137	C1-15		Frente a Huarangal (Valle de Pisco)	-13.721666	-76.0261583	Liquefaction	
138	C1-16		Cerca de caserío de Paracas (valle de Pisco)	-13.7295248	-76.003618	Settlement and cracking	
139	C1-17		San Juan de Cóndor (Valle de Pisco)	-13.6909536	-76.0414203	Debris/earth lateral spread	
140	C1-18		Cabeza deToro (Valle dePisco)	-13.6389212	-76.0266781	Liquefaction	
141	C1-19		Cabeza de Toro (Valle de Pisco)	-13.6387981	-76.0258363	Liquefaction	
142	C1-20		José Olaya(Valle dePisco)	-13.6748851	-76.0612559	Liquefaction	
143	C1-21		Toscanía (Valle de Pisco)	-13.664912	-76.0636058	Liquefaction	
144	C1-22		Manrique hacia Montalbán y Benavides (Valle de Pisco)	-13.6597752	-76.049114	Liquefaction	
145	C1-23		Sector Salinas(La Hoyada)	-13.6698154	-76.1692846	Liquefaction	
146	C1-24		Camacho / San Martín	-13.5995734	-76.1704918	Liquefaction	
147	C1-25		Callejón(Camacho)	-13.5944381	-76.1724814	Liquefaction	
148	C1-26		Polvareda Mariategui y Santa Cruz	-13.6621948	-76.2087598	Liquefaction	
149	C1-27		Tambo de Mora (Calle Nueva)	-13.4540813	-76.1822974	Liquefaction	
150	C1-28		Penal de Tambo de Mora (Chincha)	-13.4318381	-76.1867972	Liquefaction	
151	C1-29		Entre Penal y carretera a Sunampe (Chincha)	-13.4318611	-76.1819114	Settlement and cracking	
152	C1-30		Casaya hasta cerca de carretera (San Clemente, Pisco)	-13.7090407	-76.1484048	Liquefaction	
153	C1-31		Fundo DonOscar (Cañete)	-13.0505671	-76.4611363	Liquefaction	
154	C1-32		Puente La quebrada / canal San Miguel (Cañete)	-13.0456288	-76.404428	Settlement	
155	C1-33		La Quebrada(San Luis, Cañete)	-13.0347048	-76.3983639	Liquefaction	
156	C1-34		Compradores y sector de La Huaca (San Luis, Cañete)	-13.0221964	-76.3977497	Liquefaction	
157	C1-35		Canta Gallo (San Luis, Cañete)	-13.0098395	-76.4042263	Settlement and cracking	
		2		-12.578949	-76.704961	Debris/earth lateral spread	4875
		3		-12.578241	-76.704392	Debris/earth lateral spread	2400
		4		-12.576867	-76.702954	Debris/earth lateral spread	5600
		5		-12.576696	-76.703523	Debris/earth lateral spread	3200

Landslide Inventory Combined from 3 Sources: INGEMMET, Zavala, and Wartman							
INGEMMET ID	Zavala ID	Wartman ID	Name	Latitude	Longitude	LS type	volume (m^3)
		11		-13.805212	-76.293526	Debris/earth lateral spread	128100
		15		-13.832828	-76.248636	Debris/earth lateral spread	5040
		61-1		-13.696428	-76.157231	Rock fall	1851
		61-2		-13.696022	-76.157633	Rock fall	4519
		61-3		-13.695861	-76.157881	Rock fall	1800
		62		-13.686583	-76.158595	Rock fall	294
		64		-13.682302	-76.107686	Debris/earth lateral spread	3384
		65		-13.726999	-75.940756	Rock fall	18
		71		-13.686133	-75.803277	Rock fall	94
		72		-13.684679	-75.798267	Rock fall	450
		80		-13.661177	-75.756306	Rock fall	360
		81		-13.65754	-75.748715	Rock fall	10
		100		-13.611487	-75.646325	Rock fall	15
		113		-13.608134	-75.562152	Rock fall	25
		116		-13.571211	-75.540383	Rock fall	22
		117		-13.570363	-75.539986	Rock fall	20
		118		-13.56922	-75.539294	Rock fall	18
		119		-13.567997	-75.538747	Rock fall	18
		125		-13.59233	-75.500295	Rock fall	25
		129		-13.612592	-75.427848	Debris/earth fall	5000
		133		-13.611009	-75.400297	Rock fall	4500
		137		-13.608987	-75.332544	Debris/earth fall	3500
		139		-13.608037	-75.32447	Debris/earth fall	400
		143		-13.587384	-75.282644	Debris/earth fall	700
		145		-13.538273	-75.181391	Debris/earth fall	2
		153		-13.588366	-75.316097	Rock fall	35000
		157		-13.610559	-75.396901	Rock fall	42000
		225		-13.425046	-76.189182	Debris/earth lateral spread	2745000
		626		-13.922649	-76.288436	Rock slump	39840
		642		-13.923072	-76.288293	Rock slump	281996
		670		-13.9051	-76.3180918	Rock slump	18368
		681		-13.915318	-76.340096	Rock slump	89240
		694		-13.914947	-76.343779	Rock slump	5899
		697		-13.915089	-76.344268	Rock slump	4186
		880		-13.922178	-76.28792	Rock slump	99792
		900		-13.923446	-76.288664	Rock slump	179377
		905		-13.923816	-76.289217	Rock slump	58317
		910		-13.924083	-76.28957	Rock slump	6698
		913		-13.92456	-76.290059	Rock slump	11475
		919		-13.924969	-76.290413	Rock slump	5706
		927		-13.925383	-76.290852	Rock slump	22933
		937		-13.926334	-76.291541	Rock slump	86238
		950		-13.926738	-76.292199	Rock slump	22825
		960		-13.92715	-76.292745	Rock slump	28925
		973		-13.927732	-76.293803	Rock slump	51548
		986		-13.9282585	-76.294168	Rock slump	114688
		990		-13.9292	-76.294197	Rock slump	13733
		1A		-12.211545	-76.985117	Debris/earth lateral spread	2400
		1B		-12.211544	-76.985117	Debris/earth lateral spread	6000
		3A		-13.414375	-75.982924	Rock fall	25
		4A		-13.415545	-75.96185	Rock fall	7
		6A		-13.367466	-75.947468	Rock fall	75
		7A		-13.3451	-75.938845	Rock fall	25
		16A		-13.256934	-75.868747	Debris/earth fall	12
		19A		-13.255948	-75.868081	Debris/earth fall	32

Landslide Inventory Combined from 3 Sources: INGEMMET, Zavala, and Wartman							
INGEMMET ID	Zavala ID	Wartman ID	Name	Latitude	Longitude	LS type	volume (m^3)
		38A		-13.370109	-75.867979	Rock fall	50
		40A		-13.374501	-75.839363	Rock fall	1200
		44A		-13.368889	-75.764611	Rock fall	150
		46A		-13.367103	-75.751717	Debris/earth fall	50
		53A		-13.368161	-75.946971	Rock fall	50
		204A		-13.415465	-75.961769	Rock fall	202
		225A		-13.368161	-75.946971	Rock fall	151
		230A	Puente a San Miguel	-12.848864	-75.953035	Rock fall	120
		232A		-12.844352	-75.940985	Rock fall	2400
		243A		-12.909169	-75.829798	Debris/earth slump	56394
		257A		-12.9062	-75.828814	Debris/earth slump	6760
		296A		-13.710666	-75.839304	Rock fall	8000
		296A		-13.710666	-75.839304	Rock fall	8000
		334A		-13.66034	-75.761908	Rock fall	140
		358A		-13.929626	-76.294045	Rock slump	24896
		475A		-13.920119	-76.287332	Rock slump	15574
		483A		-13.919888	-76.286744	Rock slump	32167
		502A		-13.920254	-76.285817	Rock slump	21336
		505A		-13.920211	-76.28508	Rock slump	44850
		516A		-13.919693	-76.283278	Rock slump	29250
		522A		-13.901628	-76.295502	Rock slump	21670
		594A		-13.933211	-76.289048	Rock slump	15810
		605A		-13.933841	-76.288678	Rock slump	40325
		611A		-13.935507	-76.287246	Rock slump	3980
		613A		-13.93605	-76.286425	Rock slump	9585
		619A		-13.936023	-76.28549	Rock slump	15300
		626A		-13.936395	-76.284539	Rock slump	14910
		630A		-13.94308	-76.276987	Rock slump	25512
		646A		-13.954719	-76.270936	Rock slump	433080
		660A		-13.952515	-76.271815	Rock slump	159960
		704A		-13.95666	-76.271248	Rock slump	18272
		716A		-13.957812	-76.27161	Rock slump	72668
		733A		-13.959153	-76.272578	Rock slump	80298
		762A		-13.961394	-76.271858	Rock slump	11150
		771A		-13.962173	-76.271503	Rock slump	3887
		783A		-13.963296	-76.271038	Rock slump	21728
		803A		-13.964984	-76.270771	Rock slump	469620
		815A		-13.967628	-76.270356	Rock slump	141723
		832A		-13.969472	-76.269635	Rock slump	67459
		A		-13.39745	-76.196286	Debris/earth avalanche	520000
		B		-13.414117	-76.189478	Debris/earth slump	67000
		A36		-13.717097	-76.154353	Debris/earth lateral spread	900
		A37		-13.708965	-76.152353	Debris/earth lateral spread	375
		A38		-13.69983	-76.151518	Debris/earth lateral spread	375
		A39		-13.697677	-76.152678	Debris/earth lateral spread	16100
		A41		-13.691563	-76.156006	Debris/earth lateral spread	47000
		A42		-13.69056	-76.156192	Debris/earth lateral spread	375
		A43		-13.691107	-76.155376	Debris/earth lateral spread	1500
		A45		-13.694335	-76.15303	Debris/earth lateral spread	3750
		A46		-13.69659	-76.153147	Debris/earth lateral spread	23000
		A126		-13.730499	-76.157933	Debris/earth lateral spread	300

Landslide Inventory Combined from 3 Sources: INGEMMET, Zavala, and Wartman							
INGEMMET ID	Zavala ID	Wartman ID	Name	Latitude	Longitude	LS type	volume (m^3)
		A127		-13.715946	-76.154101	Debris/earth lateral spread	300
		A128		-13.709308	-76.152375	Debris/earth lateral spread	300
		A131		-13.682337	-76.10706	Debris/earth lateral spread	10000
		P69		-13.921578	-76.357173	Rock slump	60240
		P88		-13.90166	-76.295341	Rock slump	14762
		P95		-13.919748	-76.283475	Rock slump	17544
		P104		-13.919899	-76.284557	Rock slump	24196
		P109		-13.920206	-76.285838	Rock slump	36680
		P121		-13.919857	-76.287087	Rock slump	31464
		P128		-13.92145	-76.287714	Rock slump	16688
		S1		-13.9136172	-76.3632428	Rock slump	30450
		S2		-13.9131927	-76.3654011	Rock slump	65472
		S3		-13.8180307	-76.3671057	Rock slump	83040
		S4		-13.8027976	-76.3617984	Rock slump	59150
		S5		-13.8017705	-76.3404051	Rock slump	50184
		S6		-13.800925	-76.3373186	Rock slump	3738
		S7		-13.9075721	-76.2913221	Rock slump	15844

Appendix B: Tavera et al. Evaluation of Attenuation Relationships

Introduction

The tables and graphs in Appendix B were extracted directly from Tavera et al., (2008) and include information about the PGA attenuation relationships evaluated, as well as graphs and a table comparing the equations' predicted values with those measured by accelerographs.

Predictive Equations for Ground Motion Events

Table 5 Predictive equations for ground-motions from subduction events used in the present study

Reference	Geographic coverage	Ground-motion parameter	Horizontal component definition	Database metadata coverage	Site classification scheme
Atkinson and Boore (2003)	Cascadia, Japan, Mexico, El Salvador, Pacific northwest, Alaska, Central Chile and Peru and the Solomon Islands	PGA, PSA	Random	M_w 5.5–8.3 R_{rup} 11–550 km	NEHRP site classes based on $V_{S,30}$ value. Only four classes (B to E) are modelled.
Kanno et al. (2006)	Japan, supplemented by 377 overseas records	PGA, PGV, PSA	Vectorially resolved	M_w 5.0–8.2 R_{rup} 1–450 km	Explicit consideration of $V_{S,30}$ through application of an empirical correction factor to the regression results obtained without the site term.
McVerry et al. (2006)	New Zealand, supplemented by 66 overseas records	PGA, PSA	Geometric mean	M_w 5.2–6.8 R_{rup} 30–400 km	Three site classes following New Zealand site classification, which is based on description of surface geology, geotechnical properties of the materials and depth to bedrock. Classes A and B are lumped into a single category, class E is not modelled.
Zhao et al. (2006b)	Japan, supplemented by 208 overseas records	PGA, PSA	Geometric mean	M_w 5.0–8.3 R_{rup} 0–300 km	Four site classes determined based on $V_{S,30}$ value and natural period T of the site. Provide an equivalence with NEHRP classification.
Ruiz and Saragoni (2005)	Chile	PGA	Larger PGA	M_S 6.2–7.8 R_{hyp} 36–315 km	Two site classes (rock and hard soil) based on description of surface geology.

Comparison between Recorded PGA Values and Predictions

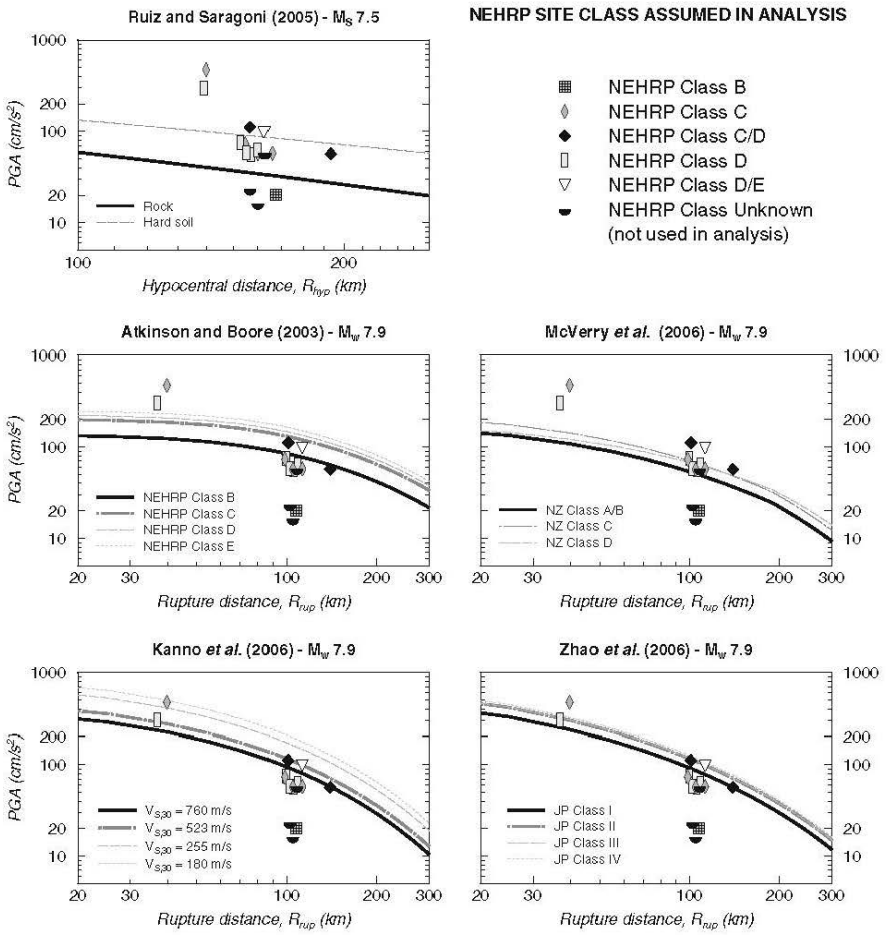

Fig. 11 Comparison between recorded PGA values and predictions of selected GMPE for subduction-zone environments, as well as the equation of Ruiz and Saragoni (2005) based on Chilean data

Comparison of Observed Ground Motions and Predictions

Table 6 Comparison of observed ground motions with predictions from selected equations, using the method of Scherbaum et al. (2004)

		PGA	SA5% at 0.05 s[a]	SA5% at 0.10 s	SA5% at 0.20 s	SA5% at 0.40 s	SA5% at 1.00 s	SA5% at 2.00 s	SA5% at 3.00 s
Scherbaum et al. (2004) classification[b]	Atkinson and Boore (2003)	D	D	D	D	D	D	D	D
	McVerry et al. (2006)	A	–	C	B	D	D	C	C
	Kanno et al. (2006)	C	B	B	B	C	D	D	D
	Zhao et al. (2006b)	C	B	B	C	D	D	D	D
Atkinson and Boore (2003)[c]	MEANNR	−1.064	−0.992	−0.641	−0.976	−1.035	−0.928	−0.712	−0.420
	MEDNR	−1.392	−1.007	−0.770	−1.146	−1.387	−1.169	−1.016	−0.808
	STDNR	1.211	0.977	0.974	1.011	1.111	0.798	0.876	1.005
	MEDLH	0.135	0.176	0.363	0.234	0.120	0.242	0.305	0.418
McVerry et al. (2006)	MEANNR	0.233	–	0.624	−0.327	−0.617	−0.636	−0.663	−0.368
	MEDNR	0.017	–	0.610	−0.235	−0.987	−1.046	−0.740	−0.666
	STDNR	0.951	–	0.750	0.800	1.141	1.081	0.987	1.109
	MEDLH	0.741	–	0.531	0.631	0.257	0.203	0.273	0.499
Kanno et al. (2006)	MEANNR	−0.655	−0.426	−0.256	−0.389	−0.553	−1.048	−1.206	−1.513
	MEDNR	−0.636	−0.422	−0.184	−0.406	−0.572	−1.083	−1.392	−1.658
	STDNR	0.551	0.661	0.528	0.571	0.560	0.437	0.522	0.784
	MEDLH	0.525	0.514	0.667	0.561	0.517	0.279	0.163	0.093
Zhao et al. (2006b)	MEANNR	−0.570	−0.297	−0.375	−0.578	−0.725	−0.875	−1.069	−1.150
	MEDNR	−0.666	−0.332	−0.420	−0.587	−0.994	−0.804	−1.184	−1.347
	STDNR	0.617	0.600	0.493	0.525	0.678	0.507	0.530	0.673
	MEDLH	0.505	0.576	0.609	0.557	0.320	0.421	0.236	0.177

The upper part of the table gives an overall rating of the performance of each equation for the ground-motion parameter of interest, while the lower part provides details of the parameters calculated to assign this rating

[a] Coefficients are not available for this period for the Atkinson and Boore (2003) and McVerry et al. (2006) equations. For Atkinson and Boore (2003), the analysis for 0.04 s is used as a proxy

[b] Assessment of capability of equation to predict the observed ground motions, using the following ranking scheme : : Rank A (high capability): MEANNR < 0.25, MEDNR < 0.25, STDNR < 1.125 and MEDLH > 0.4; Rank B (intermediate capability): MEANNR < 0.50, MEDNR < 0.50, STDNR < 1.250 and MEDLH > 0.3; Rank C (low capability): MEANNR < 0.75, MEDNR < 0.75, STDNR < 1.50 and MEDLH > 0.2; Rank D (unacceptable capability): all other combinations of parameters

[c] The calculations of the predicted values of the Atkinson and Boore (2003) model have been corrected for a data error affecting the tabulated coefficients at 2.5 and 5 Hz, as explained in Atkinson and Boore (2008)

Appendix C: McVerry Attenuation Relationship

Introduction

The pages in Appendix C were extracted directly from McVerry et al., (2006) and include the equations, parameters, and tables of coefficients for the McVerry attenuation relationship. Also included are definitions of the New Zealand site classes.

For the Pisco earthquake analysis, the subduction zone model was used. See Appendix E for MATLAB implementation of the McVerry attenuation model.

Equations and Parameters

ground accelerations for the two models obtained from the two datasets to obtain the values $SA_{A/B,C,D}(T)$ which together with the pga model $PGA_{A/B,C,D}$ from the larger dataset provide the recommended model from this study. The reason for the multiplication by the pga ratio is that for some subsets of earthquake motions, notably on rock or deep soil sites for crustal earthquakes, the pga estimates $PGA'_{A/B,C,D}$ from the response spectrum dataset were considerably smaller than the estimates $PGA_{A/B,C,D}$ derived from the complete pga dataset, particularly near-source. As the $PGA_{A/B,C,D}$ values were more in line with those from models from western US data, it was decided to scale the $SA'(T)$ values by the ratio of the pgas from the two models to obtain the final values of $SA(T)$, even though this introduces a bias to the final model with respect to the New Zealand data. Note that this scaling applies for the particular set of independent parameters (magnitude, distance, mechanism, tectonic class, site class) that applies in a particular case, so varies continuously as a function of these parameters. For parameter combinations where the models are well constrained by the data so that the pga estimates are similar for the two models, the scaling by the pga ratio has little effect. For parameter values, such as at short distances, where the $PGA'_{A/B,C,D}$ values are poorly constrained, the scaling may be more substantial. The standard deviations are taken as those with from the regression analyses, with no modification to account for any bias introduced by the pga scaling procedure.

The crustal model takes the form:

$$\begin{aligned}\ln SA'_{A/B}(T) = {} & \mathbf{C_1'(T)} + C_{4AS}(M-6) \\ & + C_{3AS}(T)\,(8.5-M)^2 \\ & + \mathbf{C_5'(T)}\,r + (\mathbf{C_8'(T)} \\ & + C_{6AS}(M-6))\,\ln(r^2 + C_{10AS}^2(T))^{1/2} \\ & + \mathbf{C_{46}'(T)}\,r_{VOL} \\ & + C_{32}\,CN + C_{33AS}(T)\,CR + F_{HW}(M,r)\end{aligned} \qquad (1)$$

The subduction zone model takes the form:

$$\begin{aligned}\ln SA'_{A/B}(T) = {} & \mathbf{C_{11}'(T)} + (C_{12Y} + (C_{15}'(T) \\ & - \mathbf{C_{17}'(T)})\,C_{19Y})\,(M-6) \\ & + C_{13Y}(T)(10-M)^3 \\ & + \mathbf{C_{17}'(T)}\,\ln(r + C_{18Y}\exp(C_{19Y}\,M)) \\ & + \mathbf{C_{20}'(T)}\,H_C + \mathbf{C_{24}'(T)}\,SI \\ & + \mathbf{C_{46}'(T)}\,r_{VOL}\,(1-DS)\end{aligned} \qquad (2)$$

where

$$C_{15}'(T) = C_{17Y}(T) \qquad (3)$$

In both the crustal and subduction zone models

$$\begin{aligned}\ln SA'_{C,D}(T) = {} & \ln SA'_{A/B}(T) + \mathbf{C_{29}'(T)}\,\delta_C \\ & + (C_{30AS}(T)\,\ln(PGA'_{A/B}+0.03) \\ & + \mathbf{C_{43}'(T)})\,\delta_D\end{aligned} \qquad (4)$$

where

$$PGA'_{A/B} = SA'_{A/B}(T=0) \qquad (5)$$

The expressions for $PGA_{A/B,C,D}$ take the same form as those for $PGA'_{A/B,C,D}$, but are differentiated by using unprimed versions of the coefficients. Finally,

$$SA_{A/B,C,D}(T) = SA'_{A/B,C,D}(T) * (PGA_{A/B,C,D} / PGA'_{A/B,C,D}) \qquad (6)$$

The complicated form of the coefficient of the magnitude term for subduction-zone earthquakes results from applying a near-source constraint at distance $r=0$. The magnitude-dependence of the model is constrained to be the same as that of the Youngs *et al.* model at zero distance, to retain the same degree of magnitude saturation at zero distance. This constraint is discussed further in Section 6.3. Note that although the coefficients $C_{15}'(T)$ are the same as $C_{17Y}(T)$, and the subduction zone expression is perhaps easier to understand with this substitution made, this notation is used so as to identify where the values are listed in Tables 5 and 6. The notation C_{12Y} and $C_{17Y}(T)$ is used to indicate the coefficients of the *(M-6)* and *ln(distance)* terms respectively in the Youngs *et al.* expression.

The parameters of these models are:

M = moment magnitude

r = shortest distance in km from the site to source

r_{VOL} = length in km of the part of the source-to-site path in

the volcanic zone (see Section 9.1)

H_C = centroid depth in km

CN = -1 for normal mechanism crustal earthquakes, 0 otherwise

CR = 0.5 for reverse/oblique mechanism crustal earthquakes, 1.0 for reverse mechanism crustal earthquakes, 0 otherwise

The source mechanisms are defined in terms of rake angle at the end of Section 2.2.

$F_{HW}(M,r)$ = hanging wall factor of the Abrahamson & Silva model (see Section 6.1).

SI = 1 for subduction interface earthquakes, 0 otherwise

DS = 1 for deep slab earthquakes, 0 otherwise

Interface and subduction slab earthquakes are defined in Section 2.1

δ_C = 1 for site class C, 0 otherwise

δ_D = 1 for site class D, 0 otherwise

$C_i(0)$ and $C'_i(T)$ = coefficients of the attenuation model, listed in Tables 5 & 6.

TABLE 6: COEFFICIENTS FOR GEOMETRIC-MEAN OF THE 5% DAMPED ACCELERATION RESPONSE SPECTRA COMPONENTS

period	0.000	0.000	0.075	0.10	0.20	0.30	0.40	0.50	0.75	1.00	1.50	2.00	3.00	
1	0.14274	0.07713	1.22050	1.53365	1.22565	0.21124	0.10541	-0.14260	-0.65968	-0.51404	-0.95399	-1.24167	-1.56570	free
3	0.00000	0.00000	0.03000	0.02800	-0.01380	-0.03600	-0.05180	-0.06350	-0.08620	0.10200	-0.12000	-0.12000	0.17260	fixed
4	-0.14400	-0.14400	-0.14400	-0.14400	-0.14400	-0.14400	-0.14400	-0.14400	-0.14400	-0.14400	0.14400	-0.14400	-0.14400	fixed
5	-0.00989	0.00898	-0.00914	-0.00903	-0.00975	-0.01032	-0.00941	-0.00878	-0.00802	-0.00647	-0.00713	-0.00713	-0.00623	free
6	0.17000	0.17000	0.17000	0.17000	0.17000	0.17000	0.17000	0.17000	0.17000	0.17000	0.17000	0.17000	0.17000	fixed
8	-0.68744	-0.73728	-0.93059	-0.96506	-0.75855	-0.52400	-0.50802	-0.52214	-0.47264	-0.58672	-0.49268	-0.49268	-0.52257	free
10	5.60000	5.60000	5.58000	5.50000	5.10000	4.80000	4.52000	4.30000	3.90000	3.70000	3.55000	3.55000	3.50000	fixed
11	8.57343	8.08611	8.69303	9.30400	10.41628	9.21783	8.01150	7.87495	7.26785	6.98741	6.77543	6.48775	5.05424	free
12	1.41400	1.41400	1.41400	1.41400	1.41400	1.41400	1.41400	1.41400	1.41400	1.41400	1.41400	1.41400	1.41400	fixed
13	0.00000	0.00000	0.00000	-0.00110	-0.00270	-0.00360	-0.00430	-0.00480	-0.00570	-0.00640	-0.00730	-0.00730	-0.00890	fixed
15	-2.55200	-2.55200	-2.70700	-2.65500	-2.52800	-2.45400	-2.40100	-2.36000	-2.28600	-2.23400	-2.16000	-2.16000	-2.03300	fixed
17	-2.56592	-2.49894	-2.55903	-2.61372	-2.70038	-2.47356	-2.30457	-2.31991	-2.28460	-2.28256	-2.27895	-2.27895	-2.05560	free
18	1.78180	1.78180	1.78180	1.78180	1.78180	1.78180	1.78180	1.78180	1.78180	1.78180	1.78180	1.78180	1.78180	fixed
19	0.55400	0.55400	0.55400	0.55400	0.55400	0.55400	0.55400	0.55400	0.55400	0.55400	0.55400	0.55400	0.55400	fixed
20	0.01545	0.01590	0.01821	0.01737	0.01531	0.01304	0.01426	0.01277	0.01055	0.00927	0.00748	0.00748	-0.00273	free
24	-0.49963	-0.43223	-0.52504	-0.61452	-0.65966	-0.56604	-0.33169	-0.24374	-0.01583	0.02009	-0.07051	-0.07051	-0.23967	free
29	0.27315	0.38730	0.27879	0.28619	0.34064	0.53213	0.63272	0.58809	0.50708	0.33002	0.07445	0.07445	0.09869	free
30	-0.23000	-0.23000	-0.28000	-0.28000	-0.24500	-0.19500	-0.16000	-0.12100	-0.05000	0.00000	0.04000	0.04000	0.04000	fixed
32	0.20000	0.20000	0.20000	0.20000	0.20000	0.20000	0.20000	0.20000	0.20000	0.20000	0.20000	0.20000	0.20000	fixed
33	0.26000	0.26000	0.26000	0.26000	0.26000	0.19800	0.15400	0.11900	0.05700	0.01300	-0.04900	-0.04900	-0.15600	fixed
43	-0.33716	-0.31036	-0.49068	-0.46604	-0.31282	-0.07565	0.17615	0.34775	0.72380	0.89239	0.77743	0.77743	0.60938	free
46	-0.03255	-0.03250	-0.03441	-0.03594	-0.03823	-0.03535	-0.03354	-0.03211	-0.02857	-0.02500	-0.02008	-0.02008	-0.01587	free
SigmaM6	0.4871	0.5099	0.5297	0.5401	0.5599	0.5456	0.5556	0.5658	0.5611	0.5573	0.5419	0.5419	0.5809	
Sigslope	-0.1011	-0.0259	-0.0703	-0.0292	0.0172	-0.0566	-0.1064	-0.1123	-0.0836	-0.0620	0.0385	0.0385	0.1403	
Tau	0.2677	0.2469	0.3139	0.3017	0.2583	0.1967	0.1802	0.1440	0.1871	0.2073	0.2405	0.2405	0.2053	
SigtotM6	0.5558	0.5666	0.6157	0.6187	0.6166	0.5800	0.5840	0.5839	0.5915	0.5946	0.5929	0.5929	0.6161	

Model GMMRFTMP

TABLE 5: COEFFICIENTS OF THE ATTENUATION MODEL P2MRF5AC FOR THE STRONGER HORIZONTAL COMPONENT

period	0.000	0.000	0.075	0.10	0.20	0.30	0.40	0.50	0.75	1.00	1.50	2.00	3.00	
1	0.28815	0.18130	1.36561	1.77717	1.39535	0.44591	0.01645	0.14826	-0.21246	-0.10451	0.48665	-0.77433	-1.30916	free
3	0.00000	0.00000	0.03000	0.02800	-0.01380	0.03600	0.05180	0.06350	0.08620	-0.10200	-0.12000	-0.12000	-0.17260	fixed
4	-0.14400	-0.14400	0.14400	-0.14400	-0.14400	-0.14400	-0.14400	-0.14400	-0.14400	0.14400	-0.14400	-0.14400	-0.14400	fixed
5	0.00967	0.00846	-0.00889	-0.00837	-0.00940	-0.00987	-0.00923	-0.00823	-0.00738	-0.00588	-0.00630	-0.00630	0.00553	free
6	0.17000	0.17000	0.17000	0.17000	0.17000	0.17000	0.17000	0.17000	0.17000	0.17000	0.17000	0.17000	0.17000	fixed
8	-0.70494	-0.75519	-0.94568	-1.01852	-0.78199	-0.56098	-0.51281	-0.56716	-0.55384	-0.65892	-0.58222	-0.58222	-0.57009	free
10	5.60000	5.60000	5.58000	5.50000	5.10000	4.80000	4.52000	4.30000	3.90000	3.70000	3.55000	3.55000	3.50000	fixed
11	8.68354	8.10697	8.68782	9.37929	10.61479	9.40776	8.50343	8.46463	7.30176	7.08727	6.93264	6.64496	5.05488	free
12	1.41400	1.41400	1.41400	1.41400	1.41400	1.41400	1.41400	1.41400	1.41400	1.41400	1.41400	1.41400	1.41400	fixed
13	0.00000	0.00000	0.00000	-0.00110	-0.00270	-0.00360	-0.00430	-0.00480	-0.00570	-0.00640	-0.00730	-0.00730	-0.00890	fixed
15	-2.55200	-2.55200	-2.70700	-2.65500	-2.52800	-2.45400	-2.40100	-2.36000	-2.28600	-2.23400	-2.16000	-2.16000	-2.03300	fixed
17	-2.56727	-2.48795	-2.54215	-2.60945	-2.70851	-2.47668	-2.36895	-2.40630	-2.26512	-2.27668	-2.28347	-2.28347	-2.03050	free
18	1.78180	1.78180	1.78180	1.78180	1.78180	1.78180	1.78180	1.78180	1.78180	1.78180	1.78180	1.78180	1.78180	fixed
19	0.55400	0.55400	0.55400	0.55400	0.55400	0.55400	0.55400	0.55400	0.55400	0.55400	0.55400	0.55400	0.55400	fixed
20	0.01550	0.01622	0.01850	0.01740	0.01542	0.01278	0.01426	0.01287	0.01080	0.00946	0.00788	0.00788	-0.00265	free
24	-0.50962	-0.41369	-0.48652	-0.61973	-0.67672	-0.59339	-0.30579	-0.24839	-0.01298	0.06672	-0.02289	-0.02289	-0.20537	free
29	0.30206	0.44307	0.31139	0.34059	0.37235	0.56648	0.69911	0.63188	0.51577	0.34048	0.12468	0.12468	0.14593	free
30	-0.23000	-0.23000	-0.28000	-0.28000	-0.24500	-0.19500	-0.16000	-0.12100	-0.05000	0.00000	0.04000	0.04000	0.04000	fixed
32	0.20000	0.20000	0.20000	0.20000	0.20000	0.20000	0.20000	0.20000	0.20000	0.20000	0.20000	0.20000	0.20000	fixed
33	0.26000	0.26000	0.26000	0.26000	0.26000	0.19800	0.15400	0.11900	0.05700	0.01300	-0.04900	-0.04900	-0.15600	fixed
43	-0.31769	-0.29648	-0.48366	-0.43854	-0.29906	-0.05184	0.20301	0.37026	0.73517	0.87764	0.75438	0.75438	0.61545	free
46	-0.03279	-0.03301	-0.03452	-0.03595	-0.03853	-0.03604	-0.03364	-0.03260	0.02877	0.02561	0.02034	-0.02034	-0.01673	free
SigmaM6	0.4865	0.5035	0.5281	0.5398	0.5703	0.5505	0.5627	0.5680	0.5562	0.5629	0.5394	0.5394	0.5701	
Sigslope	-0.1261	-0.0635	-0.0970	-0.0673	-0.0243	-0.0861	-0.1405	-0.1444	-0.0932	-0.0749	-0.0056	-0.0056	0.0934	
Tau	0.2687	0.2598	0.3217	0.3088	0.2726	0.2112	0.2005	0.1476	0.1794	0.2053	0.2411	0.2411	0.2406	
SigtotM6	0.5558	0.5666	0.6184	0.6219	0.6321	0.5896	0.5973	0.5869	0.5844	0.5992	0.5909	0.5909	0.6188	

Model P2MRF5AC

New Zealand Site Class Definitions

TABLE 3: NEW ZEALAND SITE CLASS DEFINITIONS

(now adopted in NZS1170.5:2004)

Class	Definition
Class A – Strong Rock	Strong to extremely-strong rock with: (a) unconfined compressive strength greater than 50 MPa, and (b) an average shear-wave velocity over the top 30 m greater than 1500 m/s, and (c) not underlain by materials having a compressive strength less than 18 MPa or a shear wave velocity less than 600 m/s .
Class B – Rock	Rock with: (a) a compressive strength between 1 and 50 MPa, and (b) an average shear-wave velocity over the top 30 m greater than 360 m/s, and (c) not underlain by materials having a compressive strength less than 0.8 MPa or a shear wave velocity less than 300 m/s. A surface layer of no more than 3 m depth of highly-weathered or completely-weathered rock or soil (a material with a compressive strength less than 1 MPa) may be present
Class C – Shallow Soil Sites	Sites that: (a) are not class A , class B or class E sites, and (b) have low amplitude natural period less than or equal to 0.6 s, or (c) have depths of soil not exceeding those listed in Table 4
Class D – Deep or Soft Soil Sites	Sites that: (a) are not class A , class B or class E sites, and (b) have a low-amplitude natural period greater than 0.6 s, or (c) have depths of soils exceeding those listed in Table 4, or (d) are underlain by less than 10 m of soils with an undrained shear-strength less than 12.5 kPa or soils with SPT N-values less than 6.
Class E – Very Soft Soil Sites	Sites with: (a) more than 10 m of very soft soils with undrained shear-strength less than 12.5 kPa, (b) more than 10 m of soils with SPT N values less than 6 (c) more than 10 m depth of soils with shear wave velocities of 150 m/s or less, or (d) more than 10 m combined depth of soils with properties as described in (a), (b) and (c) above.

Appendix D: Geologic Units and Maps

About the Geologic Maps

The geologic maps used for the Paracas Peninsula and the Coastal Plains were downloaded as .jpg images from the INGEMMET website, http://www.ingemmet.gob.pe/form/Inicio.aspx#.

An identical INGEMMET map was downloaded from OneGeology, http://portal.onegeology.org/, as a .kml file and placed as an overlay in Google Earth.

The geologic map used for the Andes Mountains region (Mapa Litológico) was scanned from a paper map published by INGEMMET.

Leyenda del Mapa Geólogico

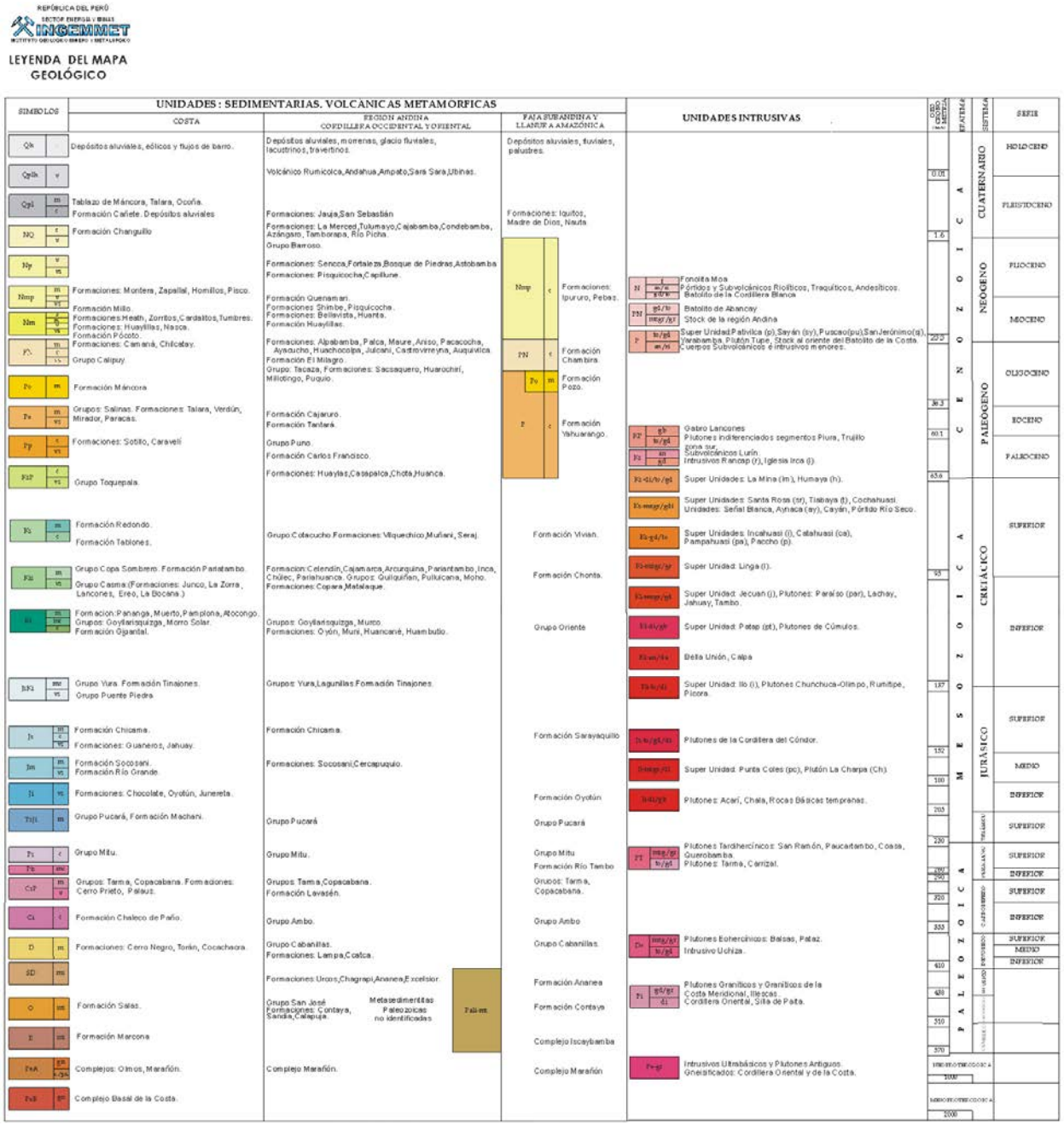

Mapa Geológico del Departmento de Lima

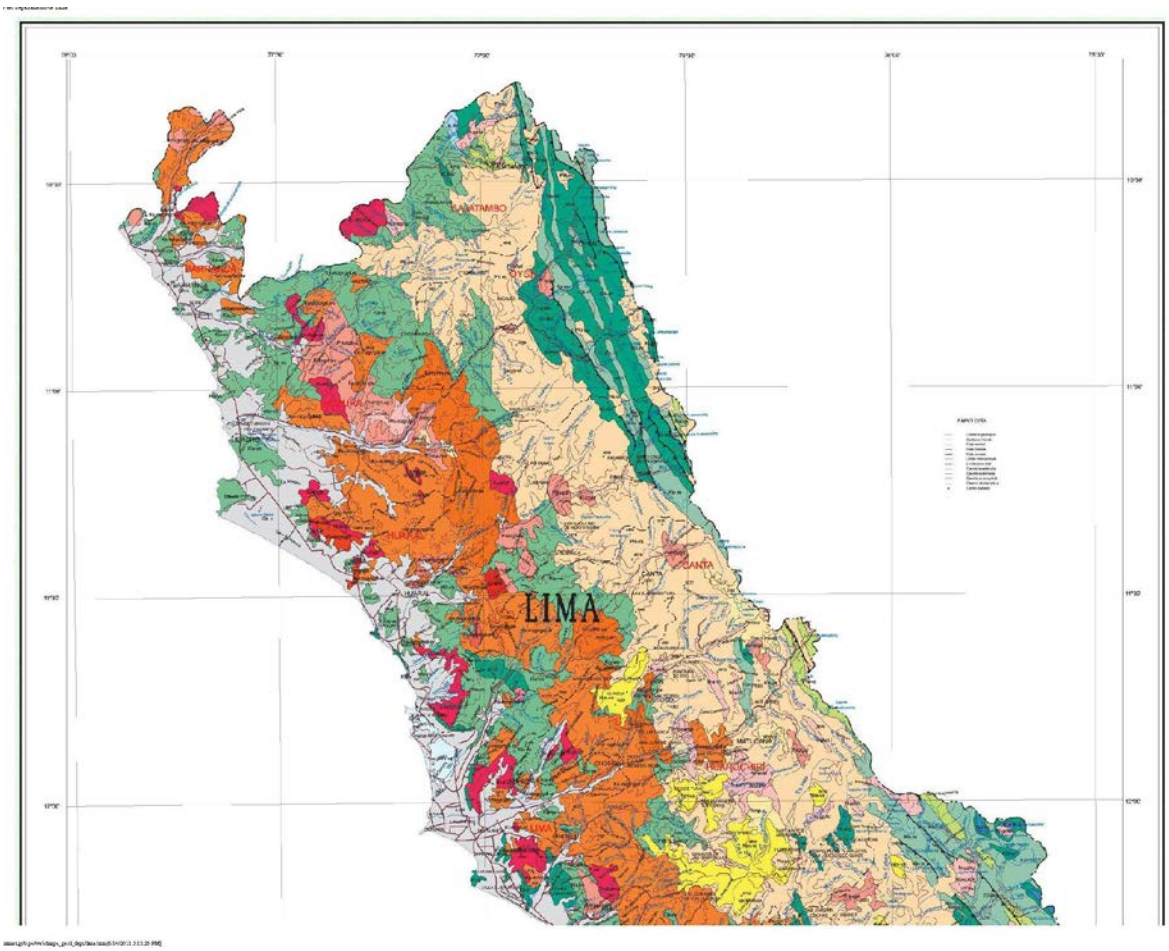

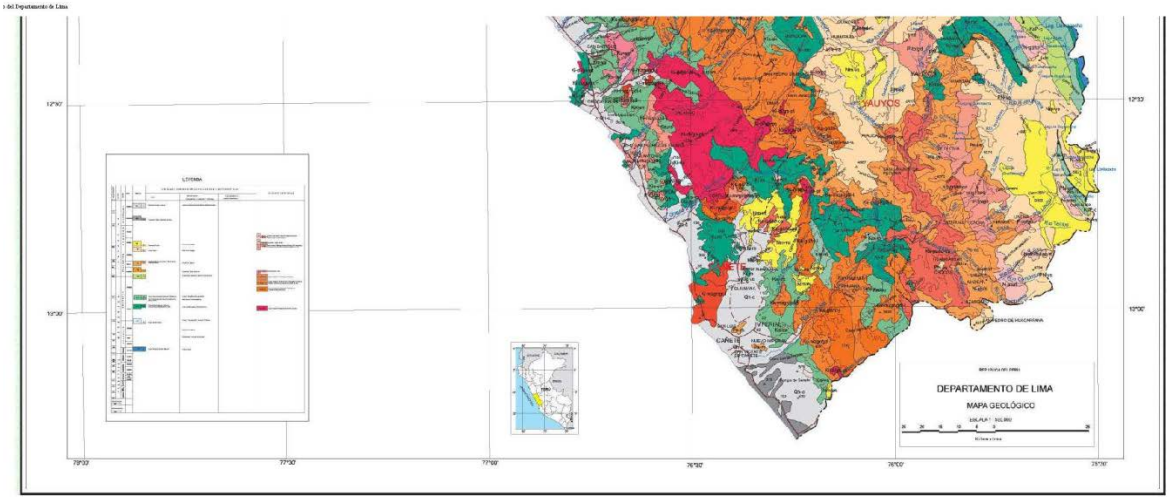

Mapa Geólogico del Departmento de Huancavelica

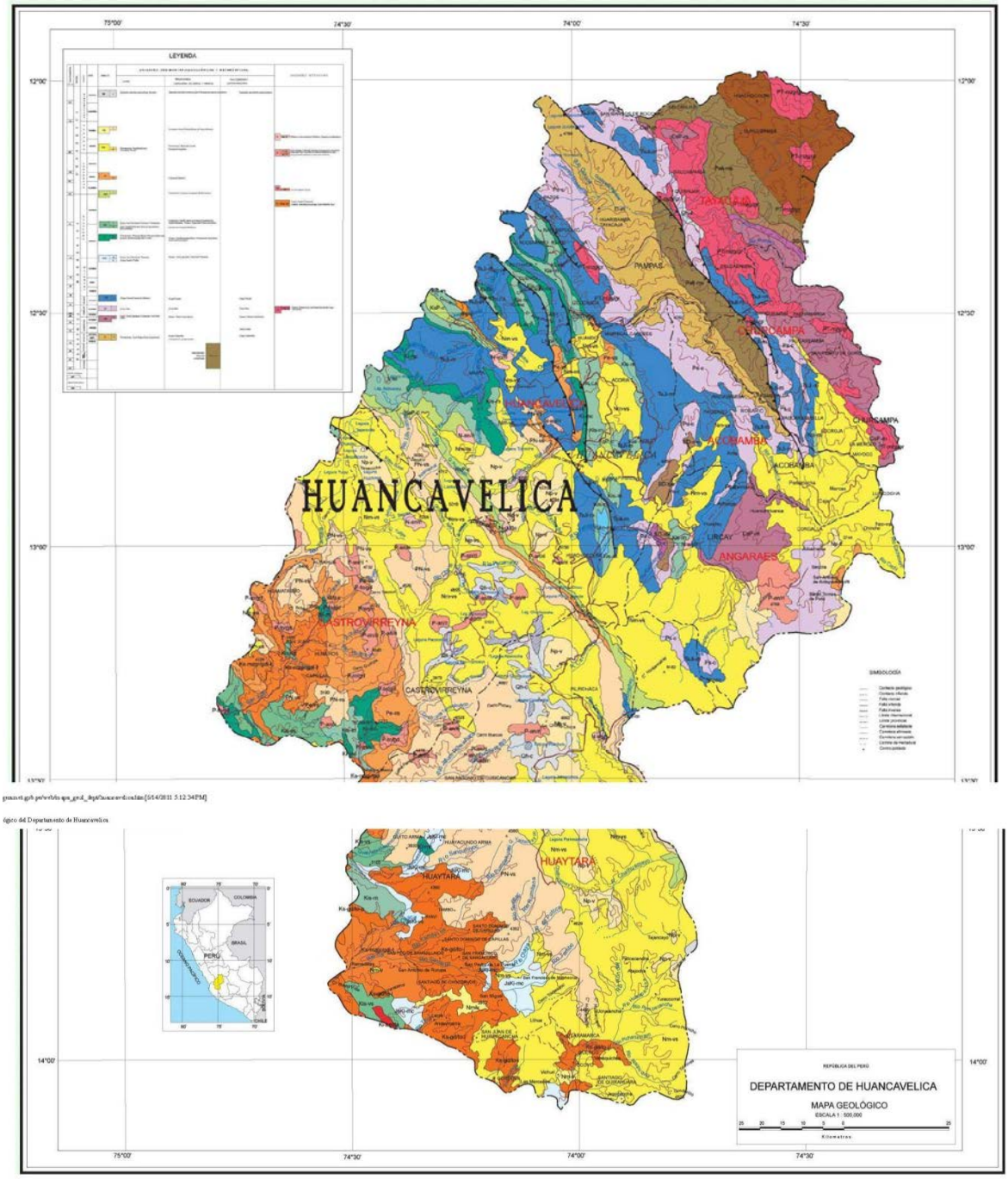

Leyenda del Mapa Litológico

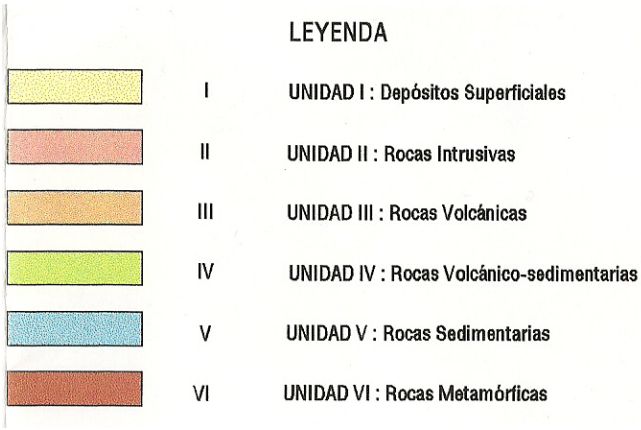

UNIDAD	SUB-UNIDAD	LITOLOGÍA	FORMACIÓN GEOLÓGICA EQUIVALENTE
I Depósitos Superficiales	I	Depósitos aluviales, proluviales, fluviales, fluvioglaciales, eólicos, coluviales, marinos, piroclásticos, lacustres	
II Rocas Intrusivas	II	Sienogranito, granito, granodiorita,diorita, gabro	Batolito de San Nicolás, Granito de San Miguel Granito de Querobamba, Batolito de la Costa
III Rocas Volcánicas	III-1	Lavas, tufos	Grupo Barroso
	III-2	Tufos	Fms. Sencca, Quenamari, Rumihuasi, Omaconga
IV Rocas Volcánico-sedimentarias	IV	Piroclastos de cenizas, limolitas, calizas negras, lutitas, tobas cristalolíticas, andesitas y riolitas	Fms. Pisco, Ayacucho, Puente Inga, Chocolate
V Rocas Sedimentarias	V-1	Cuarcitas, areniscas, lutitas, carbón	Grupo Ambo, Grupo Yura
	V-2	Pizarras, lutitas, areniscas y esquistos	Grupo Excelsior, Grupo Cabanillas, Fm. Celendín
	V-3	Areniscas rojas, lutitas y yeso	Grupo Puno, Fms. Huanta, Socos
	V-4	Calizas, areniscas y lutitas	Grupo Copacabana, Fms. Arcurquina, Fm. Atocongo
	V-5	Conglomerados, areniscas, lutitas, evaporitas	Grupo Mitu, Fms. Casapalca
VI Rocas Metamórficas	VI	Esquistos, gneis	Complejo del Marañon

Mapa Litológico

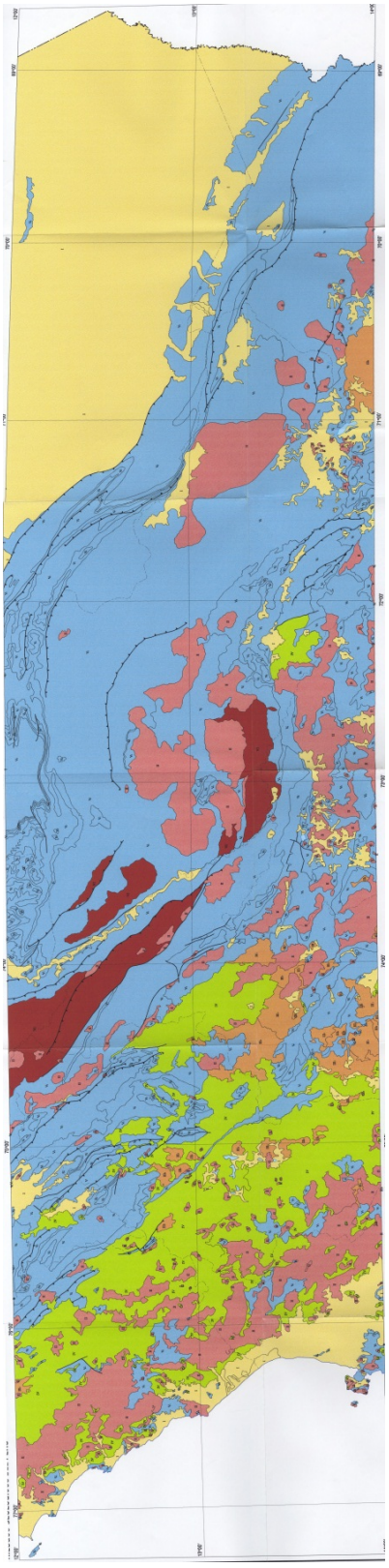

Appendix E: MATLAB Programs

About the MATLAB Programs

The **Closest Plane** MATLAB program calculates the shortest distance from a point on the surface of the earth (given by latitude and longitude) to the fault plane, given by the latitude, longitude, and elevation of each of the 4 corners of the fault plane. The program divides the plane into 4 quadrants, finds the center of each quadrant, and calculates the distance from the center of each quadrant to the point in question. It then selects the quadrant with the shortest distance and repeats this procedure until the length of one side of a quadrant is less than or equal to one meter, returning the final distance. This program was written by Adrian Rodriguez-Marek.

The **McVerry Attenuation** program implements the subduction model of the McVerry attenuation relationship; it was originally written by Adrian Rodriguez-Marek and modified by myself (parts modified/corrected are commented in the program.) The parameters used for implementation of the relationship were:

$M = 7.9$	Moment magnitude
$r_{VOL} = 0$	Length in km of source-to-site path in volcanic zone (NZ only)
$H_C = 18$	Centroid depth in km
$CN = 0$	Normal mechanism crustal earthquake
$CR = 1$	Reverse mechanism crustal earthquake
$SI = 1$	Subduction interface earthquakes
$\delta_C = 0$	New Zealand site class C, shallow soil
$\delta_D = 0$	New Zealand site class D, deep soft soil

The **Newman Power Law Distribution** program reproduces Newman's method of reducing the "noise" found in the tails of power-law distributed datasets, using an artificially constructed dataset of random numbers with a known power-law distribution. The program is then re-purposed with the Pisco landslide data in order to evaluate whether the data fits an inverse power-law relationship. **Clauset's PLFIT Function** is used to determine 2 of the parameters, alpha and x_{min}, needed for the best-fit power law curve.

The **Malamud 3-Parameter Inverse Gamma Distribution** program calculates average, total, and maximum landslide areas and volumes given the total number of landslides in the inventory (assuming self-similarity.) It also plots the Pisco inventory on a log-log frequency density versus landslide area graph, along with isolines for landslide magnitude.

Closest Plane

```
5/16/12 6:46 PM  C:\Users\Jennifer\Graduate School\Pisc...\closest plane working.m  1 of 3

%function result = closest_plane_2007(lat,lon)
%closest_plane_2007(lat,lon)
%gives distance to plane in m

%you must do first

 load topo
 figure
 axesm('globe','geoid',almanac('earth','radius','m'));
 meshm(topo,topolegend);demcmap(topo);
 view(3);


%lath = -13.354; %hypocenter latitute
%lonh = -76.509 %hypocenter long.
%aeleh = -39000 %hypocenter elev.

latVector=xlsread('C:\Users\Jennifer\Graduate School\Pisco Research\MatLab↙
Files\FinalInventory.xlsx', 'Sheet1', 'h3:h292');
lonVector=xlsread('C:\Users\Jennifer\Graduate School\Pisco Research\MatLab↙
Files\FinalInventory.xlsx', 'Sheet1', 'i3:i292');




%we will define a square that corresponds to the fault plane
%  x(1),y(1),z(1)            x(2),y(2)
%
%
%  x(4),y(4)            x(3),y(3)



%Coordinates below match the UCSB Finite Fault Solution
fault =[-76.15410      -14.63120        -3.73340  %SW 4
       -77.19620      -13.24690        -3.73340   %NW 1
       -76.48660      -12.74130       -52.18070   %NE 2
       -75.44460      -14.12560       -52.18070]; %SE 3

result=0;
for loop = 1:size(latVector,1)
lat = latVector(loop);
lon = lonVector(loop);

tol=1;
el = 0;
[x,y,z]=mfwdtran(lat,lon,el);
P = [ x y z]';

[X(1,1) X(2,1) X(3,1)]=mfwdtran(fault(2,2),fault(2,1),fault(2,3)*1000);
```

```
[X(1,2) X(2,2) X(3,2)]=mfwdtran(fault(3,2),fault(3,1),fault(3,3)*1000);
[X(1,3) X(2,3) X(3,3)]=mfwdtran(fault(4,2),fault(4,1),fault(4,3)*1000);
[X(1,4) X(2,4) X(3,4)]=mfwdtran(fault(1,2),fault(1,1),fault(1,3)*1000);


flag=1;
%start iteration
counter = 0;
while(flag)
    counter = counter+1;
    %disp(counter);


M = [ (X(:,1)+X(:,2))/2 (X(:,2)+X(:,3))/2 (X(:,3)+X(:,4))/2 (X(:,4)+X(:,1))/2];

Y = mean(X')';  %Y = midpoint

%take the midpoint of four regions
%       x1      m1       x2
%       m4      y        m2
%       x4      m3       x3

flagr = 0;
R = 1e10;
for k=1:4
    if(k>1) mindex = k-1;else mindex = 4;end
    Mid = (X(:,k)+Y+M(:,k)+M(:,mindex))/4;
%    plot3(Mid(1),Mid(2),Mid(3),'mx');
    temp = sqrt( (P - Mid)'*(P-Mid));
    if(temp<R)
        R = temp;
        flagr=k;
    end
end
% end of taking the midpoint, selected region in flagr

%redefine X
if(flagr==1)
    X=[X(:,1) M(:,1) Y M(:,4)];
elseif(flagr==2)
    X=[M(:,1) X(:,2) M(:,2) Y];
elseif(flagr==3)
    X=[Y M(:,2) X(:,3) M(:,3)];
elseif(flagr==4)
    X=[M(:,4) Y M(:,3) X(:,4)];
else
    echo 'problemproblemproblem'
end


%we stop when the distance between two edges is less than tol m
```

```
if(sqrt((X(:,1)-X(:,4))'*(X(:,1)-X(:,4))) < tol)
    flag = 0;
    result(loop)= R;
    write (loop,:) = R;


end
end
end


 SUCCESS = XLSWRITE('C:\Users\Jennifer\Graduate School\Pisco Research\MatLab↙
Files\FinalInventory.xlsx', write, 'Sheet1', 'ab3:ab292');
```

McVerry Attenuation

```
8/2/12 7:12 PM  C:\Users\Jennifer\Dropbox\Pisco Research\MatL...\McVerry working.m  1 of 6

%function [R,Sa]=mcverry(R,T,M,Hc,faulttype,siteclass,rvol)
% Usage [R,Sa]=mcverry(T,M,Hc,faulttype,siteclass,rvol)
% Computes the Attenuation relation from McVerry et al (2006)
% for subduction type earthquakes only
%
% T period at which Sa is needed, for PGA use T=0
% M
% Hc centroid depth (km)
% faultmech: Fault Mechanism 1-> Subduction Interface; 2-> Deep Slab event
% siteclass: Site class 1-> A/B; 2-> C; 3-> D
% path:      Distance (km) of the source to site path that includes volcanic zone
%
%
%
%R=[100 110 120];
R=xlsread('C:\Users\Jennifer\Graduate School\Richard\PGAs.xlsx', 'sheet1', 'J2:J6');
T=0;
M=7.9;
Hc=18;
faulttype=1;% changed from 2 to 1
siteclass=1;
rvol=0;

%Here input table5 & table6
table5=[0.28815 0.18130 1.36561 1.77717 1.39535 0.44591 0.01645 0.14826 -0.21246↙
-0.10451    -0.48665    -0.77433    -1.30916
0.00000 0.00000 0.03000 0.02800 -0.01380    -0.03600    -0.05180    -0.06350    -0.08620↙
-0.10200    -0.12000    -0.12000    -0.17260
-0.14400    -0.14400    -0.14400    -0.14400    -0.14400    -0.14400    -0.14400↙
-0.14400    -0.14400    -0.14400    -0.14400    -0.14400    -0.14400
-0.00967    -0.00846    -0.00889    -0.00837    -0.00940    -0.00987    -0.00923↙
-0.00823    -0.00738    -0.00588    -0.00630    -0.00630    -0.00553
0.17000 0.17000 0.17000 0.17000 0.17000 0.17000 0.17000 0.17000 0.17000 0.17000↙
0.17000 0.17000
-0.70494    -0.75519    -0.94568    -1.01852    -0.78199    -0.56098    -0.51281↙
-0.56716    -0.55384    -0.65892    -0.58222    -0.58222    -0.57009
5.60000 5.60000 5.58000 5.50000 5.10000 4.80000 4.52000 4.30000 3.90000 3.70000 3.55000↙
3.55000 3.50000
8.68354 8.10697 8.68788 9.37929 10.61479    9.40776 8.50343 8.46463 7.30176 7.08727↙
6.93264 6.44960 5.05488
1.41400 1.41700 1.41400 1.41400 1.41400 1.41400 1.41400 1.41400 1.41400 1.41400 1.41400↙
1.41400 1.41400
0.00000 0.00000 0.00000 -0.00110    -0.00270    -0.00360    -0.00430    -0.00480↙
-0.00570    -0.00640    -0.00730    -0.00730    -0.00890
-2.55200    -2.55200    -2.70700    -2.65500    -2.52800    -2.45400    -2.40100↙
-2.36000    -2.28600    -2.23400    -2.16000    -2.16000    -2.03300
-2.56727    -2.48795    -2.54215    -2.60945    -2.70851    -2.47668    -2.36895↙
-2.40630    -2.26512    -2.27668    -2.28347    -2.28347    -2.30500
1.78180 1.78180 1.78180 1.78180 1.78180 1.78180 1.78180 1.78180 1.78180 1.78180 1.78180↙
1.78180 1.78180
0.55400 0.55400 0.55400 0.55400 0.55400 0.55400 0.55400 0.55400 0.55400 0.55400 0.55400↙
```

```
0.55400 0.55400
0.01550 0.16220 0.01850 0.01740 0.01542 0.01278 0.01426 0.01287 0.01080 0.00946 0.00788↙
0.00788 -0.00265
-0.50962    -0.41369    -0.48652    -0.61973    -0.67672    -0.59339    -0.30579↙
-0.24839    -0.01298    0.06672 -0.02289    -0.02289    -0.20537
0.30206 0.44307 0.31139 0.34059 0.37235 0.56648 0.69911 0.63188 0.51577 0.34034 0.12468↙
0.12468 0.14593
-0.23000    -0.23000    -0.28000    -0.28000    -0.24500    -0.19500    -0.16000↙
-0.12100    -0.05000    0.00000 0.04000 0.04000 0.04000
0.20000 0.20000 0.20000 0.20000 0.20000 0.20000 0.20000 0.20000 0.20000 0.20000 0.20000↙
0.20000 0.20000
0.26000 0.26000 0.26000 0.26000 0.26000 0.19800 0.15400 0.11900 0.05700 0.01300 -0.04900↙
-0.07900    -0.15600
-0.31769    -0.29648    -0.48366    -0.43854    -0.29991    -0.05118    0.20301 0.37026↙
0.73517 0.87764 0.75438 0.75438 0.61545
-0.03279    -0.03301    -0.03452    -0.03595    -0.03853    -0.03604    -0.03364↙
-0.03260    -0.02877    -0.02561    -0.02034    -0.02034    -0.01673
0.48650 0.50350 0.52810 0.53980 0.57030 0.55050 0.56270 0.56800 0.55620 0.56290 0.53940↙
0.53940 0.57010
-0.12610    -0.06350    -0.09700    -0.06730    -0.02430    -0.08610    -0.14050↙
-0.14440    -0.09320    -0.07490    -0.00560    -0.00560    0.00934
0.26870 0.25980 0.32170 0.30880 0.27260 0.21120 0.20050 0.14760 0.17940 0.20530 0.24110↙
0.24110 0.24060
0.55580 0.56660 0.61840 0.62190 0.63210 0.58960 0.59730 0.58690 0.58440 0.59920 0.59090↙
0.59090 0.61880];
table6=[0.14274 0.07713 1.22050 1.53365 1.22565 0.21124 -0.10541    -0.14260    -0.65968↙
-0.51404    -0.95399    -1.24167    -1.56570
0.00000 0.00000 0.03000 0.02800 -0.01380    -0.03600    -0.05180    -0.06350    -0.08620↙
-0.10200    -0.12000    -0.12000    -0.17260
-0.14400    -0.14400    -0.14400    -0.14400    -0.14400    -0.14400    -0.14400↙
-0.14400    -0.14400    -0.14400    -0.14400    -0.14400    -0.14400
-0.00989    -0.00898    -0.00914    -0.00903    -0.00975    -0.01032    -0.00941↙
-0.00878    -0.00802    -0.00647    -0.00713    -0.00713    -0.00623
0.17000 0.17000 0.17000 0.17000 0.17000 0.17000 0.17000 0.17000 0.17000 0.17000 0.17000↙
0.17000 0.17000
-0.68744    -0.73782    -0.93059    -0.96506    -0.75855    -0.52400    -0.50802↙
-0.52214    -0.47264    -0.58672    -0.49268    -0.49268    -0.52257
5.60000 5.60000 5.58000 5.50000 5.10000 4.80000 4.52000 4.30000 3.90000 3.70000 3.55000↙
3.55000 3.50000
8.57343 8.08611 8.69303 9.30400 10.41628    9.21783 8.01150 7.87495 7.26785 6.98741↙
6.77543 6.48775 5.05424
1.41400 1.41400 1.41400 1.41400 1.41400 1.41400 1.41400 1.41400 1.41400 1.41400 1.41400↙
1.41400 1.41400
0.00000 0.00000 0.00000 -0.00110    -0.00270    -0.00360    -0.00430    -0.00480↙
-0.00570    -0.00640    -0.00730    -0.00730    -0.00890
-2.55200    -2.55200    -2.70700    -2.65500    -2.52800    -2.45400    -2.40100↙
-2.36000    -2.28600    -2.23400    -2.16000    -2.16000    -2.03300
-2.56592    -2.49894    -2.55903    -2.61372    -2.70038    -2.47356    -2.30457↙
-2.31991    -2.28460    -2.28256    -2.27895    -2.27895    -2.05560
1.78180 1.78180 1.78180 1.78180 1.78180 1.78180 1.78180 1.78180 1.78180 1.78180 1.78180↙
1.78180 1.78180
```

```
0.55400 0.55400 0.55400 0.55400 0.55400 0.55400 0.55400 0.55400 0.55400 0.55400 0.55400↙
0.55400 0.55400
0.01545 0.01590 0.01821 0.01737 0.01531 0.01304 0.01426 0.01277 0.01055 0.00927 0.00748↙
0.00748 -0.00273
-0.49963    -0.43223    -0.52504    -0.61452    -0.65966    -0.56604    -0.33169↙
-0.24374    -0.01583    0.02009 -0.07051    -0.07051    -0.23967
0.27315 0.38730 0.27879 0.28619 0.34064 0.53213 0.63272 0.58809 0.50708 0.33002 0.07445↙
0.07445 0.09869
-0.23000    -0.23000    -0.28000    -0.28000    -0.24500    -0.19500    -0.16000↙
-0.12100    -0.05000    0.00000 0.04000 0.04000 0.04000
0.20000 0.20000 0.20000 0.02000 0.20000 0.20000 0.20000 0.20000 0.20000 0.20000 0.20000↙
0.20000 0.20000
0.26000 0.26000 0.26000 0.26000 0.26000 0.19800 0.15400 0.11900 0.05700 0.01300 -0.04900↙
-0.04900    -0.15660
0.33716 -0.31036    -0.49068    -0.46604    -0.31282    -0.07565    0.17615 0.34775↙
0.72380 0.89239 0.77743 0.77743 0.60938
-0.03255    -0.03250    -0.03441    -0.03594    -0.03823    -0.03535    -0.03354↙
-0.03211    -0.02857    -0.02500    -0.02008    -0.02008    -0.01587
0.48710 0.50990 0.52970 0.54010 0.55990 0.54560 0.55560 0.56580 0.56110 0.55730 0.54190↙
0.54190 0.58090
-0.10110    -0.02590    -0.07030    -0.02920    0.01720 -0.05660    -0.10640    -0.11230↙
-0.08360    -0.06200    0.03850 0.03850 0.14030
0.26770 0.24690 0.31390 0.30170 0.25830 0.19670 0.18020 0.14400 0.18710 0.20730 0.24050↙
0.24050 0.20530
0.55580 0.56660 0.61570 0.61870 0.61660 0.58000 0.58400 0.58390 0.59150 0.59460 0.59290↙
0.59290 0.61610];
if faulttype==1
    SI=1;
else
    SI=0;
end
if faulttype==2
    DS=1;
else
    DS=0;
end
%R=logspace(log10(50),log10(300),15);
Sa=zeros(size(R));%[];
periods=[0 0.05 0.075 0.1 0.2 0.3 0.4 0.5 0.75 1 1.5 2 3];%changed second column heading↙
from 0 to 0.05
sitecoeff=zeros(3,1); sitecoeff(siteclass)=1;

C=table5(:,1);%changed back to first T=0 column
Cpr=table6(:,1);%changed back as above
c1=C(1); c3=C(2); c4=C(3); c5=C(4); c6=C(5); c8=C(6); c10=C(7);
c11=C(8); c12=C(9); c13=C(10); c15=C(11); c17=C(12); c18=C(13);
c19=C(14); c20=C(15); c24=C(16); c29=C(17); c30=C(18); c32=C(19);
c33=C(20); c43=C(21); c46=C(22);
c1pr=Cpr(1);   c3pr=Cpr(2); c4pr=Cpr(3); c5pr=Cpr(4); c6pr=Cpr(5); c8pr=Cpr(6);↙
c10pr=Cpr(7);
c11pr=Cpr(8);  c12pr=Cpr(9); c13pr=Cpr(10); c15pr=Cpr(11); c17pr=Cpr(12); c18pr=Cpr(13);
```

```
pr=Cpr(14); c20pr=Cpr(15); c24pr=Cpr(16); c29pr=Cpr(17); c30pr=Cpr(18); c32pr=Cpr↙
);
pr=Cpr(20); c43pr=Cpr(21); c46pr=Cpr(22);


isempty(find(periods==T,1))
 m=find(periods<T);
 n=find(periods>T);
 T1=periods(m(length(m)));
 T2=periods(n(1));

 m=find(periods==T1);

 D=table5(:,m(1));
 Dpr=table6(:,m(1));

 d1=D(1); d3=D(2); d4=D(3); d5=D(4); d6=D(5); d8=D(6); d10=D(7);
 d11=D(8); d12=D(9); d13=D(10); d15=D(11); d17=D(12); d18=D(13);
 d19=D(14); d20=D(15); d24=D(16); d29=D(17); d30=D(18); d32=D(19);
 d33=D(20); d43=D(21); d46=D(22);
 d1pr=Dpr(1);   d3pr=Dpr(2); d4pr=Dpr(3); d5pr=Dpr(4); d6pr=Dpr(5); d8pr=Dpr(6);↙
pr=Dpr(7);
 d11pr=Dpr(8);  d12pr=Dpr(9); d13pr=Dpr(10); d15pr=Dpr(11); d17pr=Dpr(12); d18pr=Dpr↙
);
 d19pr=Dpr(14); d20pr=Dpr(15); d24pr=Dpr(16); d29pr=Dpr(17); d30pr=Dpr(18); d32pr=Dpr↙
);
 d33pr=Dpr(20); d43pr=Dpr(21); d46pr=Dpr(22);
 Sa1=[];
 for i=1:length(R)
     r=R(i);
     PGAabpr=exp(c11pr+(c12+(c15pr-c17pr)*c19)*(M-6)+c13*(10-M)^3+...
         c17pr*log(r+c18*exp(c19*M))+c20pr*Hc+c24pr*SI+c46pr*rvol*(1-DS));

     PGAab=exp(c11+(c12+(c15-c17)*c19)*(M-6)+c13*(10-M)^3+...
         c17*log(r+c18*exp(c19*M))+c20*Hc+c24*SI+c46*rvol*(1-DS));

     lnSAabpr=d11pr+(d12+(d15pr-d17pr)*d19)*(M-6)+d13*(10-M)^3+...
         d17pr*log(r+d18*exp(d19*M))+d20pr*Hc+d24pr*SI+d46pr*rvol*(1-DS);

     lnSAcdpr=lnSAabpr+[d29pr (d30*log(PGAabpr+0.03)+d43pr)]*sitecoeff(2:3);
     PGAabcdpr=log(PGAabpr)+[c29pr (c30*log(PGAabpr+0.03)+c43pr)]*sitecoeff(2:3);
     PGAabcd=log(PGAab)+[c29 (c30*log(PGAab+0.03)+c43)]*sitecoeff(2:3);


     SApr=exp(lnSAcdpr);
     Sa1(i)=SApr*PGAabcd/PGAabcdpr;

 end
 m=find(periods==T2);

 D=table5(:,m(1));
```

```
    Dpr=table6(:,m(1));

    d1=D(1); d3=D(2); d4=D(3); d5=D(4); d6=D(5); d8=D(6); d10=D(7);
    d11=D(8); d12=D(9); d13=D(10); d15=D(11); d17=D(12); d18=D(13);
    d19=D(14); d20=D(15); d24=D(16); d29=D(17); d30=D(18); d32=D(19);
    d33=D(20); d43=D(21); d46=D(22);
    d1pr=Dpr(1);   d3pr=Dpr(2); d4pr=Dpr(3); d5pr=Dpr(4); d6pr=Dpr(5); d8pr=Dpr(6);↙
d10pr=Dpr(7);
    d11pr=Dpr(8);  d12pr=Dpr(9); d13pr=Dpr(10); d15pr=Dpr(11); d17pr=Dpr(12); d18pr=Dpr↙
(13);
    d19pr=Dpr(14); d20pr=Dpr(15); d24pr=Dpr(16); d29pr=Dpr(17); d30pr=Dpr(18); d32pr=Dpr↙
(19);
    d33pr=Dpr(20); d43pr=Dpr(21); d46pr=Dpr(22);
    Sa2=[];
    for i=1:length(R)
        r=R(i);
        PGAabpr=exp(c11pr+(c12+(c15pr-c17pr)*c19)*(M-6)+c13*(10-M)^3+...
            c17pr*log(r+c18*exp(c19*M))+c20pr*Hc+c24pr*SI+c46pr*rvol*(1-DS));

        PGAab=exp(c11+(c12+(c15-c17)*c19)*(M-6)+c13*(10-M)^3+...
            c17*log(r+c18*exp(c19*M))+c20*Hc+c24*SI+c46*rvol*(1-DS));

        lnSAabpr=d11pr+(d12+(d15pr-d17pr)*d19)*(M-6)+d13*(10-M)^3+...
            d17pr*log(r+d18*exp(d19*M))+d20pr*Hc+d24pr*SI+d46pr*rvol*(1-DS);

        lnSAcdpr=lnSAabpr+[d29pr (d30*log(PGAabpr+0.03)+d43pr)]*sitecoeff(2:3);
        PGAabcdpr=log(PGAabpr)+[c29pr (c30*log(PGAabpr+0.03)+c43pr)]*sitecoeff(2:3);
        PGAabcd=log(PGAab)+[c29 (c30*log(PGAab+0.03)+c43)]*sitecoeff(2:3);


        SApr=exp(lnSAcdpr);
        Sa2(i)=SApr*PGAabcd/PGAabcdpr;

    end
    for i=1:length(R)
    Sa=interp1([T1 T2],[Sa1(i) Sa2(i)],T,'log')';
    end
else
    m=find(periods==T);

    D=table5(:,m(1));
    Dpr=table6(:,m(1));

    d1=D(1); d3=D(2); d4=D(3); d5=D(4); d6=D(5); d8=D(6); d10=D(7);
    d11=D(8); d12=D(9); d13=D(10); d15=D(11); d17=D(12); d18=D(13);
    d19=D(14); d20=D(15); d24=D(16); d29=D(17); d30=D(18); d32=D(19);
    d33=D(20); d43=D(21); d46=D(22);
    d1pr=Dpr(1);   d3pr=Dpr(2); d4pr=Dpr(3); d5pr=Dpr(4); d6pr=Dpr(5); d8pr=Dpr(6);↙
d10pr=Dpr(7);
    d11pr=Dpr(8);  d12pr=Dpr(9); d13pr=Dpr(10); d15pr=Dpr(11); d17pr=Dpr(12); d18pr=Dpr↙
(13);
```

```
    d19pr=Dpr(14); d20pr=Dpr(15); d24pr=Dpr(16); d29pr=Dpr(17); d30pr=Dpr(18); d32pr=Dpr(19);
    d33pr=Dpr(20); d43pr=Dpr(21); d46pr=Dpr(22);


    for i=1:length(R)
        r=R(i);
        PGAabpr=exp(c11pr+(c12+(c15pr-c17pr)*c19)*(M-6)+c13*(10-M)^3+...
            c17pr*log(r+c18*exp(c19*M))+c20pr*Hc+c24pr*SI+c46pr*rvol*(1-DS));

        PGAab=exp(c11+(c12+(c15-c17)*c19)*(M-6)+c13*(10-M)^3+...
            c17*log(r+c18*exp(c19*M))+c20*Hc+c24*SI+c46*rvol*(1-DS));

        lnSAabpr=d11pr+(d12+(d15pr-d17pr)*d19)*(M-6)+d13*(10-M)^3+...
            d17pr*log(r+d18*exp(d19*M))+d20pr*Hc+d24pr*SI+d46pr*rvol*(1-DS);

        lnSAcdpr=lnSAabpr+[d29pr (d30*log(PGAabpr+0.03)+d43pr)]*sitecoeff(2:3);
        %PGAabcdpr=log(PGAabpr)+[c29pr(c30*log(PGAabpr+0.03)+c43pr)]*sitecoeff(2:3);
original code
        PGAabcdpr=(PGAabpr)+[c29pr (c30*log(PGAabpr+0.03)+c43pr)]*sitecoeff(2:3); %error
corrected
        %PGAabcd=log(PGAab)+[c29(c30*log(PGAab+0.03)+c43)]*sitecoeff(2:3); original code
        PGAabcd=(PGAab)+[c29 (c30*log(PGAab+0.03)+c43)]*sitecoeff(2:3); %error corrected


        SApr=exp(lnSAcdpr);
        Sa(i)=SApr*PGAabcd/PGAabcdpr;
        %Sa(i)= SApr;

    end
end
SUCCESS = XLSWRITE('C:\Users\Jennifer\Graduate School\Richard\PGAs.xlsx',Sa, 'sheet1',
'K2:K6');
```

Newman Power Law Distribution – Artificial Data

8/2/12 7:34 PM C:\Users\Jennifer\Dropbox\The...\Pisco Newman artificial dataset.m 1 of 4

```
% Reproduce Newman's method of analyzing data

clear all;
clc;

% Need one million numbers in a power-law distribution
clear all;
alpha = 2.5; %given in Newman paper
xMin = 1; %from eyeballing graphs
C = (alpha-1)*xMin^(alpha-1); %from Clauset and Newman, 2009
r = rand(1,10^6); %gives one million random numbers between 0 and 1
x = xMin.*(1-r).^(-1/(alpha-1)); %transforms uniform distribution into power-law
distribution

% start uniform binning, bins size .1 starting with 1
k=1;
for i=1:.1:500;
binCenter(k) = i+.05;
px(k)= C*binCenter(k)^(-alpha); %function to plot against random data; equation (1) from
Newman paper
k=k+1;
end

[n,bin] = hist(x,binCenter); %find out how many numbers, n, from our power-law
distribution, x, are in each bin
prob = n./10^6/.1; %normalize by total n, bin size

figure (1);
subplot (1,2,1);
bar (bin, prob, 'hist'); %make a bar graph of the probability of a number being in each
bin
g = findobj(gca,'Type','patch');
set(g,'FaceColor','b','EdgeColor','k')
axis ([0 8 0 1.5]);
set(gca,'FontSize',16);
title('(A)', 'Units', 'normalized', ...
'Position', [.05 1], 'HorizontalAlignment', 'left');
xlabel ('value of x', 'FontSize', 16);
ylabel ('probability of x, %', 'FontSize', 16);
hold on;
plot (bin, px, '--','linewidth', 3, 'color', 'r');
text (1.75, 1.25, 'blue: artificial dataset, bin size = .1', 'color', 'b', 'FontSize',
16);
text (1.75, 1.1, 'red: p(x) = 1.5*x\^(-2.5)', 'color', 'r', 'FontSize', 16);

subplot(1,2,2); %plot previous graph in log-log space
loglog (bin,prob, 'linewidth', 2);
set(gca,'FontSize',16);
title('(B)', 'Units', 'normalized', ...
'Position', [.05 1], 'HorizontalAlignment', 'left');
xlabel ('value of x', 'FontSize', 16);
```

```
ylabel ('probability of x, %', 'FontSize', 16);
hold on;
loglog (bin, px, '--','linewidth', 3, 'color', 'r');
axis ([1 200 10^-5 10^0]);

%total prob should be 1, check area under graphs
totalProb = 0;
totalProbEV = 0;
for j=1:length(prob);
    totalProb = totalProb + prob(j)*.1;
    totalProbEV = totalProbEV + px(j)*.1;
end


% start log2-binning graphs
p = 1;
logBinEdge(p) = 1; %start at binEdge = 1, increase by .1, .2, .4, .8 etc
for m=0:20;
    p=p+1;
    logBinEdge(p) = logBinEdge(p-1) + .1*2^m; %creates logBins 1, 1.1, 1.3, 1.7, etc
    logBinSize(p-1) = .1*2^m; %size of log bins, will use for normalizing later
    logBinCenter(p-1) = (logBinEdge(p-1) + logBinEdge(p) )/2; %will use for graphing
power law function to compare with random data
end
logBinSize(p) = .1*2^(m+1); %need extra element to make vectors the same length, since
there is one more edge than center
logBinCenter(p) = logBinEdge(p) + .5*logBinSize(p);
N = histc(x,logBinEdge); %find out how many numbers, N, from our power-law distribution,
x, are in each log-2 bin
probLog = N./10^6./logBinSize; %normalized by bin width

figure (2);
subplot (1,2,1);
bar (logBinEdge, probLog, 'histc');
h = findobj(gca,'Type','patch');
set(h,'FaceColor','b','EdgeColor','k')
set(gca,'FontSize',16);
axis ([0  8 0 1.5]);
title('(A)', 'Units', 'normalized', ...
'Position', [.05 1], 'HorizontalAlignment', 'left');
xlabel ('value of x', 'FontSize', 16);
ylabel ('probability of x, %', 'FontSize', 16);
hold on;
loglog (bin, px, '--','linewidth', 3, 'color', 'r');
text (1.75, 1.25, 'blue: artificial dataset, log-2 bins', 'color', 'b', 'FontSize', 16);
text (1.75, 1.1, 'red: p(x) = 1.5*x\^(-2.5)', 'color', 'r', 'FontSize', 16);

subplot (1,2,2);
loglog (logBinCenter, probLog, 'linewidth', 3);
axis ([1 200 10^-5 10^0]);
set(gca,'FontSize',16);
```

```
title('(B)', 'Units', 'normalized', ...
'Position', [.05 1], 'HorizontalAlignment', 'left');
xlabel ('value of x', 'FontSize', 16);
ylabel ('probability of x, %', 'FontSize', 16);
hold on;
loglog (bin, px, '--','linewidth', 3, 'color', 'r');


%plot equation to check graph of random numbers
%expected value (probability)for the kth bin is
%C*(a^(alpha-1)-1)/(alpha-1)*(xmin*a^k)^(-alpha+1)
%where C=1.5, alpha=2.5, xmin=1, and a=2 (b/c of log2 bins)
a=2;
xMin = .1;
alpha = 2.5;

for q=1:length(N)-1;
   %EV(q) = C*(a^(alpha-1)-1)/(alpha-1)*(xMin*a^q)^(1-alpha); %this is from but Newman,
but has problems
   EV(q) = C/(1-alpha)*( logBinEdge(q+1)^(1-alpha)-logBinEdge(q)^(1-alpha) )/logBinSize
(q);
end
EV(q+1) = EV(q);

figure (3);
subplot (1,2,1);
plot(logBinCenter,EV, '--','linewidth',3, 'color', 'r');

%check area under curves for log binning graphs--should equal 1
totalProbLog = 0;
totalProbLogEV = 0;
for s=1:length(probLog);
    totalProbLog = totalProbLog + probLog(s)*logBinSize(s);
    totalProbLogEV = totalProbLogEV + EV(s)*logBinSize(s);
end

%start cumulative plot
%probability of x being equal to or greater than x
sortAscending = sort(x);
c=1;
row=2;
table = zeros(10^6,4);
table(1,1)=sortAscending(1); %value of x
table(1,2)=1; %number of that value
table (1,3)=10^6; %number greater than or equal to that value
table (1,4)=1; %cumulative probability of x being greater than x
for index=2:length(x)-1;
    if sortAscending(index)==sortAscending(index+1);
        c=c+1;
    else
        table(row,1) = sortAscending(index); %value of x
```

```
        table(row,2) = c; %number of that value
        table(row,3) = table(row-1,3)-table(row-1,2);%number greater than of equal to x
        table(row,4) = table(row,3)/10^6;%cumulative probability of being greater than
or equal to x
        row=row+1;
        c=1;
    end
end


%plotting artificial data set cumulatively
%subplot (2,2,4);
loglog (table(:,1),table(:,4), 'linewidth', 3);
axis ([1 10^4 10^-5.5 10^.2]);
set(gca,'FontSize',16);
xlabel ('value of x', 'FontSize', 16);
ylabel ('cumulative probability of x, %', 'FontSize', 16);
hold on;

% function to match data
for u = 1:length(EV);
 EVcum(u) = C/(alpha-1)*logBinCenter(u)^-(alpha-1);
end
plot (logBinCenter, EVcum, '--','linewidth', 3, 'color', 'r');
text (10^1.1, 10^-1, 'blue: artificial dataset', 'color', 'b', 'FontSize', 16);
text (10^1.4, 10^-1.6, 'red: p (X>x) =  C/(alpha-1) * x^(^a^l^p^h^a^-^1^) ', 'color',
'r', 'FontSize', 16);
text (10^2, 10^-2.1, 'C = 1.5,  alpha = 2.5', 'color', 'r', 'FontSize', 16);
```

Newman Power Law Distribution – Pisco Data


```
% Reproduce Newman's method of analyzing data

clear all;
clc;

x = xlsread('C:\Users\Jennifer\Dropbox\Thesis\Power Law Figures and Papers\LS volumes
for analysis.xlsx', 'Sheet1', 'a1:a254');
%make a vector of landslide volumes from excel spreadsheet column

alpha = 2.1309; %from Clauset's plfit function
xmin = 50184; %from Clauset's plfit function
C = (alpha-1)*xmin^(alpha-1);

%best fit line
 n = length(x);
        c = [sort(x) (n:-1:1)'./n]; %colum 1 sorts x in ascending order, col 2 100% down
to 1/254
        q = sort(x(x>=xmin)); %sort x from xmin to xmax
        cf = [q (q./xmin).^(1-alpha)];
        cf(:,2) = cf(:,2) .* c(find(c(:,1)>=xmin,1,'first'),2); %multiply column cf(:,2)
by value of c(:,2)at index of first value equal to xmin


% start uniform binning
k=1;
for i=1:3000:3*10^6; %gives us 1000 bins, size 3000, from 1 to 3 million
binCenter(k) = i+1500; %gives us the centers of bins
px(k)= C*binCenter(k)^(-alpha); %function to plot against random data; equation (1) from
Newman paper
k=k+1;
end

[n,bin] = hist(x,binCenter); %find out how many numbers, n, from our power-law
distribution, x, are in each bin
prob = n./length(x)/3000; %normalize by total n, bin size

figure (1);
subplot (1,2,1);
bar (bin, prob,'hist'); %make a bar graph of the probability of a number being in each
bin
g = findobj(gca,'Type','patch');
set(g,'FaceColor','b','EdgeColor','k')
y = C.*x.^(-alpha);
hold on;
axis ([-1500 5*10^4 0 .00023]);
title('(A)', 'FontSize', 16, 'Units', 'normalized', ...
'Position', [.1 1], 'HorizontalAlignment', 'left');
xlabel ('landslide volume, m^3', 'FontSize', 16);
ylabel ('probability, %', 'FontSize', 16);
text (10^4, 1.5*10^-4, 'blue: Pisco data, bin size = 3000 m^3', 'color', 'b',
'FontSize', 16);
```

```
subplot(1,2,2); %plot previous graph in log-log space
loglog (bin,prob, 'o--', 'linewidth', 2, 'color', 'b');
hold on;
xlabel ('landslide volume, m^3', 'FontSize', 16);
ylabel ('probability, %', 'FontSize', 16);
hold on;
axis ([10^3 10^6 10^-6 .00023]);
title('(B)','FontSize', 16, 'Units', 'normalized', ...
'Position', [.1 1], 'HorizontalAlignment', 'left');


%start cumulative plot
%probability of x being equal to or greater than x
sortAscending = sort(x);
count=1;
row=2;
table = zeros(length(x),4);
table(1,1)=sortAscending(1); %value of x
table(1,2)=1; %number of that value
table (1,3)=length(x); %number greater than or equal to that value
table (1,4)=1; %cumulative probability of x being greater than x
for index=2:length(x)-1;
    if sortAscending(index)==sortAscending(index+1);
        count=count+1;
    else
        table(row,1) = sortAscending(index); %value of x
        table(row,2) = count; %number of that value
        table(row,3) = table(row-1,3)-table(row-1,2);%number greater than of equal to x
        table(row,4) = table(row,3)/length(x);%cumulative probability of being greater
than or equal to x
        row=row+1;
        count=1;
    end
end


%plotting Pisco data set cumulatively
figure (2);
%subplot (1,2,1);
loglog (table(:,1),table(:,4), 'linewidth', 2, 'color', 'b');
hold on;
xlabel ('landslide volume, m^3', 'FontSize', 16);
ylabel ('cumulative probability, %', 'FontSize', 16);
axis ([1 10^6 10^-2.5 10^.2]);

%plotting best fit line from Clauset Matlab function
loglog(cf(:,1),cf(:,2),'r--','LineWidth',3);
text (10^.6, 10^-1.0, 'blue: Pisco volume data', 'color', 'b', 'FontSize', 18);
text (10^.6, 10^-1.2, 'red: p(X \geq x) =  C/(alpha-1) * x^-^(^a^l^p^h^a^-^1^) ',
'color', 'r', 'FontSize', 18);
```

```
text (10^.6, 10^-1.4, 'C = 2.3404 x 10^5', 'color', 'k', 'FontSize', 18);
text (10^.6, 10^-1.6, 'alpha = 2.1309', 'color', 'k', 'FontSize', 18);
text (10^.6, 10^-1.8, 'x_m_i_n = 50184', 'color', 'k', 'FontSize', 18);

figure (3);
%subplot(1,2,2); %plot previous graph in log-log space
loglog (bin,prob, 'o--', 'linewidth', 2, 'color', 'b');
hold on;
loglog(x(227:254,:),y(227:254,:), 'g--', 'linewidth', 3);
loglog(x(1:254,:),y(1:254,:), 'g--', 'linewidth', 3);
xlabel ('landslide volume, m^3', 'FontSize', 16);
ylabel ('probability, %', 'FontSize', 16);
hold on;
axis ([10^3 10^6 10^-6 .00023]);
text (10^5.1, 10^-4.0, 'blue: Pisco volume data', 'color', 'b', 'FontSize', 18);
text (10^5.1, 10^-4.2, 'green: p(x) =  Cx^-^a^l^p^h^a ', 'color', 'g', 'FontSize', 18);
text (10^5.1, 10^-4.4, 'C = 2.3404 x 10^5', 'color', 'k', 'FontSize', 18);
text (10^5.1, 10^-4.6, 'alpha = 2.1309', 'color', 'k', 'FontSize', 18);
text (10^5.1, 10^-4.8, 'x_m_i_n = 50184', 'color', 'k', 'FontSize', 18);
```

Clauset's PLFIT Function


```
function [alpha, xmin, L]=plfit(x, varargin)
% PLFIT fits a power-law distributional model to data.
%    Source: http://www.santafe.edu/~aaronc/powerlaws/
%
%    PLFIT(x) estimates x_min and alpha according to the goodness-of-fit
%    based method described in Clauset, Shalizi, Newman (2007). x is a
%    vector of observations of some quantity to which we wish to fit the
%    power-law distribution p(x) ~ x^-alpha for x >= xmin.
%    PLFIT automatically detects whether x is composed of real or integer
%    values, and applies the appropriate method. For discrete data, if
%    min(x) > 1000, PLFIT uses the continuous approximation, which is
%    a reliable in this regime.
%
%    The fitting procedure works as follows:
%    1) For each possible choice of x_min, we estimate alpha via the
%       method of maximum likelihood, and calculate the Kolmogorov-Smirnov
%       goodness-of-fit statistic D.
%    2) We then select as our estimate of x_min, the value that gives the
%       minimum value D over all values of x_min.
%
%    Note that this procedure gives no estimate of the uncertainty of the
%    fitted parameters, nor of the validity of the fit.
%
%    Example:
%       x = (1-rand(10000,1)).^(-1/(2.5-1));
%       [alpha, xmin, L] = plfit(x);
%
%    The output 'alpha' is the maximum likelihood estimate of the scaling
%    exponent, 'xmin' is the estimate of the lower bound of the power-law
%    behavior, and L is the log-likelihood of the data x>=xmin under the
%    fitted power law.
%
%    For more information, try 'type plfit'
%
%    See also PLVAR, PLPVA

% Version 1.0    (2007 May)
% Version 1.0.2  (2007 September)
% Version 1.0.3  (2007 September)
% Version 1.0.4  (2008 January)
% Version 1.0.5  (2008 March)
% Version 1.0.6  (2008 July)
% Version 1.0.7  (2008 October)
% Version 1.0.8  (2009 February)
% Version 1.0.9  (2009 October)
% Version 1.0.10 (2010 January)
% Version 1.0.11 (2012 January)
% Copyright (C) 2008-2012 Aaron Clauset (Santa Fe Institute)
% Distributed under GPL 2.0
% http://www.gnu.org/copyleft/gpl.html
% PLFIT comes with ABSOLUTELY NO WARRANTY
```

```
%
% Notes:
%
% 1. In order to implement the integer-based methods in Matlab, the numeric
%    maximization of the log-likelihood function was used. This requires
%    that we specify the range of scaling parameters considered. We set
%    this range to be [1.50 : 0.01 : 3.50] by default. This vector can be
%    set by the user like so,
%
%       a = plfit(x,'range',[1.001:0.001:5.001]);
%
% 2. PLFIT can be told to limit the range of values considered as estimates
%    for xmin in three ways. First, it can be instructed to sample these
%    possible values like so,
%
%       a = plfit(x,'sample',100);
%
%    which uses 100 uniformly distributed values on the sorted list of
%    unique values in the data set. Second, it can simply omit all
%    candidates above a hard limit, like so
%
%       a = plfit(x,'limit',3.4);
%
%    Finally, it can be forced to use a fixed value, like so
%
%       a = plfit(x,'xmin',3.4);
%
%    In the case of discrete data, it rounds the limit to the nearest
%    integer.
%
% 3. When the input sample size is small (e.g., < 100), the continuous
%    estimator is slightly biased (toward larger values of alpha). To
%    explicitly use an experimental finite-size correction, call PLFIT like
%    so
%
%       a = plfit(x,'finite');
%
%    which does a small-size correction to alpha.
%
% 4. For continuous data, PLFIT can return erroneously large estimates of
%    alpha when xmin is so large that the number of obs x >= xmin is very
%    small. To prevent this, we can truncate the search over xmin values
%    before the finite-size bias becomes significant by calling PLFIT as
%
%       a = plfit(x,'nosmall');
%
%    which skips values xmin with finite size bias > 0.1.

vec     = [];
sample  = [];
xminx   = [];
```

```
limit   = [];
finite  = false;
nosmall = false;
nowarn  = false;

% parse command-line parameters; trap for bad input
i=1;
while i<=length(varargin),
  argok = 1;
  if ischar(varargin{i}),
    switch varargin{i},
        case 'range',         vec     = varargin{i+1}; i = i + 1;
        case 'sample',        sample  = varargin{i+1}; i = i + 1;
        case 'limit',         limit   = varargin{i+1}; i = i + 1;
        case 'xmin',          xminx   = varargin{i+1}; i = i + 1;
        case 'finite',        finite  = true;
        case 'nowarn',        nowarn  = true;
        case 'nosmall',       nosmall = true;
        otherwise, argok=0;
    end
  end
  if ~argok,
    disp(['(PLFIT) Ignoring invalid argument #' num2str(i+1)]);
  end
  i = i+1;
end
if ~isempty(vec) && (~isvector(vec) || min(vec)<=1),
    fprintf('(PLFIT) Error: ''range'' argument must contain a vector; using default.
\n');
    vec = [];
end;
if ~isempty(sample) && (~isscalar(sample) || sample<2),
    fprintf('(PLFIT) Error: ''sample'' argument must be a positive integer > 1; using
default.\n');
    sample = [];
end;
if ~isempty(limit) && (~isscalar(limit) || limit<min(x)),
    fprintf('(PLFIT) Error: ''limit'' argument must be a positive value >= 1; using
default.\n');
    limit = [];
end;
if ~isempty(xminx) && (~isscalar(xminx) || xminx>=max(x)),
    fprintf('(PLFIT) Error: ''xmin'' argument must be a positive value < max(x); using
default behavior.\n');
    xminx = [];
end;

% reshape input vector
x = xlsread('C:\Users\Jennifer\Dropbox\Thesis\Power Law Figures and Papers\LS volumes
for analysis.xlsx', 'Sheet1', 'a1:a254');
x = reshape(x,numel(x),1);
```

```
% select method (discrete or continuous) for fitting
if     isempty(setdiff(x,floor(x))), f_dattype = 'INTS';
elseif isreal(x),    f_dattype = 'REAL';
else                 f_dattype = 'UNKN';
end;
if strcmp(f_dattype,'INTS') && min(x) > 1000 && length(x)>100,
    f_dattype = 'REAL';
end;

% estimate xmin and alpha, accordingly
switch f_dattype,

    case 'REAL',
        xmins = unique(x);
        xmins = xmins(1:end-1);
        if ~isempty(xminx),
            xmins = xmins(find(xmins>=xminx,1,'first'));
        end;
        if ~isempty(limit),
            xmins(xmins>limit) = [];
        end;
        if ~isempty(sample),
            xmins = xmins(unique(round(linspace(1,length(xmins),sample))));
        end;
        dat   = zeros(size(xmins));
        z     = sort(x);
        for xm=1:length(xmins)
            xmin = xmins(xm);
            z    = z(z>=xmin);
            n    = length(z);
            % estimate alpha using direct MLE
            a    = n ./ sum( log(z./xmin) );
            if nosmall,
                if (a-1)/sqrt(n) > 0.1
                    dat(xm:end) = [];
                    xm = length(xmins)+1;
                    break;
                end;
            end;
            % compute KS statistic
            cx   = (0:n-1)'./n;
            cf   = 1-(xmin./z).^a;
            dat(xm) = max( abs(cf-cx) );
        end;
        D     = min(dat);
        xmin  = xmins(find(dat<=D,1,'first'));
        z     = x(x>=xmin);
        n     = length(z);
        alpha = 1 + n ./ sum( log(z./xmin) );
        if finite, alpha = alpha*(n-1)/n+1/n; end; % finite-size correction
```

```
        if n < 50 && ~finite && ~nowarn,
            fprintf('(PLFIT) Warning: finite-size bias may be present.\n');
        end;
        L = n*log((alpha-1)/xmin) - alpha.*sum(log(z./xmin));

    case 'INTS',

        if isempty(vec),
            vec  = (1.50:0.01:3.50);    % covers range of most practical
        end;                            % scaling parameters
        zvec = zeta(vec);

        xmins = unique(x);
        xmins = xmins(1:end-1);
        if ~isempty(xminx),
            xmins = xmins(find(xmins>=xminx,1,'first'));
        end;
        if ~isempty(limit),
            limit = round(limit);
            xmins(xmins>limit) = [];
        end;
        if ~isempty(sample),
            xmins = xmins(unique(round(linspace(1,length(xmins),sample))));
        end;
        if isempty(xmins)
            fprintf('(PLFIT) Error: x must contain at least two unique values.\n');
            alpha = NaN; xmin = x(1); D = NaN;
            return;
        end;
        xmax   = max(x);
        dat    = zeros(length(xmins),2);
        z      = x;
        fcatch = 0;

        for xm=1:length(xmins)
            xmin = xmins(xm);
            z    = z(z>=xmin);
            n    = length(z);
            % estimate alpha via direct maximization of likelihood function
            if fcatch==0
                try
                    % vectorized version of numerical calculation
                    zdiff = sum( repmat((1:xmin-1)',1,length(vec)).^-repmat(vec,xmin-
1,1) ,1);
                    L = -vec.*sum(log(z)) - n.*log(zvec - zdiff);
                catch
                    % catch: force loop to default to iterative version for
                    % remainder of the search
                    fcatch = 1;
                end;
            end;
```

```
            if fcatch==1
                % force iterative calculation (more memory efficient, but
                % can be slower)
                L       = -Inf*ones(size(vec));
                slogz   = sum(log(z));
                xminvec = (1:xmin-1);
                for k=1:length(vec)
                    L(k) = -vec(k)*slogz - n*log(zvec(k) - sum(xminvec.^-vec(k)));
                end
            end;
            [Y,I] = max(L);
            % compute KS statistic
            fit = cumsum((((xmin:xmax).^-vec(I))./ (zvec(I) - sum((1:xmin-1).^-vec
(I))));
            cdi = cumsum(hist(z,xmin:xmax)./n);
            dat(xm,:) = [max(abs( fit - cdi )) vec(I)];
        end
        % select the index for the minimum value of D
        [D,I] = min(dat(:,1));
        xmin  = xmins(I);
        z     = x(x>=xmin);
        n     = length(z);
        alpha = dat(I,2);
        if finite, alpha = alpha*(n-1)/n+1/n; end; % finite-size correction
        if n < 50 && ~finite && ~nowarn,
            fprintf('(PLFIT) Warning: finite-size bias may be present.\n');
        end;
        L     = -alpha*sum(log(z)) - n*log(zvec(find(vec<=alpha,1,'last')) - sum((1:
xmin-1).^-alpha));

    otherwise,
        fprintf('(PLFIT) Error: x must contain only reals or only integers.\n');
        alpha = [];
        xmin  = [];
        L     = [];
        return;
end;
```

Implementation of PLFIT

9/7/12 12:08 PM C:\Users\Jennifer\Dropbox\Thesis\P...\Inverse power law Newman5.m 1 of 1

```
clear all;
clc;

x = xlsread('C:\Users\Jennifer\Dropbox\Thesis\Power Law Figures and Papers\LS volumes
for analysis.xlsx', 'Sheet1', 'a1:a254');

[alpha, xmin, L] = plfit(x);

 n = length(x);
        c = [sort(x) (n:-1:1)'./n];
        q = sort(x(x>=xmin));
        cf = [q (q./xmin).^(1-alpha)];
        cf(:,2) = cf(:,2) .* c(find(c(:,1)>=xmin,1,'first'),2);

        figure;
        h(1) = loglog(c(:,1),c(:,2),'b','LineWidth',2'); hold on;
        h(2) = loglog(cf(:,1),cf(:,2),'r--','LineWidth',3); hold off;
        xr  = [10.^floor(log10(min(x))) 10.^ceil(log10(max(x)))];
        xrt = (round(log10(xr(1))):2:round(log10(xr(2))));
        if length(xrt)<4, xrt = (round(log10(xr(1))):1:round(log10(xr(2)))); end;
        yr  = [10.^floor(log10(1/n)) 1];
        yrt = (round(log10(yr(1))):2:round(log10(yr(2))));
        if length(yrt)<4, yrt = (round(log10(yr(1))):1:round(log10(yr(2)))); end;
        set(gca,'XLim',xr,'XTick',10.^xrt);
        set(gca,'YLim',yr,'YTick',10.^yrt,'FontSize',16);
        ylabel('p(X \geq x)','FontSize',16);
        xlabel('x','FontSize',16)
```

Malamud 3-Parameter Inverse Gamma Distribution


```
% 3 parameter inverse gamma distribution

clear all;
clc;

%make a vector of landslide volumes in m^3 from excel spreadsheet column
x = xlsread('C:\Users\Jennifer\Dropbox\Thesis\Power Law Figures and Papers\LS volumes
for analysis.xlsx', 'Sheet1', 'a1:a254');

% use Larsen et al. (2010) to estimate landslide areas given volumes
alpha = 10^-.836;
gamma = 1.35; % gamma for rock; gamma for soil = 1.145
x(:,2) = (x(:,1)./alpha).^(1/gamma); % Larsen empirical scaling relationship, area in
m^2
%x(:,2) = (x(:,1)./.05).^(2/3) % Hovius et al. 1997
x(:,3) = (x(:,2)./1000^2); %area in km^2
area = x(:,3);

% parameters for Malamud et. al
rho = 1.4;  %power law decay
a = 1.28*10^-3;  %location of maximum probability
s = -1.32*10^-4;  %exponential rollover
Nlt = length(x);  %total number of landslides associated with event
gamma = .88726;

% code for landslide area probability density
% will need to log-bin data, get number of LS in each bin
% probability density for each bin is number of LS in that bin,
% divided by total number of landslides
% divided by the width of the bin


% create log bins from 10^-6 to 10^-1
numBins = 50;
binEdges(1) = 10^-6;
for k = 2:numBins+1;
binEdges(k) = 10^(-6.1+.1*k);
binSizes(k-1) = binEdges(k)-binEdges(k-1);
binCenters(k-1) = binEdges(k-1)+ binSizes(k-1)/2;
end
N = hist(area, binCenters);

% find probability density
pAl = 1./Nlt .* N./binSizes;


figure (1);
%subplot (1,2,1);
Al(1) = 10^-6;
for j=1:350;
Al(j+1) = 1.1*Al(j);
```

```
end
func = (1/a/gamma).*(a./(Al-s)).^(rho+1).*exp(-a./(Al-s));
loglog (Al, func, 'linewidth', 2, 'color', [.8 .8 .8]);
xlabel ('landslide area, km^2');
ylabel ('probability density, km^-^2');
axis ([10^-5.3 10^0.4 10^-5 10^4.5]);
hold on;
loglog (binCenters, pAl, 'o', 'MarkerEdgeColor', 'k', 'MarkerFaceColor', 'k',↙
'MarkerSize',3);
%loglog (binC, pAl, 'linewidth', 2);
legend ('3-parameter inverse gamma probability distribution', 'Pisco data, log-10 bins',↙
'Location', 'SouthWest');

figure (2);
%subplot (1,2,2);
plot (Al, func, 'linewidth', 2, 'color', [.8 .8 .8]);
axis ([0 .01 0 700]);
%xlabel ('landslide area, km^2');
%ylabel ('probability density, km^-^2');
hold on;
plot (binCenters, pAl, 'o', 'MarkerEdgeColor', 'k', 'MarkerFaceColor', 'k',↙
'MarkerSize',4);

% make frequncy density versus landslide area graph
% add landslide magnitude lines mL = 1 - 8 where mL = log Nlt

fAl = pAl.*Nlt;
for i=1:8;
    mL(i,:) = func.*10^i;
end


figure (3);
loglog (binCenters, fAl, 'o', 'MarkerEdgeColor', 'k', 'MarkerFaceColor', 'k',↙
'MarkerSize',3);
axis ([10^-5 10^1 10^0 10^8]);
xlabel ('landslide area, km^2');
ylabel ('frequency density, km^-^2');
hold on;
loglog (Al, mL, 'linewidth', 2, 'color', [.8 .8 .8]);
legend ('Pisco data', 'landslide event magnitude', 'Location', 'SouthWest');
loglog (binCenters, fAl, 'o', 'MarkerEdgeColor', 'k', 'MarkerFaceColor', 'k',↙
'MarkerSize',3);
text (10^-1.9, 10^.3, '\bf \it m_L = 1', 'FontSize', 10);
text (10^-1.1, 10^.3, '\bf \it 2', 'FontSize', 10);
text (10^-.7, 10^.3, '\bf \it 3', 'FontSize', 10);
text (10^-.3, 10^.3, '\bf \it 4', 'FontSize', 10);
text (10^.1, 10^.3, '\bf \it 5', 'FontSize', 10);
text (10^.55, 10^.3, '\bf \it 6', 'FontSize', 10);
text (10^.55, 10^1.3, '\bf \it 7', 'FontSize', 10);
text (10^.55, 10^2.3, '\bf \it 8', 'FontSize', 10);
```

```
% make figure with rockfall frequency curve
x(:,4) = x(:,1)./1000^3; % volume in km^3
volume = x(:,4);
%fVr = -1.07.*log10(volume) + .37;

% create log bins from 10^-9 to 10^-2 for rockfall volumes in km^3
numBinsR = 70;
binEdgesR(1) = 10^-9;
for h = 2:numBinsR+1;
binEdgesR(h) = 10^(-9.1+.1*h);
binSizesR(h-1) = binEdgesR(h)-binEdgesR(h-1);
binCentersR(h-1) = binEdgesR(h-1)+ binSizesR(h-1)/2;
end
Nr = hist(volume, binCentersR);

% find frequency density for Pisco volume data, km^3
fVr = Nr./binSizesR;

% find power-law correlation for rock (Malamud, 2003)
% Vr gives us log-10 spaced x-values
% funcR gives us the power-law correlation value at Vr
Vr(1) = 10^-9;
for g=1:350;
Vr(g+1) = 1.1*Vr(g);
funcR(g) = 10^(-1.07.*log10(Vr(g)) + .37);
end
funcR(g+1) = 10^(-1.07.*log10(Vr(g+1)) + .37);

% find landslide magnitude curves in terms of volume instead of area
% func = (1/a/gamma).*(a./(Al-s)).^(rho+1).*exp(-a./(Al-s));
funcR2 = (1/a/gamma).*(a./((Vr./.05).^(2/3)-s)).^(rho+1).*exp(-a./((Vr./.05).^(2/3)-s));
for f=1:7;
    mLr(f,:) = funcR2.*10^f.*254;
end

figure (4);
loglog (binCentersR, fVr, 'o', 'MarkerEdgeColor', 'k', 'MarkerFaceColor', 'k',↙
'MarkerSize',3);
axis ([10^-8 10^0 10^0 10^11]);
xlabel ('landslide volume, km^3');
ylabel ('frequency density, km^-^3');
hold on;
loglog (Vr, funcR, '--', 'linewidth', 2, 'color', 'k');
loglog (Vr, 4.*funcR, '--', 'linewidth', 2, 'color', 'r');
loglog (Vr, mLr(1:2:7,:),'linewidth', 2, 'color', [.8 .8 .8]);
legend ('Pisco data', 'rockfall power-law correlation', 'landslide event magnitude',↙
'Location', 'SouthWest');
text (10^-3.7, 10^3, '\bf \it 1', 'FontSize', 10);
text (10^-3.7, 10^5, '\bf \it 3', 'FontSize', 10);
text (10^-3.7, 10^7, '\bf \it 5', 'FontSize', 10);
```

```
text (10^-4.2, 10^9, '\bf \it m_L = 7', 'FontSize', 10);
loglog (binCentersR, fVr, 'o', 'MarkerEdgeColor', 'k', 'MarkerFaceColor', 'k',↙
'MarkerSize',3);
loglog (Vr, funcR, '--', 'linewidth', 2, 'color', 'k');


%SUCCESS = XLSWRITE('C:\Users\Jennifer\Dropbox\Thesis\Power Law Figures and Papers\LS↙
volumes for analysis.xlsx', binCentersR', 'Sheet3', 'a1:a70');
%SUCCESS = XLSWRITE('C:\Users\Jennifer\Dropbox\Thesis\Power Law Figures and Papers\LS↙
volumes for analysis.xlsx', fVr', 'Sheet3', 'b1:b70');
```